UNIVERSITAT DE
BARCELONA

Bioreduction of iron (hydr)oxides from mine tailings under marine conditions

Robert Benaiges Fernández

ADVERTIMENT. La consulta d'aquesta tesi queda condicionada a l'acceptació de les següents condicions d'ús: La difusió d'aquesta tesi per mitjà del servei TDX (**www.tdx.cat**) i a través del Dipòsit Digital de la UB (**diposit.ub.edu**) ha estat autoritzada pels titulars dels drets de propietat intel·lectual únicament per a usos privats emmarcats en activitats d'investigació i docència. No s'autoritza la seva reproducció amb finalitats de lucre ni la seva difusió i posada a disposició des d'un lloc aliè al servei TDX ni al Dipòsit Digital de la UB. No s'autoritza la presentació del seu contingut en una finestra o marc aliè a TDX o al Dipòsit Digital de la UB (framing). Aquesta reserva de drets afecta tant al resum de presentació de la tesi com als seus continguts. En la utilització o cita de parts de la tesi és obligat indicar el nom de la persona autora.

ADVERTENCIA. La consulta de esta tesis queda condicionada a la aceptación de las siguientes condiciones de uso: La difusión de esta tesis por medio del servicio TDR (**www.tdx.cat**) y a través del Repositorio Digital de la UB (**diposit.ub.edu**) ha sido autorizada por los titulares de los derechos de propiedad intelectual únicamente para usos privados enmarcados en actividades de investigación y docencia. No se autoriza su reproducción con finalidades de lucro ni su difusión y puesta a disposición desde un sitio ajeno al servicio TDR o al Repositorio Digital de la UB. No se autoriza la presentación de su contenido en una ventana o marco ajeno a TDR o al Repositorio Digital de la UB (framing). Esta reserva de derechos afecta tanto al resumen de presentación de la tesis como a sus contenidos. En la utilización o cita de partes de la tesis es obligado indicar el nombre de la persona autora.

WARNING. On having consulted this thesis you're accepting the following use conditions: Spreading this thesis by the TDX (**www.tdx.cat**) service and by the UB Digital Repository (**diposit.ub.edu**) has been authorized by the titular of the intellectual property rights only for private uses placed in investigation and teaching activities. Reproduction with lucrative aims is not authorized nor its spreading and availability from a site foreign to the TDX service or to the UB Digital Repository. Introducing its content in a window or frame foreign to the TDX service or to the UB Digital Repository is not authorized (framing). Those rights affect to the presentation summary of the thesis as well as to its contents. In the using or citation of parts of the thesis it's obliged to indicate the name of the author.

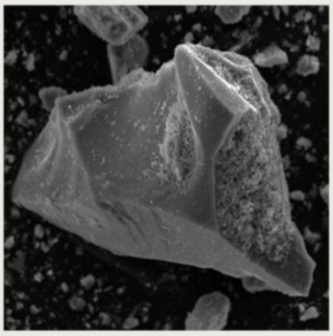

BIOREDUCTION OF IRON (HYDR)OXIDES FROM MINE TAILINGS UNDER MARINE CONDITIONS

ROBERT BENAIGES FERNÁNDEZ

UNIVERSITAT DE BARCELONA

FACULTAT DE BIOLOGIA

BIOREDUCTION OF IRON (HYDR)OXIDES FROM MINE TAILINGS UNDER MARINE CONDITIONS

ROBERT BENAIGES-FERNÁNDEZ, 2020

UNIVERSITAT DE BARCELONA

FACULTAT DE BIOLOGIA

DEPARTAMENT DE GENÈTICA, MICROBIOLOGIA I ESTADÍSTICA

PROGRAMA DE DOCTORAT DE BIOTECNOLOGIA

BIOREDUCTION OF IRON (HYDR)OXIDES FROM MINE TAILINGS UNDER MARINE CONDITIONS

Memòria presentada per Robert Benaiges Fernández per optar al títol de doctor
per la Universitat de Barcelona

Director
Dr. Jordi Cama i Robert

Director i tutor
Dr. Jordi Urmeneta Masó

Doctorand
Robert Benaiges Fernández

When you eat right through it, you see everything alive
It is inside spirit, with enough grit to survive

If you think that it's pretentious, you've been taken for a ride
Look across the mirror, sonny, before you choose, decide

It is here, It is now!

It, Genesis. The lamb lies down on Broadway. 1974

Agraïments/Acknowledgments

M’agradaria agrair l’ajuda que he tingut durant la realització d’aquesta tesi a molta gent. Durant aquests 4 anys he coincidit amb moltes persones i d’alguna manera segur que hi ha una mica de totes aquestes vivències en aquest document (i les que porto amb mi).

Als meus directors de tesi:

Al Dr. Jordi Cama per tota la feina (moltíssima feina), tot el que he après, tot el que he treballat i tot lo bé que m’ho he passat, ja sigui a BCN o al pol nord. Moltes gràcies per tot.

Al Dr. Jordi Urmeneta per tota la feina. Moltes gràcies per donar-me aquesta oportunitat i per confiar en mi molt abans que tot això comencés.

A tota la gent que m’ha ajudat:

Al Dr. Jordi Palau, el tercer director de tesi en l’ombra. Moltes gràcies per tots els consells, per tota la feina, per ensenyar-me tant i per la teva ajuda incommensurable, tant científicament com personal.

Al Dr. Franceso Offeddu, el meu italià preferit. Moltes gràcies per tot el que m’has ajudat en aquests anys que hem compartit en el laboratori. La feina amb tu i amb Siglo XXI sempre es més amena.

La tesi presentada en aquest document és tant seva com meva.

A tota la gent amb qui he compartit estones:

Moltes gràcies a la gent de l’IDAEA, per totes les converses, tots els cafès... Amb companys de viatge així qualsevol aventura és divertida. Hauria de posar molts noms en aquesta llista i no m’hi cabrien. La gent a la qui estic agraïda ja ho sap i li he comentat personalment. M’agradaria però fer una menció honorífica al senyor Jordi Bellès, la paciència personificada. Moltes gràcies per la teva ajuda.

Moltes gràcies a la gent del Departament de microbiologia, de la mateixa manera. He tingut sort de poder tenir companys a tot arreu i certament les penes són menys feixugues

quan les comparteixes. Moltes gràcies a tots. Moltes gràcies a la Sandra i a la Míriam per la seva ajuda d'última hora.

A tota la gent que m'acompanya:

A tots els meus amics i companys de la universitat, de Barcelona i del Poble. No només pel que m'heu ajudat anímicament durant la tesi, sinó per tots els moments que hem viscut junts. Ja sé que aquí no hi pinta res, però és tant bon lloc com un altre perquè quedi escrit. Menció honorífica als meus germans del 4rt, la majoria dels quals estan passant pel mateix. Moltes gràcies Gerard, Àlex, Maria, Uri, Marc, Sergi, Álvaro, Núria...

A la meva família:

Tot el suport que he rebut de la meva família, que han entès i s'han preocupat per la meva feina, Padrí, Padrina, Tieta, Pili, Diego, Pol, Marc, Maria, Biel, Irene.

A la meva àvia Dolores i a la meva àvia Rosita, perquè m'han ensenyat des de ben petit moltes coses, però principalment a no rendir-se mai i a mirar sempre endavant.

A la meva mare Carme, per ensenyar-me des de ben petit la cultura de l'esforç, a tenir esperit crític i a perseverar davant les adversitats.

Al meu pare Robert, per ensenyar-me des de ben petit que cal lluitar pel què creus, encara que el món se't posi en contra. I que de vegades, contra tot pronòstic les coses surten bé.

Els dos m'han ensenyat a gaudir d'aprendre, tant de les ciències com de les lletres. Espero arribar algun dia a ser tant persona com són ells.

I finalment a la Núria, podria escriure una tesi sencera amb les coses que t'hauria d'agrair, em passaria molt de temps escrivint, i prefereixo passar aquest temps al teu costat. Moltes gràcies.

Forth Eorlingas!

ABSTRACT

Mining industry faces environmental problems concerning waste management. Given the environmental issues associated with storage of mine wastes on land, one disposal option that has gained attraction is submarine tailings disposal (STD). This practice involves disposal of mine tailings under seawater through underwater pipelines. Discharged mine wastes may be geochemically altered by microbial communities that living in the seabed have an ecophysiology that is compatible with the mine tailings. These communities (e.g., *Shewanella, Geobacter*) would be able to reduce the structural Fe(III) of oxides and oxyhydroxides (henceforth referred to as (hydr)oxides) of iron contained in the tailings, leading to a release of Fe(II) and Trace Elements (TEs) into the marine environment.

The present study aimed at understanding the reaction of bioreduction of iron (hydr)oxides that are contained in mine tailings and assessing the environmental impact of STD. For this purpose, different samples of iron (hydr)oxides and mine tailings were reacted in batch and column experiments in the presence of *Shewanella loihica*, a dissimilatory iron reducing bacteria. The release of Fe(II) and TE was monitored throughout the experiments, and the surface of the reacted oxides were examined. Geochemical simulations of the experimental data were used to quantify the extent of the overall reductive dissolution reaction. Furthermore, to understand the influence of aqueous iron in the ocean's nitrogen cycle, a series of experiments were carried out with Fe(II) released from bioreduced iron oxides in the presence of nitrite.

Results showed that *Shewanella loihica* bioreduces Fe(III) from the iron (hydr)oxides contained in the mine tailings under marine conditions. The dissolution process leads to a release of Fe(II) and TEs, which are harmful for the marine environment. It was deduced that the reactive surface area of the iron (hydr)oxides is a key factor in the bioreduction process as it provides available Fe(III) and available surface, on which *Shewanella loihica* attach for electron transferring. However, adsorption of some of released Fe(II) onto the surface leads to a decrease in the reactive surface area, which lowers the total available Fe(III), and to a transformation of the former oxide to a new biogenic phase containing Fe^{2+}/Fe^{3+} (i.e. magnetite). Moreover, it was demonstrated that the Fe(II) released promotes a nitrite removal, interfering thus with the nitrogen cycle of the ocean. The nitrite removal was

characterized using chemical and isotopic analyses, which allowed a better understanding of the mechanisms controlling the Fe(II)-N interaction and an identification of the source of nitrite reduction in the sea.

From the results, it is inferred that STD can become a major environmental concern because (1) the Fe(II) released may lead to fertilization and eutrophication of disposal sites, resulting in an oxygen depletion and an expansion of the oxygen minimum zone and (2) the TEs released bioaccumulate in the environment and trophic webs, ultimately affecting human health and social economic development.

RESUM

La indústria minera s'encara a un problema de gestió dels residus produïts. Degut als problemes mediambientals que provoca l'emmagatzematge terrestre de les cues mineres, la deposició submarina de les cues (STD) és una opció que ha guanyat interès en els darrers anys. Aquesta pràctica implica el dipòsit dels residus al fons marí mitjançant canonades submergides des de les indústries mineres. Aquestes cues es poden veure afectades geoquímicament per les poblacions microbianes que viuen en el fons marí i que poden tenir una ecofisiologia compatible amb els residus. Aquestes comunitats (per exemple, *Shewanella, Geobacter*) poden bioreduir el ferro fèrric dels òxids i/o hidròxids continguts en els residus miners, alliberant Fe (II) i elements traça (TE) al medi marí.

El principal objectiu d'aquest treball va ser entendre el procés de bioreducció dels òxids i hidròxids de ferro presents en els residus miners i avaluar les conseqüències mediambientals dels dipòsits de residus al fons marí.

Per dur a terme aquest propòsit, es van fer experiments de tipus batch i de columna amb diverses mostres d'òxids i hidròxids de ferro i de residus miners, les quals van reaccionar amb *Shewanella loihica*, un bacteri desassimilatori del ferro capaç de dur a terme la dissolució reductiva del ferro. Es va monitoritzar l'alliberament de Fe(II) i de TEs, es van observar les superfícies dels sòlids reaccionats i es va fer un model geoquímic per quantificar la bioreducció. A més a més, per tal d'entendre millor la influència del ferro en el cicle del nitrogen de l'oceà es van dur a terme uns experiments batch on el ferro bioreduït interaccionava amb nitrit.

Els resultats han demostrat que la *Shewanella loihica* pot bioreduir els òxids i/o hidròxids de ferro continguts en residus miners en condicions semblants a les del fons marí. Aquesta dissolució bioreductiva comporta l'alliberament de Fe(II) i de TEs que poden arribar a ser perjudicials per l'ambient. S'ha deduït que la superfície reactiva dels òxids i/o hidròxids é un factor clau en la bioreducció perquè proveeix Fe(III) per bioreduir i superfície perquè els bacteris transfereixin electrons.. Ara bé, l'adsorció de Fe(II) en la superfície comporta, per una banda, la disminució de la superfície reactiva

i del Fe(III) disponible i, per altra banda, la formació d'una nova fase mineral biogènica que conté Fe^{2+}/Fe^{3+}, és a dir una transformació a magnetita

També s'ha demostrat que el Fe(II) alliberat per la bioreducció pot interferir, amb el cicles biogeoquímic del nitrogen de l'oceà. Així, el Fe(II) bioproduït desencadena l'eliminació del nitrit en el mar. Aquest procés s'ha caracteritzat utilitzant anàlisis químiques i isotòpiques. Les dades isotòpiques han servit per entendre millor els mecanismes que regulen la interacció Fe(II)-nitrogen, i per identificar l'origen de la reducció de nitrit en el medi marí.

A partir dels resultats obtinguts, es dedueix que el dipòsit de residus miners al mar (STD) és un problema mediambiental perquè (1) l'alliberament de Fe(II) pot provocar una fertilització i eutrofització dels llocs on es dipositin els residus amb una disminució de l'oxigen dissolt i una expansió de la zona mínima d'oxigen i (2) l'alliberament d'ETs pot provocar una bioacumulació d'aquests elements a les xarxes tròfiques. Tot plegat afecta no només l'equilibri d'altres cicles biogeoquímics a l'oceà sinó també la salut humana i l'economia de la societat.

LIST OF FIGURES

Figure 1. 1. Variation in concentration of lactate, acetate and total aqueous Fe over time in the bioreductive dissolution experiments with synthetic and commercial iron oxide samples 28

Figure 1. 2. Variation in concentration of lactate, acetate and total aqueous Fe over time in the bioreductive dissolution experiments with field powdered samples. 29

Figure 1. 3. Iron bioreduction coefficients of the iron oxides mediated by *S. loihica* 30

Figure 1. 4. pH and Eh values during the bioreduction experiments with all the minerals reacted. 33

Figure 1. 5. Ferrous iron adsorption isotherm onto ferrihydrite in the marine medium 34

Figure 1. 6. XRD patterns of non-reacted pure ferrihydrite (red) and reacted ferrihydrite after adsorption experiments (black) 35

Figure 2. 1. Trace element content (ppm) of magnetite determined by LA-ICP-MS in this study and from the literature. 55

Figure 2. 2. Evolution of lactate, acetate and dissolved Fe(II) during the experiments. Solid lines represent the trends obtained by model simulations. 57

Figure 2. 3. Elements detected in solution during the iron bioreduction experiments with the magnetite ore samples and the tailings sample. 58

Figure 2. 4. Evolution of dissolved Fe(II) and selected TEs during the experiments. Solid lines represent the model simulations 61

Figure 3. 1. Mine disposal sites in Spain and Chile 73

Figure 3. 2. Schematics that show: a) a column with the five layers of glass beads, sand and tailings sample and b) the experimental setup. 76

Figure 3. 3. Variation of (a) the concentrations of Fe (II), Zn and Mn, and (b) lactate and acetate and (c) pH and (d) Eh as a function of time in the PORT column. 80

Figure 3. 4. Variation in the concentration of trace element as a function of time in the PORT column 81

Figure 3. 5. Variation in the concentrations of Fe, Mn and Zn (a) and trace metals (Pb, V and Ti) (b) as a function of time in the batch experiment with Portman tailings.....82

Figure 3. 6. Variation in the concentrations of (a) Fe, Mn and Zn, (b) lactate and acetate, (c) pH and Eh (d) as a function of time in the CT column....83

Figure 3. 7. TE release as a function of time in the CT column: a) Vanadium, b) Titanium, c) Nickel, d) Cd, e) Copper, f) Lead. 84

Figure 3. 8. Variation in the bioreduction rate (mol s^{-1}) as a function of: a) time and b) Fe(II) concentration (mM) in the PORT column; variation in the bioreduction rate (mol s^{-1}) as a function of: c) time and d) Fe concentration (mM) in the CT column. 87

Figure 4. 1. Fe(II) bio-production experiment describing microbial reductive dissolution of ferrihydrite. 105

Figure 4. 2. Characterization of the solid sample 106

Figure 4. 3. Variation in concentrations of Fe(II) and NO_2^- throughout the experiments (left panels) and nitrite second-order decay fits using Eqs. (EA2.1 and EA2.2 in AP2) 108

Figure 4. 4. Dual N-O isotope plot for the abiotic and biotic nitrite reduction experiments. 113

Figure 4. 5 Correlation between the NO_2^- isotopic composition and the Ln Fe(II) concentration. 115

Figure A1. 1. Trace element content (ppm) of hematite determined by LA-ICP-MS for the C4 sample. 139

Figure A1. 2. Comparison of the TEs content (ppm) of magnetite determined by LA-ICP-MS in C1 and S1 samples and with data from the literature 140

Figure A1. 3. Trace element content (ppm) of magnetite determined by EMPA. 141

Figure A1. 4. (A) Uptake of Fe(II) from solution in an experiment with nonstoichiometric magnetite (Fe^{2+}/Fe^{3+} = 0.33) 147

Figure A1. 5. Evolution of lactate, acetate and dissolved Fe(II) during the experiments. 148

Figure A1. 6. ATR-FTIR spectra of: (a) synthetic magnetite, (b) ferrihydrite used in the experiments and (c, d) solid sample retrieved at the end of the experiments with ferrihydrite. 151

Figure A1. 7. ATR-FTIR spectra of: (a) natural siderite (86.6 wt.% $FeCO_3$), (b) C3, (c, d) CT and (e) C2. 152

Figure A1. 8. Cell viable counts (*aqueous phase*) 153

Figure A2. 1. Fe(II) adsorption onto ferrihydrite (experiment A2). 160

Figure A2. 2. Heterotrophic nitrite reduction mediated by *S.loihica* in the absence of Fe(II) and ferrihydrite. 161

Figure A2. 3. Linear regressions based on Eq. (EA2.2): $A = 1/Fe(II)0 - \alpha NO2 - 0$ and $B = NO2 - 0FeII0 - \alpha X/FeII0NO2 - 0 - X$ 164

Figure A2. 4. Linear correlation between the natural logarithm of the substrate remaining fraction and the determined isotope ratios. 167

LIST OF TABLES

Table 1. 1. Surface area and mineralogical composition (wt.%) of the studied samples. Contractions: Hem (hematite), Gt (goethite), Mag (Magnetite), Fh (ferrihydrite). ..23

Table 1. 2. Microbial bioreduction activity coefficients calculated from measured acetate and ferrous iron concentrations..31

Table 3. 1. Mineralogical composition (wt. %) of the Portman Bay (PORT) and Ensenada Chapaco (CT) tailings used in the experiments. 75

Table 3. 2. Chemical composition of the marine medium..77

Table 4. 1. Initial conditions for the different experiments. 110

Table 4. 2 Average nitrite reduction rates (mM^{-1} d^{-1}), $\varepsilon^{15}N_{NO2}$, $\varepsilon^{18}O_{NO2}$ and $\varepsilon^{18}O/\varepsilon^{15}N$ ratio in the experiments. 112

Table 4. 3 $\varepsilon^{15}N$, $\varepsilon^{18}O$ (in ‰) and $\varepsilon^{18}O/\varepsilon^{15}N$ ratio reported in the literature for the NO_2^- reduction. 118

Table A1. 1. Solid sample, mineralogical composition, deposit type (IOA: Iron Oxide Apatite; IOCG: Iron Oxide Copper Gold) and specific surface area. 133

Table A1. 2. Laser ablation and Q-ICP-MS operation conditions.. 136

Table A1. 3. Stoichiometric coefficients of the reactions with magnetite-bearing samples simulated with PHREEQC.. 144

Table A1. 4. Parameters used for the Monod rate expressions (eqs. 2.1 and 2.3 in chapter 2). 145

Table A1. 5. Results obtained by model simulations with PHREEQC 146

Table A2. 1. Control experiments filled with SSW and Tris-HCl buffer solution. 162

Table A2. 2. Parameters used in Eq. (EA2.2) and calculated half-life values of NO_2^-. 165

TABLE OF CONTENT

LIST OF FIGURES 1

LIST OF TABLES 4

TABLE OF CONTENT 7

INTRODUCTION 11

STATE OF THE ART 11
MOTIVATION 13
OBJECTIVES 13
METHODOLOGY 13
THESIS OUTLINE 15
REFERENCES 16

CHAPTER 1. BIOREDUCTION OF IRON (HYDR)OXIDES: MECHANISMS 19

1.1.INTRODUCTION 20
1.2.MATERIALS AND METHODS 22
  1.2.1. Sample characterization 22
  1.2.2. Bacterial culture 23
  1.2.3. Batch experiments with powdered samples 24
  1.2.4. Chemical analyses 25
  1.2.5. Fe (II)-ferrihydrite adsorption experiments 25
  1.2.6. Experiments with microbial cells and field samples 26
1.3.RESULTS AND DISCUSSION 27
  1.3.1. Bioreductive dissolution of Fe-oxides 27
  1.3.2. Fe(II)-ferrihydrite adsorption 29
  1.3.3. Bacteria and Fe-oxide surfaces 30
  1.3.4. Aqueous chemistry 32
  1.3.5. *Shewanella loihica* and Fe-(hydr)oxide surfaces 36
1.4.CONCLUSIONS 38
1.5.REFERENCES 39

CHAPTER 2. IRON (HYDR)OXIDE BIOREDUCTION PROCESS: MONOD KINETICS AND TRACE ELEMENT RELEASE 45

2.1.INTRODUCTION 45
2.2.MATERIALS AND METHODS 48
  2.2.1. Solid samples 48
  2.2.2. Solid characterization 49
  2.2.3. Batch experiments 49
  2.2.4. Geochemical modelling 51
2.3.RESULTS AND DISCUSSION 53
  2.3.1. Geochemical composition of iron oxides 53
  2.3.2. Magnetite bioreduction experiments 55
  2.3.3. Release of Fe(II) and trace elements to the aqueous phase during magnetite bioreduction 59
2.4.CONCLUSIONS 63
2.5.REFERENCES 64

CHAPTER 3. IRON (HYDR)OXIDE BIOREDUCTION PROCESS: COLUMN EXPERIMENTS 71

3.1.INTRODUCTION 72
3.2.MATERIALS AND METHODS 74
  3.2.1. Tailings characteritzation 74
  3.2.2. Experimental setup 75
  3.2.3. Bacterial culture and marine medium 77
  3.2.4. Chemical analysis 77
3.3.RESULTS AND DISCUSSION 78
  3.3.1. Tailings composition 78
  3.3.2. Aqueous chemistry: Portman tailings 79
  3.3.3. Aqueous chemistry: CT tailings 82
  3.3.4. Comparison between PORT and CT tailings 84
3.4.CONCLUSIONS 88
3.5.REFERENCES 89

CHAPTER 4. IRON BIOREDUCTION AND ITS IMPLICATION WITH NITROGEN CYCLE 95
4.1.INTRODUCTION 96
4.2.MATERIALS AND METHODS 98
4.2.1. Solutions 98
4.2.2. Bacterial culture 99
4.2.3. Ferrihydrite: synthesis and characterization 99
4.2.4. Experimental setup and sampling procedure 100
4.2.5. Isotopic analyses 103
4.3.RESULTS AND DISCUSSION 104
4.3.1. Bioreduction of ferrihydrite 104
4.3.2. NO_2^- reduction coupled with Fe(II) oxidation 107
4.3.3. Biotic (heterotrophic) NO2- reduction by *S. loihica* 111
4.3.4. Isotopic fractionation during abiotic NO_2^-reduction owing to dissolved or solid-bound Fe(II) 111
4.3.5. Use of isotopic tools to distinguish between abiotic and biotic NO2- reduction in the field 114
4.4.CONCLUSIONS 119
4.5.REFERENCES 121
CHAPTER 5. SUMMARY AND CONCLUSIONS 128
APPENDIX 1 133
APPENDIX 2 159
APPENDIX 3 169

INTRODUCTION

STATE OF THE ART

Mining industry faces environmental problems concerning waste management. High-grade mineral deposits worldwide are lowering, inducing the mining sector to find lower-grade mineral deposits. Exploitation of low-grade ores with low element/waste ratios may increase the production of mine waste in the near future. Negative environmental impacts related to mine wastes are widely known. For instance, a major environmental impact is due to acid mine drainage (AMD) [1], which is caused by the oxidative dissolution of pyrite in exploited metal sulfide ores, mine tailings dams and open-pit mines.

Given the environmental issues associated with storage of mine wastes on land, one disposal option that has gained attraction is submarine tailings disposal (STD)) [2]. This practice involves disposal of mine wastes under sea water at depths that vary between 25 m and 800 m through submarine pipelines. STD could therefore prevent AMD on land. Moreover, the advantages of STD with respect to conventional land storage are better geochemical and physical stability of the wastes, low oxygen-reducing conditions, avoidable collapse incidents (important in countries with limited usable land (i.e., in Chile and Norway)) and non-maintenance requirements.

Although STD appears to be plausible from a geochemical point of view, the reality in nature is more complex. Marine contamination associated with continuous STD has been reported elsewhere (e.g., Chañaral Bay (Atacama region, Chile) in northern coast of Chile [19, 20] and Portman Bay in the south-east coast of Spain [1]). To date, however, little is known about the STD environmental impacts on marine systems (e.g., hyper-sedimentation, seabed toxicity, seawater turbidity).

It should be borne in mind that discharges of mine wastes may be geochemically affected by microbial communities that live in the seabed, whose ecophysiology is compatible with the mine tailings. This is the case of iron-reducing bacteria (Dissimilatory Iron Reducing Bacteria DIRB) [3]. DIRBs are facultative anaerobic bacteria that can degrade organic matter by reducing ferric iron (Fe(III)), which acts as terminal acceptor (TEA). This metabolism is considered one of the most archaic forms of prokaryotic metabolism [4]. These bacteria are able to reduce structural Fe(III) from the iron (hydr)oxides that are present in mine wastes under marine conditions. This process (i.e., reductive dissolution) can lead to severe ecological impacts on marine ecosystems. For instance, it induces the release of trace elements (i.e., metal(loids): Cu, Ni, Zn, Cd, Pb, V, Cr Se and As) from the disposal sites into the environment. These elements are environmentally toxic as they affect fish and shellfish and bioaccumulate in the food web, eventually reaching humans [5]. In addition, STD results in stress for benthic organisms and for seafloor habitats, reducing the abundance and biodiversity of the species.

Iron is one of the most common elements on Earth but is biologically unavailable [6]. Iron redox states (Fe^0, Fe^{2+} and Fe^{3+}) can persist in solids under aerobic conditions, although ferric iron (Fe^{3+}) is the thermodynamically stable one. This persistence is due to the poor solubility of iron phases at neutral pH and in aerobic environments. In addition, iron is one of the most necessary trace elements for terrestrial and marine organisms, since it is necessary to form metalloenzymes used in many essential processes in life, such as photosynthesis. Thus, the low bioavailability of iron makes it to be an element that regulates terrestrial and marine ecosystems. Furthermore, iron has played a major role in modulating atmospheric CO_2 concentrations in the geological past (e.g., the iron hypothesis) [7].

Finally, iron can interfere with the ocean’s nitrogen cycle. The iron and nitrogen cycles are related in anaerobic environments, where bioreduction of iron (hydr)oxides may induce nitrite reduction and Fe(II) oxidation [8]. It is necessary to understand the nitrite-Fe(II) interaction under marine conditions to assess the environmental impact of STD on coastal marine environments.

MOTIVATION

The environmental hazards associated with STD [2 and the references therein] could be minimized, i.e. predicted and prevented, if mineralogical and biogeochemical data were available at the decision-making time. It is therefore essential to carry out a mineralogical and biogeochemical study of the processes occurring in STD operations to predict the geochemical behavior of the tailings for a comprehensive assessment of the environmental impact on the marine environment.

OBJECTIVES

The aim of the present thesis is to study the bioreduction of iron (hydr)oxides contained in mine tailings under marine conditions in an attempt to evaluate the impact on the marine environment of STD.

The specific objectives are:

- To elucidate the mechanisms by which *Shewanella loihica* reduces Fe(III) from iron (hydr)oxides under marine conditions.
- To study the bioreduction kinetics and to quantify the release of trace elements.
- To evaluate the effect of Fe-oxide bioreduction on aqueous nitrogen under marine conditions.

METHODOLOGY

To accomplish the objectives, the research in this PhD study was carried out by conducting laboratory batch and column experiments under conditions similar to those in ongoing STD sites (e.g. Ensenada Chapaco in Chile). Iron (hydr)oxides from distinct mine ores and two tailings samples were used. A geochemical modeling was performed to reproduce the experimental data employing the PHREEQC code. The experimental and modeling results allowed me to understand the overall bioreduction reaction and to evaluate the extent of the release of bioreduced Fe(III) and associated trace elements.

In Chapter 1, Fe(III) (hydr)oxides (synthetic ferrihydrite, commercial goethite, magnetite and hematite and field specimens with different contents of iron oxides and other minerals) were reacted in batch experiments in the presence of *Shewanella loihica* strain PV-4, whose ecophysiology makes it optimal for Fe(III)-bioreduction under marine conditions. Two different experiments were performed to elucidate the kinetics of Fe(III)-bioreduction and to examine the bacteria-mineral surface interaction.

In Chapter 2, the batch experiments were performed using a number of magnetite ore samples from Chilean and Swedish mines and the mine tailings sample from the iron oxide pellet plant at Ensenada Chapaco (Huasco) in Chile. Chemical analysis were used to investigate the kinetics of iron mineral bioreduction under marine conditions and the potential release of trace elements. The microbial reduction of Fe(III) was geochemically modeled on the basis of Monod kinetics using the PHREEQC code.

In Chapter 3, two column experiments and one batch experiment were performed using the mine tailings samples from two STD locations (Portman Bay (Spain) and Ensenada Chapaco (Chile). Bioreduction and trace metal release in the columns and batch experiments were monitored over time and compared.

In Chapter 4, biotic and abiotic NO_2^- reduction experiments using synthetic and bio-produced Fe(II) were performed in an anoxic microcosms. The chemical and isotopic analyses shed light into the kinetics of NO_2^- reduction in marine environments. Moreover, the isotopic analysis could be useful to distinguish between abiotic and biotic (heterotrophic) NO_2^- reduction.

THESIS OUTLINE

This thesis consists of five chapters after the introductory one. In the first Chapter, I describe the mechanisms for bioreduction of iron (hydr)oxides that are present in mine tailings under marine conditions. The bioreduction kinetics and the release of metals are accounted for in the second and third Chapters. A kinetic model to quantify the biogeochemical process observed in the batch experiments is presented in Chapter 2. In the fourth Chapter, I address the influence of bioreduced Fe(III) on nitrite stability. Chapter 5 summarizes the main contributions of this thesis.

A first article with the study presented in chapter one was published in Marine Environmental Research: Benaiges-Fernandez, R., Palau, J., Offeddu, F. G., Cama, J., Urmeneta, J., Soler, J. M., & Dold, B. (2019). Dissimilatory bioreduction of iron (III) oxides by *Shewanella loihica* under marine sediment conditions. *Marine environmental research*, *151*, 104782. See Appendix 3.

A second article with the study presented in chapter two was submitted for publication in Journal of Hazardous Materials: Palau, J., Benaiges-Fernandez, R., Offeddu, F. G., Urmeneta, J., Soler, J. M., Cama, J., & Dold, B. (2020).

A third article with the study presented in chapter three is about to be submitted in Applied Geochemistry: Benaiges-Fernandez, R., , Cama, J., Urmeneta, J., Soler, J. M. (2020).

A fourth article with the study presented in chapter four was published in Chemosphere: Benaiges-Fernandez R., Offeddu G. F., Margalef-Marti R., Palau J., Urmeneta J., Carrey R., Otero N., & Cama J. (2020). Geochemical and isotopic study of abiotic nitrite reduction coupled to biologically produced Fe (II) oxidation in marine environments. *Chemosphere, 260,* 127554. See Appendix 3.

REFERENCES

1. Johnson, D.B. and K.B.J.S.o.t.t.e. Hallberg, *Acid mine drainage remediation options: a review.* 2005. **338**(1-2): p. 3-14.

2. Dold, B.J.M., *Submarine tailings disposal (STD)—A review.* 2014. **4**(3): p. 642-666.

3. Lovley, D.R., *Dissimilatory Fe (III) and Mn (IV) reduction.* Microbiology and Molecular Biology Reviews, 1991. **55**(2): p. 259-287.

4. Weber, K.A., L.A. Achenbach, and J.D.J.N.R.M. Coates, *Microorganisms pumping iron: anaerobic microbial iron oxidation and reduction.* 2006. **4**(10): p. 752-764.

5. Johnson, D.B.J.F.m.e., *Biodiversity and ecology of acidophilic microorganisms.* 1998. **27**(4): p. 307-317.

6. Raiswell, R. and D.E.J.G.p. Canfield, *The iron biogeochemical cycle past and present.* 2012. **1**(1): p. 1-2.

7. Martin, J.H.J.P., *Glacial-interglacial CO2 change: The iron hypothesis.* 1990. **5**(1): p. 1-13.

8. Kampschreur, M.J., et al., *Reduced iron induced nitric oxide and nitrous oxide emission.* Water Research, 2011. **45**(18): p. 5945-5952.

CHAPTER 1.

BIOREDUCTION OF IRON (HYDR)OXIDES:

MECHANISMS

This chapter presents the study of bioreduction mechanisms of iron oxides under coastal marine conditions. *Shewanella* is a genus of marine bacteria capable of dissimilatory iron reduction (DIR). In the context of deep-sea mining activities or submarine mine tailings disposal, dissimilatory iron reducing bacteria may play an important role in biogeochemical reactions concerning iron oxides placed on the sea bed. In this study, batch experiments were performed to evaluate the capacity of *Shewanella loihica* PV-4 to bioreduce different iron oxides (ferrihydrite, magnetite, goethite and hematite) under conditions similar to those in anaerobic sea sediments. Results showed that bioreduction of structural Fe(III) via oxidation of labile organic matter occurred in all these iron oxides. Based on the aqueous Fe (II) released, derived Fe(II)/acetate ratios and bioreduction coefficients seem to be only up to about 4% of the theoretical ones, considering the ideal stoichiometry of the reaction. A loss of aqueous Fe (II) was caused by adsorption and mineral transformation processes. Scanning electron microscope images showed that *Shewanella lohica* was attached to the Fe(III)-oxide surfaces during bioreduction. Our findings suggest that DIR of Fe(III) oxides from mine waste placed in marine environments could result in adverse ecological impacts such as liberation of trace metals in the environment.

1.1. INTRODUCTION

Iron is one of the most important elements on Earth due to its involvement in key biological processes, such as photosynthesis. However, the low solubility of Fe makes it not much bioavailable in most environments [1]. Iron is one of the controlling elements in many ecosystems, especially in marine environments [2, 3]. Some studies have shown that iron stimulates the growth of phytoplankton in high-nitrate, low-chlorophyll waters, which account for 25% of the ocean [4]. Furthermore, iron participates in important biological processes such as atmospheric carbon dioxide consumption, dimethyl sulfide (DMS) production and organic matter (OM) degradation in sediments [5]. Bioavailability of iron in the sea also played a crucial role in the modulation of carbon dioxide concentration in the atmosphere in the geological past [6].

A marine sediment is an aphotic nutrient-rich and low-production zone where most microorganisms are heterotrophic [7]. In anoxic reduced zones of the sediment, there are OM-degrading anaerobic microorganisms that use inorganic compounds other than oxygen as terminal electron acceptors (TEAs) for the electron transport respiratory chain [8]. Dissimilatory iron reduction mediated by microorganisms uses Fe(III) as TEA to produce Fe(II) species. This process is coupled to the degradation of simple OM and is carried out by different genera of bacteria, like *Geobacter* or *Shewanella [9]*. In marine sediments, metabolic products of degradation serve as electron donors for the terminal oxidizing bacteria, which use inorganic TEAs for a complete oxidation of organic matter. Moreover, iron reduction besides sulfate reductors are the most important terminal oxidation processes in the upper anoxic zone [10]. For instance, in artic marine sediments lactate (among acetate, propionate and isobutyrate) is degraded in the marine sediment by iron and sulfate reducers [11].

The *Shewanella* genus is well known for itspresence in marine sediments and for its metabolic capacity [12]. *Shewanella* can use oxygen, nitrate and heavy metals as TEAs. Some strains may even degrade recalcitrant organic compounds, such as chlorinated solvents, providing the genus with the potential to be applied in bioremediation studies [13]. *Shewanella loihica* is a species from the genus *Shewanella* isolated from a submarine volcano in Loihi, Hawaii [14]. The metabolic versatility and ubiquitous presence in the marine environment make *Shewanella loihica* a suitable candidate for bioreduction studies. Earlier studies on the capacity and mechanisms of *Shewanella* to bioreduce ferric iron in fresh water have shown that (i) it is able to reduce not only soluble Fe (III) compounds but also (Fe) (III)-bearing minerals such as magnetite (Fe_3O_4) through polysaccharide attachment [15] and that (ii) biotic iron reduction coupled to OM degradation requires a direct contact between the microorganisms and the poorly soluble mineral surface [16]. However, bioreduction of magnetite and other iron oxides and hydroxides (ferrihydrite, goethite and hematite) under marine conditions has not yet been studied.

The fate of iron oxides in seafloor sediments has a major interest for potential sea water contamination caused by deep-sea mining activities or marine disposal of mine tailings, which were practices widely spread worldwide [17] although currently banned in most of the countries [18]. For instance, marine contamination associated with continuous tailings disposal has been reported in. Chañaral Bay in northern coast of Chile [19, 20] and Portman Bay in the south-east coast of Spain [21]. In mine tailings originated from sulfide-rich ores the contained Fe(III)-oxides incorporate Mn, Al, Cr, Co, Ni, Zn, V, Pb and As [22, 23]. Valence II and III metal cations can be adsorbed on the iron oxides or isomorphously substitute iron in the crystalline oxide structure [24]. Offshore disposal of these mine tailings may result in adverse ecological impacts as bioreductive dissolution of Fe(III) oxides releases aqueous Fe(II) together with trace metals and metalloids co-precipitated or structurally incorporated in Fe (III) oxides [25]. Thus, an undesired bioaccumulation of metals and metalloids in sea sediments, in secondary plumes and in the water column and an increase in trophic transfer of metals could occur [26, 27]. A better understanding of the interaction between Fe(III) oxides and microorganisms capable to bioreduce Fe(III) sheds new light on the bioavailability of iron in the ocean and on potential environmental consequences of sea mining activities and marine disposal of mine tailings.

To this end, Fe(III) oxides (synthetic ferrihydrite, commercial goethite, magnetite and hematite and field specimens with different contents of iron oxides and other minerals) were reacted in the laboratory in the presence of *Shewanella loihica* strain PV-4, whose ecophysiology makes it optimal for Fe(III)-bioreduction under marine sediment conditions. Two different experiments were performed to elucidate the kinetics of Fe(III) bioreduction and to examine the bacteria-mineral surface interaction.

1.2. MATERIALS AND METHODS

1.2.1. Sample characterization

The iron oxide samples used in this chapter have three different sources: three samples were commercial powders of magnetite, hematite and goethite purchased from Sigma Aldrich; one sample of 2L ferrihydrite was synthesized in the laboratory following the procedure described by Cornel and Shwertmann [28]; and three samples were field specimens with different contents of magnetite (V1 from Distrito Algarrobo, Chile, TB from Lago Sur, Chile, and M1 from Malmberget, Sweden). Sample V1 also contained hematite. Powder X-ray diffraction (XRD) analysis and Rietveld refinement [29], using a Bruker D8 A25 Advance X-ray diffractometer θ- θ with CuKα1 radiation, showed that the commercial and synthesized samples were composed of the respective iron oxides and no accessory minerals were identified. Rietveld analysis confirmed that no impurities were present in the samples. As for the field samples, magnetite was present in all of them (ranging from 19 to 89 wt.% for V1 and M1, respectively), hematite was only present in V1 (40 wt.%) and goethite was not detected (Table 1.1). Other minerals identified were silicates (hornblende, and Fe-actinolite) and phosphates (hydroxyapatite) (Table 1.1).

The size fraction of the commercial powders was about 5 μm. Synthesized 2L ferrihydrite was ground using an agate mortar and pestle and sieved to a size fraction of 5 - 60 μm. Fragments of field samples were similarly ground and sieved to a size fraction of 60 - 100 μm. These powdered samples were used in batch experiments to study the Fe(III) bioreduction reaction. The specific surface area of all these samples was determined by the Brunauer-Emmett-Teller (BET) method [30] using a Gemini 2370 surface area analyzer and 5-point N_2 adsorption isotherms. Sample degassing with nitrogen lasted for 2 h at 137 °C. Data uncertainty was around 10%. Synthesized ferrihydrite showed the largest value (181 m^2 g^{-1}) and M1 and TB the lowest ones (0.6 and 0.2 m^2 g^{-1}, respectively; Table 1.2).

Table 1. 1. Surface area and mineralogical composition (wt.%) of the studied samples. Contractions: Hem (hematite), Gt (goethite), Mag (Magnetite), Fh (ferrihydrite).

Sample	**Hem**	**Gt**	**Mag**	**Fh**	**V1**	**M1**	**TB**
hydroxylapatite ($Ca_5(PO_4)_3(OH)$)						16%	11%
magnetite ($Fe^{2+}Fe^{3+}_2O_4$)			100%		19%	79%	89%
horblende ($Ca_2(Mg, Fe, Al)_5 (Al, Si)_8O_{22}(OH)_2$)					41%		
hematite (Fe_2O_3, α-Fe_2O_3)	100%				40%		
ferro-actinolyte ($Ca_2(Mg_{2.5-0.0}Fe^{2+}_{2.5-5.0})Si_8O_{22}(OH)_2$)						5%	
goethite (α-$FeO(OH)$)		100%					
ferrihydrite($(Fe^{3+})_2O_3{\cdot}0.5H_2O$)				100%			

1.2.2. Bacterial culture

Shewanella loihica strain PV-4 was obtained from the German Collection of Microorganisms and Cell Cultures (DSMZ 17748). To obtain a bacterial suspension for the starting inoculum, cells were cultivated in M1 medium [14] supplemented with 10 mM of sodium lactate as electron donor and carbon source and 10 mM of Fe(III) citrate as electron acceptor. Cultures were incubated anaerobically for 24 h at 30 ºC and then harvested by centrifugation (5000 rpm for 10 min). The pellet was re-suspended in synthetic seawater prepared previously following the standard protocol D1141-98 (ATSM International). Centrifugation and pellet re-suspension were repeated three times as a washing step.

A medium simulating seawater (hereafter referred to as marine medium) was developed for the experiments. A basal medium of synthetic seawater (ASTM D1141-98) was amended with sodium lactate (10 mM) as an electron donor and carbon source, ammonium chloride (1.87 mM) as a source of nitrogen, and TRIS-HCl (10 mM) as a pH-buffer. The pH of the medium was adjusted to 8.2 with 0.1 N NaOH solution. The final medium was sterilized by autoclave (121 °C for 20 min).

1.2.3. Batch experiments with powdered samples

In all batch experiments, 0.25 ± 0.01 g of powdered sample were placed in 25 mL glass vials capped with Teflon plugs and then sterilized by autoclave (121 °C for 20 min). Previous studies [31, 32] showed a thermal transformation of ferrihydrite to hematite could occur. A test performed with ferrihydrite showed that XRD analyses after the sterilization revealed no mineral changes in this stage.

The vials were filled with 25 mL of marine medium, keeping a 1% solid/liquid ratio (g/mL), and inoculated with *Shewanella loihica* to an approximate final number of $1 \cdot 10^7$ colony-forming units (cfu) mL^{-1}, measured by agar culture (LB). The vials were sealed with screw caps, leaving a minimal head space (small air bubble) to prevent overpressure, and statically immersed in a thermostatic water bath at 10 ± 1 °C in the dark. These conditions with the use of the marine medium mimicked the suboxic zone in marine sediments [33, 34]. Abiotic controls without inoculum of *Shewanella loihica* were also prepared under the same conditions as biotic experiments.

For each solid sample, a single-point batch experiment was carried out. Five vials were prepared as replicates, and each one was sacrificed at different time spans (13, 27, 47, 70 and 111 days). Sampling was performed in a glove box with N_2 atmosphere to maintain the anoxic conditions. The vials were shaken just before sampling and then the medium from the vial was totally recovered, sampled and filtered using a sterile syringe and syringe filters (0.22 μm pore size). Sample aliquots were used for pH/Eh measurements and for chemical analyses of cations and anions. To evaluate the carbon and energy source consumption, lactate and acetate, being the latter the oxidation end product under anaerobic conditions, were measured. For ion analysis a volume of 10 mL was preserved at $pH < 2$ by adding 100 μL of 60% (v/v) HNO_3 solution. For Fe(II)/Fe(III) measurements by Phenanthroline colorimetry [35], an additional volume of 10 mL was preserved with the addition of 100 μL of 6 M HCl solution. Thereafter, all samples were stored at 4 °C in the dark until analysis.

1.2.4. Chemical analyses

Measurements of pH (± 0.02 pH units) and Eh (± 10 mV) were performed in the glove box using pH and Eh electrodes (Crison and SenTix ORP, Ag/AgCl, WTW, respectively). Oxidation-reduction potential readings were converted to standard Eh values by correcting for the electrode potential of the reference hydrogen electrode. Total iron was analyzed by Inductively Coupled Plasma Mass Spectrometry (ICP-MS, Perkin- Elmer 3000). Owing to the high dissolved iron concentrations in the experiments with ferrihydrite, iron measurements were performed using ICP–Optical Emission Spectroscopy (ICP-OES). The uncertainty of the ICP-MS (and ICP-OES) measurements was better than ± 5%. Total iron measured was checked to be Fe (II) with a modified protocol of the Phenanthroline method [35]. Lactate and acetate concentrations were determined by high performance liquid chromatography (HPLC). The equipment used consisted of a Waters 600 HPLC pump controller equipped with an Aminex HPX-87H column (300 x 7.8 mm), BioRad, and a Waters 717 plus autoinjector. Triplicates were performed for iron, lactate and acetate measurements.

1.2.5. Fe (II)-ferrihydrite adsorption experiments

Fe(II) adsorption on powdered ferrihydrite in marine medium (0.5 g of ferrihydrite and 50 mL of solution, 1% w/v) was determined in gently mixed batch experiments at room temperature (23 ± 2 ^{0}C). Different amounts of $FeCl_2$ were added to distinct vials, from 0.4 to 40 mM, in order to get a wide range of initial Fe(II) aqueous concentration in the experiment. Samples were collected after reaching equilibrium at 24 h [36] to measure total and ferrous iron by the phenanthroline method. At the end of the experiments the solid fractions were retrieved, freeze dried and preserved under nitrogen atmosphere until analysis. Subsequently, XRD-Rietveld analyses and measurement of BET specific surface areas were performed. The concentration of adsorbed Fe(II) was determined by subtracting the aqueous ferrous iron concentration after equilibration from the initial concentration according to (eq. 1.1):

$$C_{Fe-ads} = (C_{Fe-i} - C_{Fe-eq}) \cdot \frac{V}{M} \qquad (1.1)$$

where $C_{Fe\text{-}ads}$ is the amount of adsorbed iron per gram of ferrihydrite, $C_{Fe\text{-}i}$ and $C_{Fe\text{-}eq}$ are the initial and equilibrium aqueous concentrations of Fe(II), respectively, V is the volume of solution and M is the mass of ferrihydrite.

1.2.6. Experiments with microbial cells and field samples

Surface mineral-bacteria interaction was investigated by scanning electron microscope (SEM). Fragments of field samples (M1 and TB) were cut down to small rectangular pieces (surface of $\approx$ 10 mm^2 and $\approx$ 3 mm thick) in order to fit into sample holders used for the critical point drying technique. These pieces were used to study the interaction between *Shewanella* and the surface of the iron oxides. Top surfaces were polished by conventional metallographic polishing to improve the observation of the surface mineral-bacteria interaction by SEM. The M1 and TB pieces were placed in 200 mL bottles filled with marine medium (synthetic sea water) without head space and incubated with $1\cdot10^7$ cfu mL^{-1} of *Shewanella loihica.* Experiments were conducted in the N_2-atmosphere glove box in the dark for 115 days at 25 ^{0}C.

At the end of the experiments, the pieces incubated with *Shewanella* were retrieved and treated for 2 h with a glutaraldehyde 2.5% w/v in 0.1 M phosphate buffered saline (PBS) cell- fixation solution. Several washes with PBS (10 min each) were done, and post-fixation of the mineral pieces was carried out using 1% osmium tetraoxide and 0.8% potassium ferricyanide in 0.1 M PBS for up to 2 h in darkness. To evaluate potential effects of the dehydration process on the bacteria structure, two different dehydration methods were carried out. In one dehydration method the critical point drying technique was performed by replacing water in the samples with increasing concentrations of ethanol (50-100%) [37]. In the other method sample dehydration was performed using a hexamethyldisilazane (HMDS) solution [38]. Thereafter, all samples were coated with carbon before SEM observation (Hitachi H-4100FE instrument under a 15–20 kV potential in a high vacuum) using the backscattered electron detector (BSD) in Field Emission (FE) and an energy-dispersive spectrometer (EDS).

1.3. RESULTS AND DISCUSSION

1.3.1. Bioreductive dissolution of Fe-oxides

Dissolution of the iron oxide minerals and production of aqueous Fe(II) did not take place in the abiotic control experiments. In contrast, bioreductive dissolution occurred in all experiments inoculated by *Shewanella loihica*. Figure 1.1 shows the variation of total aqueous iron concentration over time for the experiments with synthetic and commercial samples. Measured total aqueous iron in all the experiments was confirmed to be Fe (II) by the phenanthroline method. Aqueous iron concentration increased over time in the experiment with hematite (Fig. 1.1a), initially increased and then decreased in the case of goethite (Fig. 1.1b) and increased and levelled off in the experiments with magnetite and ferrihydrite (Fig. 1.1c,d). The highest Fe(II) concentration (1.3 mM) was reached in the ferrihydrite experiment. In all experiments, the change in aqueous ferrous iron concentration was accompanied by consumption of lactate and production of acetate. Only in the case of ferrihydrite experiment lactate was totally consumed. For the experiments prepared with field samples, reductive dissolution of the iron oxides showed similar trends (Fig. 1.2), in which iron increased in different steps (Fig. 1.2a,c) or gradually (Fig. 1.2b). The concentrations of released iron were lower than those of the synthetic and commercial samples (< 0.03 mM). As observed for the experiments with synthetic and commercial samples, consumption of lactate and production of acetate accompanied the ferrous iron release.

The measured ferrous iron and acetate concentrations throughout the experiments were used to estimate initial bioreduction coefficients based on the initial release of iron and acetate associated with the microbial activity. These coefficients were calculated by linear regression of the first two sampling points for ferrihydrite and the first three ones for the other oxide experiments using the following expressions (eq 1.2, 1.3):

$$k_{biored-Fe} = \frac{c_{Fe(II)} \cdot V}{\Delta t \cdot M} \qquad (1.2) \qquad k_{biored-Ac} = \frac{c_{acetate} \cdot V}{\Delta t \cdot M} \qquad (1.3)$$

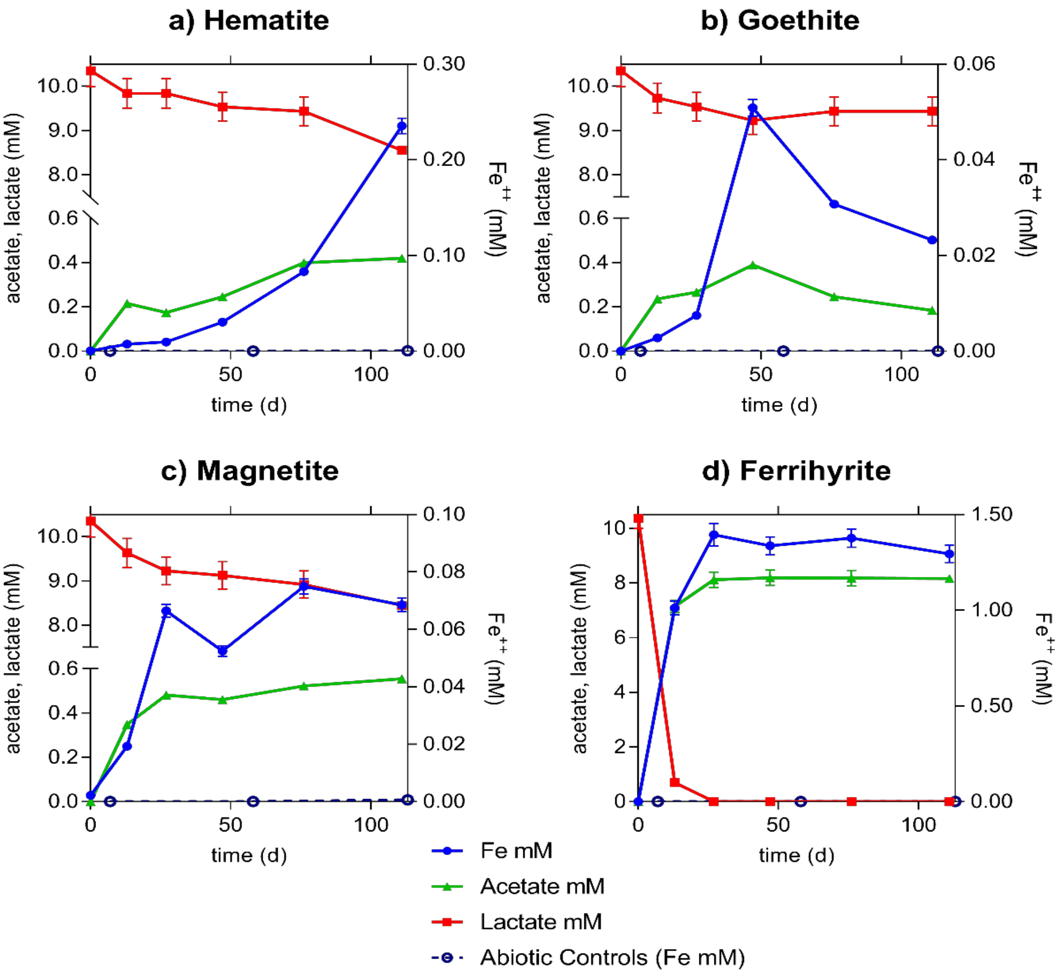

Figure 1. 1. Variation in concentration of lactate, acetate and total aqueous Fe over time in the bioreductive dissolution experiments with synthetic and commercial iron oxide samples: a. Hematite , b. Goethite , c. Magnetite , d. Ferryhydrite . Key: (□) Lactate; (▲) Acetate; (●) Total dissolved iron and (o) Abiotic controls. Error bars correspond to the analytical uncertainty (SD).

where $C_{Fe(II)}$ and $C_{acetate}$ are the measured iron and acetate concentrations (μM), V is the solution volume (L), M is the Fe(III)-oxide mass (g) and t is time (d). Linear regressions showed R^2 values between 0.8 and 0.99. The values of the iron and acetate bioreduction coefficients are listed in Table 1.2. Figure 1.3a shows that the bioreduction coefficient (μmol g_{oxide}^{-1} d^{-1}) for the ferrihydrite experiment is much larger than those of the other samples. However, when the coefficients are normalized with the specific BET surface area (μmol m^{-2} d^{-1}) the coefficients of magnetite are higher (Fig. 1.3b).

In all experiments, pH slightly decreased from 8.2 to an average pH of 7.8 (Fig. 1.4) whereas Eh significantly decreased from 300 mV to an average value of 18.5 mV (Fig. 1.4).

1.3.2. Fe(II)-ferrihydrite adsorption

Due to the high specific surface area of ferrihydrite (181 m^2 g^{-1}) compared to the other iron oxides investigated (Table 1.1), this phase was used to evaluate Fe(II) adsorption on Fe(III)-oxides in the marine medium. Figure 1.5 shows the measured adsorption of Fe(II) on powdered ferrihydrite. The amount of adsorbed Fe (II) increased with Fe (II) aqueous concentration, exceeding the theoretical adsorption capacity of ferryhydrite (0.6 mmol g^{-1}) [39]. The XRD patterns and Rietveld semi-quantitave analysis of the retrieved ferrihydrite allowed us to elucidate the mineralogical change at the end of the experiment and showed the presence of both ferrihydrite (≈10 wt.%) and magnetite (≈ 90 wt.%) (Fig. 1.5).

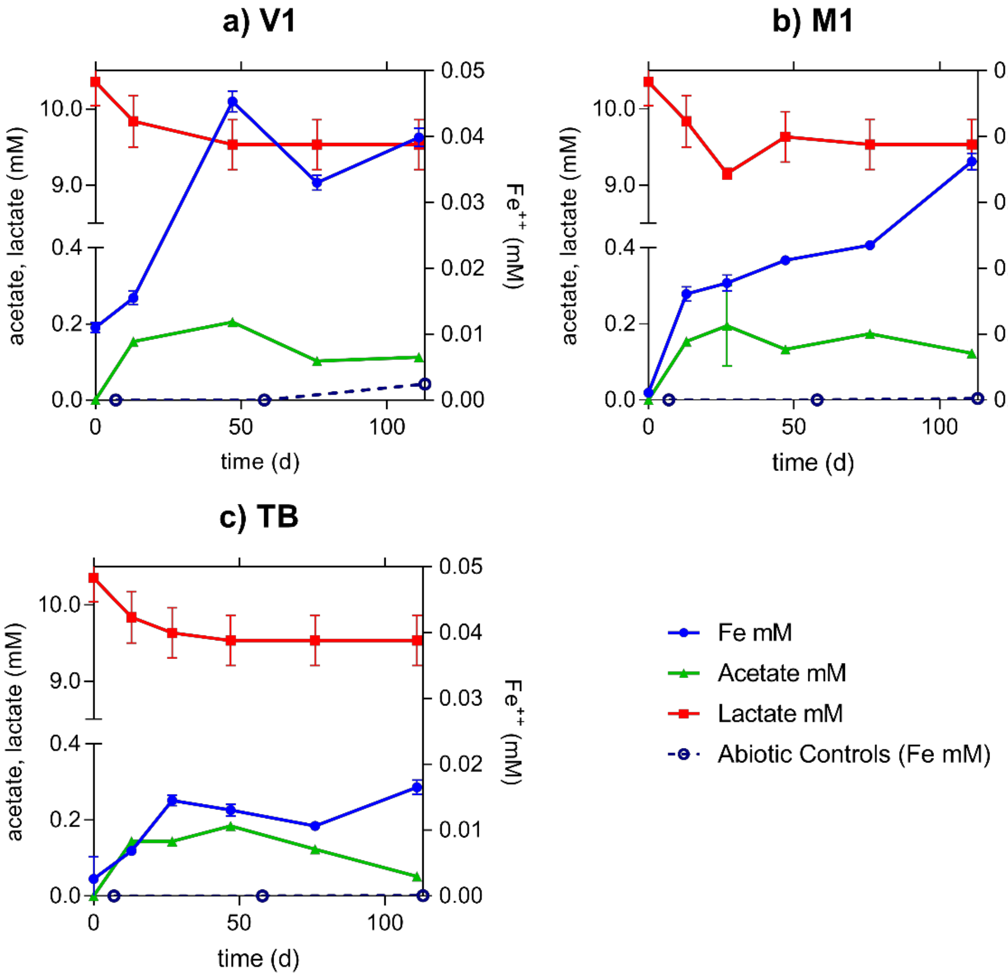

Figure 1. 2. Variation in concentration of lactate, acetate and total aqueous Fe over time in the bioreductive dissolution experiments with field powdered samples. a. Sample V1 (Distrito Algarrobo, Chile); b. Sample M1 (Malmberget, Sweden); c. Sample TB (Lago Sur, Chile). Key: (□)

Lactate; (▲) Acetate; (●) Total dissolved iron and (o) Abiotic controls. Error bars correspond to the analytical uncertainty (SD).

1.3.3. Bacteria and Fe-oxide surfaces

Independently of the dehydration technique used to preserve the bacteria structure, SEM images of the reacted field samples showed the presence of bacteria (*S. loihica*) attached on the iron-oxide surfaces (Fig. 1.6). Bacteria cells colonized the iron-oxide surfaces, either as individual cells or forming clusters. Most of the cells were attached preferably on the iron-oxide surfaces rather than on the surfaces of the other minerals present in the field samples (Fig. 1.6a). Extracellular structures by *S. loihica* have been observed suggesting that bacteria connect with the mineral surface and with other cells (Fig. 1.6b,c).

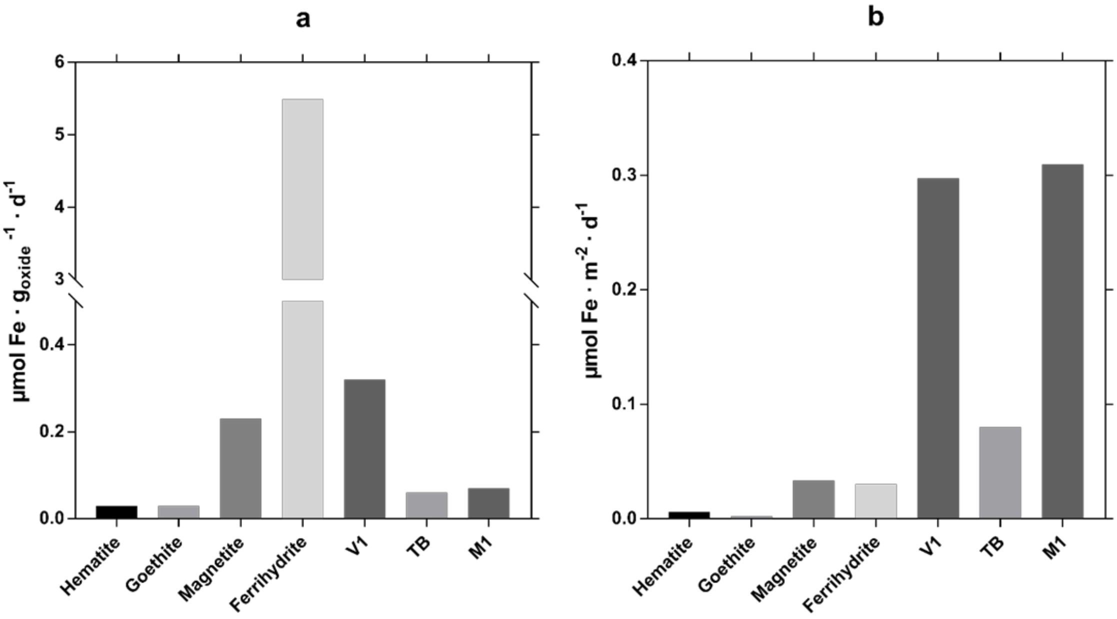

Figure 1. 3. Iron bioreduction coefficients of the iron oxides mediated by *S. loihica*: a) values normalized to mass and b) normalized to surface area.

Table 1. 2. Microbial bioreduction activity coefficients calculated from measured acetate and ferrous iron concentrations.

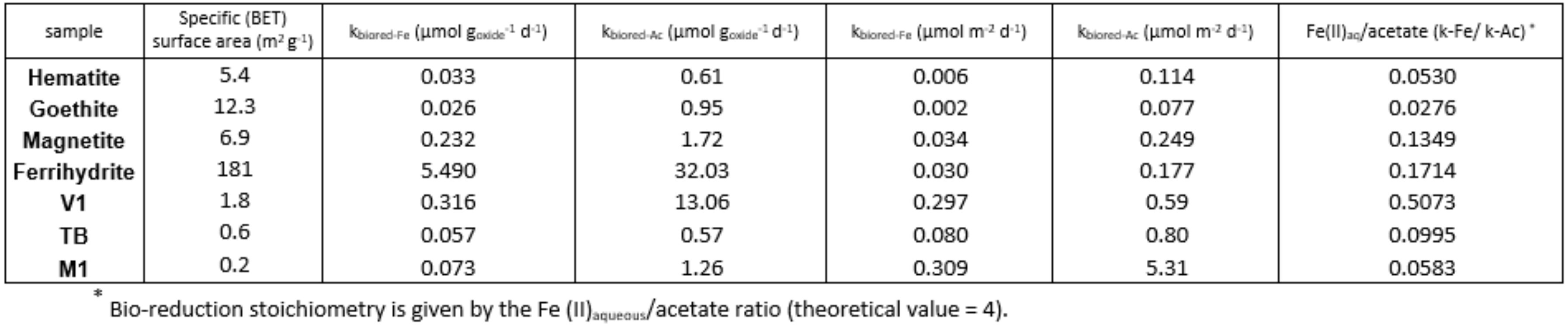

sample	Specific (BET) surface area ($m^2\ g^{-1}$)	$k_{biored-Fe}$ (µmol $g_{oxide}^{-1}\ d^{-1}$)	$k_{biored-Ac}$ (µmol $g_{oxide}^{-1}\ d^{-1}$)	$k_{biored-Fe}$ (µmol $m^{-2}\ d^{-1}$)	$k_{biored-Ac}$ (µmol $m^{-2}\ d^{-1}$)	$Fe(II)_{aq}$/acetate (k-Fe/ k-Ac) *
Hematite	5.4	0.033	0.61	0.006	0.114	0.0530
Goethite	12.3	0.026	0.95	0.002	0.077	0.0276
Magnetite	6.9	0.232	1.72	0.034	0.249	0.1349
Ferrihydrite	181	5.490	32.03	0.030	0.177	0.1714
V1	1.8	0.316	13.06	0.297	0.59	0.5073
TB	0.6	0.057	0.57	0.080	0.80	0.0995
M1	0.2	0.073	1.26	0.309	5.31	0.0583

* Bio-reduction stoichiometry is given by the Fe $(II)_{aqueous}$/acetate ratio (theoretical value = 4).

1.3.4. Aqueous chemistry

The capacity of *Shewanella* to reduce soluble (e.g. iron citrate) or structural (e.g. biogenic magnetite) ferric iron has been studied [40], but its capacity to reduce magnetite and other iron-oxide minerals under marine conditions remained unknown. Our study demonstrates that *S. loihica* was able to bioreduce not only magnetite, but also hematite, goethite and ferrihydrite in conditions similar to those found in anoxic marine environments, such as in seafloor sediments and in offshore mine-tailings disposal sites [27]. It appeared that *S. loihica* used the structural ferric iron of the iron oxides as an electron acceptor in the respiratory chain [16]. In the experiments, a simultaneous consumption of light organic matter (lactate) to produce acetate was observed along with an increase in aqueous Fe(II). Production of acetate was attributed to the anaerobic metabolism of the bacteria during ferric iron reduction. This finding is in agreement with previous studies showing that the metabolism of *S. loihica* was sustained by the production of acetate from lactate, which acts as electron donor [41, 42].

Bioreduction may be expressed in a simple form as [8] (eq 1.4):

$$\text{Lactate}^- + 4Fe^{3+} + 2H_2O \rightarrow \text{acetate}^- + HCO_3^- + 4Fe^{2+} + 5H^+ \qquad (1.4)$$

where one and four moles of acetate and ferrous iron are respectively produced (i.e., Fe(II)/acetate ratio = 4). Experiments with high lactate consumption and acetate formation correlated well with those having high aqueous ferrous iron concentration. In the ferrihydrite experiment, however, bioreduction was halted by total exhaustion of lactate (Fig 1.1d). Mass balance between lactate consumption and acetate production showed carbon deficit in all experiments (lactate consumed > acetate produced). In a first stage (≈ <12h) of bioreduction experiments, *Shewanella loihica* consumed all the remaining oxygen in solution in the full oxidation of lactate to CO_2 via the aerobic metabolic pathway. The observed carbon mismatch (reaching up to ≈20%) was attributed to both carbon assimilation in biomass formation during microbial growth and the use of the aerobic metabolic pathway in oxygen consumption by *Shewanella loihica*.

According to the bioreduction reaction (Eq. 1.4), a significant deficit of ferrous iron, based on measured aqueous Fe(II) relative to acetate, was found in all experiments. The Fe(II)/acetate ratios range between 0.03 and 0.17, which is between 0.7% and 4.3% of the stoichiometric ratio (Table 1. 2). Several previous studies [43-45] reported a similar Fe(II) deficit, suggesting that (1) the apparent extent of bioreduction based on measured aqueous Fe(II) reached only about 3% solubilization of initial Fe(III) and (2) Fe(III) reduction could then be largely underestimated due to adsorption of Fe(II) on the dissolving iron oxides and/or formation of secondary mineral phases containing structural Fe(II).

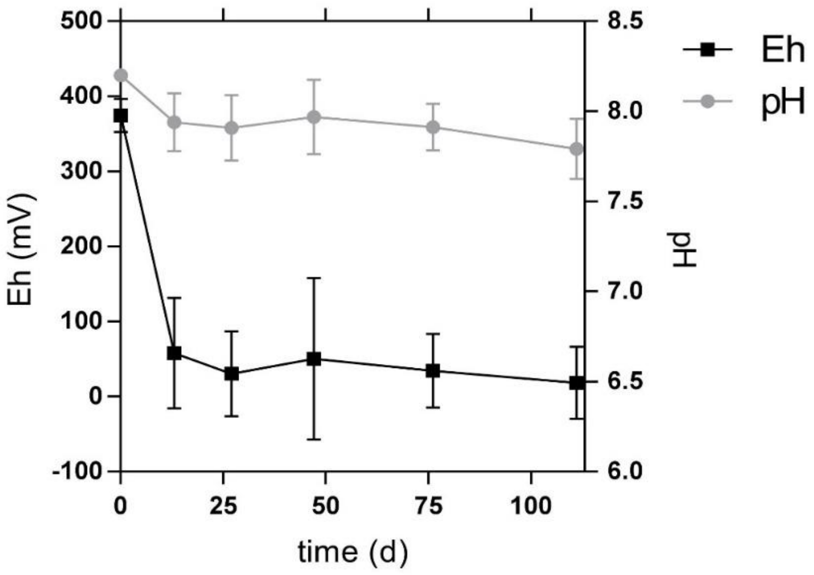

Figure 1. 4. pH and Eh values during the bioreduction experiments with all the minerals reacted. Key: (□) Eh; (●) pH

In the current study, the measurement of adsorption of Fe(II) on powdered ferryhidrite in marine medium (Fig. 1.5) indicated a probable adsorption of solubilized ferrous iron, as it has also been found for other Fe(III)-oxides in previous studies using aqueous solutions with a composition different than in our study [46, 47]. Considering the adsorption capacity of ferryhidrite (0.6 mmol g^{-1}) and the released acetate in the ferrihydrite bioreduction experiment (Fig. 1.1d), a Fe(II)/acetate ratio of 3.25 would be obtained if only adsorption of ferrous iron had occurred. Therefore, the marked Fe deficit observed (Fe(II)/acetate = 0.17; Table 1. 2) cannot be explained by adsorption of ferrous iron alone. Moreover, the Fe(II)-ferrihydrite adsorption experiments showed that the adsorbed Fe(II) exceeded the maximum capacity (0.6 mmol g^{-1}; Fig. 1.5). This indicated that an additional process, such as ferrihydrite transformation to magnetite, could be responsible for the extra Fe(II) uptake. A comparison between the XRD patterns of non-reacted and reacted ferrihydrite samples showed the presence of magnetite, a more crystalline phase (Fig. 1.6), confirming the occurrence of magnetite formation. Previous studies suggested that the Fe(III)-oxide-magnetite transformation is driven by an electron transfer between the adsorbed Fe(II) and Fe(III) in iron oxides, resulting in the formation of nano-crystalline, stoichiometric magnetite [48, 49]. This mineralogical transformation may be expressed as (eq 1.5):

$$2Fe(OH)_3 + Fe^{2+} \leftrightarrow Fe_3O_4 + 2H_2O + 2H^+ \qquad (1.5).$$

It is suggested that in alkaline environments magnetite is the most stable iron oxide phase [50], in contrast to lepidocrocite and goethite in neutral environments [51]. Simultaneous Fe(II) adsorption and mineral transformation could therefore explain the systematically high deficit of aqueous ferrous iron. These two processes, which act as a sink for dissolved biogenic ferrous iron, were also observed in *Geobacter* mediated ferrihydrite bioreduction [52].

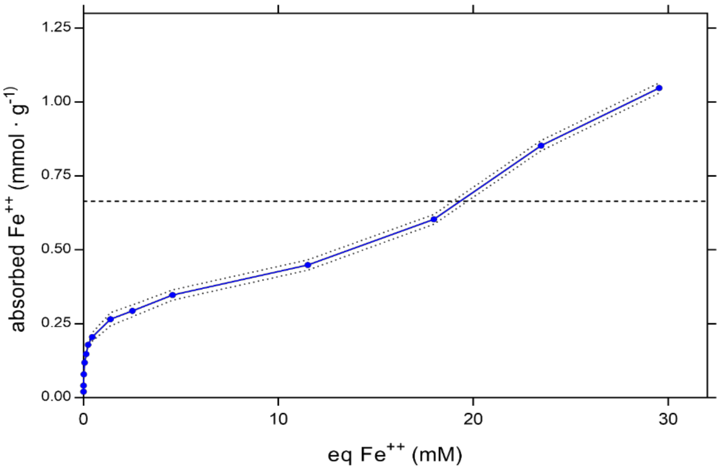

Figure 1. 5. Ferrous iron adsorption isotherm onto ferrihydrite in the marine medium. Dashed line indicates the saturation point based on the calculated number of sorption sites for ferrihydrite. Dotted lines indicate the SD of the experiment.

The estimated initial bioreduction coefficients differed between the different oxides studied (Table 1.2). Bioreduction kinetics is dependent on the reactive surface area of the iron oxides, which plays a key role in the process [53]. Ferrihydrite has the largest surface area (Table 1.1), up to three orders of magnitude higher than that of the other minerals. As a result, the bioreduction coefficient of ferrihydrite shows the highest value (5.49 μmol of Fe(II) g_{oxide}^{-1} d^{-1};Fig. 1.3a). In contrast, the lowest bioreduction coefficient corresponds to goethite (Table 1.2), commercial powder (0.026 μmol of Fe(II) g_{oxide}^{-1} d^{-1}; Fig. 1.3a). Nevertheless, when microbial bioreduction coefficients were normalized with the specific surface area of the oxides, magnetite, either synthetic or natural (Magnetite and M1) shows the highest bioreduction coefficient (0.034 μmol Fe(II) m^{-2} d^{-1} for Magnetite and 0.309 μmol Fe(II) m^{-2} d^{-1} for M1; Fig. 1.3b). According to the normalized acetate coefficients, both commercial and field magnetite samples showed the highest acetate production compared to other commercial and synthetic samples (0.249 μmol acetate m^{-2} d^{-1} and 5.31 μmol acetate m^{-2} d^{-1}, respectively).

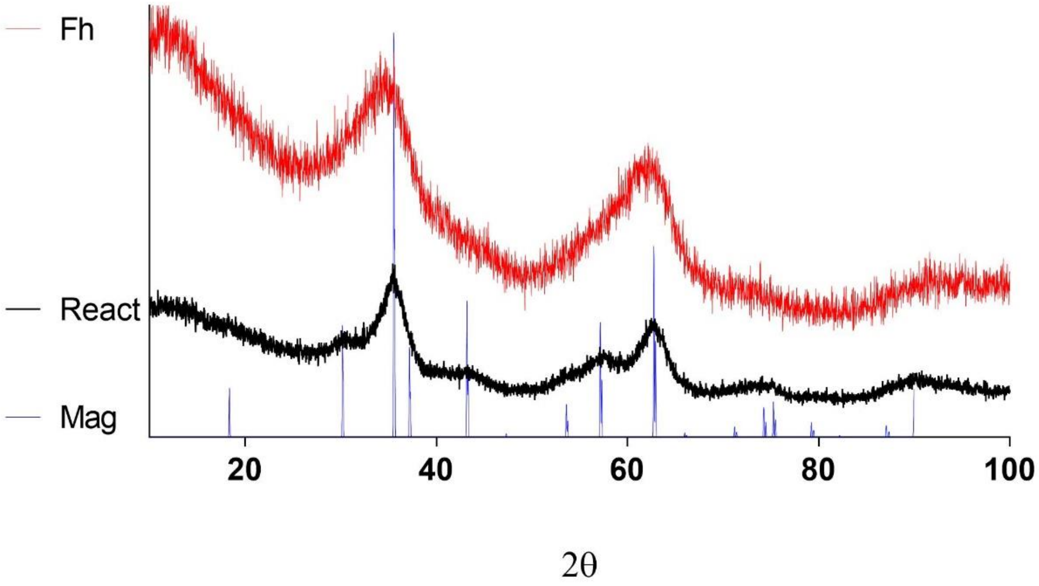

Figure 1. 6. XRD patterns of non-reacted pure ferrihydrite (red) and reacted ferrihydrite after adsorption experiments (black). Blue lines indicate the position of the main XRD peaks of pure crystalline magnetite (blue) obtained from Ruff database. Most of the reacted ferrihydrite transformed to magnetite after surface adsorption of iron (II). Rietveld analysis of the reacted sample indicates that 10% of the sample is ferrihydrite and 90% is magnetite with nanocrystalline morphology.

These phases therefore show high preference for *Shewanella*'s bioreduction. Yet, the high values of the magnetite bioreduction coefficient could be also associated with an extra release of ferrous iron from the lattice of the magnetite [40]. Furthermore, if

Fe(III) of the magnetite lattice is reduced to Fe(II), an increase in crystal radius (with IV coordination) from 63 to 77 pm might destabilize magnetite structure, yielding high coefficient values [54]. The variability in the bioreduction coefficients of the studied iron oxides could be attributed to the differences in the intrinsic mineral properties, such as the degree of crystallinity, grain size and impurity content [55, 56].

1.3.5. *Shewanella loihica* and Fe-(hydr)oxide surfaces

Bacteria use several strategies to perform bioreduction process. A well-known strategy is the contact of bacteria with mineral surfaces, allowing the electron transport [53]. SEM images showed *Shewanella loihica* cells colonizing the iron-oxide surfaces (Fig. 1.7a), either as individual cells or forming clusters. In addition, the SEM images revealed the presence of extracellular structures apparently connecting single cells with the mineral surface and/or with other cells (Fig. 1.7b,c). In fact, previous studies have shown that the genera *Shewanella* is able to develop extracellular structures to perform the electron exchange in the bioreduction process (i.e. nanowires) [57-59]. A similar morphology between the extracellular structures in our study and those reported in previous studies exist. Nevertheless, to fully prove the electron-exchange capacity of the extracellular structures observed in this work, further studies are necessary.

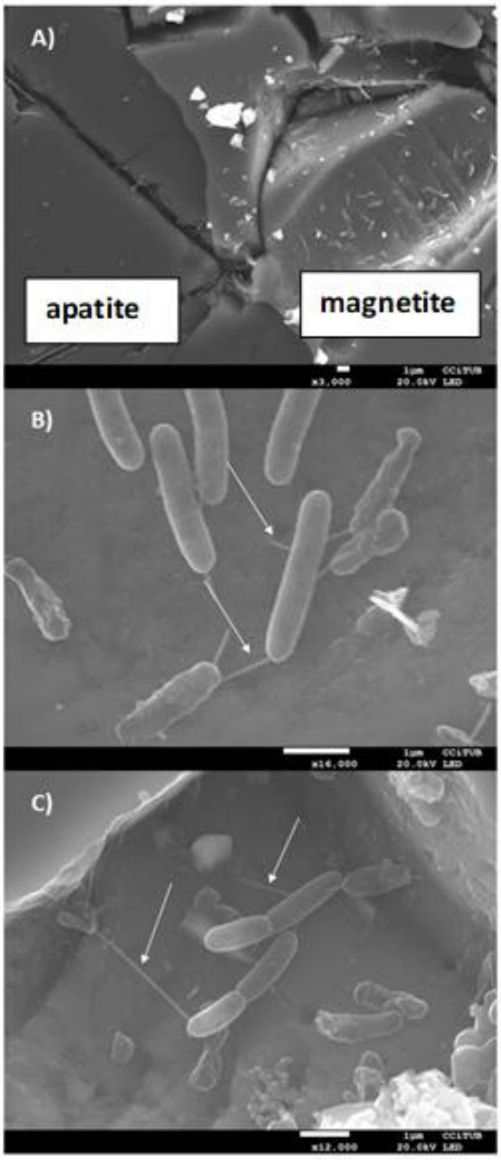
A)
apatite
magnetite
1µm CCiTUB
x3,000 20.0kV LED
B)
1µm CCiTUB
x16,000 20.0kV LED
C)
1µm CCiTUB
x12,000 20.0kV LED

Figure 1.7. SEM images of *S. loihica* cells colonizing an iron-oxide surface: a) bacteria growing preferably on the oxide surfaces (magnetite); b,c) bacteria growing on the surface of magnetite (M1) with developed extracellular structures (see arrows) interconnecting cells and/or connecting cells with the mineral surface.

1.4. CONCLUSIONS

Shewanella loihica is able to dissolve Fe(III) oxides via dissimilatory iron reduction under conditions of anoxic marine sediments. The deficit of aqueous ferrous iron relative to acetate produced during bioreduction was explained by adsorption of Fe(II) on the dissolving iron oxides and transformation of the iron oxides into stoichiometric magnetite. Hence, calculated bioreduction coefficients based on measured aqueous Fe(II) account for only up to about 4% of the actual reaction, considering the theoretical release of Fe(II) and acetate productions. During bioreduction, *Shewanella loihica* colonizes the surface of the iron oxides.

Results indicate a potential unfavorable role of iron-oxide bioreduction in deep-sea mining activities or coastal mine-tailings disposal, where release of trace and toxic metals represents an environmental threat. Furthermore, the iron released from metal mine tailings disposed offshore could affect primary production, jeopardizing the resilience of offshore ecosystems. However, a positive implication of iron-oxide bioreduction is found for biotechnology as iron-oxide bioleaching could potentially be used for recovery of iron and trace elements in metallurgical treatments.

1.5. REFERENCES

1. Raiswell, R. and D.E. Canfield, *The iron biogeochemical cycle past and present.* Geochemical perspectives, 2012. **1**(1): p. 1-2.

2. Field, C.B., et al., *Primary production of the biosphere: integrating terrestrial and oceanic components.* science, 1998. **281**(5374): p. 237-240.

3. Morel, F. and N. Price, *The biogeochemical cycles of trace metals in the oceans.* Science, 2003. **300**(5621): p. 944-947.

4. De Baar, H.J., et al., *Synthesis of iron fertilization experiments: from the iron age in the age of enlightenment.* Journal of Geophysical Research: Oceans, 2005. **110**(C9).

5. Boyd, P. and M. Ellwood, *The biogeochemical cycle of iron in the ocean.* Nature Geoscience, 2010. **3**(10): p. 675.

6. Martin, J.H., S.E. Fitzwater, and R.M. Gordon, *Iron deficiency limits phytoplankton growth in Antarctic waters.* Global Biogeochemical Cycles, 1990. **4**(1): p. 5-12.

7. Fenchel, T., *The ecology of marine microbenthos IV. Structure and function of the benthic ecosystem, its chemical and physical factors and the microfauna commuities with special reference to the ciliated protozoa.* Ophelia, 1969. **6**(1): p. 1-182.

8. Lovley, D.R., *Dissimilatory Fe (III) and Mn (IV) reduction.* Microbiological reviews, 1991. **55**(2): p. 259-287.

9. Lovley, D.R. and E.J. Phillips, *Organic matter mineralization with reduction of ferric iron in anaerobic sediments.* Applied and environmental microbiology, 1986. **51**(4): p. 683-689.

10. Thamdrup, B., *Bacterial manganese and iron reduction in aquatic sediments*, in *Advances in microbial ecology*. 2000, Springer. p. 41-84.

11. Finke, N., V. Vandieken, and B.B. Jørgensen, *Acetate, lactate, propionate, and isobutyrate as electron donors for iron and sulfate reduction in Arctic marine sediments, Svalbard.* FEMS Microbiology Ecology, 2007. **59**(1): p. 10-22.

12. Hau, H.H. and J.A. Gralnick, *Ecology and biotechnology of the genus Shewanella.* Annu. Rev. Microbiol., 2007. **61**: p. 237-258.

13. Roh, Y., et al., *Metal reduction and iron biomineralization by a psychrotolerant Fe (III)-reducing bacterium, Shewanella sp. strain PV-4.* Applied and Environmental Microbiology, 2006. **72**(5): p. 3236-3244.

14. Gao, H., et al., *Shewanella loihica sp. nov., isolated from iron-rich microbial mats in the Pacific Ocean.* International Journal of Systematic and Evolutionary Microbiology, 2006. **56**(8): p. 1911-1916.

15. Dong, H., et al., *Mineral transformations associated with the microbial reduction of magnetite.* Chemical Geology, 2000. **169**(3-4): p. 299-318.

16. Tugel, J.B., M.E. Hines, and G.E. Jones, *Microbial iron reduction by enrichment cultures isolated from estuarine sediments.* Applied and environmental microbiology, 1986. **52**(5): p. 1167-1172.

17. Ellis, D. and K. Ellis, *Very deep STD.* Marine Pollution Bulletin, 1994. **28**(8): p. 472-476.

18. Dold, B., *Submarine tailings disposal (STD)—A review.* Minerals, 2014. **4**(3): p. 642-666.

19. Medina, M., et al., *Biodiversity of rocky intertidal benthic communities associated with copper mine tailing discharges in northern Chile.* Marine Pollution Bulletin, 2005. **50**(4): p. 396-409.

20. Dold, B., *Element flows associated with marine shore mine tailings deposits.* Environmental science & technology, 2006. **40**(3): p. 752-758.

21. Manteca, J.I., et al., *The beach placer iron deposit of Portman Bay, Murcia, SE Spain: the result of 33 years of tailings disposal (1957–1990) to the Mediterranean seaside.* Mineralium Deposita, 2014. **49**(6): p. 777-783.

22. Nadoll, P., et al., *The chemistry of hydrothermal magnetite: A review.* Ore geology reviews, 2014. **61**: p. 1-32.

23. Knipping, J.L., et al., *Trace elements in magnetite from massive iron oxide-apatite deposits indicate a combined formation by igneous and magmatic-hydrothermal processes.* Geochimica et Cosmochimica Acta, 2015. **171**: p. 15-38.

24. Cornell, R. and U. Schwertmann, *The Iron Oxides: Structures, Properties, Reactions, Occurrences and Uses.* VCH Verlagsgesellshaft GMBH, Weinheim, Germany, 1996: p. 533-559.

25. Zachara, J.M., et al., *Solubilization of Fe (III) oxide-bound trace metals by a dissimilatory Fe (III) reducing bacterium.* Geochimica et Cosmochimica Acta, 2001. **65**(1): p. 75-93.

26. Morello, E.B., et al., *The ecological impacts of submarine tailings placement*, in *Oceanography and Marine Biology*. 2016, CRC Press. p. 323-374.

27. Ramirez-Llodra, E., et al., *Submarine and deep-sea mine tailing placements: a review of current practices, environmental issues, natural analogs and knowledge gaps in Norway and internationally.* Marine Pollution Bulletin, 2015. **97**(1-2): p. 13-35.

28. Cornel, R. and U. Shwertmann, *Iron oxides in the laboratory. Preparation and characterization.* VCH Editions, Weinhein, Germany, 1991.

29. Young, R., *The Rietveld Method, International Union of Crystallography Monographs on Crystal and Oxford Science Publications*. 1995, Oxford, UK.

30. Brunauer, S., P.H. Emmett, and E. Teller, *Adsorption of gases in multimolecular layers.* Journal of the American chemical society, 1938. **60**(2): p. 309-319.

31. Das, S., M.J. Hendry, and J. Essilfie-Dughan, *Transformation of two-line ferrihydrite to goethite and hematite as a function of pH and temperature.* Environmental science & technology, 2010. **45**(1): p. 268-275.

32. Mazzetti, L. and P. Thistlethwaite, *Raman spectra and thermal transformations of ferrihydrite and schwertmannite.* Journal of Raman Spectroscopy, 2002. **33**(2): p. 104-111.

33. Rosselló-Mora, R., et al., *The response of the microbial community of marine sediments to organic carbon input under anaerobic conditions.* Systematic and Applied Microbiology, 1999. **22**(2): p. 237-248.

34. Jørgensen, B. and S. Kasten, *Marine geochemistry.* Bacteria and, 2006.

35. Stucki, J., *The quantitative assay of minerals for Fe2+ and Fe3+ using 1, 10-phenanthroline: II. A photochemical method 1.* Soil Science Society of America Journal, 1981. **45**(3): p. 638-641.

36. Dzombak, D.A. and F. Morel, *Surface complexation modeling: hydrous ferric oxide*. 1990: John Wiley & Sons.

37. Anderson, T.F., *TECHNIQUES FOR THE PRESERVAATION OF THREE-DIMENSIONAL STRUCTURE IN PREPARING SPECIMENS FOR THE ELECTRON MICROSCOPE.* Transactions of the New York Academy of Sciences, 1951. **13**(4 Series II): p. 130-134.

38. Nation, J.L., *A new method using hexamethyldisilazane for preparation of soft insect tissues for scanning electron microscopy.* Stain technology, 1983. **58**(6): p. 347-351.

39. Hiemstra, T., *Surface and mineral structure of ferrihydrite.* Geochimica et Cosmochimica Acta, 2013. **105**: p. 316-325.

40. Kostka, J.E. and K.H. Nealson, *Dissolution and reduction of magnetite by bacteria.* Environmental Science & Technology, 1995. **29**(10): p. 2535-2540.

41. Scott, J.H. and K.H. Nealson, *A biochemical study of the intermediary carbon metabolism of Shewanella putrefaciens.* Journal of Bacteriology, 1994. **176**(11): p. 3408-3411.

42. Tang, Y.J., et al., *Anaerobic central metabolic pathways in Shewanella oneidensis MR-1 reinterpreted in the light of isotopic metabolite labeling.* Journal of Bacteriology, 2007. **189**(3): p. 894-901.

43. Roden, E.E., M.M. Urrutia, and C.J. Mann, *Bacterial reductive dissolution of crystalline Fe (III) oxide in continuous-flow column reactors.* Applied and environmental microbiology, 2000. **66**(3): p. 1062-1065.

44. Bonneville, S., P. Van Cappellen, and T. Behrends, *Microbial reduction of iron (III) oxyhydroxides: effects of mineral solubility and availability.* Chemical Geology, 2004. **212**(3-4): p. 255-268.

45. Benner, S.G., et al., *Reductive dissolution and biomineralization of iron hydroxide under dynamic flow conditions.* Environmental Science & Technology, 2002. **36**(8): p. 1705-1711.

46. Larese-Casanova, P. and M.M. Scherer, *Fe (II) sorption on hematite: New insights based on spectroscopic measurements.* Environmental science & technology, 2007. **41**(2): p. 471-477.

47. Rajput, S., C.U. Pittman Jr, and D. Mohan, *Magnetic magnetite (Fe3O4) nanoparticle synthesis and applications for lead (Pb2+) and chromium (Cr6+) removal from water.* Journal of colloid and interface science, 2016. **468**: p. 334-346.

48. Williams, A.G. and M.M. Scherer, *Spectroscopic evidence for Fe (II)– Fe (III) electron transfer at the iron oxide– water interface.* Environmental science & technology, 2004. **38**(18): p. 4782-4790.

49. Byrne, J., et al., *Control of nanoparticle size, reactivity and magnetic properties during the bioproduction of magnetite by Geobacter sulfurreducens.* Nanotechnology, 2011. **22**(45): p. 455709.

50. Tronc, E., et al., *Transformation of ferric hydroxide into spinel by iron (II) adsorption.* Langmuir, 1992. **8**(1): p. 313-319.

51. Boland, D.D., et al., *Effect of solution and solid-phase conditions on the Fe (II)-accelerated transformation of ferrihydrite to lepidocrocite and goethite.* Environmental science & technology, 2014. **48**(10): p. 5477-5485.

52. Chen, Z., et al., *Maghemite (γ-Fe2O3) nanoparticles enhance dissimilatory ferrihydrite reduction by Geobacter sulfurreducens: Impacts on iron mineralogical change and bacterial interactions.* Journal of Environmental Sciences, 2018.

53. Burdige, D.J., S.P. Dhakar, and K.H. Nealson, *Effects of manganese oxide mineralogy on microbial and chemical manganese reduction.* Geomicrobiology Journal, 1992. **10**(1): p. 27-48.

54. Shannon, R.D., *Revised effective ionic radii and systematic studies of interatomic distances in halides and chalcogenides.* Acta crystallographica section A: crystal physics, diffraction, theoretical and general crystallography, 1976. **32**(5): p. 751-767.

55. Li, X., et al., *Reduction of structural Fe (III) in oxyhydroxides by Shewanella decolorationis S12 and characterization of the surface properties of iron minerals.* Journal of soils and sediments, 2012. **12**(2): p. 217-227.

56. O'Loughlin, E.J., et al., *Effects of oxyanions, natural organic matter, and bacterial cell numbers on the bioreduction of lepidocrocite (γ-FeOOH) and the formation of secondary mineralization products.* Environmental Science & Technology, 2010. **44**(12): p. 4570-4576.

57. Pirbadian, S., et al., *Shewanella oneidensis MR-1 nanowires are outer membrane and periplasmic extensions of the extracellular electron transport components.* Proceedings of the National Academy of Sciences, 2014. **111**(35): p. 12883-12888.

58. Shi, L., et al., *Extracellular electron transfer mechanisms between microorganisms and minerals.* Nature Reviews Microbiology, 2016. **14**(10): p. 651.

59. Gorby, Y.A., et al., *Electrically conductive bacterial nanowires produced by Shewanella oneidensis strain MR-1 and other microorganisms.* Proceedings of the National Academy of Sciences, 2006. **103**(30): p. 11358-11363.

CHAPTER 2

IRON (HYDR)OXIDE BIOREDUCTION PROCESS: MONOD KINETICS AND TRACE ELEMENT RELEASE

Mine industry is facing mine tailings management problems. Given the environmental issues associated with mine tailings on land disposal, submarine tailings disposal (STD) is an attractive alternative for tailings deposition. A better understanding of tailings reactivity under marine conditions, likely controlled by bioreduction of iron (hydr)oxides, is therefore crucial for a reliable STD assessment. This chapter presents the study of the bioreduction kinetics of magnetite, an abundant Fe(III)-oxide mineral in iron-rich mine tailings, and the subsequent TE release.

2.1. INTRODUCTION

An adverse impact of metal mine tailings on sediment and water quality is a major environmental problem.[1, 2] Mine tailings are waste produced after the target metal is extracted from the ore by crushing and milling. Ore grades in many exploited metal ore reserves will probably decrease in the future leading to an increase of the waste/metal production ratio and the volume of mine tailings.[3, 4] Due to environmental issues associated with deposition of mine tailings on land (e.g., acid mine drainage [5] and tailings dam failures [6]), alternative options for tailings management such as submarine tailings disposal (STD) are being considered and used in some countries [7, 8]. However, severe ecological impacts of STD in active and historical sites were reported worldwide [7-10].

In addition to the physical impacts of STD on the seafloor biota due to massive tailings discharge and extremely high sedimentation rates (i.e., hyper-sedimentation), toxic effects may occur due to heavy metals (e.g., Cu, Zn, Ni, Pb, Cr, V, Cd etc.) and metalloids (e.g., As) release [7-9, 11]. Most of the field studies on marine environment contamination by metal(loid)s from mining activities investigated are sites impacted by sulphide ore tailings [7, 11-14]. Recent laboratory studies also investigated the potential impacts of metal sulfide minerals and sulfide-containing tailings on marine environments.[15, 16] Embile et al. [15] evaluated the release of Cu, Pb and Fe from sulfide-containing tailings in seawater and Simpson et al. [16] studied the toxicity and bioavailability of several metal sulphide minerals to benthic marine invertebrates. However, iron oxide minerals such as magnetite and hematite can also contribute to metal contamination of marine sediment and pore water in those sites impacted by disposal of sulfide ore tailings [7]. For instance, Pb-Zn ore tailings directly released to the Mediterranean Sea between 1957 and 1990 in Portman Bay (Spain) contained an iron oxide (magnetite, hematite and goethite) concentration of 15.6% (mineral treated during 1973) [17].

Iron oxide ore (mainly magnetite) tailings in submarine environments were deposited in Norway (from 2009 to 2015) and in Chile (from 1978 to 2019) [7, 8, 18]. At the moment, field or laboratory studies on the potential contamination by trace metals from submarine iron ore tailings disposal are scarce. Wong et al. [19] observed that the contents of heavy metals (i.e., Fe, Mn, Pb and Zn) of two different marine algae found on iron ore tailings were higher than those measured in algae collected from two locations far away from the tailings. A more recent review provided information from an environmental monitoring conducted at a site affected by iron oxide tailings disposal and higher accumulation of Fe and Al was determined in blue mussels closer to the outlet [8].

In the present study, iron oxides in most of the samples investigated are mainly composed of magnetite ($Fe^{2+}Fe^{3+}{}_2O_4$). Magnetite is an iron ore [20, 21] (72.36% Fe) and also a common mineral in sulfide ore bodies and their host rocks [22-24]. It forms under a wide variety of geologic conditions and a large range of minor and trace elements can be incorporated in its spinel structure [22-26]. For instance, cations such as Mn, Zn, Ni and Co may substitute Fe^{2+}, whereas others like Al, Cr, V and Ga can replace Fe^{3+} sites [23, 26]. As a result, elements such as Al, Ti, V, Cr, Mn, Co, Ni, Zn and Ga are commonly present in magnetite at concentrations from 10 to > 1000 ppm [26]. Based on the potential amounts of trace metals in magnetite, STD of magnetite-bearing mine tailings could adversely affect the quality of marine sediments. In addition, sea currents and tidal waves can lead to a gravimetric classification of the tailings material in some sites, yielding a high fraction of dense iron oxides [17]. According to reported sediment quality guidelines (SQGs) for the assessment of metal contamination in marine environments, threshold concentration values (ppm dry weight) above which adverse effects are frequently expected are 43, 271 and 160 for Ni, Zn and Cr, respectively [27].

The magnitude of the impact on marine biota depends on the amount of metal that is bioavailable. Dissolved species and free metal cations are considered the most bioavailable forms [8, 9, 16]. In sediments where reducing conditions prevail, iron oxides may be affected by microbial reductive dissolution, [28, 29] which can lead to trace element release into the aqueous phase. In contrast, sulfide minerals are relatively stable under such conditions [7, 9]. When the rate of carbon rain to the sediments is high, dissolved oxygen (DO) penetration depths in the sediment are shallow whereas when the rate is low, penetration depths increase [30]. Morello et al. (and references herein) [9] indicated that DO penetration depths in fine sediments were typically no more than 1 cm in highly productive coastal waters and up to 5-20 cm in deep-ocean sediments due to the lower biological activity.

Ribet et al. [31] studied the potential of metal release by reductive dissolution of weathered sulfide ore tailings from a mine tailings impoundment on land. These authors indicated that high concentrations of metals including Ni, Cr and Cu are potentially releasable by reductive dissolution of Fe^{3+}-bearing secondary minerals such as goethite. Zachara et al. [32] studied the solubilization of coprecipitated Co(III) and Ni(II) from goethite during Fe^{3+}-bioreduction at circumneutral pH. However, the conditions and/or metal oxides investigated in these previous studies are different than those in natural marine environments impacted by iron oxides from mine tailings. Trace metal release and bioavailability will depend on the properties and characteristics of the metal and host mineral(s) as well as on the geochemical conditions of the STD site. Therefore, further research on potential trace metal release from iron oxide ores such as magnetite in conditions closer to marine environments is necessary for the assessment of potential environmental impacts associated to STD.

Batch experiments were performed using a number of magnetite ore samples from Chilean and Swedish mines and a mine tailings sample. The overall goal was to investigate the extent and kinetics of iron ore minerals bioreduction under marine conditions and the potential release of trace elements. The magnitude of microbial reduction of Fe(III) was evaluated using a geochemical model that included Monod kinetics.

2.2. MATERIALS AND METHODS

2.2.1. Solid samples

The solids used for the experiments were seven iron ore samples, one iron ore tailings sample and four synthetic monomineralic samples. Five iron ore samples were from different mines in Chile (C1 to C5-T) and two samples from Swedish mines (S1 and S2) (Table A1.1 in Appendix 1 (AP1)). Since these mine samples were from iron ore deposits formed under different geological conditions, variations in trace element composition of the iron oxides were expected [26] . Before experiments and analyses, ore subsamples were crushed to powder with a size between 60 and 100 μm and subsequently homogenized. The iron oxide ore tailings sample was collected at the iron concentration plant (80th percentile value of 44 μm) of the mine from where the C5-T sample was extracted (see details in Sections 1 and 2 in AP1).

As for the monomineralic samples, synthetic ferrihydrite 2-Line ($Fe^{3+}_5HO_8·4H_2O$, particle size < 60 μm) was produced in the laboratory according to Schwertmann and

Cornell [33] (i.e., sample F), whereas synthetic powder (< 5 μm) samples of magnetite ($Fe^{2+}Fe^{3+}{}_2O_4$), hematite ($Fe^{3+}{}_2O_3$) and goethite ($Fe^{3+}O(OH)$) were purchased from Sigma-Aldrich (i.e., M, H and G, respectively).

2.2.2. Solid characterization

Samples were analyzed using X-ray diffraction (XRD) analysis and Rietveld refinement [34], scanning electron microscopy (SEM) and energy dispersive X-ray spectrometry (EDS), electron microprobe analysis (EMPA) and laser ablation inductively coupled plasma mass spectrometry (LA-ICP-MS). Details on the equipment and settings used are available in AP1 (Table A1.2). For the iron ore samples, the mineralogical study indicated that, except for sample C4 with about 40 wt.% of hematite, the metal oxide fraction was composed of magnetite with contents ranging from approximately 5 to 90 wt.% (Table A1.1 in AP1). This wide range covers well the content of iron oxides in sediments impacted by STD in active and historical sites. In some samples, other major constituents (> 10 wt.%) were silicates (amphibole, chlorite and plagioclase) and phosphates (apatite-(CaOH)). In the C3 sample, there was a substantial amount of chalcopyrite ($CuFeS_2$, ≈ 13 wt.%) (Table A1.1 in AP1). The tailings sample was mainly composed of gangue minerals, primarily silicates (amphibole, chlorite, plagioclase and talc), plus a minor amount (< 5 wt.%) of unrecoverable iron oxide minerals (mainly magnetite). The XRD analyses showed that the commercial and synthesized samples were composed of the respective iron (hydr)oxides with a lack of minor phases. The specific surface area of all samples was determined by the Brunauer-Emmett-Teller (BET) method [35] (Table A1.1).

Quantitative elemental analyses of the iron oxide minerals and other phases in the tailings and iron oxide ore samples were performed by EMPA and LA-ICP-MS. Bulk sample elemental composition was determined by total acid digestion and ICP analysis (see details in AP1).

2.2.3. Batch experiments

In the Fe(III) bioreduction experiments with iron (hydr)oxides, a marine bacterium *Shewanella loihica* PV-4 [36, 37]was used as a model microorganism (see cultivation details in Section 1.2 in Chapter 1. It is capable to grow under both oxic and anoxic conditions using oxygen or ferric iron as terminal electron acceptor (TEA), respectively [36, 37]. 55 glass tubes of 25 mL (nominal volume) were used for the microcosm (5 tubes for each solid sample) and 33 tubes for the abiotic controls (3 tubes for each solid). 0.25 g of powder sample were placed in each tube, which were subsequently filled with artificial seawater (ASW) under atmospheric conditions (see details in Section 3 in AP1). ASW was amended with sodium lactate (10 mM) as electron donor and carbon source and ammonium chloride (1.87 mM) as a source of nitrogen.

Tris(hydroxymethyl)aminomethane hydrochloride (TRIS-HCl, 10 mM) was used as a pH-buffer and the ASW solution was adjusted to pH of 8.2 with 1 N NaOH solution. In contrast to nutrient-rich solutions, the minimal growth medium used in this study may better represent the conditions in STD sites. No exogenous electron carrier substances (e.g., anthraquinone-2,6-disulfonate, AQDS) or reducing agents (e.g, cysteine) were added to the solution.

Except for the abiotic controls, *S. loihica* was aseptically inoculated into the tubes containing the medium and the solid previously sterilized to a final number of $1{\cdot}10^7$ colony-forming units (cfu) mL^{-1} (measured by agar culture, LB). The microcosms and abiotic controls were tightly closed using closed-top screw caps with butyl liner and sealed with Parafilm M. A minimal headspace was left to avoid cracking of the tubes due to overpressure. The solid/liquid ratio was approximately 9.5 g/L.

Thereafter, all tubes were stirred for approximately 15 s by a vortex mixer and immediately placed horizontally for incubation into a thermostatic water bath at 10 ± 1 °C without agitation in the dark until sampled. The relatively low incubation temperature and the static conditions were selected to be similar to marine sediment environments in STD sites. The horizontal disposition allowed the solid to settle down in a thin layer (thickness ≤ 1 mm) over the side of the tubes, maximizing the solid–liquid contact. Additional abiotic controls were prepared under anoxic conditions using degassed (O2-free) ASW or Milli-Q water (see details in AP1).

The experiments lasted 113 days and, during which, microcosms and controls were removed from the thermostatic bath at different times and placed immediately in the anoxic glovebox for sampling. The liquid was collected to measure the concentrations of lactate and acetate (high performance liquid chromatography (HPLC)) and metal(loid)s (ICP coupled to optical emission spectroscopy (ICP-OES) and ICP-MS). Uncertainties were estimated based on the analysis of sample replicates with different concentrations (see AP1). Measurements of dissolved iron speciation were performed by phenanthroline colorimetry. The solution pH, Eh and dissolved oxygen (DO) concentration were also measured. The solid was retrieved and preserved for XRD-Rietveld analysis, Field Emission SEM-EDS and Attenuated Total Reflectance-Fourier Transform Infrared Spectroscopy (ATR-FTIR). Detailed information on the analytical techniques, sampling and sample preservation is provided in AP1.

2.2.4. Geochemical modelling

The variation of the concentrations of lactate, acetate and the release of iron and TEs throughout the experiments were simulated using a kinetic model developed with the PHREEQC [38] code. A Monod kinetic rate expression for substrate (i.e., lactate) utilization coupled to cell growth was used [39, 40]. Monod kinetic equations allow to describe the competitive use of different TEAs (e.g., dissolved oxygen, Mn(IV), Fe(III), etc.) by the bacteria:

$$r = \frac{dS}{dt} = -k_{max} \cdot X \cdot \frac{S}{K_S + S} \cdot \frac{TEA}{K_{TEA} + TEA} \cdot \frac{K_{In}}{K_{In} + In} \tag{2.1}$$

where r is the rate of consumption of substrate S (mol L^{-1} s^{-1}), k_{max} is the maximum substrate consumption rate (s^{-1}), X, S, TEA and In are the concentration of the cell biomass, substrate, particular TEA and inhibiting substance (mol L^{-1}), respectively, KS and KTEA are the Monod half-saturation constants with respect to S and TEA (mol L^{-1}), respectively, and K_{In} corresponds to the respective inhibition constant (mol L^{-1}). Under reducing conditions, magnetite bioreduction in the experiments performed in this study is expressed as

$$C_3H_5O_3^- + 0.15\ NH_4^+ + 1.5\ Fe^{2+}Fe^{3+}{}_2O_4 + 8.35\ H^+ \rightarrow$$

$$0.75\ C_2H_3O_2^- + 0.75\ HCO_3^- + 0.15\ C_5H_7O_2N + 4.5\ Fe(II) + 4.95\ H_2O \tag{2.2}$$

where $C_3H_5O_3^-$ and $C_2H_3O_2^-$ are lactate and acetate, respectively. A cell biomass formula of $C_5H_7O_2N$ was assumed according to previous studies [41, 42] to convert measurements of cfu to moles of cell biomass (see details in Section 9 in AP1). Cell biomass changes (e.g., growth or decay) during the experiment were simulated by a simple model that includes a first-order decay rate [43, 44]:

$$\frac{dX}{dt} = Y \cdot r - \mu_{dec} \cdot X \cdot In_{dec} \tag{2.3}$$

where r is the rate of substrate consumption from Eq.(2.1), Y is the molar biomass yield, such that Y = mol of biomass (i.e., $C_5H_7O_2N$) produced/mol of substrate (i.e., $C_3H_5O_3^-$) consumed, and μ_{dec} is the decay rate coefficient (s^{-1}). An inhibition factor, $In_{dec} = 1 - (Xmin / X)$, which inhibits the decay at low cell concentrations (i.e., X_{min}) was used (Table A1.4 in AP1). Microbial growth was simulated by including biomass (i.e., $C_5H_7O_2N$) as a product in the reaction stoichiometry Eq. (2.2)) and according to Y (Eqs. (2.2 and 2.3)). This requires different reaction stoichiometries for different values of Y.

Details on the parameters used in Eqs. (2.1 and 2.3) and the stoichiometric coefficients of the reactions simulated with PHREEQC (Eq. (2.2)) are available in AP1 (Tables A1.3 and A1.4). Potential formation of secondary minerals (magnetite and/or siderite ($Fe^{2+}CO_3$)) by produced Fe(II) (Eq. 2.2) reacting with and iron (hydr)oxides or anions in solution, respectively, was considered in the calculations (Eqs. (EA1.2) and (EA1.3) in AP1). In Eq. (2.2), magnetite is assumed to be stoichiometric (i.e., $Fe^{2+}/Fe^{3+} = 0.5$). However, as partially oxidized magnetite ($Fe^{2+}/Fe^{3+} < 0.5$, commonly referred to as nonstoichiometric magnetite) is also possible [45] a nonstoichiometric magnetite was also utilized in the simulations (see discussion below). Throughout this chapter, “Fe(II)” and “Fe^{2+}” refer to dissolved ferrous iron and structural ferrous iron, respectively.

2.3. RESULTS AND DISCUSSION

2.3.1. Geochemical composition of iron oxides

The TEs content measured by in-situ LA-ICP-MS of magnetite in C1, C2, C3, S1, S2 and CT samples is illustrated in Fig. 2.1. For the C4 sample, with approximately 40 wt.% of hematite (Table A1.1 in AP1), the TEs composition of hematite is shown in Fig. A1.1 in AP1. The elemental composition of the C5-T sample was determined by EMPA and total acid digestion. LA-ICP-MS elemental compositions of magnetite from ore samples of the same mine are available in the literature and were used for comparison [21].

The C1, C2 and C3 ore samples (Fig. 2.1a) showed high concentrations of Al and Mg (> 2000 ppm), V (685-11188 ppm), Mn (147-2060 ppm), Ni (69-522 ppm), Zn (48-132 ppm) and Co (28-186 ppm). Variable amounts were observed for Ti (16-2114 ppm), Cu (2-407 ppm), Cr (2-363 ppm) and Ga (2-126 ppm), and a relatively low one for Pb (< 2 ppm). The highest values of Cu and Cr in magnetite were observed for the C3 sample, which also contained chalcopyrite. In general, the Swedish S1 and S2 ore samples (Fig. 2.1b) exhibited a TEs composition pattern of magnetite relatively similar to that observed for the C1 and C2 samples from the Chilean IOA-type deposits (Fig. 2.1a). Nevertheless, the S2 sample showed lower concentrations of Zn, Cu, Pb and Y. In addition to the elements shown in Fig. 2.1, As was also detected and showed average values of up to ≈ 230 ppm in S2 and C5-T. Further comparison between TEs composition in magnetite from different deposits in Chile and Sweden and literature data is shown in Fig. A1.2 in AP1.

The elemental composition of the magnetite present in the processed ore tailings sample (CT) is illustrated in Fig. 2.1c, and the As concentration range determined by LA-ICP-MS and EMPA was 143-213 ppm. Reported TEs concentrations in magnetite ore samples from this deposit (LC-04\05 and LC-14, [21] Fig. 2.1c) generally fall within the range of those of the magnetite ore samples of the present study (shaded area in Fig. 2.1). Except for Cr and Ti, most of the average TEs concentrations of the magnetite grains in the CT sample were higher than those in the LC-04\05 and LC-14 samples [21]. Likewise, the average concentrations of several elements in the CT sample (e.g., Co, Mg and Al) were much higher than the range obtained for the magnetite ore samples measured in this study (shaded area in Fig. 2.1)

For a better characterization of the TEs concentrations in the magnetite from the tailings, EMPA analyses were carried out on the CT sample and a magnetite ore sample from the mine (C5-T) (Fig. A1.3 in AP1). The elemental composition of the CT-5 sample determined by total acid digestion agreed well with literature bulk rock measurements [21]. EMPA results showed that the concentration of most of the elements was higher in the magnetite of the tailings (CT) than that in the magnetite ore sample (CT-5). Moreover, the differences in the TEs concentrations of magnetite between the CT and CT-5 samples (Fig. A1.3 in AP1) are in general smaller than those observed between CT and LC-04\05 and LC-14 samples by LA-ICP-MS (Fig. 2.1c). Therefore, LA-ICP-MS and EMPA results indicate elevated contents of TEs in the magnetite of the tailings (Fig. 2.1c and Fig. A1.3 in AP1), which are even higher than in the magnetite ore samples from the same deposit (i.e., non-processed material). A hypothesis for the high content of TEs in the tailings magnetite could be the TEs enrichment during the iron separation process at the processing plant (further information in Section 4 in AP1). The accurate determination of the TEs concentrations performed is relevant to evaluate the potential impact of TEs release on marine environments affected by STD.

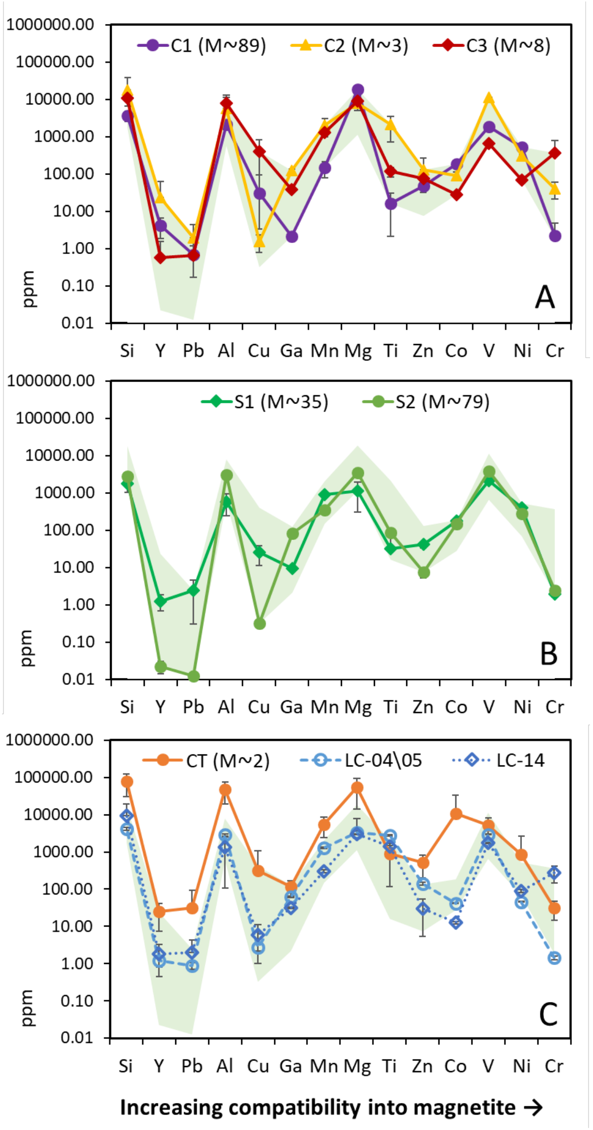

Figure 2. 1. Trace element content (ppm) of magnetite determined by LA-ICP-MS in this study and from the literature. A. Samples from Chilean deposits: C1 and C2 are from Iron Oxide Apatite (IOA) deposits and C3 is from an Iron Oxide Cupper Gold (IOCG) deposit. B. Samples S1 and S2 are from iron IOA-type deposits in Sweden. C. Iron ore tailings sample obtained at the outlet of a plant that processes magnetite ore from an IOA-type deposit. Data of ore samples (i.e., LC-04\05 and LC-14) from the same deposit available in the literature were also illustrated. [21]. The green area corresponds to the range of average concentrations determined for C1-3, S1 and S2 samples. Weight % of magnetite (M) in the samples of this study is in brackets.

2.3.2. Magnetite bioreduction experiments

In the biotic experiments, the measured concentrations of dissolved iron) were much higher than those in the abiotic controls (either prepared under atmospheric or anoxic conditions; Fig. 2.2 and Fig. A1.5 in AP1). In the biotic experiments, acetate formation coupled to lactate consumption indicated ferric iron bioreduction (Eq. (2.2)). Iron speciation measurements indicated that aqueous iron was ferrous iron Fe(II). Moreover, values of pH, Eh and DO agree with the values (pH (8.0 ± 0.1, ± 1s), Eh_{std} (45 ± 24, ± 1s) and DO (< 0.05 mg/L)) observed during the experiments with the magnetite-bearing samples and the PHREEQC speciation calculations.

As the bioreduction experiments were prepared under oxic conditions (atmospheric pressure), iron reduction started after oxygen consumption. Some previous tests prepared similarly, using either ferric-citrate or ferrihydrite as the source of Fe(III), showed that oxic conditions lasted approximately 2 days. Thus, lactate was initially consumed by aerobic oxidation to CO_2 and microbial growth (Eq. (EA1.1) in AP1). The aerobic metabolic pathway was also included in the geochemical model and Y values used in Eq. (2.3) for oxic and anoxic conditions are indicated in Table A1.4 in AP1. In fact, a transition from (sub)oxic to anoxic (iron reducing) conditions is likely to occur in seabed sediments impacted by STD. Strong redox gradients are common in the sediment-water interface [46, 47], and typical DO penetration depths in fine sediments in highly productive coastal waters are no more than 1 cm [9]. In the experiments with ferryhidrite, initial lactate concentration (10 mM) was totally consumed after 20 days (F in Fig. A1.5 in AP1). By contrast, the estimated total lactate consumption (as electron donor and carbon source) for the experiments with magnetite ranged from 8.1 to 13.3% (Fig. 2.2 and Table A1.5 in AP1). Similar values were obtained for the experiments with hematite and goethite (Table A1.5 in AP1).The maximum substrate consumption rates (k_{max}, Eq. 2.1) under oxic (4.4×10^{-5} s^{-1} for all experiments) and anoxic conditions (from $6.6 \cdot 10^{-7}$ to $2.5 \cdot 10^{-6}$ s^{-1} for experiments with magnetite; Table A1.4 in AP1) were derived by model calibration, based on both the lactate consumption and acetate formation during the experiments. Similar values were determined for the experiments with hematite and goethite, with the exception of the higher value obtained for ferrihydrite ($2.3 \cdot 10^{-5}$ s^{-1}), which is consistent with the much higher specific surface area of this sample (Table A1.1 in AP1). For the experiments with magnetite samples, the highest k_{max} value was obtained for the experiments with synthetic magnetite ($2.5 \cdot 10^{-6}$ s^{-1}), which also had a specific surface area higher than those of the magnetite ore samples (Table A1.1 in AP1). Nevertheless, the magnetite experiments showed a relatively narrow range of k_{max} values (average value of $1.3\cdot 10^{-6} \pm 0.7\cdot 10^{-6}$ s^{-1}, ± 1σ, n = 8; Table A1.4 in AP1).

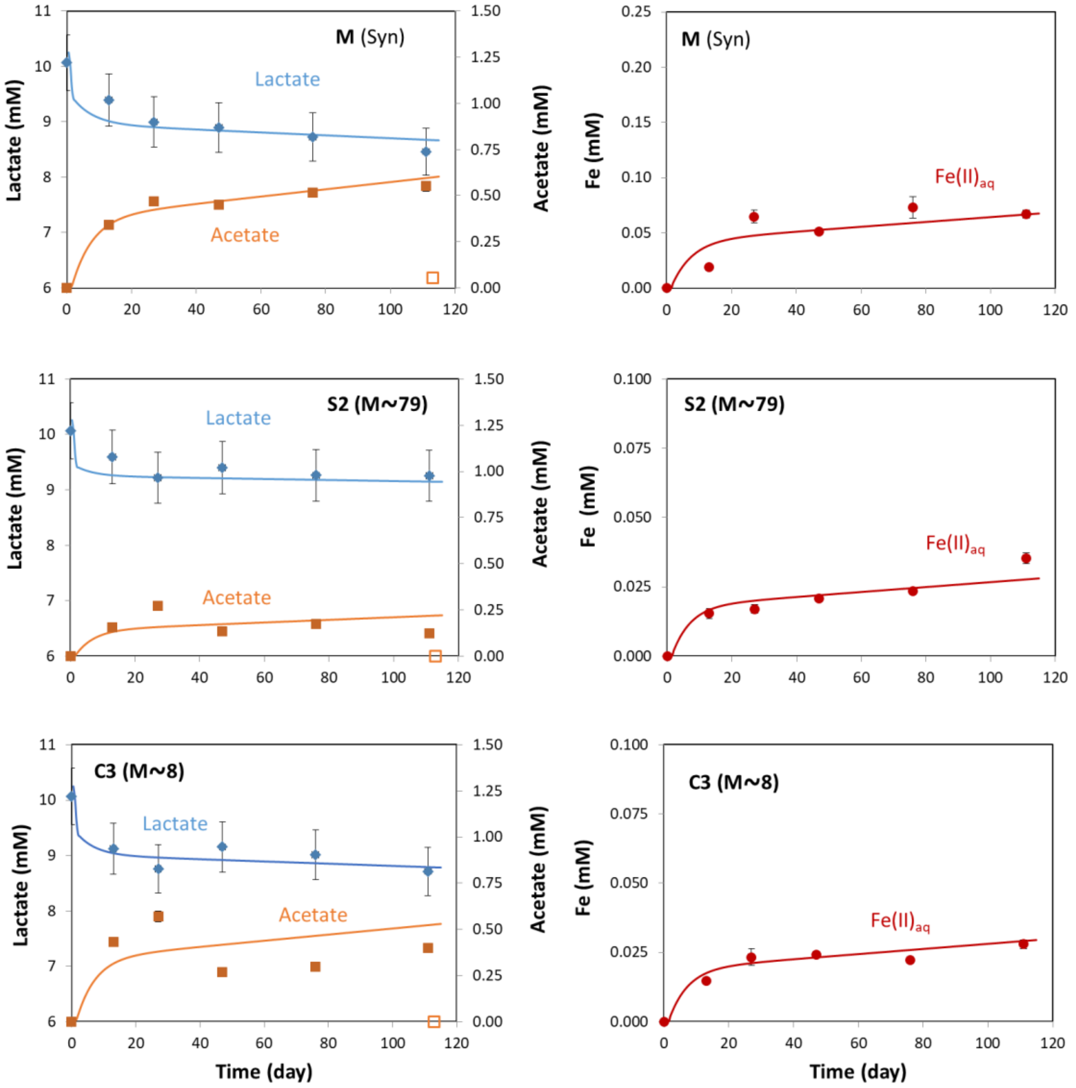

Figure 2. 2. Evolution of lactate, acetate and dissolved Fe(II) during the experiments. Solid lines represent the trends obtained by model simulations. Representative experiments with synthetic magnetite and ore samples from different locations (Chile and Sweden) and with different amounts of magnetite were selected. Weight % of magnetite (M) in the samples is indicated in brackets. Concentration data plots for the other magnetite-bearing samples and synthetic iron minerals are available in AP1 (Fig. A1.4)

Simulations reproduced satisfactorily the experimental lactate consumption and acetate formation (Fig. 2.2 and Fig. A1.5 in AP1). Under the conditions investigated, the consumption of lactate was higher under oxic conditions, except for the ferrihydrite experiments, in which lactate was mainly consumed via oxidation to acetate under anoxic conditions (F in Fig. A1.5 in AP1). Under anoxic conditions, concentrations of acetate and dissolved Fe(II) showed a similar evolution for most of the experiments regardless of the solid sample used (Fig. 2.2 and Fig. A1.5 in AP1). Concentrations of acetate and dissolved Fe(II) exhibited a relatively rapid increase for approximately 10 days. Thereafter, the rate of the increase was much lower or close to zero (e.g., sample CT, Fig. A1.5 in AP1).

With the model parameters (Table A1.4 in AP1), the numerical simulations indicate an increase in cell biomass under oxic conditions (i.e., X in Eqs. (2.1 and 2.3)) that is followed by a reduction of biomass when solid Fe^{3+} is the electron acceptor (see AP1). Ferrihydrite is an exception, since microbial growth could take place under iron reducing conditions. Compared to the other Fe^{3+}-bearing minerals used in the other experiments, Fe^{3+} in ferrihydrite is more bioavailable due to the low crystallinity and high surface area of this phase (Table A1.1 in AP1). Therefore, under the investigated conditions, a reduction of cell biomass can explain the attenuation of iron reduction in the experiments. This reduction could be interpreted either as a decrease in the number of active cells or as a constant number of cells with a slower metabolism. It reflects the lower bioavailability of solid Fe^{3+} in iron (hydr)oxides compared to dissolved electron acceptors (e.g., oxygen or ferric-citrate) and a potential occurrence of processes inhibiting Fe(III) bioreduction. For instance, previous studies investigated the inhibitory effect of Fe(II) on bacterial activity.[40, 48, 49].

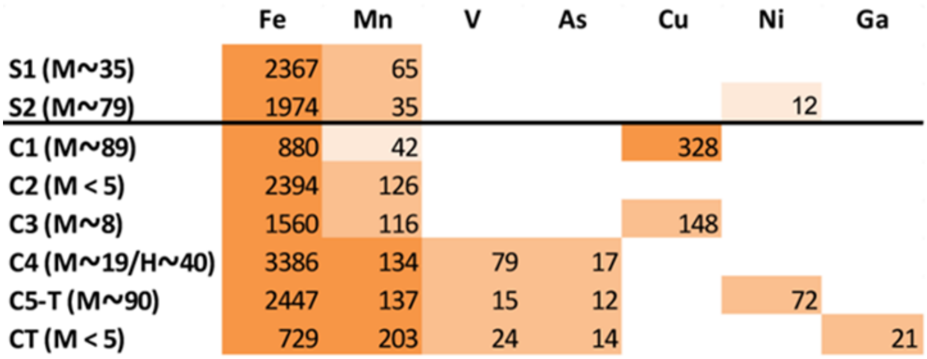

	Fe	Mn	V	As	Cu	Ni	Ga
S1 (M~35)	2367	65					
S2 (M~79)	1974	35				12	
C1 (M~89)	880	42			328		
C2 (M < 5)	2394	126					
C3 (M~8)	1560	116			148		
C4 (M~19/H~40)	3386	134	79	17			
C5-T (M~90)	2447	137	15	12		72	
CT (M < 5)	729	203	24	14			21

Figure 2. 3. Elements detected in solution during the iron bioreduction experiments with the magnetite ore samples and the tailings sample. *Dark orange*: elements detected in all the tubes. *Orange*: elements detected in all the tubes at lower concentrations, *Pale orange*: elements detected at very low concentrations or in some of the tubes. The highest concentrations (mg L^{-1}) determined for each solid used in the experiments (n = 5) are indicated.

2.3.3. Release of Fe(II) and trace elements to the aqueous phase during magnetite bioreduction

On the basis of lactate consumption and acetate formation in the experiments with magnetite-bearing samples, estimates of total ferric iron reduction with respect to the initial content of Fe^{3+} in the solid samples (Table A1.5 in AP1) ranged between 1.3% and 3.7% for the samples with high amounts of ferric iron (from 31.8 to 88.4 mM Fe^{3+}) and between 33.2% and 90.1% for the samples with low amounts (from 1.9 to 7.7 mM Fe^{3+}). The highest relative amount of ferric iron reduction (up to 90.1%) occurred with the iron ore tailings, where iron reduction ceased after 20 days (Fig. A1.5 in AP1, sample CT). For the experiments with synthetic hematite and goethite samples, lower reductions were observed (1.1% and 1.4%, respectively) compared to those of synthetic magnetite (3.7%). By contrast the iron reduction was higher for ferrihydrite (35.4%).

According to the estimated total Fe(III) bioreduction in the experiments, the expected aqueous Fe(II) concentrations were much higher than those measured, suggesting that dissolved Fe(II) only represented a minor fraction of the total ferric iron reduced. Previous studies showed that aqueous Fe(II) reacts on the surface of iron oxide minerals such as hematite, goethite, ferrihydrite and magnetite (see [50] and references therein). In accordance with these studies, adsorbed Fe(II) on magnetite oxidizes to Fe(III) by electron transfer to the mineral phase, resulting in magnetite growth. Detailed experiments in these studies revealed that the uptake of Fe(II) from the aqueous phase is controlled by the ratio of Fe^{2+}/Fe^{3+} in magnetite (e.g., for stoichiometric magnetite ($Fe^{2+}Fe^{3+}{}_2O_4$) the Fe^{2+}/Fe^{3+} ratio is 0.5), being higher in experiments with partially oxidized magnetite (i.e., Fe^{3+}-enriched, $Fe^{2+}/Fe^{3+} < 0.5$) [51]. In this study, therefore, the role of magnetite was considered in the geochemical model for the experiments with magnetite-bearing samples (see AP1). The Fe^{2+}/Fe^{3+} ratios of magnetite (from 0.20 to 0.35, Table A1.5 in AP1) were derived by model calibration and constrained with literature values [51, 52] (Table A1.3 in AP1). Note that during reductive dissolution of partially oxidized magnetite a lesser amount of structural Fe^{2+} per mole of magnetite dissolved is released to the solution as compared with the stoichiometric magnetite.

Simulations indicated that the uptake of dissolved Fe(II) by oxidation on magnetite could account for the variation in the aqueous Fe(II) concentrations in the experiments with samples containing relatively high amounts of magnetite (i.e., > 30 wt.%). In samples with lower fractions of magnetite (i.e., < 10 wt.%), oxidation of dissolved Fe(II) and magnetite growth partially account for the measured aqueous Fe(II) concentrations. This suggests a potential precipitation of other secondary Fe^{2+}-bearing minerals (e.g., siderite ($Fe^{2+}CO_3$)). Secondary siderite precipitation was observed in previous studies of Fe(III) bioreduction of magnetite [53], goethite [54] and ferric-citrate [55] at circumneutral pH. Hence, siderite precipitation was taken into account in the geochemical modeling (Eq. EA1.3, Tables A1.3 and A1.5 in AP1) of the experiments with samples containing low amounts of magnetite (< 10 wt.%). The saturation index (SI) with respect to siderite at the end of the experiments with magnetite-containing samples was calculated using PHREEQC and wateq4f.dat database. The SI values ranged from -0.42 to 0.41 (Table A1.5 in AP1), indicating near-equilibrium conditions. The examination of the solid samples retrieved at the end of the experiments (see details in AP1) back up the formation of magnetite as the main biogenic Fe^{2+}-bearing mineral during iron bioreduction under the investigated conditions. Hence, experimental and model results suggest that the amount of magnetite in sediments impacted by STD could become an important factor to control the formation of different secondary Fe^{2+}-bearing minerals (e.g., magnetite and/or siderite). This could have strong implications on the distribution of trace metals eventually released in the environment during iron (hydr)oxides reductive dissolution.

The maximum increase in the rates of aqueous Fe(II) concentration (Fig. 2.2 and Fig. A1.5 in AP1) were estimated from the simulations. Values from 0.07 to 0.26 $\mu M\ h^{-1}$ were calculated for the experiments with magnetite containing samples. The rates for the experiments with synthetic hematite and goethite were within the range of magnetite containing samples, whereas the rate determined for ferrihydrite (4.4 $\mu M\ h^{-1}$) was clearly above.

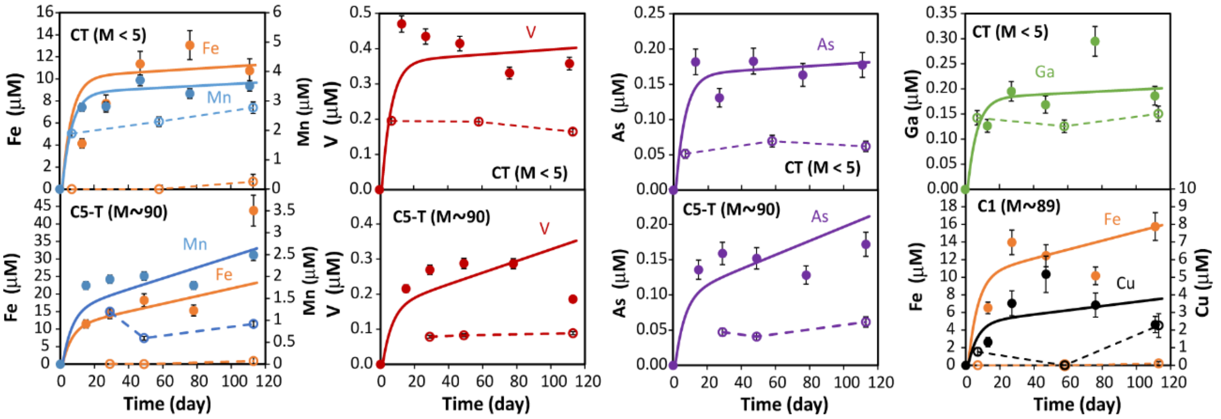

Figure 2. 4. Evolution of dissolved Fe(II) and selected TEs during the experiments. Solid lines represent the model simulations. Empty symbols and dashed lines correspond to the concentrations determined in the abiotic controls. Weight % of magnetite (M) in the samples is in brackets.

Along with Fe, several trace metal(loid)s (Mn, V, As and Cu) were detected in solution (< 1 mg L^{-1}) (Fig. 2.3). According to PHREEQC inorganic speciation calculations, the elements released in solution were present as free species and chloride complexes (i.e., Fe^{2+}, Mn^{2+}, $FeCl^{+}$, $MnCl^{+}$, $CuCl_3^{2-}$, $CuCl^{-}$). Arsenic was mainly found as As(III) (i.e., H_3AsO_3), which is more toxic than As(V) [56]. It might increase the concentrations of labile TEs in sediments impacted by STD. Mn and V were among those TEs with high concentrations in the magnetite ore samples (Fig. 2.1). Other elements (Ni and Ga) were detected in solution only in few samples and/or at lower concentrations (Fig. 2.3). However, Ni concentrations in the magnetite ore samples were in general relatively high, similar to those of Mn (Fig. 2.1). Despite Co and Ti concentrations were above 100 mg Kg^{-1} in some magnetite samples, their concentrations were below detection limit (2 and 7 mg L^{-1}, respectively). These results suggest that other processes such as coprecipitation within secondary biogenic Fe^{2+}-minerals may control the fate of Ni, Co and Ti during reductive dissolution of magnetite under the investigated conditions. This is in agreement with the observations of previous Fe(III) bioreduction studies [57, 58] using synthetic oxyhydroxides coprecipitated with either Co or Ni. For instance, the incorporation and site occupancies of Co and Ni into the structure of biogenic magnetite were determined [58]. Data from the literature is available in AP1.

For a better understanding of the fate of TEs, a stoichiometric release of TEs to the aqueous phase during magnetite reductive dissolution was simulated for the C1 and C5-

T magnetite ore samples and the CT tailings sample (Fig. 2.4). The calculated stoichiometric coefficients for the different elements were compared with those expected from the TEs composition of magnetite in the respective samples (AP1). The results suggest that part of As and V released by reductive dissolution of magnetite in C5-T and CT samples could be incorporated into secondary biogenic minerals (mainly magnetite) and/or adsorbed on the remaining magnetite and gangue minerals. A previous study [59] showed removal of As(III) and As(V) from solution at neutral pH (higher from As(III)- than from As(V)-solution) associated with coprecipitation of Fe(III) oxides and subsequent adsorption of As on the fresh Fe(III) oxides. Wang et al., [60] investigated the interaction of aqueous As(III) during magnetite precipitation experiments at neutral pH. They observed arsenite sequestration via surface adsorption and surface precipitation reactions. In the present study, As in solution was mainly H_3AsO_3 suggesting that the effect of adsorption could be limited by the lack of electrostatic attraction compared to other aqueous As species.

2.4. CONCLUSIONS

Our data show that iron oxides such as magnetite can undergo reductive dissolution under marine sediment conditions, leading to a potential release of Fe and associated TEs to the marine environment.

As most ore deposits contain iron (hydr)oxides and sulfides, the resulting tailings most likely contain both mineral groups, which are unstable under anoxic and oxic conditions, respectively.

It is also known that the geochemical regime along continental shelves like those in South America (e.g. Chile, Peru) can change from reducing (Oxygen Minimum Zone; OMZ) to oxidizing conditions during upwelling or ENSO (El Niño–Southern Oscillation) events in days or weeks [61]. Therefore, the presence of both reactive mineral groups (metal oxides and sulfides) in the tailings and the continuous changes of the geochemical conditions can result in i) a permanent reactivity of the minerals in the changing marine environment and ii) the release of Fe and TEs. It depends on the amount of reactive minerals and associated TEs in the tailings whether might be a toxicological risk for the marine fauna.

Moreover, solubilization of Fe, a limiting nutrient for phytoplankton production [62] might lead to additional fertilization and subsequent eutrophication, which may result in oxygen depletion and expansion of the OMZ along the continental shelfs [63]. Thus, besides the known smothering of benthic organisms and physical alteration of seabed habitats [8, 9] geochemical processes leading to dissolution of reactive minerals and subsequent release of associated nutrients and TEs have to be regarded as potential negative impacts on the marine ecosystem.

Due to the complexity of the reactive mineralogy and geochemical conditions in the marine environment, a stable situation where no dissolution reactions occur is thus unlikely, increasing thus the risk for unpredicted reactivity of STD.

2.5. REFERENCES

1. Younger, P.L.B., S. A.; Hedin, R. S., *Mine Water - Hydrology, Pollution, Remediation*. 2002, Dordrecht: Kluwer Academic Publishers. 442.

2. Lottermoser, B.G., *Mine Wastes: Characterization, Treatment and Environmental Impacts*. Mine Wastes: Characterization, Treatment and Environmental Impacts. 2010, Berlin: Springer-Verlag Berlin. 1-400.

3. Mudd, G.M., *Global trends in gold mining: Towards quantifying environmental and resource sustainability?* Resources Policy, 2007. **32**(1-2): p. 42-56.

4. Franks, D.M., et al., *Sustainable development principles for the disposal of mining and mineral processing wastes.* Resources Policy, 2011. **36**(2): p. 114-122.

5. Dold, B., *Evolution of Acid Mine Drainage Formation in Sulphidic Mine Tailings.* Minerals, 2014. **4**(3): p. 621-641.

6. Rico, M., G. Benito, and A. Diez-Herrero, *Floods from tailings dam failures.* J Hazard Mater, 2008. **154**(1-3): p. 79-87.

7. Dold, B., *Submarine Tailings Disposal (STD)-A Review.* Minerals, 2014. **4**(3): p. 642-666.

8. Ramirez-Llodra, E., et al., *Submarine and deep-sea mine tailing placements: A review of current practices, environmental issues, natural analogs and knowledge gaps in Norway and internationally.* Mar Pollut Bull, 2015. **97**(1-2): p. 13-35.

9. Morello, E.B., et al., *The ecological impacts of submarine tailings placement*, in *Oceanography and Marine Biology: An Annual Review, Vol 54*, R.N. Hughes, et al., Editors. 2016, Crc Press-Taylor & Francis Group: Boca Raton. p. 315-366.

10. Hughes, D.J., et al., *Ecological impacts of large-scale disposal of mining waste in the deep sea.* Scientific Reports, 2015. **5**: p. 11.

11. Koski, R.A., *Metal Dispersion Resulting from Mining Activities in Coastal Environments: A Pathways Approach.* Oceanography, 2012. **25**(2): p. 170-183.

12. Pedersen, K.B., et al., *Long-term dispersion and availability of metals from submarine mine tailing disposal in a fjord in Arctic Norway.* Environ Sci Pollut Res Int, 2018. **25**(33): p. 32901-32912.

13. Sternal, B., et al., *The impact of submarine copper mine tailing disposal from the 1970s on Repparfjorden, northern Norway.* Mar Pollut Bull, 2017. **120**(1-2): p. 136-153.

14. Angel, B.M., et al., *Trace metals associated with deep-sea tailings placement at the Batu Hijau copper-gold mine, Sumbawa, Indonesia.* Marine Pollution Bulletin, 2013. **73**: p. 306-313.

15. Embile, R.F., Jr., et al., *Cu, Pb and Fe release from sulfide-containing tailings in seawater: Results from laboratory simulation of submarine tailings disposal.* Mar Pollut Bull, 2018. **137**: p. 582-592.

16. Simpson, S.L. and D.A. Spadaro, *Bioavailability and Chronic Toxicity of Metal Sulfide Minerals to Benthic Marine Invertebrates: Implications for Deep Sea Exploration, Mining and Tailings Disposal.* Environ Sci Technol, 2016. **50**(7): p. 4061-70.

17. Ignacio Manteca, J., et al., *The beach placer iron deposit of Portman Bay, Murcia, SE Spain: the result of 33 years of tailings disposal (1957-1990) to the Mediterranean seaside.* Mineralium Deposita, 2014. **49**(6): p. 777-783.

18. Trannum, H.C., et al., *Effects of submarine mine tailings on macrobenthic community structure and ecosystem processes.* Sci Total Environ, 2018. **630**: p. 189-202.

19. Wong, M.H., et al., *Metal contents of the two marine algae found on iron ore tailings.* Marine Pollution Bulletin, 1979. **10**(2): p. 56-59.

20. Nystrom, J.O. and F. Henriquez, *Magmatic features of iron-ores of the Kiruna type in Chile and Sweden - Ore textures and magnetite geochemistry.* Economic Geology and the Bulletin of the Society of Economic Geologists, 1994. **89**(4): p. 820-839.

21. Knipping, J.L., et al., *Trace elements in magnetite from massive iron oxide-apatite deposits indicate a combined formation by igneous and magmatic-hydrothermal processes.* Geochimica Et Cosmochimica Acta, 2015. **171**: p. 15-38.

22. Nadoll, P., et al., *Geochemistry of magnetite from porphyry Cu and skarn deposits in the southwestern United States.* Mineralium Deposita, 2015. **50**(4): p. 493-515.

23. Makvandi, S., et al., *Principal component analysis of magnetite composition from volcanogenic massive sulfide deposits: Case studies from the Izok Lake (Nunavut, Canada) and Halfmile Lake (New Brunswick, Canada) deposits.* Ore Geology Reviews, 2016. **72**: p. 60-85.

24. Boutroy, E., et al., *Magnetite composition in Ni-Cu-PGE deposits worldwide: application to mineral exploration.* Journal of Geochemical Exploration, 2014. **145**: p. 64-81.

25. Dare, S.A.S., et al., *Trace elements in magnetite as petrogenetic indicators.* Mineralium Deposita, 2014. **49**(7): p. 785-796.

26. Nadoll, P., et al., *The chemistry of hydrothermal magnetite: A review.* Ore Geology Reviews, 2014. **61**: p. 1-32.

27. Hubner, R., K.B. Astin, and R.J. Herbert, *Comparison of sediment quality guidelines (SQGs) for the assessment of metal contamination in marine and estuarine environments.* J Environ Monit, 2009. **11**(4): p. 713-22.

28. Lovley, D.R., D.E. Holmes, and K.P. Nevin, *Dissimilatory Fe(III) and Mn(IV) reduction*, in *Advances in Microbial Physiology, Vol. 49*, R.K. Poole, Editor. 2004. p. 219-286.

29. Kappler, A. and K.L. Straub, *Geomicrobiological cycling of iron*, in *Molecular Geomicrobiology*, J.E. Banfield, J. CerviniSilva, and K.H. Nealson, Editors. 2005. p. 85-108.

30. Devol, A.H., *Denitrification, anammox, and N(2) production in marine sediments.* Ann Rev Mar Sci, 2015. **7**: p. 403-23.

31. Ribet, I., et al., *The potential for metal release by reductive dissolution of weathered mine tailings.* Journal of Contaminant Hydrology, 1995. **17**(3): p. 239-273.

32. Zachara, J.M., et al., *Solubilization of Fe(III) oxide-bound trace metals by a dissimilatory Fe(III) reducing bacterium.* Geochimica et Cosmochimica Acta, 2001. **65**: p. 75-93.

33. Schwertmann, U. and R.M. Cornell, *Iron oxides in the laboratory: preparation and characterization*. 2008: John Wiley & Sons.

34. Bish, D.L. and S. Howard, *Quantitative phase analysis using the Rietveld method.* Journal of Applied Crystallography, 1988. **21**(2): p. 86-91.

35. Brunauer, S., P.H. Emmett, and E. Teller, *Adsorption of gases in multimolecular layers.* Journal of the American chemical society, 1938. **60**(2): p. 309-319.

36. Gao, H., et al., *Shewanella loihica sp. nov., isolated from iron-rich microbial mats in the Pacific Ocean.* International Journal of Systematic and Evolutionary Microbiology, 2006. **56**(8): p. 1911-1916.

37. Roh, Y., et al., *Metal reduction and iron biomineralization by a psychrotolerant Fe (III)-reducing bacterium, Shewanella sp. strain PV-4.* Applied and Environmental Microbiology, 2006. **72**(5): p. 3236-3244.

38. Parkhurst, D.L. and C. Appelo, *User's guide to PHREEQC (Version 2)(Equations on which the program is based).* Water-Resources Investigations Report, 1999. **99**: p. 4259.

39. Watson, I.A., et al., *Modeling kinetic processes controlling hydrogen and acetate concentrations in an aquifer-derived microcosm.* Environmental science & technology, 2003. **37**(17): p. 3910-3919.

40. Liu, C., et al., *Microbial reduction of Fe (III) and sorption/precipitation of Fe (II) on Shewanella putrefaciens strain CN32.* Environmental science & technology, 2001. **35**(7): p. 1385-1393.

41. Roden, E.E. and Q. Jin, *Thermodynamics of microbial growth coupled to metabolism of glucose, ethanol, short-chain organic acids, and hydrogen.* Applied and environmental microbiology, 2011. **77**(5): p. 1907-1909.

42. Maier, R.M. and I.L. Pepper, *Bacterial growth*, in *Environmental microbiology*. 2015, Elsevier. p. 37-56.

43. Thullner, M., P. Van Cappellen, and P. Regnier, *Modeling the impact of microbial activity on redox dynamics in porous media.* Geochimica et Cosmochimica Acta, 2005. **69**(21): p. 5005-5019.

44. Thullner, M., P. Regnier, and P. Van Cappellen, *Modeling microbially induced carbon degradation in redox-stratified subsurface environments: concepts and open questions.* Geomicrobiology Journal, 2007. **24**(3-4): p. 139-155.

45. Usman, M., et al., *Magnetite and green rust: synthesis, properties, and environmental applications of mixed-valent iron minerals.* Chemical reviews, 2018. **118**(7): p. 3251-3304.

46. Santschi, P., et al., *Chemical processes at the sediment-water interface.* Marine chemistry, 1990. **30**: p. 269-315.

47. Devol, A.H., *Denitrification, anammox, and N2 production in marine sediments.* Annual review of marine science, 2015. **7**: p. 403-423.

48. Urrutia, M., et al., *Microbial and surface chemistry controls on reduction of synthetic Fe (III) oxide minerals by the dissimilatory iron-reducing bacterium Shewanella alga.* Geomicrobiology Journal, 1998. **15**(4): p. 269-291.

49. Burgos, W.D., et al., *Theoretical and experimental considerations related to reaction-based modeling: A case study using iron (III) oxide bioreduction.* Geomicrobiology Journal, 2002. **19**(2): p. 253-287.

50. Gorski, C.A. and M.M. Scherer, *Fe2+ sorption at the Fe oxide-water interface: A revised conceptual framework*, in *Aquatic Redox Chemistry*. 2011, ACS Publications. p. 315-343.

51. Gorski, C.A. and M.M. Scherer, *Influence of magnetite stoichiometry on FeII uptake and nitrobenzene reduction.* Environmental science & technology, 2009. **43**(10): p. 3675-3680.

52. Cheng, W., R. Marsac, and K. Hanna, *Influence of magnetite stoichiometry on the binding of emerging organic contaminants.* Environmental science & technology, 2018. **52**(2): p. 467-473.

53. Dong, H., et al., *Mineral transformations associated with the microbial reduction of magnetite.* Chemical Geology, 2000. **169**(3-4): p. 299-318.

54. Liu, C., et al., *Kinetic analysis of the bacterial reduction of goethite.* Environmental Science & Technology, 2001. **35**(12): p. 2482-2490.

55. Castro, L., et al., *Heavy metal adsorption using biogenic iron compounds.* Hydrometallurgy, 2018. **179**: p. 44-51.

56. Jain, C. and I. Ali, *Arsenic: occurrence, toxicity and speciation techniques.* Water research, 2000. **34**(17): p. 4304-4312.

57. Zachara, J.M., et al., *Solubilization of Fe (III) oxide-bound trace metals by a dissimilatory Fe (III) reducing bacterium.* Geochimica et Cosmochimica Acta, 2001. **65**(1): p. 75-93.

58. Coker, V.S., et al., *Probing the site occupancies of Co-, Ni-, and Mn-substituted biogenic magnetite using XAS and XMCD.* American Mineralogist, 2008. **93**(7): p. 1119-1132.

59. Guo, H., D. Stüben, and Z. Berner, *Adsorption of arsenic (III) and arsenic (V) from groundwater using natural siderite as the adsorbent.* Journal of colloid and interface science, 2007. **315**(1): p. 47-53.

60. Wang, Y., et al., *Arsenite sorption at the magnetite–water interface during aqueous precipitation of magnetite: EXAFS evidence for a new arsenite surface complex.* Geochimica et Cosmochimica Acta, 2008. **72**(11): p. 2573-2586.

61. Ulloa, O., et al., *Evolution and biological effects of the 1997–98 El Nino in the upwelling ecosystem off northern Chile.* Geophysical Research Letters, 2001. **28**(8): p. 1591-1594.

62. Boyd, P.W., et al., *A mesoscale phytoplankton bloom in the polar Southern Ocean stimulated by iron fertilization.* Nature, 2000. **407**(6805): p. 695-702.

63. Breitburg, D., et al., *Declining oxygen in the global ocean and coastal waters.* Science, 2018. **359**(6371).

CHAPTER 3.

IRON (HYDR)OXIDES BIOREDUCTION PROCESS:

COLUMN EXPERIMENTS

Bioreduction of Fe-oxides contained in mine tailings deposited under marine conditions releases Fe and associated trace elements (e.g., Ti, Ni, Cd, Pb, etc.). This process leads to a potential contamination of the marine environment. Two column experiments filled with samples from the mine tailings of two STD sites (Portman Bay in Spain and Ensenada Chapaco in Chile) were carried out to study the bioreduction process under marine conditions, in which organic matter (i.e., lactate) is permanently provided. The results obtained were compared with those from batch experiments performed under similar conditions.

This chapter describes how bioreduction took place in the experiments. In the column filled with Portman Bay tailings, the high content of magnetite provides a high magnetite surface area and a high number of available Fe(III), yielding an initially high release of Fe(II) and TE. As Fe(II) adsorbs onto the magnetite surface decreasing the Fe(III) availability, the magnetite bioreduction and the consequent TE release decrease after 2000 h. By contrast, in the column filled with Ensenada Chapaco tailings, the magnetite bioreduction lasts longer (3000 h). The reason is that the lower magnetite content in the tailings provides less reactive surface area yielding less available Fe(III). As a consequence, the concentrations of Fe(II) and TE in the output solutions are lower, slowing down the Fe(II) adsorption onto magnetite and resulting in a longer magnetite bioreduction. In the column experiments, bioreduction is regulated by the Fe(III) availability in contrast with the previous batch experiments.

From the experimental results, a variation in the bioreduction rate is calculated as a function of time and Fe(II) concentration. Moreover, the concentrations of TE released from the two bioreduced tailings exceed the elemental concentrations found under natural marine conditions.

3.1. INTRODUCTION

As explained in the previous chapters, sea tailings disposal is a major environmental concern regarding mine waste management. Flotation process revolutionized mining activity in the early twentieth century owing to the strong capacity to exploit low-grade ores and thus increasing considerably the volume of tailings. Tailings are waste that remains after the ore is passed through crushing, milling and flotation stages in order to extract the target minerals, but also overburden and the country was rock extracted in the mining process [1]. Historically a relatively small number of mines have discharged tailings and mining waste into the marine environment [2]. In 2015, only 16 of the current 2500 large industrialized mines worldwide utilized STD [3], restricted to a few countries (e.g., Norway, Papua New Guinea, Chile). Nowadays, large active mines in Norway continue using STD [4, 5]. Yet 15-20 mines are considering STD as a future disposal option [4, 6, 7]. The international legislation framework for STD (Convention on the Prevention of Marine Pollution by Dumping of Wastes and Other Matter 1972, also known as the “London Convention” and the “London Protocol” from 1996) prohibits all dumping of wastes into the sea, except for wastes “inert, inorganic geological material” under which tailings may fall [8, 9].

In the present work, the mine tailings of two STD cases are studied. The first one is related to the deposition that took place in Portman Bay (La Unión, Spain) from 1958 to 1991. The second one relates to the STD at Ensenada Chapaco (Huasco, Chile) that lasted from 1978 to 2018. Metal contamination of sea water associated with STD has been reported for Chañaral Bay (North of Chile) [10, 11] and Portman Bay [12].

Portman Bay is located at La Unión municipality (Murcia, SE Spain). Due to its proximity to the Sierra de Cartagena-La Unión mining district, an ore concentration facility was opened in the bayside (Lavadero Roberto) to treat complex ores from the mining deposits [13]. In the 33 years of Lavadero Roberto functioning, tailings were pumped directly to the sea (Fig. 3.1), until the end of exploitation in 1991. About 60 Mt of tailings were disposed onto the sea, leaving behind hazardous (metal-rich) artificial soils and moving the shoreline 500-600 m to the sea. This caused the most critical case of pollution by mine wastes in the western Mediterranean and contributed to 50% of the heavy metal input and around 90% of the solid waste input to the Mediterranean Sea. At present, more than 80% of Portman Bay is filled with tailings, corresponding to 70 ha previously occupied by the sea [14].

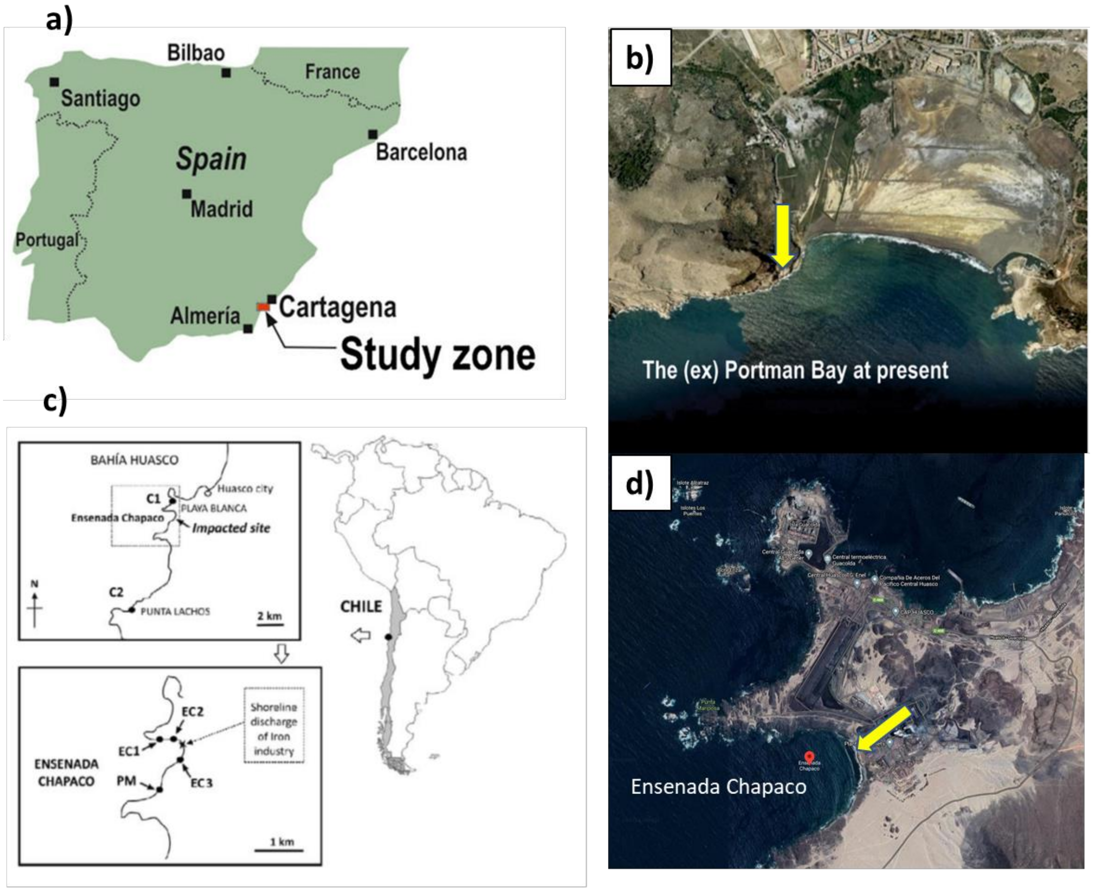
a)
Bilbao
France
Santiago
Spain
Barcelona
Madrid
Portugal
Almería
Cartagena
Study zone
b)
The (ex) Portman Bay at present
c)
BAHÍA HUASCO
Huasco city
C1
PLAYA BLANCA
Ensenada Chapaco
Impacted site
N
C2
PUNTA LACHOS
2 km
CHILE
ENSENADA CHAPACO
EC2
EC1
PM
EC3
Shoreline discharge of Iron industry
1 km
d)
Ensenada Chapaco

Figure 3. 1. Mine disposal sites in Spain and Chile: a) location of Portman Bay in La Unión, southern Iberian Peninsula; b) aerial photograph of Portman Bay filled with the tailings; c) location of Ensenada Chapaco in Huasco, northern Chile and d) aerial photograph of Ensenada Chapaco where an iron oxide pellet plant is located. The yellow arrows indicate the location of the tailings disposal pipes [12] [15].

Ensenada Chapaco belongs to the Huasco municipality (Atacama region, Chile). An iron oxide pellet plant is located in the bayside and receives mining material mainly from Los Colorados mine, an iron oxide-apatite (IOA) mineral deposit, and from the El Algarrobo and Los Cristales mines. The mining activity began in 1978 and ended in 2018. The plant generated daily 4000 Mt of tailings that were disposed into the sea at 500 m offshore (Fig. 3.1). Earlier studies evaluated the effect of 16 years of tailings disposal in the intertidal zone (1978–1994) on the macro benthic community. A prolonged deposition of mine tailings in the sea bed caused a significantly suffering of in terms of abundance, species richness, diversity and high dominance, and caused deep changes in community structure due to the tailings deposition [16].

The environmental impact of STD is a major concern that affects not only the ocean ecosystems but also sea fishing and pollution. It is therefore necessary to understand the geochemical evolution of tailings depositions into the sea, where iron-mineral bioreduction with the consequent release of iron and trace metals (TEs) can perniciously impact the marine ecosystems.

In this study, a quantitative interpretation of the release of Fe and TE from the tailings, i.e., Fe-oxide bioreduction, is performed for a better understating of the environmental impact of tailings disposal on the sea sediments. To this end, two column experiments filled with the mine tailings from Portman Bay and Ensenada Chapaco were carried out under marine conditions similar to those of these sites. Moreover, a batch experiment with the Portman Bay tailings sample was performed to compare the magnitude of the bioreduction process in a column (open system) with that in a batch (closed system). In both experiments, the release of Fe(II) and trace metals was monitored over time.

3.2. MATERIALS AND METHODS

3.2.1. Tailings characteritzation

The tailings used in this study were from the tailings deposition sites of Portman Bay (PORT) and Ensenada Chapaco (CT). The PORT column was filled with tailings from Portman Bay accumulated at the seashore. The sample was collected from the top 50 cm using a hand core sampler and placed in sterile zip-lock plastic bags that were stored in the freezer at 4 ^{0}C until use. Subsequently, the sample was ground and sieved to a size fraction between 60 and 100 μm. Powder XRD-Rietveld analysis was performed for the mineralogical characterization of the sample (Table 3.1). The CT column was filled with tailings from the iron oxide pellet plant. The tailings sample was obtained from the treatment plant and placed in a sterile zip-lock plastic bag to be stored at room temperature. Some amount was centrifuged 3 times in order to remove pore water. The resulting sample was sieved to a size fraction between 60 and 100 µm. Powder XRD-Rietveld analysis was carried to determine the mineralogical composition of the sample (Table 3.1). Both tailings samples were autoclaved before filling the columns, and an additional powder XRD analysis was performed to detect any possible new mineral. No mineralogical changes occurred.

Table 3. 1. Mineralogical composition (wt. %) of the Portman Bay (PORT) and Ensenada Chapaco (CT) tailings used in the experiments.

Mineral	CT	PORT
Magnetite	1	15
Chlorite	22	
Hornblende	30	
Albite	28	
Hydrocalcite	3	
Talc	16	
Pyrite		37
Siderite		32
Jarosite		8
Marcasite		5
Quartz		3

3.2.2. Experimental setup

3.2.2.1. Column experiments

Two column experiments were conducted using two methacrylate columns of 8 cm in diameter and 10 cm long. The columns were filled from bottom to top with five layers of glass beads, acid washed sand and tailings sample (Fig. 3.2a). All layers were 1.6 cm thick with a volume of 0.08 L. The bottom layer was made of glass beads, the second layer of acid washed sand, the third layer was composed of inoculated tailings samples (CT and PORT), the fourth layer was made of acid washed sand, and the top layer was made of glass beads (Fig. 3.2a). The porosities of the tailings layers were 60% (CT) and 40% (PORT). Thereafter, the filled columns were saturated with marine medium and allowed to equilibrate overnight.

A peristaltic pump was used to circulate the marine medium through the columns from bottom to top (Fig. 3.2b). The flow rates were maintained constant at approximately 0.003 mL min^{-1}, yielding residence times of 7.4 d and 11.1 d in the PORT and CT layers, respectively.

The columns were immersed in a water bath at 10 ºC (Fig. 3.2b). The bath was covered with an opaque lid to guarantee dark conditions. Colum immersion prevented O_2 diffusion through the wall columns. A bottle with the input marine medium solution was placed in a glove box purged with N_2 to ensure anoxic conditions (Fig. 3.2b). Metal tubing (stainless steel, 0.02 m inner diameter) was used to connect the input and output solution bottles with the columns in order to prevent O_2 diffusion. Input and output solutions were collected from the respective bottles placed in the anoxic glove box. The experiments lasted 167 days.

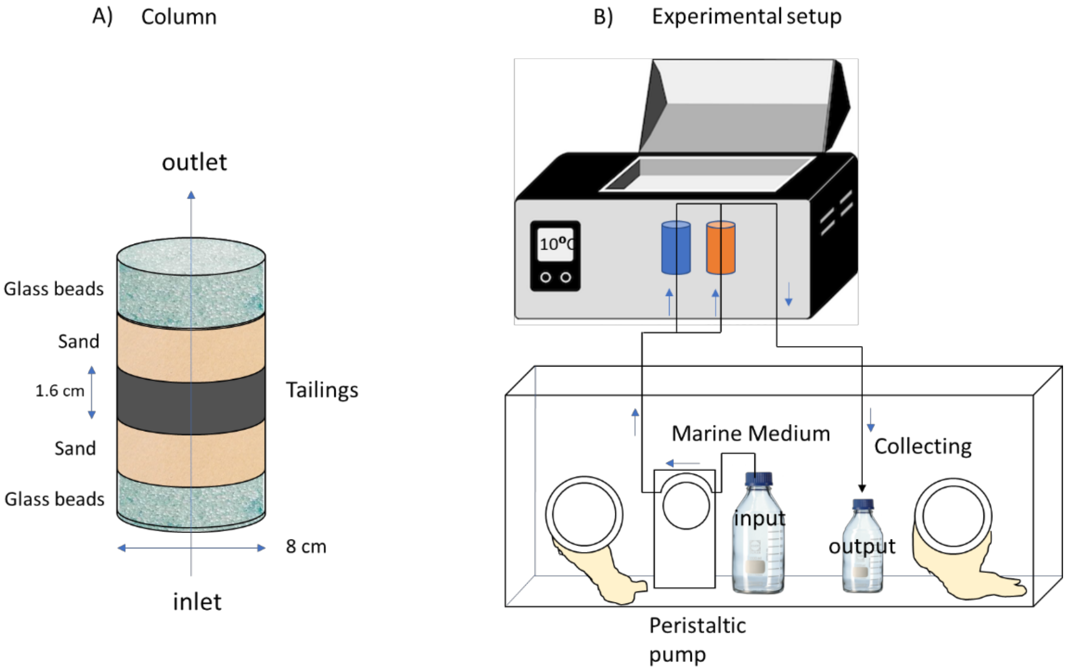
A) Column
outlet
Glass beads
Sand
1.6 cm
Tailings
Sand
Glass beads
8 cm
inlet
B) Experimental setup
10ºC
Marine Medium
Collecting
input
output
Peristaltic pump

Figure 3. 2. Schematics that show: a) a column with the five layers of glass beads, sand and tailings sample and b) the experimental setup.

3.2.2.2. Batch experiments

One batch experiment with the PORT tailings sample was performed following the procedure described in Section 2.3 (Chapter 2).

3.2.3. Bacterial culture and marine medium

Bacterial culture and medium preparation were carried out following the procedure described in Section 2.2 (Chapter 2). The marine medium composition is shown in Table 3.2. Before the experiments, the marine medium was sterilized in an autoclave and bubbled with a constant N_2 flow to remove dissolved oxygen.

Table 3. 2. Chemical composition of the marine medium.

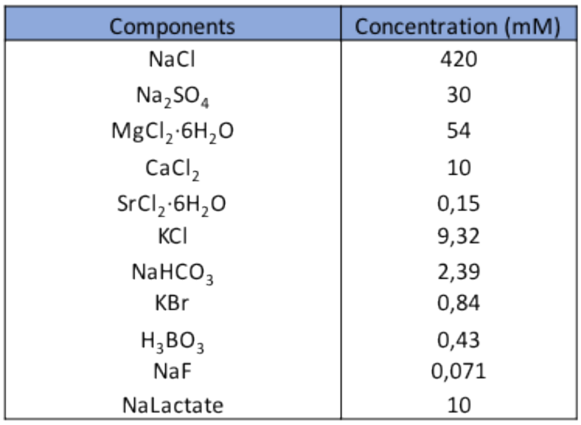

Components	Concentration (mM)
NaCl	420
Na_2SO_4	30
$MgCl_2·6H_2O$	54
$CaCl_2$	10
$SrCl_2·6H_2O$	0,15
KCl	9,32
$NaHCO_3$	2,39
KBr	0,84
H_3BO_3	0,43
NaF	0,071
NaLactate	10

3.2.4. Chemical analysis

Measurements of pH (± 0.02 pH units) and Eh (± 10 mV) were performed using pH and Eh electrodes (Crison and SenTix ORP, Ag/AgCl, WTW, respectively) in the glove box under anoxic conditions. Oxidation-reduction potential readings were converted to standard Eh values by correcting for the electrode potential of the reference hydrogen electrode. At each sampling time, solutions were collected in acid washed tubes, and two aliquots were taken for analysis. One aliquot was acidified with 100 µL of fuming HCl (37%) to measure lactate and acetate by High Pressure Liquid Chromatography (HPLC). The second aliquot was acidified with 100 µL of 65% nitric acid to measure the concentrations of minor and major elements by Inductively Coupled Plasma (ICP). The aliquots were stored at 4 °C until analysis.

A Waters 600 HPLC pump controller equipped with an Aminex HPX-87H column (300 x 7.8 mm), BioRad, and a Waters 717 plus autoinjector were used for the HPLC measurements of lactate and acetate. Concentrations of minor elements were analyzed by Inductively Coupled Plasma Mass Spectrometry (ICP-MS) with a Perkin Elmer 350D spectrometer. The analysis of major elements was performed by ICP Optical Emission Spectroscopy (ICP-OES) with a Perkin Elmer Optima 8300 spectrometer equipped with a CID detector (Charge Injection Device). The uncertainty of the ICP-MS and ICP-OES measurements was better than ± 5%. Concentrations of total iron and ferrous iron (Fe(II)) were measured following a modified protocol of the Phenanthroline method [17] with a SP268 830 PLUS, Metertech Inc. spectrophotometer. Triplicate measurements were performed for iron, lactate and acetate.

3.3. RESULTS AND DISCUSSION

3.3.1. Tailings composition

Table 3.1 lists the mineralogical composition of the PORT and CT tailings. PORT tailings were mainly composed of pyrite, siderite and magnetite, having, hence, high contents of Fe(III) and Fe(II). By contrast, a 1 wt.% of magnetite in the CT tailings yielded a low Fe content. The differences in mineral composition between the two tailings are caused by the concentration processes utilized in the respective processing plants. In the Ensenada Chapaco plant, although magnetite is the main ore in Los Colorados mine, most of the profitable iron is in the pellets, leaving a poor Fe(III) content in the CT tailings [18]. Moreover, high concentrations of TEs (e.g., V, Ti, Mn, Al, Pb and Zn) were detected in the magnetite from Los Colorados deposit [19].

On the other hand, La Unión mine had different profitable sources during the years of operation. Changes in mineral extraction due to economic interests (mainly between galena and sphalerite), and the fact that the company did not recover magnetite from the tailings resulted in tailings highly enriched in magnetite. This explains the high Fe(II)-Fe(III) content in the PORT tailings [20]. Moreover, the magnetite present in the Portman Bay tailings is rich in TEs such as Pb, Zn, Cu, As and Cd [21, 22]).

3.3.2. Aqueous chemistry: Portman tailings

3.3.2.1. Column experiment

The two columns were run under an advective flow regime, in which the presence of *Shewanella loihica* prompted the oxidation of lactate to acetate coupled to reduction of Fe(III) to Fe(II). In the PORT column, Fe was highly released ([Fe] was up to 61mM) in the first 300 h (Fig. 3.3a). Thereafter, the Fe concentration gradually decreased until the end of the experiment. Manganese and zinc behaved similarly with an initial high release ([Mn] and [Zn] = 20 mM) that was followed by a gradual decrease (Fig 3.3a). Lactate followed a trend that was similar to that of iron release (Fig. 3.3b). A high lactate consumption took place in the onset of the experiment with a consequent release of acetate. Over time, lactate consumption and acetate production decreased gradually to concentrations below detection limit. The initial solution pH was 8.2, and as reactions occurred, it decreased to about 4 remaining during lactate consumption (Fig. 3.3c). Thereafter, the output pH slowly increased to reach the initial pH value. Eh decreased from 200 mV to 50 - 60 mV in the experiment (Fig 3.3d).

As for the TE release, the concentrations of Ti, V, Pb, Ni, Cd and Co decreased gradually as occurred with that of Fe(II) (Fig. 3.4a-f)). This variation indicates that the TE release is related to bioreduction, i.e., to lactate consumption. Cu is also released (Fig. 3.4g), but the release is rather constant throughout the experiment.

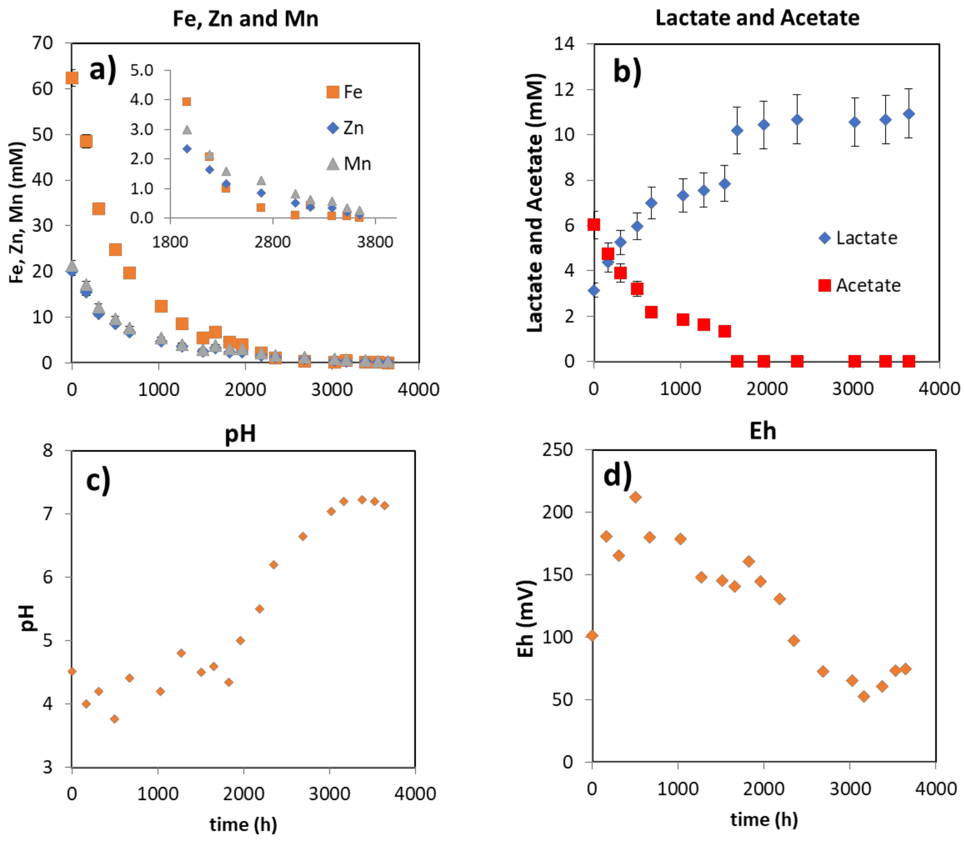

Figure 3. 3. Variation of (a) the concentrations of Fe (II), Zn and Mn, and (b) lactate and acetate and (c) pH and (d) Eh as a function of time in the PORT column.

The gradual decrease in the TE concentrations along with that of Fe(II) indicated the occurrence of magnetite bioreduction. A high microbial activity led to a high magnetite bioreduction that accounted for the elevated TE release in the first hours of the experiment (Fig. 3.3 and 3.4). A decrease in the activity of *S. loihica* was inferred from a diminishment of lactate consumption accompanied by a decrease in the concentrations of Fe (II) and TE. Note that in the column experiments, the carbon source is constant as lactate is permanently injected. Therefore, lactate consumption is not the limiting factor for bioreduction. The cease of microbial activity observed after 2000 h was caused by a low Fe(II) bioavailability in the tailings, since the Fe(II) released during magnetite bioreduction is partially adsorbed on the magnetite surface [23] as explained in Chapter 2.

The TE release was similar to that of TE and Fe(II) in the batch experiments (see Section 2.3.3 in Chapter 2). This suggests that some of the TE released from magnetite bioreduction could be incorporated into the secondary biogenic magnetite or adsorbed onto the remaining gangue minerals [24, 25].

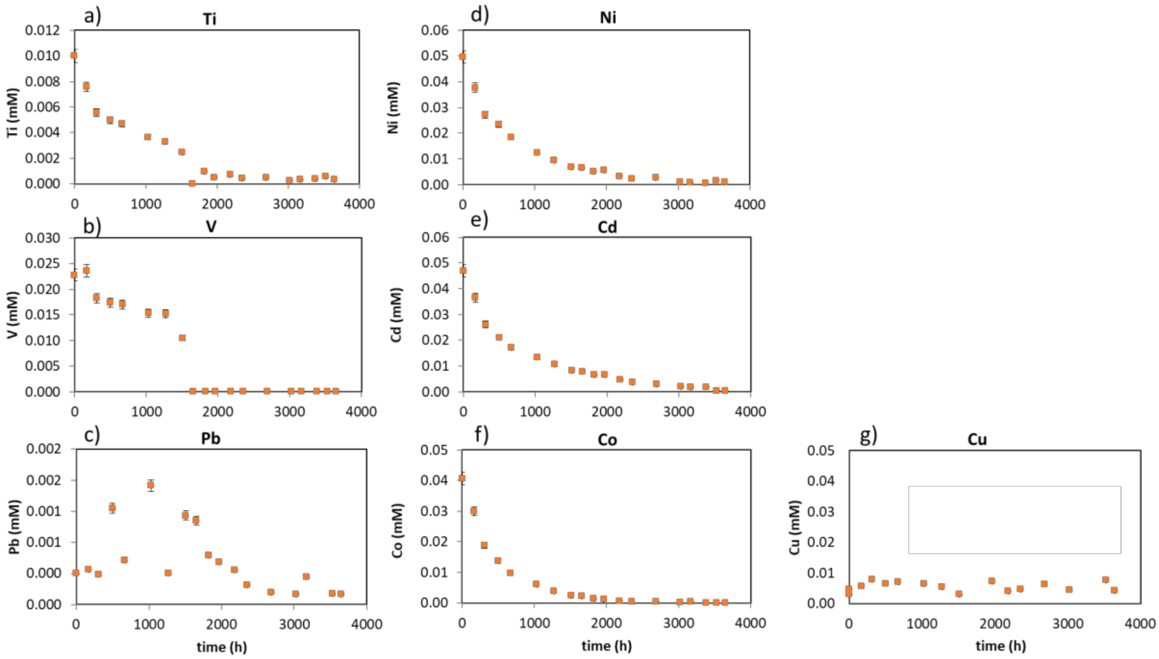

Figure 3. 4. Variation in the concentration of trace element as a function of time in the PORT column: a) Titanium, b) Vanadium, c) Lead, d) Nickel, e) Cadmium, f) Cobalt and g) Copper.

3.3.2.2. Batch experiment

In the batch experiment, bioreduction of the PORT tailings also occurred under marine conditions. At the start of the experiment, manganese was highly released before iron (Fig. 3.5a), indicating that Mn contained in the magnetite [26, 27] can also be bioreduced and that *Shewanella loihica* shows a preference for Mn before Fe [28]. Similar trends in the release in Mn were observed in magnetite with high content of Mn (see Section 2.3.3 in Chapter 2). Nevertheless, an initial Fe(II) adsorption onto magnetite cannot be ruled out [25].

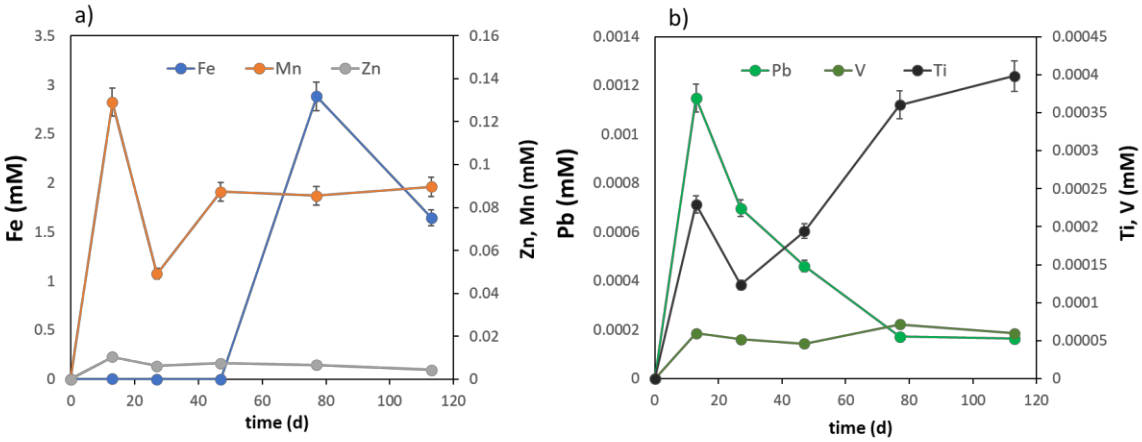

Figure 3. 5. Variation in the concentrations of Fe, Mn and Zn (a) and trace metals (Pb, V and Ti) (b) as a function of time in the batch experiment with Portman tailings.

The Fe(II) release occurred after Mn was mostly reduced after about 50 d (Fig. 3.5a). The amounts of Fe(II) released in the column and in the batch experiments were similar (1.28 mmol and 1.15 mmol Fe(II) $g_{tailing}^{-1}$, respectively). A release of TEs (Zn, Pb, V and Ti) also took place throughout the experiment (Fig. 3.5a,b). The release of Zn, Pb and V was similar to that of Mn, i.e., a fast initial increase was followed by a decrease. By contrast, the concentration of Ti increased over time along with the Fe release. The TE behavior observed in the batch was similar to that in the column experiment, suggesting the occurrence of magnetite bioreduction with Fe(II) adsorption onto the magnetite surface.

3.3.3. Aqueous chemistry: CT tailings

3.3.3.1. Column Experiment

In the CT column, a rather constant Fe release ([Fe] ≈ 10μm) occurred during the experimental run (Fig. 3.6a). Mn and Zn release was similar to that of Fe(II), i.e., rather constant ([Zn] = 20 μM; Fig. 3.6a), although a gradual increase in the Zn output concentration occurred in the first 1000 h. Lactate consumption and acetate production accompanied the Fe(II) release (Fig 3.6b), Being lactate consumption higher in the first 1000 h. As explained in Chapters 1 and 2 the produced acetate was, however, lower than the stoichiometric one (Eq. (2.2)) due to a bacterial biomass production. After 1000 h, lactate consumption decreased and remained constant until the conclusion of the experiment. The output solution pH was nearly the same as the input solution pH of 8.2 throughout the experiment (Fig 3.6c). Eh slowly dropped from 150-200 mV to 50 mV throughout the experimental (Fig 3.6d). These Eh values (50mV) indicate a level of oxide-reduction similar to the iron reduction measured in sea sediment [29].

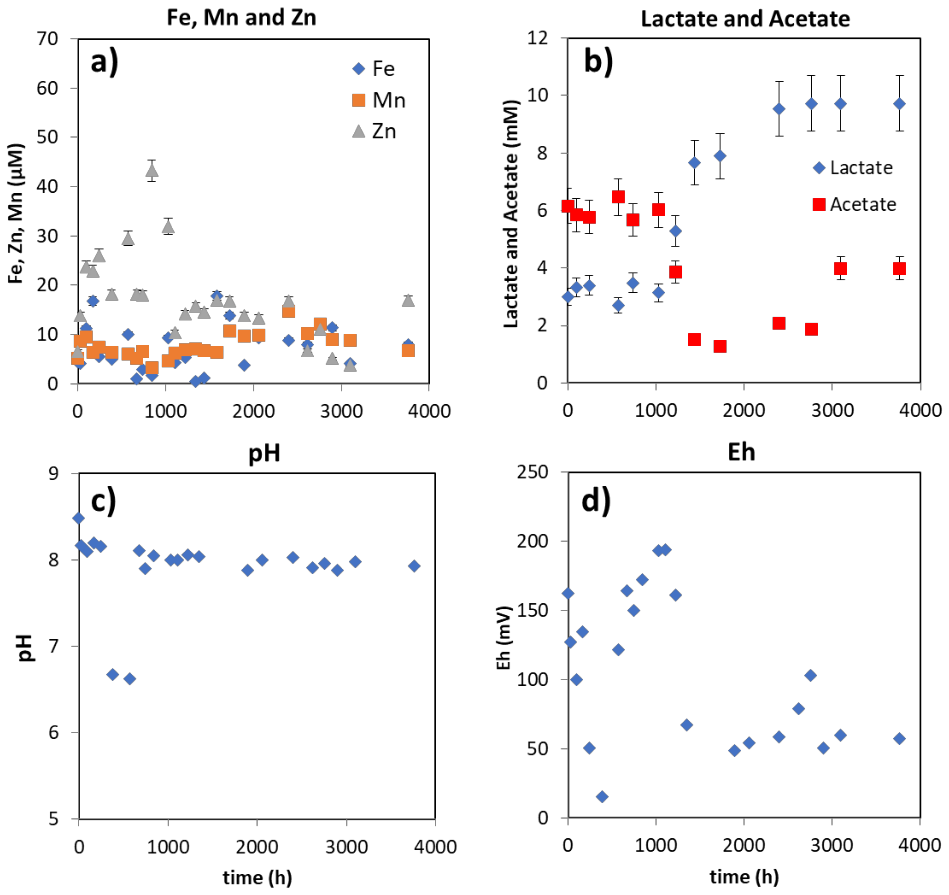

Figure 3. 6. Variation in the concentrations of (a) Fe, Mn and Zn, (b) lactate and acetate, (c) pH and Eh (d) as a function of time in the CT column.

Figure 3.7 shows the TE release over time. A high V release is observed in the first 165 h. Thereafter, the concentration drops and remains constant for the next 800 h. Subsequently, the concentration increases and remains constant until the end of the experiment (Fig. 3.7a). The Zn concentration pattern is somehow similar for the concentrations of Ti, Ni, and Cd (Fig. 3.7b-d). Cu concentration varies between 4 and 15 µM throughout the experiment (Fig. 3.7e). Pb is highly released in the first half of the experiment (≈2000 h), and thereafter it gradually decreases (Fig. 3.7f). Overall, the TE release agrees in magnitude with those observed in the batch experiments (Chapter 2) and in previous studies [30], in which an incorporation of Co and Ni into the structure of biogenic magnetite was proposed. Vanadium, Copper and Nickel high release had been observed in both batch and column experiments. Column has shown also release in Titanium, Lead and Cadmium.

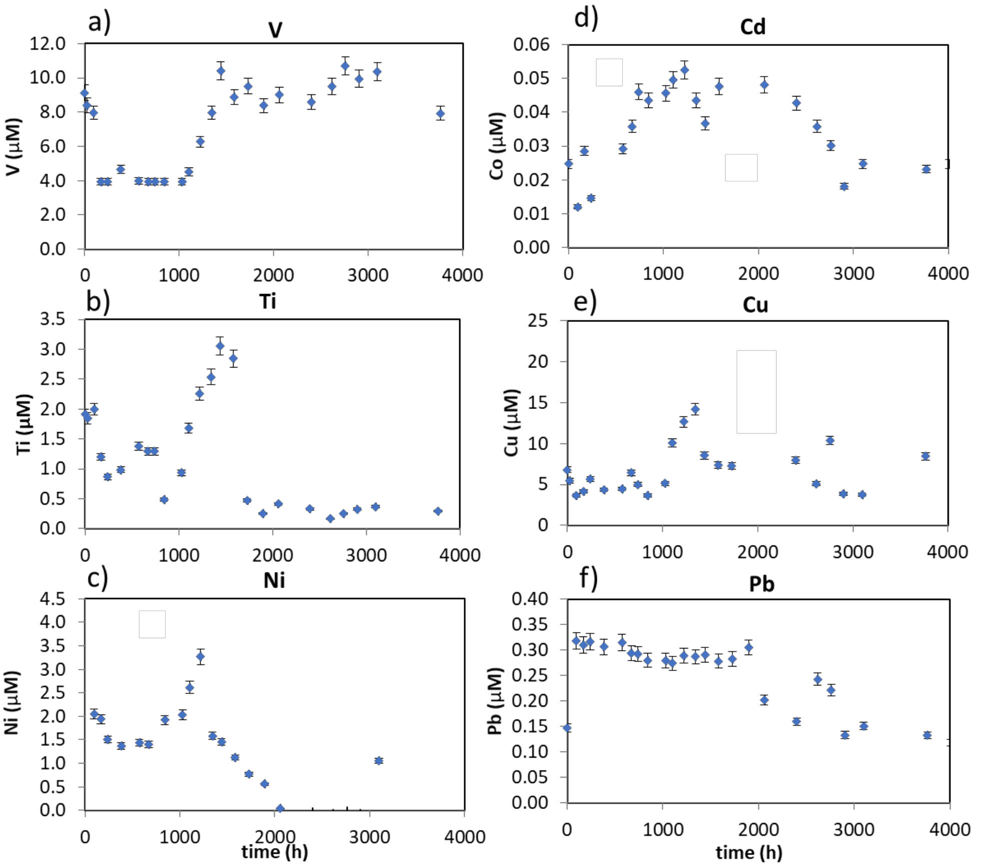

Figure 3. 7. TE release as a function of time in the CT column: a) Vanadium, b) Titanium, c) Nickel, d) Cd, e) Copper, f) Lead.

3.3.4. Comparison between PORT and CT tailings

In order to compare the occurrence of the Fe(III) bioreduction occurred between the PORT column and the CT column, the initial amount of Fe(III) in the respective tailings samples must be taken into account. The magnetite content in the CT tailings is lower than that in the PORT tailings (Table 3.1), and hence the initial content of Fe(III):

168.3 mmol and 5.4 mmol in the PORT and CT tailings, respectively. Therefore, the magnitude of bioreduction is expected to be higher in the PORT column than in the CT column.

In the PORT column, after normalizing the release of bioreduced Fe(II) to the initial content of Fe(III) in the tailings sample, a 95% of Fe(III) is practically consumed after 2000 h (Fig. 3.3a). At this point, the low microbial activity is dependent on the remaining low Fe(III) concentration. By contrast, in the CT column, the bioreduced Fe (III) was 8%. This significant difference in bioreduced Fe(III) explains the difference in Fe(II) released throughout the experiments. The decrease in the microbial activity is due to the low thermodynamic efficiency of *S. loihica* to use the Fe(III) present in the CT tailings as a terminal electron acceptor (TEA). Thus, as explained in Chapter 2, *S. loihica* is unable to maintain a sufficient bacterial population using a low profit TEA, limiting the Fe(III) bioreduction [31-33].

As explained in Chapter 1 (Section 1.4.1 and Fig 1.4), a key parameter in the bioreduction kinetics is the reactive surface area of the iron (hydr)oxide involved in the reaction. Hence, a high surface area availability enables a high bacterial attachment, increasing thus the bioreduction rate. Furthermore, a previous study [34] showed that biogenic iron mineral transformation is strongly controlled by the kinetic properties of the reaction system (e.g., chemical and biological dissolution kinetics and the presence of catalysts). Since the magnetite content in the CT tailings sample is low, there is little magnetite surface area available for *S. loihica* to attach and bioreduce [35]. Thus, a lowe reactive surface area likely leads to a low bioreduction in the CT column. In the PORT column, the magnetite content is higher than in the CT column, providing more magnetite reactive surface area for a higher bioreduction rate.

In the column experiments, in contrast with the batch experiments, lactate is permanently provided. In the batch experiments, the ratio between lactate and available Fe(III) was smaller than that in the columns. Therefore, magnetite bioreduction is controlled by available Fe(III) rather than available lactate, and the availability of Fe(III) is proportional to the magnetite reactive surface area. The geochemical model that includes the Monod kinetics [30, 36] to calculate the bioreduction rate (see Eq. (2.2) and kinetic parameterization in Section 2.4; Chapter 2) was used to determine the reactive surface area effect on the bioreduction rate in each column experiment using the PHREEQC code [37] (Fig. 3.8). Since the Fe(III) content and the magnetite surface area are higher in the PORT tailings column, the initial bioreduction rate was higher in the PORT column (≈ $7.0 \cdot 10^{-7}$ mol s^{-1}) than in the CT column ($5.6 \cdot 10^{-7}$ mol s^{-1}) (Fig. 3.8a,c).

In the PORT column, the higher magnetite surface area led to a higher bioreduction rate that induced an initially high Fe(II) release (Fig. 3.3a). However, a sharp decrease in Fe(II) took place because the Fe(II) released adsorbed onto the magnetite surface, reducing its reactive surface area. As a consequence of this latter mechanism the Fe(III) available for the bacteria diminished, leading to a decrease in the bioreduction rate (Fig. 3.8a).

In the CT column, the bioreduction rate remained constant for 1000 h (Fig 3.8b) as inferred from the constant Fe(II) concentration (Fig 3.6a). Thereafter, the rate drops in the following 1500 h until bioreduction practically ceases after 2500 h (Fig. 3.8c). However, as the initial release of Fe(II) is lower than that in the PORT experiment, the effect of Fe (II) adsorption on the bioreduction rate is smaller. In this case, Fe(II) adsorption is slower, and available Fe(III) for the bacteria to reduce remains longer. In both columns, the bioreduction rates increase with aqueous Fe(II) (Fig 3.8b,d).

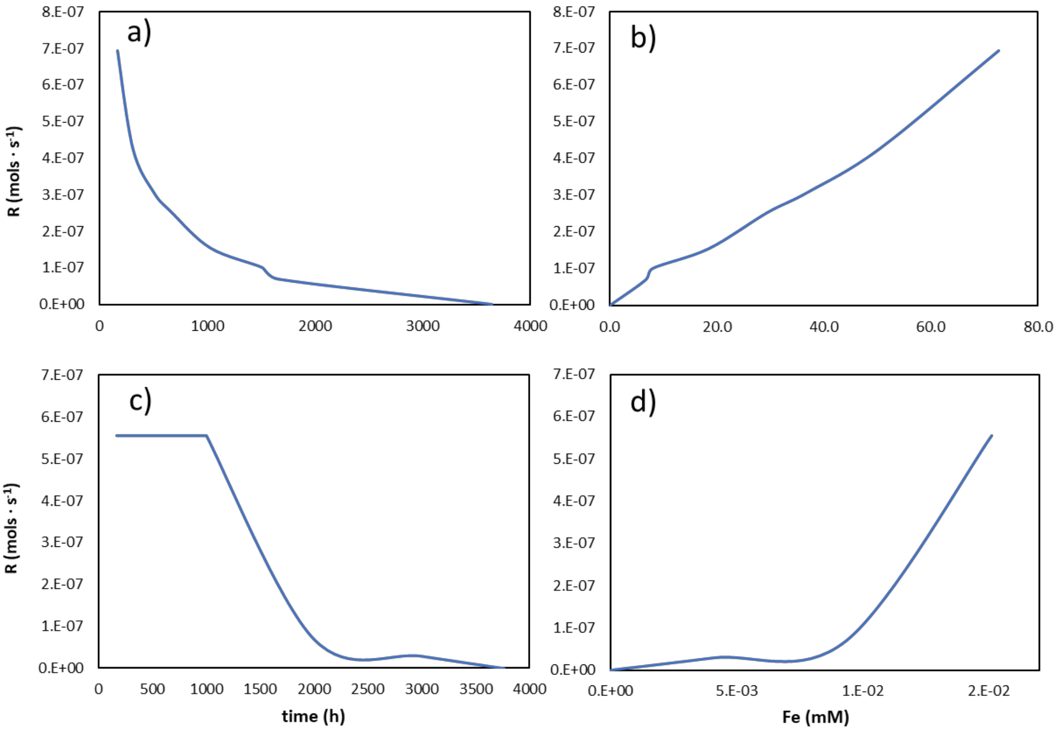

Figure 3. 8. Variation in the bioreduction rate (mol s^{-1}) as a function of: a) time and b) Fe(II) concentration (mM) in the PORT column; variation in the bioreduction rate (mol s^{-1}) as a function of: c) time and d) Fe concentration (mM) in the CT column.

3.4. CONCLUSIONS

The column experiments performed with the Portman Bay and Ensenada Chapaco tailings showed the occurrence of magnetite bioreduction under marine conditions (i.e., O_2-free atmosphere and 10 °C in the dark).

In the two columns, the trace elements contained in the magnetite were released together with Fe(II), and the release was similar to that in the batch experiments. The vanadium, copper and nickel release showed a similar trend in both the column and batch experiments. Furthermore, in the column experiments, other TE (titanium, lead and cadmium) were released

Given that lactate was permanently provided in the columns, magnetite bioreduction was only dependent on the availability of Fe(III), which depended on the content and reactive surface area of magnetite. As Fe(II) adsorbed onto magnetite inducing the formation of a secondary magnetite (biomineralization), the reactive surface area decreased, limiting the availability of Fe(III) and thus lowering the bioreduction rate. Magnetite bioreduction lasted longer in the CT column than in the PORT column (3000 h and 2000 h, respectively). Duration of bioreduction depended on the magnetite content and the resulting magnetite reactive surface area, which provided reducible Fe(III). The bioreduction rate decreased with the decrease in reactive surface area, which was caused by Fe(II) adsorption onto magnetite.

The variation of the bioreduction rates was calculated as a function of time and Fe(II) concentration. The estimates are suitable for STD management.

The overall process suggests that a continuous disposal of mine tailings in the sea could induce a lasting tailings bioreduction and the consequent TE release as long as Fe(III) is available.

The concentrations of the TE released in the columns and batch experiments exceed those found under natural marine conditions. Hence, TE release from iron oxide mine tailings augments the environmental risk by enhancing metal contamination and accumulation in the flora and fauna of the sea [38].

3.5. REFERENCES

1. Dold, B.J.M., *Submarine tailings disposal (STD)—A review.* 2014. **4**(3): p. 642-666.

2. Vare, L.L., et al., *Scientific considerations for the assessment and management of mine tailings disposal in the deep sea.* 2018. **5**: p. 17.

3. Stud., G.J.R., *Proceedings of the GESAMP International Workshop on the Impacts of Mine Tailings in the Marine Environment.(IMO/FAO/UNESCO-IOC/UNIDO/WMO/IAEA/UN/UNEP/UNDP Joint Group of Experts on the Scientific Aspects of Marine Environmental Protection).* 2016. **94**: p. 84.

4. Jensen, T. and K. Hylland, *Environmental adaptive management: application on submarine mine tailings disposal.* Integrated environmental assessment and management, 2019. **15**(4): p. 575-583.

5. Bøe, R., et al., *Marine mine tailings disposal at Lillebukt, Stjernsundet, North Norway: distribution, sedimentary processes and depositional impacts.* Norwegian Journal of Geology/Norsk Geologisk Forening, 2018. **98**(3).

6. Davies, E.J. and R. Nepstad, *In situ characterisation of complex suspended particulates surrounding an active submarine tailings placement site in a Norwegian fjord.* Regional studies in marine science, 2017. **16**: p. 198-207.

7. Ramirez-Llodra, E., et al., *Guidelines and best available techniques for submarine tailings disposal in Norwegian fjords: Recommendations from the NYKOS project.* NIVA-rapport, 2019.

8. Kwong, Y.J., et al., *Comparison of Environmental Impacts of Deep-sea Tailings Placement Versus On-land Disposal.* Water, Air, & Soil Pollution, 2019. **230**(12): p. 287.

9. Nurbani, E.S., *Tailing Disposal System: Indonesia's Policy and Future Challenges.* Journal of Liberty and International Affairs, 2020(03): p. 83-95.

10. Medina, M., et al., *Biodiversity of rocky intertidal benthic communities associated with copper mine tailing discharges in northern Chile.* Marine Pollution Bulletin, 2005. **50**(4): p. 396-409.

11. Dold, B., *Element flows associated with marine shore mine tailings deposits.* Environmental science & technology, 2006. **40**(3): p. 752-758.

12. Manteca, J.I., et al., *The beach placer iron deposit of Portman Bay, Murcia, SE Spain: the result of 33 years of tailings disposal (1957–1990) to the Mediterranean seaside.* Mineralium Deposita, 2014. **49**(6): p. 777-783.

13. Peña, J.A., et al., *Magnetic gradient map of the mine tailings in Portman Bay (Murcia, Spain) and its contribution to the understanding of the bay infilling process.* 2013. **95**: p. 115-120.

14. Ramade, F., *Conservation des écosystèmes méditerranéens: enjeux et perspectives*. 1990: UNEP-MAP/BP-RAC.

15. González, S.A., W. Stotz, and D. Lancellotti, *Effects of the discharge of iron ore tailings on subtidal rocky-bottom communities in northern Chile.* Journal of Coastal Research, 2014. **30**(3): p. 500-514.

16. Lancellotti, D. and W.J.M.P.B. Stotz, *Effects of shoreline discharge of iron mine tailings on a marine soft-bottom community in northern Chile.* 2004. **48**(3-4): p. 303-312.

17. Stucki, J., *The Quantitative Assay of Minerals for Fe2+ and Fe3+ Using 1, 10-Phenanthroline: II. A Photochemical Method.* Soil Science Society of America Journal, 1981. **45**(3): p. 638-641.

18. Knipping, J.L., et al., *Trace elements in magnetite from massive iron oxide-apatite deposits indicate a combined formation by igneous and magmatic-hydrothermal processes.* 2015. **171**: p. 15-38.

19. Knipping, J.L., et al., *Trace elements in magnetite from massive iron oxide-apatite deposits indicate a combined formation by igneous and magmatic-hydrothermal processes.* Geochimica et Cosmochimica Acta, 2015. **171**: p. 15-38.

20. Manteca, J.I., et al., *The beach placer iron deposit of Portman Bay, Murcia, SE Spain: the result of 33 years of tailings disposal (1957–1990) to the Mediterranean seaside.* 2014. **49**(6): p. 777-783.

21. Gomez-Garcia, C., et al., *Rock magnetic characterization of the mine tailings in Portman Bay (Murcia, Spain) and its contribution to the understanding of the bay infilling process.* Journal of Applied Geophysics, 2015. **120**: p. 48-59.

22. Pérez-Sirvent, C., et al., *Assessment of potentially toxic element contamination in soils from Portman Bay (SE, Spain).* Journal of Soils and Sediments, 2018. **18**(6): p. 2248-2258.

23. Boland, D.D., et al., *Effect of solution and solid-phase conditions on the Fe (II)-accelerated transformation of ferrihydrite to lepidocrocite and goethite.* Environmental science & technology, 2014. **48**(10): p. 5477-5485.

24. Williams, A.G. and M.M. Scherer, *Spectroscopic evidence for Fe (II)– Fe (III) electron transfer at the iron oxide– water interface.* Environmental science & technology, 2004. **38**(18): p. 4782-4790.

25. Gorski, C.A. and M.M. Scherer, *Fe2+ sorption at the Fe oxide-water interface: A revised conceptual framework*, in *Aquatic Redox Chemistry*. 2011, ACS Publications. p. 315-343.

26. Frietsch, R., *Chemical composition of magnetite and sphalerite in the iron and sulphide ores of central Sweden.* Geologiska Föreningen i Stockholm Förhandlingar, 1982. **104**(1): p. 43-47.

27. Lu, R. and S.K. Banerjee, *Magnetite dissolution in deep sediments and its hydrologic implication: a detailed study of sediments from site 808, leg 131.* Journal of Geophysical Research: Solid Earth, 1994. **99**(B5): p. 9051-9059.

28. Gao, H., et al., *Shewanella loihica sp. nov., isolated from iron-rich microbial mats in the Pacific Ocean.* International Journal of Systematic and Evolutionary Microbiology, 2006. **56**(8): p. 1911-1916.

29. Lovley, D.R. and E.J. Phillips, *Organic matter mineralization with reduction of ferric iron in anaerobic sediments.* Applied and environmental microbiology, 1986. **51**(4): p. 683-689.

30. Liu, C., et al., *Kinetic analysis of the bacterial reduction of goethite.* Environmental Science & Technology, 2001. **35**(12): p. 2482-2490.

31. Liu, C., et al., *Microbial reduction of Fe (III) and sorption/precipitation of Fe (II) on Shewanella putrefaciens strain CN32.* Environmental science & technology, 2001. **35**(7): p. 1385-1393.

32. Urrutia, M., et al., *Microbial and surface chemistry controls on reduction of synthetic Fe (III) oxide minerals by the dissimilatory iron-reducing bacterium Shewanella alga.* Geomicrobiology Journal, 1998. **15**(4): p. 269-291.

33. Burgos, W.D., et al., *Theoretical and experimental considerations related to reaction-based modeling: A case study using iron (III) oxide bioreduction.* Geomicrobiology Journal, 2002. **19**(2): p. 253-287.

34. Dippon, U., et al., *Secondary mineral formation during ferrihydrite reduction by Shewanella oneidensis MR-1 depends on incubation vessel orientation and resulting gradients of cells, Fe2+ and Fe minerals.* Geomicrobiology Journal, 2015. **32**(10): p. 878-889.

35. El-Naggar, M.Y., et al., *Electrical transport along bacterial nanowires from Shewanella oneidensis MR-1.* Proceedings of the National Academy of Sciences, 2010. **107**(42): p. 18127-18131.

36. Watson, I.A., et al., *Modeling kinetic processes controlling hydrogen and acetate concentrations in an aquifer-derived microcosm.* Environmental science & technology, 2003. **37**(17): p. 3910-3919.

37. Parkhurst, D.L. and C. Appelo, *User's guide to PHREEQC (Version 2)(Equations on which the program is based).* Water-Resources Investigations Report, 1999. **99**: p. 4259.

38. Halden, N. and L. Friedrich, *Trace-element distributions in fish otoliths: natural markers of life histories, environmental conditions and exposure to tailings effluence.* Mineralogical Magazine, 2008. **72**(2): p. 593-605.

CHAPTER 4.

IRON BIOREDUCTION AND ITS IMPLICATION IN THE NITROGEN CYCLE

In this chapter, I describe how bioreduced Fe(II), either as an aqueous or solid-bound species, interacts with the nitrite present in estuarine sediments, which are often rich in iron (hydr)oxides, organic matter and anthropogenic nitrogen compounds.

Nitrite reduction coupled with Fe(II) oxidation was studied performing two sets of experiments with ferrihydrite. In one set, ferrihydrite reacted in anoxic synthetic seawater in the presence of *Shewanella loihica*. Some bioproduced Fe(II) adsorbed on ferrihydrite whereas the remainder intervened in the ferrihydrite transformation to magnetite. In a second set, synthetic Fe(II) was added in the solution. With similar Fe(II) concentration in both sets, the reduction rate of abiotic NO_2^- was higher in the experiments with bioproduced Fe(II) than with those with synthetic Fe(II), yielding half-lives of 0.07 and 0.47 d, respectively.

The isotopic study of the overall process showed similar $\varepsilon^{18}O/\varepsilon^{15}N$ ratios for the abiotic experiments. A lower $\varepsilon^{18}O/\varepsilon^{15}N$ (3.3) ratio was, however, obtained for the heterotrophic denitrification of NO_2^- by *S. loihica*. Since these $\varepsilon^{18}O/\varepsilon^{15}N$ values are close to or within the wide range of values reported in the literature for the abiotic and biotic nitrite reduction, the use of this ratio to distinguish different mechanisms of nitrite reduction at field scale might be limited. Alternatively, the correlation between $\delta^{15}N$-NO_2 and the aqueous Fe(II) concentrations might be used to elucidate the processes controlling the NO_2^- fate in natural settings.

4.1. INTRODUCTION

The intensive use of organic and inorganic fertilizers and domestic and industrial waste waters are mainly responsible for nitrogen input and contamination of water resources [1]. Marine sediments in estuarine and coastal areas often contain terrigenous organic matter and other constituents such as iron and nitrogen compounds (e.g., NO_x) via riverine and submarine groundwater inputs [2]. In such environments, marine dissimilatory iron reducing bacteria (e.g., *Shewanella loihica*) are able to reduce Fe(III)-oxide minerals [3] under anoxic conditions producing aqueous and mineral-associated Fe(II) (reaction 4.1) [4]. Bio-produced Fe(II) can abiotically reduce nitrite (NO_2^-) via formation of nitrous oxide (N_2O) (reaction 4.2) [5].

$$CH_3CHOHCOO^- + 4Fe(OH)_3 + 7H^+ \rightarrow CH_3COO^- + HCO_3^- + 4Fe^{2+} + 10H_2O \quad (4.1)$$

$$4Fe^{2+} + 2NO_2^- + 5H_2O \rightarrow 4FeOOH + N_2O + 6H^+ \quad (4.2)$$

Nitrous oxide is a potent greenhouse gas and the single greatest ozone-depleting substance [6]. In recent years, nitrite reduction caused by Fe(II) oxidation, i.e., chemodenitrification, is the subject of much research given its environmental relevance [5, 7-9].

Both iron and nitrogen cycles are related in anaerobic environments where bioreduction of Fe(III)-(hydr)oxides (also referred to as hydrous ferric oxides (HFO), such as ferrihydrite (Fh)) leads to nitrite reduction coupled with Fe(II) oxidation[10]. Since nitrite reduction occurs in the presence of aqueous Fe(II) and in the absence of HFO [11, 12], higher abiotic NO_2^- reduction rates have been observed in the presence of solid iron phases [5, 13, 14]. Tai and Dempsey [5] have observed higher NO_2^- reduction rates when the aqueous Fe(II)/HFO ratio was 0.3 compared to ratios > 0.3, halting the reduction when the aqueous Fe(II) concentrations became low or null even in the presence of mineral-associated Fe(II). Furthermore, the abiotic NO_2^- reduction was negligible in the absence of HFO. In experiments with aqueous Fe(II) and nitrite, precipitation of HFO or mixed valence (Fe^{2+}, Fe^{3+}) iron minerals will probably occur owing to the oxidation of aqueous Fe(II)[8, 15].

Solid Fe(II) (also referred to as structural or solid-bound Fe(II)) may be involved in nitrite reduction [16] together with the dissolved Fe(II). Dhakal et al. [14] studied the ability of magnetite to reduce nitrite and showed that abiotic NO_2^- reduction by magnetite had a greater impact on nitrite removal than microbially mediated denitrification. However, Lu et al. [8] showed that magnetite was not able to reduce nitrite in a wide concentration range (30-280 mg L^{-1}) in the absence of solid-bound Fe(II). No information on abiotic nitrite reduction in experiments with freshly biogenic magnetite in marine environment is available to date.

To date, the evaluation of abiotic nitrogen reduction coupled with oxidation of Fe(II) in heterogenous systems at laboratory scale has been performed by with the addition of synthetic Fe(II) (e.g., $FeCl_2$) to aqueous solutions with different iron minerals [8, 11, 17]. However, in natural settings ferrous iron can derive from microbial reduction of Fe(III)-minerals. Dissimilatory Fe(III) reduction could alter the properties of the iron mineral surface or result in the formation of secondary iron mineral phases such as magnetite or siderite [18]. The evaluation of abiotic nitrite reduction is therefore required in systems closer to natural conditions.

In this study, ferrihydrite was the Fe(III) mineral used in biotic and abiotic nitrite reduction experiments where Fe(II) was either (i) added (as $FeSO_4$) or (ii) bio-produced by *Shewanella loihica* strain PV-4 at similar aqueous concentrations. The *S.loihica* strain PV-4 is able to reduce Fe(III) oxides and hydroxides in seawater under anoxic conditions [19]. Ferrihydrite is ubiquitous in the environment and is abundant in marine sediment [20]. Given its thermodynamic instability and large surface area, ferrihydrite has a high reactivity in the presence of aqueous Fe(II), which may lead to a mineral transformation made up of more crystalline phases containing Fe(II) such as magnetite [21-25].

Isotopic analysis is a useful tool for tracing NOx transformation processes. The enzymatic NO_3^- reduction provokes an enrichment in the heavy isotopes ^{15}N and ^{18}O of the unreacted substrate [26-29] unlike processes such as dilution that could lead to a decrease in concentration without influencing the isotopic signature. The same pattern is expected for the biotic reduction of all N intermediate products (e.g. NO_2^- or N_2O), which will be initially depleted in ^{15}N and ^{18}O with respect to the substrate. However, data on the dual N-O isotope systematics during the biotic reduction of intermediate compounds such as NO_2^- remain scarce [30, 31]. Moreover, two recent isotopic studies on the abiotic NO_2^- reduction by Fe(II) found results similar to what is expected from the biotic reaction [7, 9]. From the isotopic data in earlier studies, it is unclear to what degree the isotopic characterization might help in distinguishing biotic and abiotic NO_2^- reduction. Further studies on the potential of isotopic data to elucidate the process controlling the fate of nitrite in the field are therefore warranted.

In the present study, biotic and abiotic NO_2^- reduction experiments using synthetic and bio-produced Fe(II) were performed with anoxic synthetic sea water i) to shed light on the kinetics of NO_2^- reduction in marine environments and ii) to evaluate the possible use of isotopic analysis to distinguish between abiotic and biotic (heterotrophic) NO_2^- reduction. In addition, the reductive dissolution of ferrihydrite mediated by *Shweanella loihica* and the fate of bio-produced Fe(II) was investigated.

4.2. MATERIALS AND METHODS

4.2.1. Solutions

Synthetic sea water (SSW) was prepared to simulate marine sediment conditions following the standard protocol D1141-98 (ATSM International). In addition to this basal medium, 10 mM of sodium lactate as a carbon source and electron donor and 10 mM of TRIS-HCl (Tris) as a buffer (pH ≈ 8.2) were added. Hereafter, this medium will be referred to as M-SSW.

Stock solutions of Fe(II) at pH 1 (HCl) and NO_2^- (12.8 and 2.8 g L^{-1}, respectively) were prepared in an anoxic glove box dissolving suitable amounts of $FeSO_4$ and KNO_2, respectively, in ultrapure Milli-Q water (Merck Millipore) previously degassed with N_2. Both solutions were subsequently filtered (0.22 μm) and stored in sterile bottles.

All solutions used in this study were sterilized by autoclave (121 ^{0}C, 20 min) unless stated otherwise. Dissolved oxygen concentrations were measured by luminescent dissolved oxygen (LDO) probe (detection limit 0.01 mgL^{-1}).

4.2.2. Bacterial culture

Shewanella loihica strain PV-4 was purchased from the German Collection of Microorganisms and Cell Cultures (DSMZ 17748). Bacteria were recovered and cultivated in M1 medium [32] with 10 mM of lactate as electron donor and carbon source and 10 mM of Fe(III) citrate as electron acceptor. To obtain bacterial suspension, cells were cultivated for 24 h and then harvested by centrifugation (5000 rpm for 10 min). Pellet was re-suspended in SSW. This step was repeated three times as a washing protocol. *S.loihica* was inoculated with a concentration of $1\cdot10^7$ colony-forming units (cfu) mL^{-1}.

4.2.3. Ferrihydrite: synthesis and characterization

2L-ferrihydrite was synthesized according to a modified protocol of Schwertmann and Cornell (2007) (see APPENDIX 2 (AP2) for more details). The specific surface area was measured by the Brunauer-Emmett-Teller (BET) method [33] with a Gemini 2370 surface area analyzer using 5-point N_2 adsorption isotherms. Sample degassing with nitrogen lasted for 2 h at 137 °C. The BET specific surface area measured for unreacted samples varied between 140 and 180 m^{2}g^{-1}, and for the bioreacted samples it was between 144 and 152 m^2 g^{-1}.

The reacted and unreacted samples were examined by three techniques: (1) scanning electron microscopy (SEM) using a Hitachi H-4100FE instrument under a 15–20 kV potential in a high vacuum and utilizing the backscattered electron detector (BSD) in field emission (FE) and coating the samples with carbon; (2) X-ray diffraction (XRD) using a *PANalytical X'Pert PRO MPD θ/θ* Bragg-Brentano powder diffractometer of 240 mm in radius and Cu Kα radiation (λ = 1.5418 Å), and (3) Fourier transform infrared spectrometry (FTIR) utilizing a Perkin Elmer frontier/ATR diamond/detector DTGS, accumulation at 16 scans, spectral resolution 4 cm^{-1}, spectral range 4000 - 225 cm^{-1}.

4.2.4. Experimental setup and sampling procedure

Table 4.1 lists the initial experimental conditions. All batch experiments were run in the dark (bottles wrapped with aluminum foil) and in triplicate at 22 ± 2 °C. Bottles were placed in an anoxic glove box purged of N_2 and equipped with UV germicidal light for periodical sterilization. Glassware, septa, caps, tips and media solutions were sterilized by autoclave at 121 °C for 20 min before the experiments.

4.2.4.1. Abiotic nitrite reduction experiments with bio-produced Fe(II)

These batch experiments consisted of two stages. In the first stage, Fe(II) was bioproduced before NO_2^- addition (experiment Ferr; Table 4.1). The anaerobic reductive dissolution of ferrihydrite mediated by *S. loihica* strain PV-4 was performed in cultures prepared with the M-SSW medium described above. Bottles of 500 mL were capped with a screw cap, silicone o-ring and blue butyl rubber stopper and wrapped in aluminum foil to avoid exposure to light. Autoclaved ferrihydrite powder was put into the bottles (1:100 w/v ratio). Each bottle consisted of a multi-point batch experiment in which the butyl rubber stopper allowed for multiple collection of samples with a syringe along time. Before sampling, the bottles were thoroughly shaken for liquid-solid homogenization. Aliquots of 5 mL were extracted about every 48 h, filtered (0.22 µm) and acidified with 200 µL of 6 M HCl solution. One mL was used for immediate Fe(II) analysis, and 4 mL were stored in the dark at 4 ^{0}C for further lactate/acetate measurements.

In the second stage, nitrite reduction was brought about by bio-produced Fe(II) (NFerr experiment in Table 4.1). The starting conditions in this stage were therefore the ones achieved at the end of the first stage (no lactate after total consumption and halted ferrihydrite bioreduction): the concentrations of bio-produced Fe(II) and acetate were about 1 and 8 mM, respectively, for at least 10 days. At this point, 4.81 mL of a 60 mM NO_2^- stock solution were injected into the batch under anoxic conditions, resulting in a final concentration of 0.76 mM NO_2^-.

Three sample aliquots were extracted at each sampling point: two of 5 mL to measure both the aqueous Fe(II) and Fe(III) concentrations and the nitrite isotopic composition ($\delta^{15}N-NO_2^-$ and $\delta^{18}O-NO_2^-$), and one of 1 mL to measure the NO_2^- concentration. Concentrations of dissolved iron species and nitrite were analyzed immediately to prevent iron oxidation/nitrite reduction. For the isotopic analysis, samples were immediately frozen and defrosted just before measurements (see below).

4.2.4.2. Abiotic nitrite reduction experiments with synthetic Fe(II)

To investigate the role of solid and aqueous Fe(II) in nitrite reduction, three abiotic experiments were performed with synthetic Fe(II) and with or without ferrihydrite, in which the N and O isotopic composition of nitrite was also monitored over time. In the experiments containing ferrihydrite, the liquid/solid ratio was the same as in the NFerr experiment. These experiments were performed with different settings: i) dissolved Fe(II) + NO_2^- without ferrihydrite, ii) ferrihydrite + synthetic Fe(II) (totally solid-bound on by ferrihydrite) + NO_2^- in the absence of aqueous Fe(II) and iii) ferrihydrite + both solid-bound and dissolved Fe(II) + NO_2^- (i.e., A1, A2 and A3, respectively; Table 4.1). In these experiments, a basal solution of SSW supplemented by 10 mM of acetate and 10 mM of Tris-HCl buffer was used. Acetate was added to match the initial conditions in the NFerr experiment (around 8 mM of acetate; Table 4.1).

In experiment A1, abiotic reaction between aqueous Fe(II) (1.0 mM) and NO_2^- (0.65 mM) took place in multi-point batch reactors (250 mL of SSW basal solution). The decrease in aqueous Fe(II) and NO_2^- was monitored to evaluate the nitrite reduction rate. In experiment A2, multi-point batch reactors contained 2.5 g of ferrihydrite and 250 mL of SSW basal solution supplemented with 1.2 mM of Fe(II). The concentration of aqueous Fe(II) decreased in solution, reaching complete depletion in about 400 min due to its uptake on ferrihydrite (see AP2 and Fig. A2.1). Once aqueous Fe(II) was depleted, 3.16 mL of 60 mM nitrite were added into solution to reach a 0.76 mM nitrite concentration to promote its reduction by solid-bound Fe(II).

Experiment A3 contained 2.5 g of ferrihydrite and a higher amount of synthethic Fe(II) than in A2 experiment (6 mL of 101 Fe(II) mM solution to reach a 2.59 mM Fe(II) concentration; Table 4.1). As in the experiment A2, a fast uptake of approximately 1.39

mM Fe(II) occurred, yielding a fairly constant aqueous Fe(II) concentration of approximately 1.2 mM for 8 d. Thereafter, 3.16 mL of 60 mM of nitrite (0.76 mM) were injected into the reactor to induce nitrite reduction by oxidation of both solid bound and aqueous Fe(II). Note that the aqueous Fe(II) concentration in the experiments A1, A2, A3 and in the NFerr experiment, previous to the addition of nitrite, was approximately the same (i.e., around 1.2 mM). In experiments A1, A2 and A3, sample collection, preservation and analysis procedure were performed as in the NFerr experiment (see above).

4.2.4.3. Biotic nitrite reduction experiments with *S. loihica*

Bio1 and Bio2 experiments were performed to investigate the heterotrophic denitrification mediated by *S. loihica* in the absence of ferrihydrite and aqueous Fe(II) (Table 4.1). The solution was prepared with SSW, 10 mM of either lactate or acetate as electron donor and carbon source, 10 mM of buffer Tris-HCl, and 0.65 nM of nitrite. This enabled us to compare the nitrite denitrification rates with the abiotic ones and to characterize isotopically the nitrite reduction by *S. loihica*. Moreover, these experiments allowed an evaluation of a potential contribution of the heterotrophic nitrite reduction in the abiotic experiments with bio-produced Fe(II).

4.2.4.4. Control and adsorption experiments

Control experiments in SSW were performed to examine potential interferences between acetate and Fe(II), nitrite and acetate or buffer, acetate and Fe(II) and only nitrite or Fe(II) in SSW (details in AP2). Adsorption experiments were carried out to quantify the amount of Fe(II) adsorbed during reductive dissolution of synthetized ferrihydrite (see AP2). A Fe(II) adsorption isotherm was performed with increasing concentrations of aqueous Fe(II) in anoxic SSW, acetate and TRIS pH buffer to A Fe(II) adsorption isotherm to investigate the mechanisms responsible for the Fe(II) uptake on ferrihydrite Fig. 1.5 in Chapter 1).

4.2.4.5. Chemical analyses

Concentrations of dissolved iron and nitrite were both measured by spectrophotometry (SP-830 PLUS, Metertech Inc.) at wavelengths of 510 nm and 540 nm, respectively. Ferrous iron and total iron concentrations were measured immediately after sampling by the phenanthroline method. Nitrite concentration was measured after adding sulphanilamide and the N-(1-naphthyl)-ethylenediamine dihydrochloride (NED) reagents and an incubation time of 20 min, following Garcia-Robledo et al. [34]. The total iron dissolved was also measured by Inductively Coupled Plasma Optical Emission Spectroscopy (ICP-OES, Perkin- Elmer 3000) to confirm that all dissolved iron was Fe(II). Differences in Fe concentrations measured by the phenanthroline method and ICP-OES were smaller than 5%. Concentrations of lactate and acetate were measured by High Performance Liquid Chromatography (Waters 600 HPLC pump controller equipped with an Aminex HPX-87H column (300 x 7.8 mm), BioRad, and a Waters 717plus autoinjector). Associated uncertainty was better than 3%. pH (± 0.02 pH units) of the initial medium was measured in a glove box using Thermo Orion pH electrodes and periodically calibrated with standard solutions of pH 2, 4 and 7.

4.2.5. Isotopic analyses

$\delta^{15}N\text{-}NO_2^-$ and $\delta^{18}O\text{-}NO_2^-$ were determined following the azide reduction method [35, 36]. N_2O was analyzed using a Pre-Con (Thermo Scientific) coupled with a Finnigan MAT 253 Isotope Ratio Mass Spectrometer (IRMS, Thermo Scientific). Notation is expressed in terms of delta per mil (δ ‰) (i.e., $\delta = (R_{sample}\text{-}R_{standard})/R_{standard}$, where R is the ratio between the heavy (^{15}N, ^{18}O) and the light (^{14}N, ^{16}O)isotopes). Used international standards were atmospheric N_2 (AIR) for $\delta^{15}N$ and Vienna Standard Mean Oceanic Water (V-SMOW) for $\delta^{18}O$. According to Coplen [37], several international and laboratory (in-house) standards were interspersed among samples for normalization of analyses. Two international standards (USGS 34 and 35) and two internal laboratory standards (UB-$NaNO_3$ ($\delta^{15}N$ = +16.9 ‰ and $\delta^{18}O$ = +28.5 ‰) and UB-KNO_2 ($\delta^{15}N$ = -28.5 ‰)) were employed to calibrate the $\delta^{15}N\text{-}NO_2^-$ and $\delta^{18}O\text{-}NO_2^-$ raw values to the international scales. The reproducibility (1σ) of the samples, calculated from the standards systematically interspersed in the analytical batches, was ±1.0 ‰ for $\delta^{15}N\text{-}NO_2^-$ and ±1.5 ‰ for $\delta^{18}O\text{-}NO_2$.

Under closed system conditions, the isotopic fractionation values (i.e., $\varepsilon^{15}N_{NO2}$ and $\varepsilon^{18}O_{NO2}$) are calculated according to the Rayleigh distillation equation:

$$\ln\left(\frac{R_{residual}}{R_{initial}}\right) = \varepsilon \times \ln\left(\frac{C_{residual}}{C_{initial}}\right) \qquad (4.3)$$

from which ε values are obtained from the slope of the linear correlation between the natural logarithm of the substrate remaining fraction ($\ln(C_{residual}/C_{initial})$, where C refers to the analyte concentration, and the determined isotope ratios ($\ln(R_{residual}/R_{initial})$, where $R = (\delta+1)$).

4.3. RESULTS AND DISCUSSION

4.3.1. Bioreduction of ferrihydrite

Figure 4.1 shows the bioreduction experiment during which three stages were distinguished. In the first stage (approximately 10 days), a marked drop in the initial concentration of lactate (10.8 mM) was accompanied by a sharp increase in acetate concentration. However, aqueous iron was not detected. In stage two (from 10 to 30 days), a gradual decrease in lactate and a progressive increase in acetate were observed together with a significant increase in dissolved iron. In the third stage, lactate was totally depleted after about 60 days, and acetate and Fe(II) leveled off with respective concentrations of about 8 and 1.1 mM. The total consumption of lactate led to unavailability of electron donor, ending Fe(III)-bioreduction and leaving the acetate and aqueous Fe(II) concentrations constant.

On the one hand, on the basis of the bioreduction reaction (Eq. 4.1), the molar [acetate]/[lactate] ratio is 1. Nevertheless, a 20% deficit of acetate (carbon loss) was observed throughout the experiments (Fig. 4.1). This non-stoichiometric behavior was mainly attributed to the use of lactate as a carbon source for biomass formation during microbial growth [38]. On the other hand, since the stoichiometric [Fe(II)/[acetate] ratio is 4 (Eq. 4.1) and the highest measured concentrations of aqueous Fe(II) and acetate were 1.1 and 8 mM, respectively, only a minor fraction of ferrous iron produced (i.e.≈3.5 %) was found in solution. This Fe(II) deficit could be explained by a large Fe(II) adsorption on ferrihydrite. It is well known that a large surface area combined with a poor crystalline organization of ferrihydrite and a high pH (i.e. pH ≈ 8.2) may cause an exceptionally large sorption capacity of cations [39]. In order to evaluate the Fe(II) adsorption process under the investigated conditions, several Fe(II)-adsorption assays and one Fe(II) adsorption isotherm were performed (Figs. A2.1 and 1.5 in AP2 and Chapter 1). The results confirmed a maximum uptake of Fe(II) on ferrihydrite of ≈ 1.2 mM (Fig. A2.1 in AP2) and revealed that, in addition to adsorption, a simultaneous process was responsible for the Fe(II) uptake on ferrihydrite (Fig. 1.5 in Chapter 1).

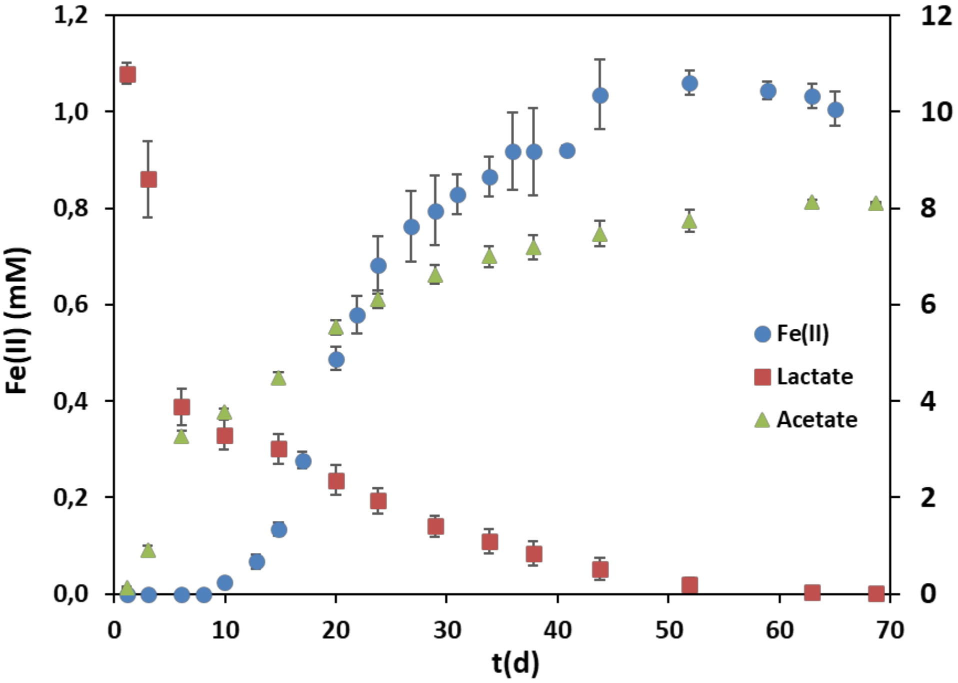

Figure 4. 1. Fe(II) bio-production experiment describing microbial reductive dissolution of ferrihydrite. The vertical error bars show the uncertainty calculated from three replicates (see text). Lactate consumption correspond to acetate and Fe(II) production. Three stages were differentiated throughout the experiment: (I) biomass production, (II) maximum release of Fe (II) and (III) halt of microbial metabolism.

Earlier studies indicated that re-adsorption of Fe(II) on ferrihydrite can result in ferrihydrite transformation to goethite, magnetite or lepidocrocite [23, 25, 40-43]. Factors as diverse as the thermodynamic properties of the minerals involved, the aqueous Fe(II) concentration and formation rates, biological and physical settings or the design of the experimental setup can play a role in ferrihydrite transformation [42]. In the SEM images (Fig. 4.2a), it is observed that the surface of the reacted ferrihydrite grains is rougher than that of the unreacted ones. XRD and FTIR analyses of the solid samples before and after the Fe(III) bioreduction process showed that ferrihydrite indeed transformed into magnetite ($Fe^{2+}Fe^{3+}{}_2O_4$) (Fig. 4.2b,c). Yang et al. [23] pointed out that this transformation is caused by the inclusion of the bio-produced Fe(II) into the mineral lattice. Figure 4.2b compares two XRD patterns after performing high statistic wide range scans of pristine and bioreduced samples. In addition to initial ferrihydrite, two new phases (nano-crystalline magnetite and microcrystalline hematite) were present in the reacted sample (NFerr experiment) with estimated amounts of 96 wt.% (magnetite) and 4 wt.% (hematite). The much smaller content of the latter was probably formed during the ferrihydrite autoclave process [44].

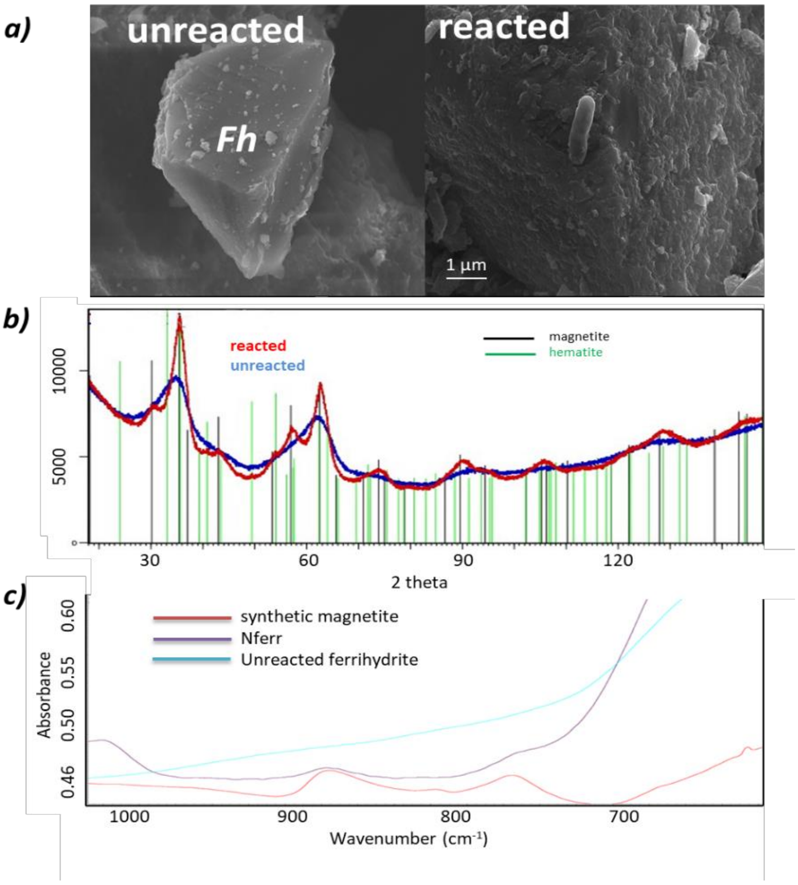

Figure 4. 2. Characterization of the solid sample: a) SEM images show an unreacted particle and a close-up surface of a reacted ferrihydrite particle with attached cell of *S.loihica*); b) X-ray powder diffraction patterns of the unreacted (blue line) and reacted (red line) ferrihydrite samples; black and green vertical lines show the 2θ positions of peaks of magnetite and hematite, respectively; c) FTIR spectra of unreacted ferrihydrite (blue line), reacted ferrihydrite (purple line) and pure magnetite (red line); magnetite peaks are visible in the reacted ferrihydrite sample.

4.3.2. NO_2^- reduction coupled with Fe(II) oxidation

Figure 4.3 shows the variation in the concentrations of nitrite and Fe(II), either synthetically (Fig 4.3a-c) or bio-produced (Fig. 4.3d), in the experiments performed to study abiotic nitrite reduction coupled with Fe(II) oxidation. Figure 4.3a shows the variation in Fe(II) and NO_2^- in a A1 representative of experiment with an initial aqueous Fe(II) concentration of ≈ 1 mM in the absence of ferrihydrite. After a week, Fe(II) depletion was approximately 50% of the initial concentration and 35% of nitrite was reduced. After a month, the Fe(II) depletion was 70% and nitrite concentration fell to a 65% of the initial concentration. The average nitrite reduction rate (k_{obs}) was estimated to be 0.059 mM^{-1} d^{-1} with a half-life value ($t_{1/2}$) of 18.7 d (second-order rate equation (Eq. (EA2.1)) and parameters in Table A2.2 in AP2).

Figure 4.3b depicts the variation in Fe(II) and nitrite concentration in a representative A2 experiment in the presence of solid bound Fe(II), i) with magnetite as a formed Fe(II)-bearing phase, and ii) adsorbed on the remaining ferrihydrite without aqueous Fe(II). About 27% of NO_2^- was reduced within 2 d, indicating that in the absence of aqueous Fe(II), Fe(II) in the solid phase was able to reduce some NO_2^- even without aqueous Fe(II). After 2 days, the reaction stopped, and nitrite concentration remained constant. An average nitrite reduction rate of 0.22 mM^{-1} d^{-1} was calculated for all replicates for the period previous to the halt of the reaction (Eq. (EA2.1)) and Table A2.2 in AP2). Figure 4.3c shows the variation in Fe(II) and nitrite concentration in a representative A3 experiment in the presence of both aqueous Fe(II) and solid bound Fe(II). NO_2^- and aqueous Fe(II) concentrations dropped to 87% and 38%, respectively, within about 2 d, yielding an average nitrite reduction rate of 0.74 mM^{-1} d^{-1} ($t_{1/2}$ = 0.47 d) (Fig. A2.3 Table A2.2 in AP2).

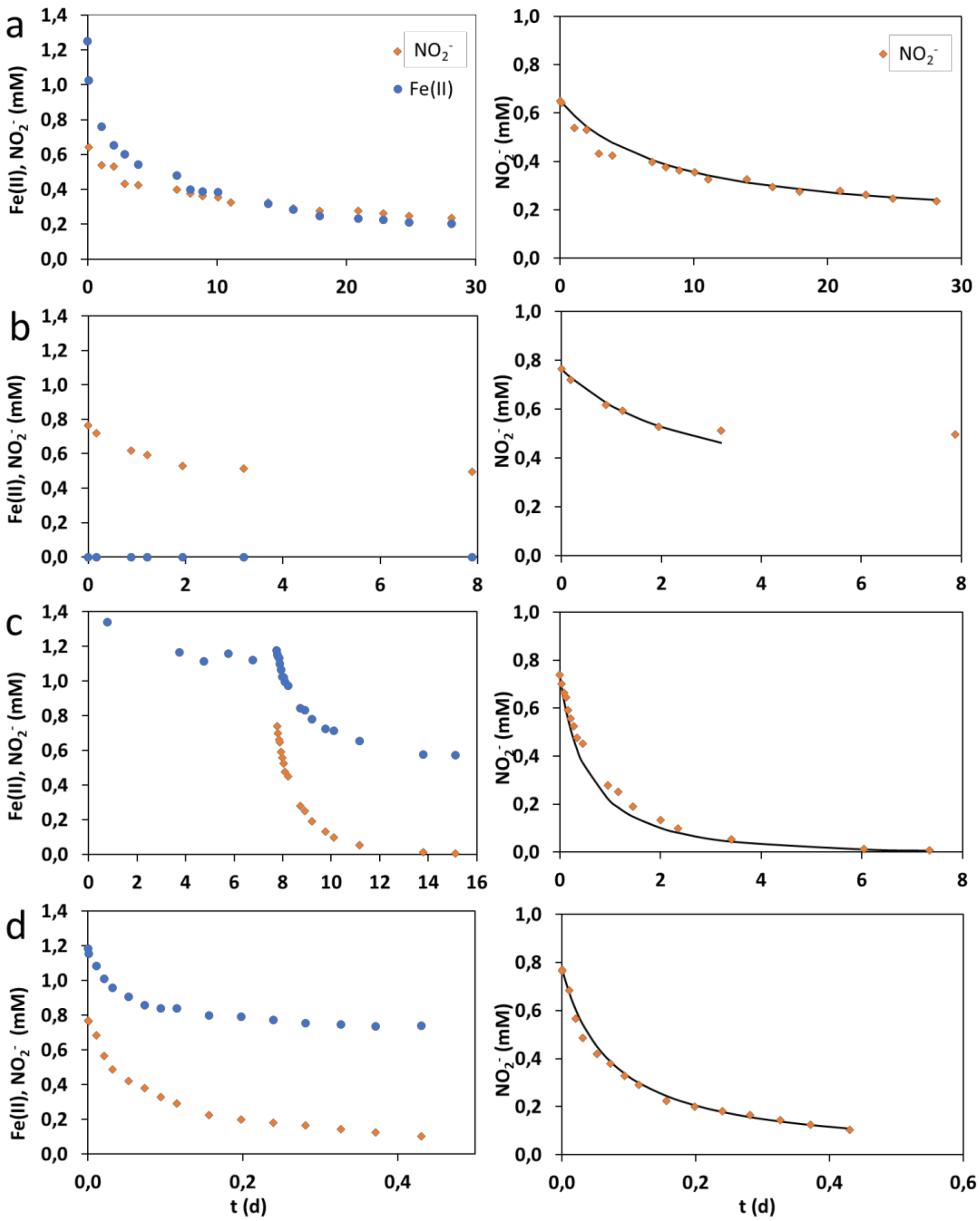

Figure 4. 3. Variation in concentrations of Fe(II) and NO_2^- throughout the experiments (left panels) and nitrite second-order decay fits using Eqs. (EA2.1 and EA2.2 in AP2) (solid line in right panels): a) initial 0.65 mM nitrite and 1 mM of aqueous Fe(II) (A1 experiment); b) initial 0.76 mM nitrite and 1.2 mM of solid-bound Fe(II) with ferrihydrite (A2 experiment); c) Initial 2.6 mM Fe(II), after 8d adsorption of 1.39 mM Fe(II) in ferrihydrite forming solid-bound Fe(II). After that addition of 0.76mM nitrite. (A3 experiment); d) initial 0.76 mM nitrite with ferrihydrite and 1.2 mM of bio-produced Fe(II).

Figure 4.3d shows the evolution of bio-produced Fe(II) after the cessation of the Fe(III) reduction in the Ferr experiment (Fig. 4.1), along with the nitrite concentration added in a representative NFerr experiment. To ensure comparability of the results, the experiment NFerr in Fig. 4.3d was selected for its high initial concentration of aqueous bio-produced Fe(II), which was similar to those of the experiments with synthetic Fe(II). Considering the reductive dissolution reaction (Eq. 4.1) and acetate production, the total concentration of bio-produced Fe(II) was estimated to be 32 mM. During the first 2 h, both nitrite and aqueous Fe(II) fell to about 50% and 30%, respectively, and after 10 h, almost all nitrite (87%) and up to 38% of the initial aqueous Fe(II) were removed. The nitrite reduction rate calculated was 6.47 mM^{-1} d^{-1} ($t_{1/2}$ = 0.07 d) (Fig. A2.3 in AP2). In NFerr experiments with lower concentrations of Fe(II) and nitrite, the rates calculated are within the same range of that from A3 experiment (Table A2.3 in AP 2).

S. loihica used for the bio-production of Fe(II) in the Ferr experiment could not be eliminated because both autoclave and antibiotics interfered with dissolved Fe(II) (Table A2.2 in AP2). However, as explained in Sections 3.3 and 3.4, the evidence that results from i) the isotopic data from the NFerr experiment (Fig. A2.4 in AP2) and ii) the results obtained from the experiments of biotic nitrite reduction by *S. loihica* using either lactate or acetate as electron donor and carbon source (see AP2), ruled out any microbial reduction of nitrite.

In accordance with the results obtained it is shown that the abiotic nitrate reduction rate was maximum in the NFerr experiment with bio-produced Fe(II) despite that aqueous Fe(II) concentrations were similar to those in the experiments with synthetic Fe(II). With regard to the experiments with synthetic Fe(II), the nitrite reduction rate was higher in the presence of both aqueous and solid Fe(II) (A3 experiment), intermediate in the presence only of solid-bound Fe(II) (A2 experiment), and lower in the experiment with only aqueous Fe(II) (A1 experiment). The much higher nitrite reduction rate observed for the NFerr experiments compared to A3 experiments, both with aqueous and solid-bound Fe(II), suggests that the larger amount of solid-bound Fe(II) obtained in the NFerr experiments (see above) could play a crucial role on the nitrite reduction rate. Previous studies suggested that solid-bound Fe(II) is able to reduce nitrite [5, 16, 45] and that an enhanced Fe(II)-rich surface (e.g.

magnetite) of bioreduced Fe(III)-amorphous oxyhydroxides is able to diminish toxic hexavalent chromium to the less harmful trivalent form.

Regarding the higher nitrite reduction rates observed in the presence of both aqueous and solid-bound Fe(II) (e.g. the NFerr and A3 experiments) compared to that in the experiments with only solid-bound Fe(II) or aqueous Fe(II), Gorski and Scherer [46] suggested that Fe(II) removal from solution by the iron oxide could affect the reduction potential of the oxide as a decrease in its oxidation leads to an increase in the oxide's reducing capacity.

Table 4. 1. Initial conditions for the different experiments. *Ferr*: Fe(II) bio-production; *NFerr*: nitrite addition after completion of Fe(II) bio-production in experiment *Ferr* (same bottle); *A1*: abiotic nitrite reduction in the absence of ferrihydrite; *A2*: abiotic nitrite reduction in the presence of ferrihydrite and solid-bound Fe(II); *A3*: abiotic nitrite reduction in the presence of ferrihydrite, solid-bound Fe(II) and aqueous Fe(II); *Bio1* and *Bio2*: biotic nitrite reduction in the absence of ferrihydrite with either lactate or acetate as carbon source, respectively. n.d. Below detection limit.

	Experiment	Ferrihydrite (g)	Volume (mL)	Aqueous bio-Fe(II) (mM)	Synthetic Fe(II) (mM) Added / Aqueous	NO_2^- (mM)	Acetate (mM)	Lactate (mM)	*S.loihica*
Fe(II) bio-production	Ferr	5	500	-	-	-	-	10	yes
Abiotic $NO_2^-{}_{red}$/Fe(II)$_{ox}$	NFerr	3.8	380	1.15	-	0.76	8	-	-
	A1	-	250	-	1 / 1	0.65	10	-	-
	A2	2.5	250	-	1.2 / n.d.	0.76	10	-	-
	A3	2.5	250	-	2.59/1.2	0.76	10	-	-
Biotic NO_2^- reduction	Bio1	-	250	-	-	0.65	-	10	yes
	Bio2	-	250	-	-	0.65	10	-	yes

4.3.3. Biotic (heterotrophic) NO_2^- reduction by *S. loihica*

Biotic experiments showed a lag in microbial activity before nitrite reduction commenced. In the cultures amended with either lactate or acetate, the time-lag lasted about 1 d and 10 d, respectively (Fig. A2.2 in AP2). Yoon et al. [47] reported a similar behavior for *Shewanella* spp. In contrast, in the abiotic NO_2^- reduction experiments with bio-produced Fe(II) and acetate, nitrite was consumed in only 10 h (Fig. 4.3d). These results suggest an absence of microbial nitrite reduction in the abiotic denitrification experiments with bio-produced Fe(II), which was confirmed with the isotope data (see below).

4.3.4. Isotopic fractionation during abiotic NO_2^- reduction owing to dissolved or solid-bound Fe(II)

In the experiments with abiotic NO_2^- reduction, while the NO_2^- concentration decreased, the unreacted NO_2^- became enriched in the heavy isotopes (^{15}N and ^{18}O), as it is commonly observed for denitrification. Table 4.2 lists the values determined for $\varepsilon^{15}N_{NO2}$, $\varepsilon^{18}O_{NO2}$ and $\varepsilon^{15}N/\varepsilon^{18}O$ that ranged from -19.7 ‰ to -8.1 ‰, from -11.4 ‰ to -4.6 ‰ and from 3.3 to ≈ 0.6 respectively (calculations shown in Fig. A2.4 in AP2). These values are within the range reported in the literature for both, the biotic (heterotrophic) and abiotic NO_2^- reductions (Table 4.3). In this study, the N-O isotopic fractionation ratio was expressed as $\varepsilon^{18}O/\varepsilon^{15}N$ instead of $\varepsilon^{15}N/\varepsilon^{18}O$ for better comparison with the slopes obtained in the dual N-O isotope plot (see below).

In the experiments to test the abiotic NO_2^- reduction with synthetic Fe(II), differences in NO_2^- isotopic fractionation were not observed (i) when using Fe(II) from biotic or synthetic source (NFerr and A3 experiments, respectively) nor (ii) when using both aqueous and solid-bound Fe(II) or only aqueous Fe(II) (A1 and A3 experiments, respectively; Table 4.2). By contrast, in the experiments with solid-bound Fe(II) in the absence of aqueous Fe(II) (A2 experiment), the $\varepsilon^{15}N_{NO2}$ and $\varepsilon^{18}O_{NO2}$ determined were higher (Table 4.2).

Table 4. 2 Average nitrite reduction rates (mM^{-1} d^{-1}), $\varepsilon^{15}N_{NO2}$, $\varepsilon^{18}O_{NO2}$ and $\varepsilon^{18}O/\varepsilon^{15}N$ ratio in the experiments. In NFerr experiment, nitrite reduction rate is calculated from a representative experiment. Figure A2.4 (AP2) shows the linear correlation between the natural logarithms of the substrate remaining fraction and the isotope ratios obtained. Values for $\varepsilon^{18}O/\varepsilon^{15}N$ are calculated from data indicated in Fig. A2.4.

	Experiment	Electron donor	electron donor distribution	Reduction rate (NO_2^-)	$\varepsilon^{15}N_{NO2}$ ‰	$\varepsilon^{18}O_{NO2}$ ‰	$\varepsilon^{18}O/\varepsilon^{15}N$
Abiotic	A1	Synthetic Fe(II)	Aqueous Fe(II)	0.059	-8.6	-6.3	0.7
	A2	Synthetic Fe(II)	Solid-bound Fe(II)	0.22	-19.7	-11.4	0.6
	A3	Synthetic Fe(II)	Aqueous & solid Fe(II)	0.74	-8.7	-5.2	0.6
	NFerr	Bio-produced Fe(II)	Aqueous & solid Fe(II)	6.47	-8.1	-4.6	0.6
Biotic	Bio1	Acetate			-1.6	-5.3	3.1

In these abiotic NO_2^- reduction experiments, the variability of $\varepsilon^{15}N_{NO2}$ and $\varepsilon^{18}O_{NO2}$ observed could be caused by the different NO_2^- reduction rates under each condition or by a different underlaying reaction mechanism during oxidation of dissolved or solid-bound Fe(II). In earlier studies, lower ε values have been associated with higher NO_2^- reduction rates [9, 30]. Buchwald et al. [9] observed differences in ε and NO_2^- removal rates using aqueous Fe(II) as electron donor or Fe(II) associated with the oxide surface. However, the present results do not show a correlation between the NO_2^- reduction rates and the isotopic fractionation values (Table 4.2). For instance, $\varepsilon^{15}N_{NO2}$ and $\varepsilon^{18}O_{NO2}$ were similar in the A3 and NFerr experiments with highly dissimilar NO_2^- reduction rates (0.75 and 6.47 mM^{-1} d^{-1}, respectively).

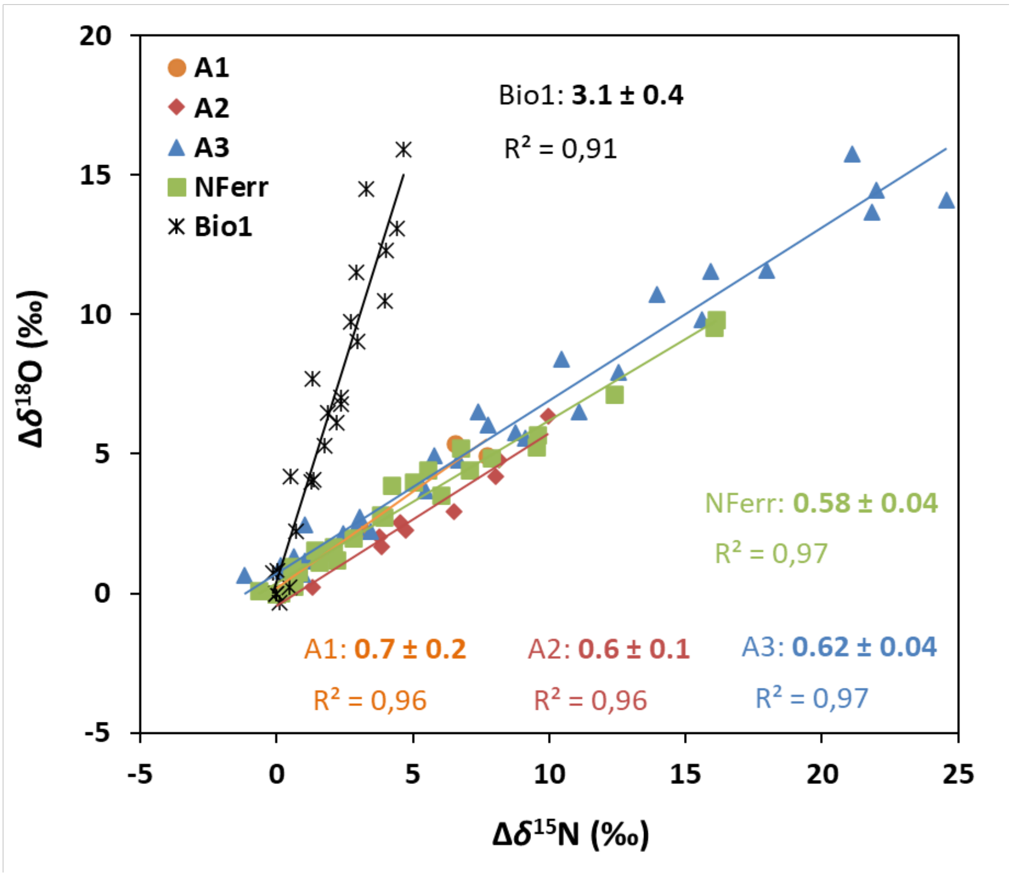

Figure 4. 4. Dual N-O isotope plot for the abiotic and biotic nitrite reduction experiments. Isotopic fractionation values respect to its initial isotopic composition for all carried out experiments are shown. Linear regression is represented by solid lines and formula.

The kinetics of the abiotic NO_2^- reduction could be affected by the initial concentration and proportion of the reactants (NO_2^- and Fe(II)), solution pH, and the presence of minerals that were added externally or that precipitated during the reaction [7, 9]. In the latter case, the amount, composition (including the Fe oxidation state) and the mineral specific surface area could have influenced the reaction. In the present study, the formation of secondary magnetite during the Fe(II) oxidation in the Ferr experiment complicates a comparison between the effect of the conditions investigated in this study and earlier studies.

It is not easy therefore to determine whether the ε variability observed is only due to differences in the reduction rates or to the differences in mechanisms (oxidation of aqueous or solid-bound Fe(II) coupled with NO_2^- reduction).

A dual element isotope approach was used to further investigate the differences in the ε values in the different experiments (Fig. 4.4). The different slopes (i.e., $\Delta\delta^{18}O/\Delta\delta^{15}N \approx \varepsilon^{18}O/\varepsilon^{15}N$) suggest the occurrence of different nitrite reduction mechanisms. The higher ε values determined in the experiment A2 (solid-bound Fe(II)) compared with the similar values in the NFerr and A3 experiments (aqueous and solid-bound Fe (II)) and the A1 experiment (aqueous Fe (II)) suggest that nitrite reduction is controlled by a different mechanism in the presence of only solid-bound Fe(II). Nevertheless, the similar slopes in the dual N-O plot for A1, A2, -A3 and NFerr ($\Delta\delta^{18}O/\Delta\delta^{15}N$ = 0.60±0.02) indicates a common nitrite reduction mechanism in the abiotic experiments. Further research is needed to elucidate the process controlling the magnitude of ε values during nitrite reduction by solid-bound Fe(II).

Another consideration in the abiotic NO_2^- reduction experiments is the possible effect of $\delta^{18}O$-NO_2^- equilibration with $\delta^{18}O$-H_2O on the $\varepsilon^{18}O$/ $\varepsilon^{15}N$ ratio, which could depend on solution salinity, temperature and/or pH [48]. Buchwald et al. (2016) [9] have shown that NO accumulated in a reversible reaction could re-oxidize to NO_2^- by incorporating an O atom from water, which could also influence the /$\varepsilon^{18}O/\varepsilon^{15}N$ ratio. Nevertheless, Martin and Casciotti (2016) [31] have shown a negligible isotopic effect of O equilibration (0.0035‰) at room temperature and pH 7.6 over 2 h between sampling and the azide reaction. Given that in this study nitrite samples in synthetic seawater were retrieved at pH between 7.8 and 8.2, immediately frozen and immediately analyzed after unfreezing, an O equilibration effect was ruled out. The similar slopes obtained in the abiotic NO_2^- reduction experiments for relatively short (NFerr experiment) and long (A3 experiment) incubation periods (Table 4.2 and Fig. 4.4) reinforce the lack of $\delta^{18}O$-NO_2^- equilibration with $\delta^{18}O$-H_2O

4.3.5. Use of isotopic tools to distinguish between abiotic and biotic NO_2^- reduction in the field

As in the abiotic reduction, in the biotic NO_2^- reduction, a decrease in concentration yielded an enrichment in the heavy isotopes (^{15}N and ^{18}O) of the unreacted substrate. The isotopic fractionation results are listed in Table 4.2 (see calculations in Fig. A2.4 in AP2). NO_2^- reduction by *S. loihica* using lactate as electron donor yielded a $\varepsilon^{15}N_{NO2}$ of -1.6 ‰, $\varepsilon^{18}O_{NO2}$ of -5.3 ‰, and /$\varepsilon^{18}O/\varepsilon^{15}N$ of 3.3. The $\varepsilon^{15}N_{NO2}$ and $\varepsilon^{18}O_{NO2}$ obtained are within the range of the values reported in the literature for both, the biotic (heterotrophic) and abiotic NO_2^- reduction (Table 4.3). Nevertheless, under the conditions of this study, the isotopic fractionation value of nitrogen (-1.6 ‰) was smaller than those from the abiotic experiments of this study. In addition, the $\varepsilon^{18}O/\varepsilon^{15}N$ ratio of 3.3 obtained differs significantly from those calculated for the abiotic experiments (Fig. 4.4 and Table 4.2), becoming one of the highest values reported in the literature (Table 4.3).

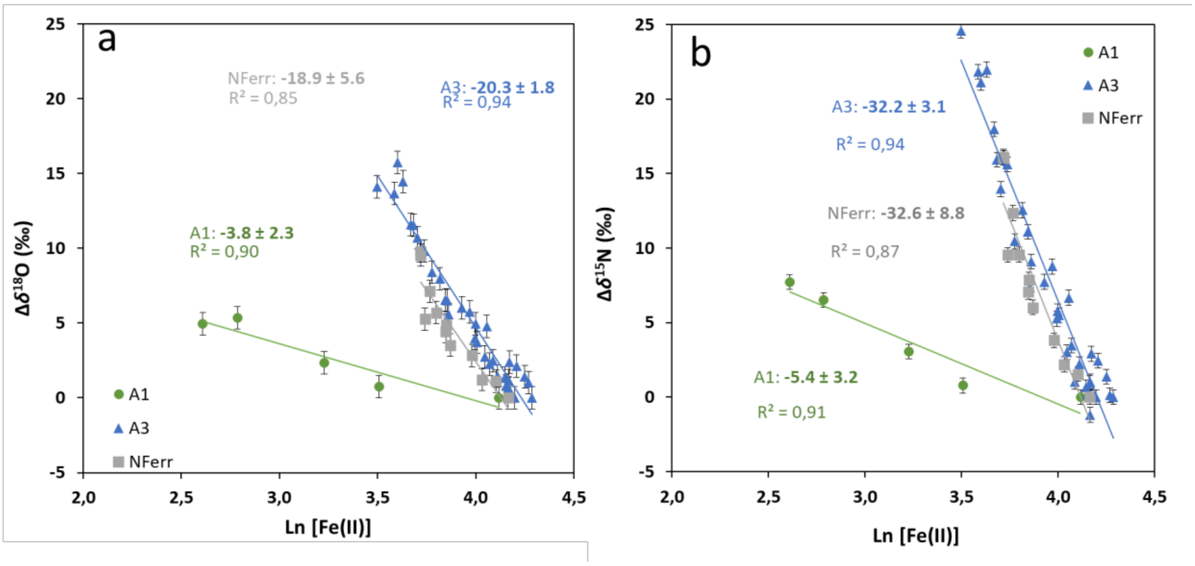

Figure 4. 5 Correlation between the NO_2^- isotopic composition and the Ln Fe(II) concentration. a) Isotopic $\delta^{18}O$-NO_2^- fractionation values respect to initial isotopic composition. b) Isotopic $\delta^{15}N$-NO_2^- fractionation values respect to initial isotopic composition. In the abiotic experiments containing dissolved Fe(II) (A1, A3 and NFerr), the linear regression of $\delta^{15}N$-NO_2^- and $\delta^{18}O$-NO_2^- is shown versus the Fe(II) concentration decrease.

In the biotic NO_2^- reduction, the magnitude of the $\varepsilon^{15}N_{NO2}$ and $\varepsilon^{18}O_{NO2}$ values could depend on the enzymes involved, on the NO_2^- transport across the cell and on the NO_2^- reduction rate, whereas pH or salinity effects are negligible as in the biotic NO_3^- reduction [49, 50]. Bacterial NO_2^- reduction can be catalyzed by two enzymes located in the periplasm (Cu containing NO_2^- reductase encoded as *nirK* (Cu-NIR) and Fe-containing NO_2^- reductase encoded as *nirS* (Fe-NIR) [51]. The $\varepsilon^{18}O/\varepsilon^{15}N$ ratio of 3.3 obtained for the biotic NO_2^- reduction by *S. loihica* bears no resemblance to those reported in a study on NO_2^- reduction with different bacterial species. Martin and Casciotti (2016) [31] attributed the variations in the $\varepsilon^{18}O/\ \varepsilon^{15}N$ ratio to the use of different enzymes since the species with Fe-NIR yielded higher $\varepsilon^{18}O/\ \varepsilon^{15}N$ ratios (from 0.3 to 1.4) than the species containing Cu-NIR (from 0.05 to 0.3). These authors suggested that Fe-NIR could produce a higher NO_2^--O isotopic fractionation because it allows cleavage of both N-O bonds since the Fe-NIR catalytic site might bind NO_2^--N [52, 53]. By contrast, the Cu-NIR catalytic site might bind both the NO_2^--O atoms and the N-O bond closest to the Asp98 residue, which is cleaved [54, 55], independently of the isotopic composition. If the NO_2^- reductase associated with *S. loihica* is Cu-NIR [56], the results of this study will not be consistent with this hypothesis. The present study showed an $\varepsilon^{18}O_{NO2}$ higher than $\varepsilon^{15}N_{NO2}$ in contrast to a lower $\varepsilon^{18}O$ associated with microorganisms containing Cu-NIR [31].

The $\varepsilon^{18}O/\varepsilon^{15}N$ of 3.3 ratio determined for the NO_2^- reduction by *S. loihica* differs significantly from the range obtained for the abiotic experiments (0.6 – 0.7; Fig. 4.4). Thus, given that *S. loihica* is the only NO_2^- reducing microorganism, the $\varepsilon^{18}O/\varepsilon^{15}N$ values calculated in the present study could allow us to distinguish the contribution of the biotic (heterotrophic) and abiotic NO_2^- reductions at the laboratory. However, taking into account the large variability of the $\varepsilon^{18}O/\ \varepsilon^{15}N$ ratio (from 0.05 to 3.3) found in the present study and in the literature for the biotic NO_2^- reduction (Tables 4.2 and 4.3), it might not be possible to distinguish between biotic and abiotic reactions in real marine environments. One reason for this is the existence of complex bacterial communities with various NO_2^- reducing enzymes. Another reason is the overlap of biotic$\varepsilon^{18}O/\ \varepsilon^{15}N$ values with the ones attributed to the abiotic reduction (0.6-2.0; Tables 4.2 and 4.3).

Alternatively, a good correlation was observed between nitrite isotopic composition $\Delta\delta^{15}N_{NO2}$ or $\Delta\delta^{18}O_{NO2}$) and dissolved ferrous iron concentration (ln[Fe(II)]) during the abiotic nitrite reduction (Fig. 4.5), which could be useful to investigate the process controlling NO_2^- reduction under field conditions. A good correlation between Δ (^{15}N or ^{18}O)-NO_2^- and ln[Fe(II)] in field samples evidences NO_2^- reduction by Fe(II) oxidation, either abiotically or biotically (chemolithotroph). By contrast, no correlation is expected for heterotrophic NO_2^- reduction. A decrease in Fe(II) concentration coupled with an increase in $\delta^{15}N_{NO2}$ and $\delta^{18}O_{NO2}$ was observed (Fig. 4.5). In the A1 experiment, the slopes for $\delta^{15}N_{NO2}$ and $\delta^{18}O_{NO2}$ (-5.4 and -3.8, respectively) were lower than those in the A3 (-32.2 and -20.3, respectively) and NFerr experiments (-32.6 and -19.0, respectively). This was due to the higher decrease in aqueous Fe(II) concentrations during the A1 experiment. In contrast to A3 and NFerr, which also contained solid-bound Fe(II) and the total amount of Fe(II) was thus higher than in A1, in the A1 experiment only aqueous Fe(II) was available for nitrite reduction (Table 4.1).

Given that under natural conditions the equilibration between δ^{18}O-NO_2^- and δ^{18}O-H_2O and the occurrence of N cycling processes (NO_2^- oxidation to NO_3^-, NO_2^- reduction to NH_4^+ or NH_4^+ oxidation to NO_2^-) could affect δ^{18}O-NO_2^-, only the variation of $\delta^{15}N_{NO2}$ versus Fe(II) concentration could provide reliability of the NO_2^- fate in the environment.

Table 4. 3 $\varepsilon^{15}N$, $\varepsilon^{18}O$ (in ‰) and $\varepsilon^{18}O/\varepsilon^{15}N$ ratio reported in the literature for the NO_2^- reduction. For NO_2^- biotic reduction, ε is calculated for conversion to N_2, whereas for NO_2^- abiotic reduction, the final product is assumed to be N_2O. n.a. = non analyzed. (1) Martin and Casciotti (2016) (average values of the data reported in Table 4.1), (2) Bryan et al. (1983), (3) Brunner et al. (2013), (4) Jacob et al. (2016), (5) Grabb et al. (2017), (6) Buchwald et al. (2016)

Reaction type	Bacteria	e^- donor	e^- acceptor	$\varepsilon^{15}N$
Biotic (heterotrophic)	*Pseudomonas aeruginosa* (Fe-NIR)	C_{org} (medium)	NO_2^-	-9.5
	Pseudomonas chlororaphis (Fe-NIR)	C_{org} (medium)	NO_2^-	-8.25
	Pseudomonas stutzeri (Fe-NIR)	C_{org} (medium)	NO_2^-	-7.0
	Pseudomonas aureofaciens (Cu-NIR)	C_{org} (medium)	NO_2^-	-20.5
	Achromobacter xylosoxidans (Cu-NIR)	C_{org} (medium)	NO_2^-	-21.0
	Ochrobactrum sp. (Cu-NIR)	C_{org} (medium)	NO_2^-	-23.5
	Pseudomonas stutzeri (Fe-NIR)	C_{org} (medium)	NO_2^-	-1.0
	Kuenenia stuttgartiensis (Fe-NIR)	C_{org} (medium)	NO_2^-	-16.0
Biotic	Environmental community	-	NO_2^-	-10
Abiotic (heterogeneous)	-	Nontronite	NO_2^-	-11.1
	-	Nontronite + Fe(II) synth	NO_2^-	-2.3
	-	Green rust	NO_2^-	-4.2 to -9.4
	-	Fe(II) synth	NO_2^-	-6.1 to -33.9
	-	Goethite + Fe(II) synth	NO_2^-	-5.9 to 44.8

4.4. CONCLUSIONS

Experiments simulating an anoxic marine medium were carried out to study nitrite reduction coupled with (bio-produced and synthetic) ferrous iron oxidation. Fe(II) bio-production was driven by ferrihydrite reduction mediated by *S.loihica*. Fe(II) released was partially re-incorporated into ferrihydrite, which transformed to nano-crystalline magnetite, producing thus solid Fe(II). Both the bio-produced aqueous Fe(II) and solid Fe(II) played a role in nitrite reduction.

Experiments with bio-produced or synthetic ferrous iron (aqueous and solid-bound Fe(II)) revealed that abiotic NO_2^- reduction is faster in a system with bio-produced Fe(II). The newly formed nano-crystalline magnetite with a high content of solid Fe(II) showed a significant reactivity in the presence of nitrite. Results obtained from the laboratory nitrite reduction experiments using synthetic Fe(II) suggest that with similar concentrations of aqueous Fe(II), nitrite reduction in natural systems could be stronger given the higher amounts of solid-bound Fe(II) obtained in the experiments with bio-produced Fe(II).

Experiments with only synthetic ferrous iron (aqueous, solid-bound Fe(II) or both) revealed that in the presence of Fe(II) in both aqueous and solid-bound forms, abiotic NO_2- reduction is faster and more efficient than in the ones with only aqueous Fe(II) or only solid-bound Fe(II).

No differences in the NO_2^- isotopic fractionation were observed in the abiotic NO_2^- reduction regarding the biotic or synthetic source of Fe(II). No significant differences were observed in $\varepsilon^{15}N_{NO2}$ and $\varepsilon^{18}O_{NO2}$ in the abiotic NO_2^- reduction by (i) aqueous Fe(II) or (ii) aqueous and solid-bound Fe(II). By contrast, the isotopic fractionation was higher in the experiments with only solid-bound Fe(II). However, the similar slopes derived in the dual N-O isotope plot suggest that the mechanisms controlling the nitrite reduction are common in the abiotic experiments. The higher slope ($\varepsilon^{18}O/\varepsilon^{15}N$ ratio of 3.3) related to the biotic (heterotrophic) experiment contrasts with those of the abiotic experiments, becoming one of the lowest values reported.

Hence, in laboratory microcosms, which mimic marine environments with *S. loihica* as the only existing NO_2^--reducing microorganism, the $\varepsilon^{18}O/\varepsilon^{15}N$ ratio calculated could be used to distinguish between biotic and abiotic NO_2^- reduction. However, given that the values of the $\varepsilon^{18}O/\varepsilon^{15}N$ ratio determined in this study fall within the wide range of values reported in the literature for the abiotic NO_2^- reduction by Fe(II) oxidation and for the NO_2^- reduction by other heterotrophic bacteria, the use of the $\varepsilon^{18}O/\varepsilon^{15}N$ ratio to distinguish different NO_2^- reduction processes (biotic or abiotic) in field studies should be used with caution.

Moreover, the correlation between $\delta^{15}N_{NO2}$ and the natural logarithm of the Fe(II) concentration observed could be used as an additional line of evidence to distinguish between NO_2^- reduction by Fe(II) oxidation, either abiotically or biotically (chemolithotroph), and heterotrophic bacteria. This observation can improve the prospect of using isotope data to investigate nitrite reduction processes in the field.

4.5. REFERENCES

1. Guerbois, D., et al., *Nitrite reduction by biogenic hydroxycarbonate green rusts: evidence for hydroxy-nitrite green rust formation as an intermediate reaction product.* Environmental science & technology, 2014. **48**(8): p. 4505-4514.

2. Jani, J. and G.S. Toor, *Composition, sources, and bioavailability of nitrogen in a longitudinal gradient from freshwater to estuarine waters.* Water research, 2018. **137**: p. 344-354.

3. Melton, E.D., et al., *The interplay of microbially mediated and abiotic reactions in the biogeochemical Fe cycle.* Nature Reviews Microbiology, 2014. **12**(12): p. 797-808.

4. Lovley, D.R., *Dissimilatory Fe (III) and Mn (IV) reduction.* Microbiology and Molecular Biology Reviews, 1991. **55**(2): p. 259-287.

5. Tai, Y.-L. and B.A. Dempsey, *Nitrite reduction with hydrous ferric oxide and Fe (II): stoichiometry, rate, and mechanism.* Water research, 2009. **43**(2): p. 546-552.

6. Ravishankara, A., J.S. Daniel, and R.W. Portmann, *Nitrous oxide (N2O): the dominant ozone-depleting substance emitted in the 21st century.* science, 2009. **326**(5949): p. 123-125.

7. Grabb, K.C., et al., *A dual nitrite isotopic investigation of chemodenitrification by mineral-associated Fe (II) and its production of nitrous oxide.* Geochimica et Cosmochimica Acta, 2017. **196**: p. 388-402.

8. Lu, Y., et al., *Microbial mediated iron redox cycling in Fe (hydr) oxides for nitrite removal.* Bioresource technology, 2017. **224**: p. 34-40.

9. Buchwald, C., et al., *Constraining the role of iron in environmental nitrogen transformations: Dual stable isotope systematics of abiotic NO2− reduction by Fe (II) and its production of N2O.* Geochimica et Cosmochimica Acta, 2016. **186**: p. 1-12.

10. Kampschreur, M.J., et al., *Reduced iron induced nitric oxide and nitrous oxide emission.* Water Research, 2011. **45**(18): p. 5945-5952.

11. Robertson, E.K., et al., *Dissimilatory nitrate reduction to ammonium coupled to Fe (II) oxidation in sediments of a periodically hypoxic estuary.* Limnology and Oceanography, 2016. **61**(1): p. 365-381.

12. Devol, A.H., *Denitrification, anammox, and N2 production in marine sediments.* Annual review of marine science, 2015. **7**: p. 403-423.

13. Wu, D., et al., *Denitrification of nitrite by ferrous hydroxy complex: effects on nitrous oxide and ammonium formation.* Chemical Engineering Journal, 2015. **279**: p. 149-155.

14. Dhakal, P., et al., *Nitrite reactivity with magnetite.* Environmental science & technology, 2013. **47**(12): p. 6206-6213.

15. Chen, D., et al., *Biological and chemical processes of microbially mediated nitrate-reducing Fe (II) oxidation by Pseudogulbenkiania sp. strain 2002.* Chemical Geology, 2018. **476**: p. 59-69.

16. Rakshit, S., C.J. Matocha, and M.S. Coyne, *Nitrite reduction by siderite.* Soil Science Society of America Journal, 2008. **72**(4): p. 1070-1077.

17. Robertson, E.K. and B. Thamdrup, *The fate of nitrogen is linked to iron (II) availability in a freshwater lake sediment.* Geochimica et Cosmochimica Acta, 2017. **205**: p. 84-99.

18. Roh, Y., et al., *Metal reduction and iron biomineralization by a psychrotolerant Fe (III)-reducing bacterium, Shewanella sp. strain PV-4.* Appl. Environ. Microbiol., 2006. **72**(5): p. 3236-3244.

19. Benaiges-Fernandez, R., et al., *Dissimilatory bioreduction of iron (III) oxides by Shewanella loihica under marine sediment conditions.* Marine environmental research, 2019. **151**: p. 104782.

20. Canfield, D.E., *Reactive iron in marine sediments.* Geochimica et Cosmochimica Acta, 1989. **53**(3): p. 619-632.

21. Tomaszewski, E.J., et al., *The role of dissolved Fe (II) concentration in the mineralogical evolution of Fe (hydr) oxides during redox cycling.* Chemical Geology, 2016. **438**: p. 163-170.

22. Boland, D.D., et al., *Effect of solution and solid-phase conditions on the Fe (II)-accelerated transformation of ferrihydrite to lepidocrocite and goethite.* Environmental science & technology, 2014. **48**(10): p. 5477-5485.

23. Yang, L., et al., *Kinetics of Fe (II)-catalyzed transformation of 6-line ferrihydrite under anaerobic flow conditions.* Environmental science & technology, 2010. **44**(14): p. 5469-5475.

24. Yee, N., et al., *The rate of ferrihydrite transformation to goethite via the Fe (II) pathway.* American Mineralogist, 2006. **91**(1): p. 92-96.

25. Hansel, C.M., et al., *Secondary mineralization pathways induced by dissimilatory iron reduction of ferrihydrite under advective flow.* Geochimica et Cosmochimica Acta, 2003. **67**(16): p. 2977-2992.

26. Böttcher, J., et al., *Using isotope fractionation of nitrate-nitrogen and nitrate-oxygen for evaluation of microbial denitrification in a sandy aquifer.* Journal of Hydrology, 1990. **114**(3-4): p. 413-424.

27. Fukada, T., et al., *A dual isotope approach to identify denitrification in groundwater at a river-bank infiltration site.* Water Research, 2003. **37**(13): p. 3070-3078.

28. Mariotti, A., et al., *Experimental determination of nitrogen kinetic isotope fractionation: some principles; illustration for the denitrification and nitrification processes.* Plant and soil, 1981. **62**(3): p. 413-430.

29. Aravena, R. and W.D. Robertson, *Use of multiple isotope tracers to evaluate denitrification in ground water: Study of nitrate from a large-flux septic system plume.* Groundwater, 1998. **36**(6): p. 975-982.

30. Bryan, B.A., et al., *Variable expression of the nitrogen isotope effect associated with denitrification of nitrite.* Journal of Biological Chemistry, 1983. **258**(14): p. 8613-8617.

31. Martin, T.S. and K.L. Casciotti, *Nitrogen and oxygen isotopic fractionation during microbial nitrite reduction.* Limnology and Oceanography, 2016. **61**(3): p. 1134-1143.

32. Gao, H., et al., *Shewanella loihica sp. nov., isolated from iron-rich microbial mats in the Pacific Ocean.* International Journal of Systematic and Evolutionary Microbiology, 2006. **56**(8): p. 1911-1916.

33. Brunauer, S., P.H. Emmett, and E. Teller, *Adsorption of gases in multimolecular layers.* Journal of the American chemical society, 1938. **60**(2): p. 309-319.

34. García-Robledo, E., A. Corzo, and S. Papaspyrou, *A fast and direct spectrophotometric method for the sequential determination of nitrate and nitrite at low concentrations in small volumes.* Marine Chemistry, 2014. **162**: p. 30-36.

35. McIlvin, M.R. and M.A. Altabet, *Chemical conversion of nitrate and nitrite to nitrous oxide for nitrogen and oxygen isotopic analysis in freshwater and seawater.* Analytical Chemistry, 2005. **77**(17): p. 5589-5595.

36. Ryabenko, E., M.A. Altabet, and D.W. Wallace, *Effect of chloride on the chemical conversion of nitrate to nitrous oxide for δ15N analysis.* Limnology and Oceanography: Methods, 2009. **7**(7): p. 545-552.

37. Coplen, T.B., *Guidelines and recommended terms for expression of stable-isotope-ratio and gas-ratio measurement results.* Rapid communications in mass spectrometry, 2011. **25**(17): p. 2538-2560.

38. Lanthier, M., K.B. Gregory, and D.R. Lovley, *Growth with high planktonic biomass in Shewanella oneidensis fuel cells.* FEMS microbiology letters, 2008. **278**(1): p. 29-35.

39. Dzombak, D.A. and F.M. Morel, *Surface complexation modeling: hydrous ferric oxide*. 1990: John Wiley & Sons.

40. Xiao, W., et al., *Use of fourier transform infrared spectroscopy to examine the Fe (II)-Catalyzed transformation of ferrihydrite.* Talanta, 2017. **175**: p. 30-37.

41. Xiao, W., et al., *Effect of Shewanella oneidensis on the kinetics of Fe (II)-catalyzed transformation of ferrihydrite to crystalline iron oxides.* Environmental science & technology, 2018. **52**(1): p. 114-123.

42. Dippon, U., et al., *Secondary mineral formation during ferrihydrite reduction by Shewanella oneidensis MR-1 depends on incubation vessel orientation and resulting gradients of cells, Fe2+ and Fe minerals.* Geomicrobiology Journal, 2015. **32**(10): p. 878-889.

43. Piepenbrock, A., et al., *Dependence of microbial magnetite formation on humic substance and ferrihydrite concentrations.* Geochimica et Cosmochimica Acta, 2011. **75**(22): p. 6844-6858.

44. Das, S., M.J. Hendry, and J. Essilfie-Dughan, *Transformation of two-line ferrihydrite to goethite and hematite as a function of pH and temperature.* Environmental science & technology, 2011. **45**(1): p. 268-275.

45. Byrne, J., et al., *Control of nanoparticle size, reactivity and magnetic properties during the bioproduction of magnetite by Geobacter sulfurreducens.* Nanotechnology, 2011. **22**(45): p. 455709.

46. Gorski, C.A. and M.M. Scherer, *Fe2+ sorption at the Fe oxide-water interface: A revised conceptual framework*, in *Aquatic Redox Chemistry*. 2011, ACS Publications. p. 315-343.

47. Yoon, S., R.A. Sanford, and F.E. Löffler, *Shewanella spp. use acetate as an electron donor for denitrification but not ferric iron or fumarate reduction.* Appl. Environ. Microbiol., 2013. **79**(8): p. 2818-2822.

48. Buchwald, C. and K.L. Casciotti, *Isotopic ratios of nitrite as tracers of the sources and age of oceanic nitrite.* Nature Geoscience, 2013. **6**(4): p. 308-313.

49. Granger, J., et al., *Nitrogen and oxygen isotope fractionation during dissimilatory nitrate reduction by denitrifying bacteria.* Limnology and Oceanography, 2008. **53**(6): p. 2533-2545.

50. Wunderlich, A., R. Meckenstock, and F. Einsiedl, *Effect of different carbon substrates on nitrate stable isotope fractionation during microbial denitrification.* Environmental science & technology, 2012. **46**(9): p. 4861-4868.

51. Kuypers, M.M., H.K. Marchant, and B. Kartal, *The microbial nitrogen-cycling network.* Nature Reviews Microbiology, 2018. **16**(5): p. 263.

52. Fülöp, V., et al., *The anatomy of a bifunctional enzyme: structural basis for reduction of oxygen to water and synthesis of nitric oxide by cytochrome cd1.* Cell, 1995. **81**(3): p. 369-377.

53. Maia, L.B. and J.J. Moura, *How biology handles nitrite.* Chemical reviews, 2014. **114**(10): p. 97.

54. Li, Y., M. Hodak, and J. Bernholc, *Enzymatic mechanism of copper-containing nitrite reductase.* Biochemistry, 2015. **54**(5): p. 1233-1242.

55. Murphy, M.E., S. Turley, and E.T. Adman, *Structure of nitrite bound to copper-containing nitrite reductase from Alcaligenes faecalis mechanistic implications.* Journal of Biological Chemistry, 1997. **272**(45): p. 28455-28460.

56. Simpson, P.J., D.J. Richardson, and R. Codd, *The periplasmic nitrate reductase in Shewanella: the resolution, distribution and functional implications of two NAP isoforms, NapEDABC and NapDAGHB.* Microbiology, 2010. **156**(2): p. 302-312.

CHAPTER 5.

SUMMARY AND CONCLUSIONS

In this work I performed experimental studies and geochemical simulations as complimentary tools to study the bioreductive dissolution of iron (hydr)oxides under marine conditions, which leads to a release of Fe(II) and associated TEs, and the influence of the released Fe(II) on nitrite stability.

The results of experimental observations lead to the following conclusions about the bioreductive dissolution:

1. Under marine conditions, *Shewanella loihica* bioreduces the structural Fe(III) of iron (hydr)oxides (e.g., magnetite, ferrihydrite) that are present in mine tailings.
2. Bioreduction of the iron (hydr)oxides brings about the release of Fe(II) and associated TEs (Mn, V, Cd, Cu, Ti, Ni, Pb and As).
3. Some of the Fe(II) released adsorbs onto the (hydr)oxide surface, leading to a transformation of the (hydr)oxide to a new biogenic phase containing Fe^{2+}/Fe^{3+} (i.e. magnetite). This mechanism results in a decrease in the (hydr)oxide reactive surface area, lowering the total available Fe(III) and, hence, the bioreduction rate.
4. From the experimental results, it is inferred that a continuous disposal of mine tailings in the sea would induce a lasting bioreduction of the (hydr)oxides contained in the tailings with the consequent TE release into the environment as long as Fe(III) is available.
5. The (hydr)oxides from distinct ore deposits in Chile and Sweden and from two mine tailings (pellet plant in Huasco (Chile) and Portman Bay (Spain)) show a high TE (Mn, V, Cd, Cu, Ti, Ni, Pb and As) content. Therefore, bioreduction of these (hydr)oxides under STD conditions will increase the concentrations of labile TE in the seabed sediments and in the water column.

6. Bioreduced Fe(II), either as an aqueous or solid-bound species, can remove nitrite, interfering thus in the nitrogen cycle of the ocean.

7. The $\varepsilon^{18}O/\varepsilon^{15}N$ ratio is useful to characterize the mechanisms involved in the Fe(II)-N interaction and to identify the source of nitrite reduction in marine systems. This finding can improve the prospect of using isotopic data to investigate nitrite reduction processes in marine systems.

The simulations lead to the following conclusions about the reductive dissolution kinetics and its environmental implications:

1. Bioreduction of iron (hydr)oxides under marine conditions was modeled using a Monod kinetic formulation.
2. Modeling suggested that the content of Fe^{2+}/Fe^{3+} of the oxides is an important factor controlling the fate and mobility of Fe(II). The stoichiometry of the newly formed magnetite (e.g., Fe^{2+}/Fe^{3+} ratio = 0.5) limits the amount of Fe(II) that can be adsorbed into the iron oxide and the transformation into new magnetite.
3. The TE release depends on the reductive dissolution rate of the iron (hydr)oxide.
4. In the tailings, the bioreduction rate coefficients are related to the Fe(III) availability, which is determined by the reactive surface area of the (hydr)oxides. Hence, a high (hydr)oxide reactive surface area yields a high Fe(II) release and Fe(II) adsorption, which induce an early bioreduction halt.
5. The kinetic model provided in this study is a useful tool to assess the environmental impacts of STD on the sea bed.

I demonstrate that the bioreduction of iron (hydr)oxides contained in mine tailings releases Fe(II) and TEs, which could increase the concentrations of labile TEs in the seabed sediments and the water column. In addition to an adverse impact of TEs on the marine fauna, solubilization of Fe, a limiting nutrient for phytoplankton production, could lead to fertilization and eutrophication of disposal sites, resulting in oxygen depletion and expansion of the oxygen minimum zone. Thus, besides the known smothering of benthic organisms and physical alteration of seabed habitats in areas affected by STD, bioreductive dissolution of iron (hydr)oxides must be considered as a process with a potential negative impact on the marine ecosystem. Hence, the submarine disposal of tailings containing iron (hydr)oxides is not recommended as an alternative to land disposal.

I suggest that a future study should focus on the following issues in order to achieve a comprehensive knowledge of the impact of STD on seabed sediments:

1. Characterization of seabed sediments affected by STD to corroborate the occurrence of bioreduction (e.g., Portman Bay and/or Ensenada Chapaco); identification of bacterial communities and bioreduced zones (altered sediments).
2. Laboratory column experiments performed with seabed sediments affected by STD to determine the extent of bioreduction; comparison with the results of the present study.
3. Use of autochthonous microorganisms in bioreduction experiments and comparison with the results of the present study.
4. Reactive transport modeling of column experiments with seabed sediments affected by STD using the Monod kinetic formulation.
5. In addition to oxygen and nitrogen isotopic analyses of seabed sediments to study nitrite reduction in marine systems, iron isotopic analysis would help to better understand the relationships between the Fe and N cycles of the ocean.

APPENDIX 1

1. Solid sample source and characterization

The source of the solid samples, mineralogical composition and specific surface area are indicated in Table A1.1

Table A1. 1. Solid sample, mineralogical composition, deposit type (IOA: Iron Oxide Apatite; IOCG: Iron Oxide Copper Gold) and specific surface area.

Iron ore and tailings samples

Sample Name	Location	Mineralogy	Deposit type	Specific surface area (m^2/g)
S1 (M~35)	Kiruna, Sweden	**Magnetite (35%)**, Hydroxylapatite (56%), Illite (8%)	IOA	0.2
S2 (M~79)	Malmberget, Sweden	**Magnetite (79%)**, Hydroxylapatite (14%), Ferro-actinolyte (< 5%)	IOA	0.3
C1 (M~89)	Laco Sur, Lower Pit, Chile	**Magnetite (89%)**, Hydroxylapatite (11%)	IOA	0.8
C2 (M<5)	Elicena Deposit, Algarrobo district, Chile	**Magnetite (< 5%)**, Hydroxylapatite (48%), Hornblende (33%), Chlorite (12%)	IOA	0.6
C3 (M~8)	Caminada drill hole, Vallenar district, Chile	**Magnetite (8%)**, Chlorite (47%), Albite (24%), Chalcopyrite (13%), Microcline (7%), Calcite (< 5%)	IOCG	2.4
C4 (H~40/M~19)	Mariposa Deposit, Algarrobo district, Chile	**Magnetite (19%)**, Actinolite (41%), **Hematite (40%)**		1.8
C5-T (M~90)	Los Colorados mine, Vallenar district, Chile	**Magnetite (90%)**, Chlorite (5%), Quarz (< 5%), Calcite (< 5%)	IOA	0.5
CT (M<5)-Tailings	Los Colorados mine, Vallenar district, Chile	**Magnetite (< 5%)**, Chlorite (22%), Actinolite (30%), Albite (28%), Talc (16%)	IOA	5.2

Synthetic monomineralic samples

Sample Name	Source	Mineralogy	Specific surface area (m^2/g)
F	IDAEA Laboratory	Ferrihydrite (100%)	181
M	Sigma - Aldrich	Magnetite (purity 95%)	6.9
G	Sigma - Aldrich	Goethite (100%)	12.3
H	Sigma - Aldrich	Hematite (purity ≥ 99%)	5.4

Samples C1-4, C5-T and CT are from deposits located at the Chilean iron belt, in the mining areas of El Laco volcano (C1), Algarrobo district (C2 and C4) and Vallenar district (C3, C5-T and CT), respectively (Table A1.1). Samples C1, C2, C5-T and CT are from Iron Oxide Apatite (IOA) deposits, an important global source of Fe ore, whereas the sample C3 is from an Iron Oxide Copper Gold (IOCG) deposit. Samples S1 and S2 are from iron IOA-type deposits located at the Kiruna – Malmberget district in Sweden (Table A1.1).

An iron ore tailings (CT) sample was obtained at the outlet of a plant that processes magnetite ore. The iron ore from the mine (mainly massive magnetite ore, up to 94%) [1] is milled and the iron mineral in the obtained micro-sized powder is concentrated by wet gravity and magnetic separation in the plant. The tailings produced are then released to the seafloor at 500 m from the coastline through a submarine pipeline. A sample of 20 L was collected every 45 minutes just at the outlet of the plant (total of 12 samples). For each sample, approximately 2 Kg of tailings slurry was recovered by centrifugation. All the samples were dried and homogenized in a single sample before further use.

Methods, equipment and settings used for solid sample characterization.

Before the preparation of the experiments, a mineralogical characterization of the samples was conducted. Powder *X-ray diffraction (XRD) analysis and Rietveld refinement* [2, 3] were performed using a Bruker D8 Advance A25 X-ray diffractometer θ-θ with CuKα1 radiation (see results in Table A1.1). For the tailings and iron ore samples, polished thin sections were examined using a *petrographic microscope* and a *scanning electron microscope (SEM)*. Samples were coated with carbon or gold before SEM observation. The SEM (Hitachi H-4100FE instrument under a 15–20 kV potential in a high vacuum) was equipped with an energy dispersive X-ray spectrometer (EDS) for the compositional analyses, and the morphology and textures were examined using backscattered (backscattered electron detector, BSD) and secondary electron modes in Field Emission (FE). All samples were also analyzed by *attenuated total reflectance - Fourier transform infrared spectroscopy (ATR-FTIR)* using a PerkinElmer frontier/ATR diamond/detector DTGS (accumulation at 16 scans, spectral resolution 4 cm^{-1}, spectral range 4000-225 cm^{-1}). Finally, the specific surface area of all the powder samples (Table A1.1) used in the experiments was determined by the *Brunauer-Emmett-Teller (BET)* method [4] using a Gemini surface area analyzer and 5-point N_2 adsorption isotherms. Sample degassing with nitrogen lasted for 2 h at 137 °C. Data uncertainty was around 10%. Synthesized ferrihydrite showed the largest value (181 $m^2 g^{-1}$) and S1 and S2 the lowest ones (0.2 and 0.3 $m^2 g^{-1}$, respectively).

2. Solid-sample elemental composition analysis

Further information on the methods used for the elemental composition analysis of i) mineral phases present in the solid samples and ii) bulk solid samples is indicated below.

Electron microprobe analysis (EMPA): The EMPA were carried out on a Jeol™ JXA-8230 WD/ED equipped with five wavelength dispersive X-ray spectrometers (WDS) and an energy dispersive X-ray spectrometer (EDS). A 5 µm diameter beam was used with an acceleration voltage of 20 kV and a beam current of 15 nA. Microprobe results were accepted only if the compound weight percent total was between 95.5 and 104.5%.

Laser ablation inductively coupled plasma mass spectrometry (LA-ICP-MS): Measurements by LA-ICP-MS were conducted at the Geochronology and Isotope Geochemistry-SGIker facility of the University of the Basque Country (UPV/EHU). The elemental analysis of minerals in ca. 100 µm thick petrographic sections was performed using a 213 nm Nd:YAG UP213 (New Wave Research, Fremont, USA) coupled to a Thermo iCAP Qc quadrupole-based ICP-MS (ThermoFisher Scientific, Bremen, Germany) with enhanced sensitivity through a dual pumping system. Spot diameters of 30 and 55 µm (depending on the grain size) associated to repetition rates of 10 Hz and laser fluence at the target of ca. 3.65 J/cm^2 were used. The ablated material was carried into helium and then mixed with argon before injection into the plasma source. Details on the system settings used during the analyses are shown in Table A1.2.

Table A1. 2. Laser ablation and Q-ICP-MS operation conditions

Q-ICP-MS	
ICP-MS	iCAP Qc
Forward Power	1550 W
Gas Flows	
Coolant (plasma)	Ar: 14 L/min
Auxiliary	Ar: 0.8 L/min
Carrier Gas	He: 0.6 L/min
Make up gas	Ar: 0.7 L/min
Analysis protocol	
Scanning mode	Peak hopping, 1 point per peak
Acquisition mode	TRA (Time Resolved Analysis)
Analysis duration	90 s (30 s background, 60 s signal)

Laser Ablation	
Laser	New Wave Research UP213
Wavelength	213 nm
Energy density	75% (ca. 3.65 J/cm^2)
Repetition rate	10 Hz
Nominal spot size	30 or 55 µm

The reference material NIST 612 [5] was used for the instrument calibration and a working standard of Durango apatite was used to control the instrument performance. Reference materials were analysed several times at the beginning of the analytical session and monitored throughout the session. Trace element (TEs) concentrations were obtained using the software Iolite 3.32 [6, 7] and the values for ^{57}Fe, ^{29}Si, ^{44}Ca and ^{140}Ce were used as internal standard depending on the minerals analyzed. For instance, to determine the TEs concentration of magnetite the iron concentrations measured by EMPA were used as internal standard for calibration of LA-ICP-MS data.

Total acid digestion of bulk solid samples: Solid samples were totally dissolved by reaction with concentrated HNO_3, HF and $HClO_4$ following a method similar to that of Torres and Auleda [8]. Briefly, 0.1 g of each solid sample first reacted with HNO_3 (2.5 mL) in a Teflon reactor for 24 h at 90 ^{0}C using a graphite oven system. Then, the sample was recovered from the reactor with ultrapure Milli-Q water (18.2 MΩ cm at 25 °C) and the liquid and remaining solid fractions were separated by centrifugation (25 minutes at 3000 rpm). The liquid was kept and the solid was immediately transferred to the Teflon reactor where reacted with HNO_3 (2.5 mL) and HF (7.5 mL) at 90 ^{0}C for 24 h. After that, the system was cooled down and $HClO_4$ (2.5 mL) was added to the Teflon reactor before it was heated on a heating plate (set a 250 ^{0}C) until dryness. Finally, the sample is recovered from the reactor by dissolving the salts with HNO_3 (2.5 mL). The obtained solution was put together with the liquid fraction collected in a previous step, diluted with Milli-Q water (2.5% HNO_3) and preserved at 4 ^{0}C until analysis.

3. Preparation of Batch experiments, sampling and analysis

Artificial seawater (ASW)

ASW was prepared according to the *ASTM D1141-98* requirements. This standard method allows the preparation of ASW with heavy metals; however, the heavy metals were not added to the ASW in other to keep their concentration levels as low as possible. A low background of heavy metals concentration in the solution can facilitate their detection during an eventual release from the solid samples. Before setting up the microcosms and controls, all the tubes, caps, solid samples, medium and other glassware used were autoclaved for 20 minutes at 121 ^{0}C.

Experiments sampling and analysis

Sampling was performed in a glove box with N_2 atmosphere to maintain the anoxic conditions. The vials were shaken just before sampling and then liquid sample aliquots were collected and filtered using a sterile syringe and syringe filters (0.22 µm pore size). Sample aliquots were used for pH / Eh / Dissolved oxygen (DO) measurements and for chemical analyses of cations and anions (lactate and acetate). For ion analysis a volume of 10 mL was preserved at pH < 2 by adding 100 µL of 60% (v/v) HNO_3 solution. For Fe(II) / Fe(III) measurements by Phenanthroline colorimetry [9] , an additional volume of 10 mL was preserved with the addition of 100 µL of 6 M HCl solution. Thereafter, all liquid samples were stored at 4 °C in the dark until analysis. After removal of the liquid fraction, the tubes with the solid were closed in the glove box and quickly frozen at -80 ^{o}C. Then, the solid samples were freeze-dried for 48h in the same tubes and preserved under a N_2 atmosphere until analysis.

Measurements of pH (± 0.02 pH units), Eh (± 10 mV) and DO (± 0.1 mg/L) were performed in the glove box using pH (Thermo Orion, Thermo Scientific), Eh (SenTix ORP, Ag/AgCl, WTW) and DO (Intellical™ LDO101) electrodes. Oxidation-reduction potential readings were converted to standard Eh values (Eh_{std}) by correcting for the electrode potential of the reference hydrogen electrode. Total iron and TEs were analyzed by ICP-MS (Perkin Elmer 3000). Only the samples from the experiments with ferrihydrite were measured by ICP-OES. The uncertainty of the ICP-MS (and ICP-OES) measurements were estimated based on the analysis of sample replicates with different concentrations: Fe (< ±5%), Mn (< ±3%), Ni (< ±5%), Cu (± 20%), As (± 10%), Co (< ±5%), V (< ±3%) and Ga (± 10%). Given the elevated ion concentrations in ASW, samples for ICP-MS analysis had to be diluted, which increased the detection limits: Fe (< 75 mg/L), Mn (< 15 mg/L), V (< 7 mg/L), As (< 7 mg/L), Cu (< 7 mg/L), Ni (< 7 mg/L), Ga (< 7 mg/L), Ti (< 7 mg/L) and Co (< 2 mg/L). Total iron measured was checked to be Fe(II) with a modified protocol of the phenanthroline method [9]. Lactate and acetate concentrations were determined by HPLC (Waters 600 HPLC pump controller equipped with an Aminex HPX-87H column (300 x 7.8 mm), BioRad, and a Waters 717 plus autoinjector).

Control experiments

Abiotic control (AC) experiments were performed in parallel with the iron bioreduction experiments. The AC tubes were prepared as the microcosms but without microbial inoculum. In addition, anoxic abiotic control (AAC) experiments were prepared in the glove box under anoxic conditions using degassed (O_2-free) ASW or Milli-Q water (18.2 MΩ cm at 25 °C). The AAC experiments with degassed Milli-Q water were performed for all the solid samples whereas those with degassed ASW for CT, C5-T, S2 and F samples. The AAC experiments lasted approximately 48 days. The AC and AAC experiments were performed and sampled in the same conditions as the iron bioreduction experiments.

4. Trace element composition of hematite in sample C4

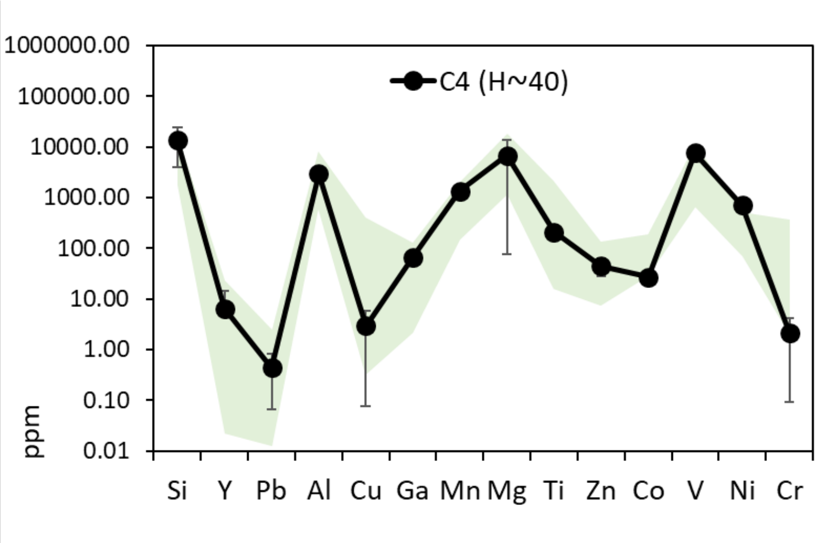

Figure A1. 1. Trace element content (ppm) of hematite determined by LA-ICP-MS for the C4 sample. The shaded area corresponds to the range of average concentrations in magnetite determined for C1-3, S1 and S2 samples. Weight % of hematite (H) in the C4 sample is indicated in brackets.

5. Comparison of TEs composition of magnetite from different deposits in Chile and Sweden and with data from previous studies

The TEs composition of magnetite from S1 and C1 samples is remarkably similar with the exception of the much higher Mg concentration values of the latter (Fig. A1.2). This result agrees very well with a previous study that measured the TEs composition of magnetite in such deposits to investigate their origin [10]. The TEs concentration values of the C1 sample are also very similar to those available in a recent study[14] investigating the origin of this magnetite deposit (L sample, Fig. A1.2).

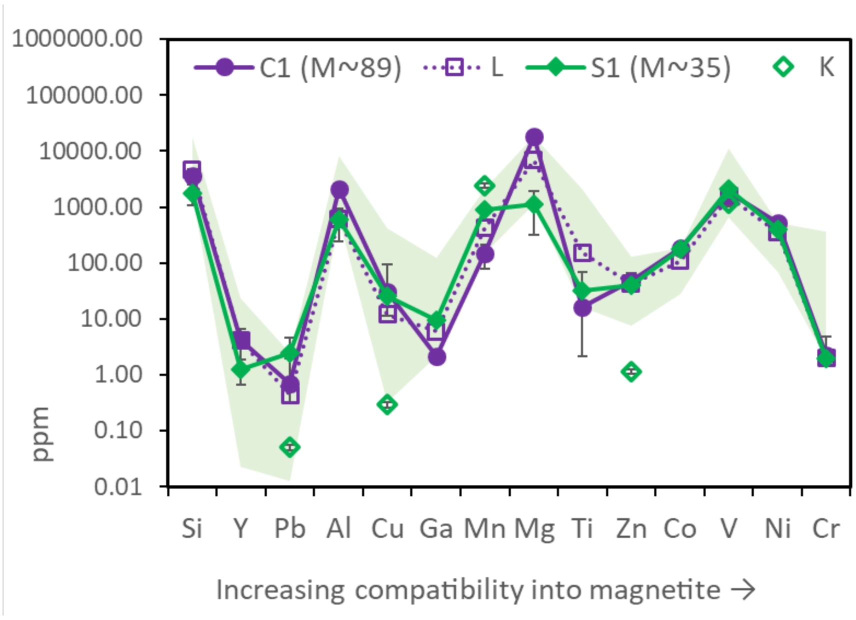

Figure A1. 2. Comparison of the TEs content (ppm) of magnetite determined by LA-ICP-MS in C1 and S1 samples and with data from the literature (i.e., L data from Dare et al. [11], and K data from Müller et al., [12]). The shaded area corresponds to the range of average concentrations determined for C1-3, S1 and S2 samples. Weight % of magnetite (M) in the samples measured in this study is indicated in brackets.

In contrast, compared to the TEs concentration values in S1 magnetite, significantly lower values were determined for elements such as Zn, Cu and Pb in magnetite samples from the same mine in a previous study by Müller et al. (sample K, Fig. S2) [12]. Unfortunately, data for the other elements illustrated in Figure A1.2 are not available in the previous study. Unlike the magnetite ore samples analyzed in the present study, which were taken directly from mines or deposits, with exception of the iron ore tailings sample, Müller et al. [12] determined the TEs composition of magnetite grains collected from different parts of the concentrating plant. In particular, data shown in Figure A1.2 were measured in magnetite grains from the primary magnetic sorter but even slightly lower mean values were determined in magnetite samples collected at the outlet of the concentrating plant [12]. This result might suggest that the concentration of TEs in magnetite from ore samples collected directly from the mine (S1 sample) and magnetite concentrate from the plant (K sample) could be different (see Section 6).

6. Trace element composition of CT and C5-T samples determined by EMPA

The results obtained by EMPA showed significantly higher average TEs concentration values (in % relative to the TEs amounts measured in the magnetite of CT-5 sample) in the tailings' magnetite (CT) for several elements such as Zn (273%), Mn (131%) and Cu (110%).

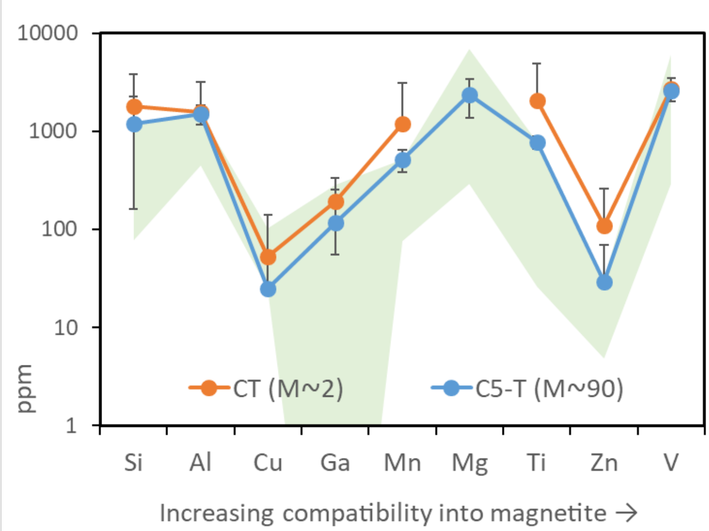

Figure A1. 3. Trace element content (ppm) of magnetite determined by EMPA. The shaded area corresponds to the range of average concentrations determined for the samples C1, C2, C3, S1, S2 and C5-T. The wt.% of magnetite (M) is indicated in brackets.

The higher concentrations of TEs observed for the tailings' magnetite compared to the magnetite in the ore samples, collected directly from the mine or deposit (i.e., non-processed) (Fig. A1.3 and Fig. 2.1C), might be explained by TEs fractionation during magnetite concentration in the plant leading to a TEs-enriched magnetite in the tailings fraction. The magnetite ore tailings investigated in this study were affected by magnetic separation in the concentration plant. Previous studies observed changes in the magnetic properties of vanadium-[13] and zinc-substituted [14] magnetite compared to pure magnetite, supporting a hypothetical effect of magnetite's TEs content on its magnetic properties. This hypothesis might also explain the magnetite composition relatively depleted in Zn, Cu and Pb observed in Figure A1.2 for the magnetite concentrate (K sample) obtained from a concentrating plant (primary magnetic sorter) in a previous study [12] . However, further research is necessary to confirm this hypothesis.

7. Geochemical model settings and additional information

Oxidation of lactate by dissolved oxygen at the beginning of all the experiments was expressed as:

$$C_3H_5O_3^- + 0.4\ NH_4^+ + 0.85\ O_2 \rightarrow 0.4\ C_5H_7O_2N + CO_2 + 1.9\ H_2O \qquad \text{(EA1.1)}$$

where $C_3H_5O_3^-$ and $C_5H_7O_2N$ are lactate and cell biomass, respectively. The stoichiometric coefficients for the reactions with magnetite-bearing samples in anoxic conditions are shown in Table A1.3. Previous studies showed that the biomass yield (also referred to as microbial growth yield, Y in eq. 2.3) for *Shewanella* strains during lactate oxidation in oxic conditions is higher than in iron reducing conditions, which agreed with the free energy (DG) calculations for the respective reactions (see [15] and references herein). In the present study, the Y values (i.e., mol of biomass produced/mol of substrate consumed) used in the geochemical simulations were 0.4 in oxic conditions and between 0.15 and 0.06 in iron reducing conditions (Table A1.4). These Y values were determined by model calibration, based on the measurements of lactate and acetate concentrations during the experiments, and were constrained according to the values from the literature. In order to avoid that biomass growth simulations result in very high cell numbers, a decay rate coefficient (m_{dec}) of $2.2 \times 10^{-6}\ s^{-1}$ was used in eq. 2.3 for all the experiments, leading to a maximum of ca. $\approx 1\cdot10^{-8}$ cells mL^{-1} in the experiments with ferrihydrite.

The lower iron reduction rate observed after 20 days for most of the experiments (Figs. 2.2 and A1.5) was simulated by including in eq. 2.3 a factor (In_{dec}) that inhibits the biomass decay at low cell concentrations (X_{min}, see Table S4). Using this biomass decay inhibition factor, a relatively small cell biomass concentration compared to the initial biomass (X_0) remains in the simulations, which is necessary for sustaining iron reduction at low rate. For the experiments with the magnetite-bearing samples, a X_{min} / X_0 ratio from 0.05 to 0.55 was determined by model calibration (Table A1.4). Concentration of colony forming units (cfu mL^{-1}) was converted to cell biomass (mol cells L^{-1}) using the dimensions of *Shewanella loihica* from Gao et al. [16] and the biovolume-to-biomass conversion factor determined by Lee and Fuhrman [17].

Secondary ferrous iron minerals

Precipitation of magnetite ($Fe^{2+}Fe^{3+}{}_2O_4$) and other potential secondary Fe^{2+}-bearing minerals such as siderite ($Fe^{2+}CO_3$) was considered in the geochemical model according with the following reactions (see Tables A1.3 and A1.5):

$$Fe^{2+} + 2Fe^{3+} + 4\ H_2O \rightarrow Fe^{2+}Fe^{3+}{}_2O_4 + 8\ H^+ \qquad \text{(EA1.2)}$$

$$Fe^{2+} + CO_3{}^{2-} \rightarrow Fe^{2+}CO_3{}^{2-} \qquad \text{(EA1.3)}$$

Table A1. 3. Stoichiometric coefficients of the reactions with magnetite-bearing samples simulated with PHREEQC.

Magnetite bioreduction

Sample	$C_3H_5O_3^-$	NH_4^+	$Fe^{2+}Fe^{3+}{}_2O_4$	H^+	→	$C_2H_3O_2^-$	HCO_3^-	$C_5H_7O_2N$	Fe(II)	H_2O	Magnetite stoichiometry (Fe^{2+}/Fe^{3+})
M (Syn)	1.0	0.15	1.39	7.45		0.75	0.75	0.15	4.05	4.50	0.35
C5-T (M~90)	1.0	0.15	1.37	7.33		0.75	0.75	0.15	3.99	4.44	0.33
C1 (M~89)	1.0	0.15	1.37	7.33		0.75	0.75	0.15	3.99	4.44	0.33
S2 (M~79)	1.0	0.15	1.39	7.45		0.75	0.75	0.15	4.05	4.50	0.35
S1 (M~35)	1.0	0.15	1.35	7.15		0.75	0.75	0.15	3.90	4.35	0.30
C3 (M~08)	1.0	0.10	1.42	7.23		0.83	0.83	0.10	4.00	4.30	0.20
C2 (M < 5)	1.0	0.10	1.42	7.23		0.83	0.83	0.10	4.00	4.30	0.20
CT (M < 5)	1.0	0.06	1.53	7.78		0.90	0.90	0.06	4.32	4.50	0.20

Secondary magnetite formation

Sample	Fe^{2+}	Fe^{3+}	H_2O	→	$Fe^{2+}Fe^{3+}{}_2O_4$	H^+	Magnetite stoichiometry (Fe^{2+}/Fe^{3+})
M (Syn)	1.32	2.64	5.28		1.32	10.56	0.5
C5-T (M~90)	1.31	2.62	5.23		1.31	10.46	0.5
C1 (M~89)	1.31	2.62	5.24		1.31	10.47	0.5
S2 (M~79)	1.32	2.64	5.27		1.32	10.54	0.5
S1 (M~35)	1.25	2.50	5.01		1.25	10.02	0.5
C3 (M~08)	0.17	0.34	0.67		0.17	1.34	0.5
C2 (M < 5)	0.20	0.41	0.82		0.20	1.63	0.5
CT (M < 5)	0.01	0.03	0.06		0.01	0.11	0.5

Siderite precipitation

Sample	Fe^{2+}	CO_3^{2-}	→	$Fe^{2+}CO_3^{2-}$
C3 (M~08)	3.45	3.45		3.45
C2 (M < 5)	3.24	3.24		3.24
CT (M < 5)	4.25	4.25		4.25

For each sample, the wt.% of magnetite (M) is indicated in brackets.

The reaction (EA1.2) was used to simulate magnetite growth in the experiments with magnetite-bearing samples. Ferric iron was formed via oxidation of adsorbed Fe(II) on the magnetite surface (see section 8). This process depends on the iron oxide mineral involved in the reaction. For instance, the reaction (EA1.4) was used to simulate magnetite formation in the experiment with hematite.

$$Fe^{2+} + Fe_2^{3+}O_3 + H_2O \rightarrow Fe^{2+}Fe^{3+}{}_2O_4 + 2\ H^+ \qquad \text{(EA1.4)}$$

The rate of siderite formation (eq. EA1.3) was directly connected to the magnetite bioreduction rate described by equation 2.1 in the Chapter 2.

Table A1. 4. Parameters used for the Monod rate expressions (eqs. 2.1 and 2.3 in chapter 2).

Oxic conditions

	K_S	K_{O2}	k_{max}	Yield[a]
Sample	mol Substrate/L	mol O_2/L	sec^{-1}	
All	1.00E-06	2.00E-05	4.40E-05	0.40

Anoxic conditions[b]

	K_S	K_{In} (O_2)	k_{max}	Yield[a]	Comments
Magnetite-bearing	mol Substrate/L	mol O_2/L	sec^{-1}		
M (Syn)	1.00E-06	2.00E-04	2.50E-06	0.15	
C5-T (M~90)	" "	" "	9.00E-07	" "	
C1 (M~89)	" "	" "	8.70E-07	" "	
S2 (M~79)	" "	" "	1.00E-06	" "	
S1 (M~35)	" "	" "	8.50E-07	" "	
C3 (M~08)	" "	" "	2.10E-06	0.10	
C2 (M < 5)	" "	" "	6.60E-07	0.10	
CT (M < 5)	" "	" "	1.90E-06	0.06	
Iron (hydr)oxides					
G (Syn)	" "	" "	2.10E-06	0.15	
F (Syn)	" "	" "	2.29E-05	0.10	
Mixed oxides					
C4 (H~40 / M~19)[c]	" "	" "	*1.30E-07*	*0.07*	*Hematite*
	" "	" "	*2.10E-06*	*0.03*	*Magnetite*
H~99.9 / MnO_2~0.1 (Syn)[d]	" "	" "	*2.80E-07*	*0.15*	*MnO_2 (K_{MnO2} = 5E-6 mol MnO_2/L)*
	" "	" "	*1.40E-06*	*0.06*	*Hematite (K_{in} (MnO_2) = 1E-5 mol MnO_2/L)*

Microbial decay

	μ_{dec}	X_{min}	X_{min} / X_0
Magnetite-bearing	sec^{-1}	mol cells/L	
M (Syn)	2.20E-06	1.00E-05	0.23
C5-T (M~90)	" "	2.00E-05	0.45
C1 (M~89)	" "	1.00E-05	0.23
S2 (M~79)	" "	" "	" "
S1 (M~35)	" "	" "	" "
C3 (M~08)	" "	" "	" "
C2 (M < 5)	" "	2.40E-05	0.55
CT (M < 5)	" "	2.00E-06	0.05
Iron (hydr)oxides			
G (Syn)	" "	1.00E-08	0.0002
F (Syn)	" "	" "	" "
Mixed oxides			
C4 (H~40 / M~19)	" "	2.00E-05	0.45
H~99.9 / MnO_2~0.1 (Syn)	" "	4.50E-05	1.02

The Monod parameters K_S (1 mM), K_{O2} (20 mM) and K_{in} (O_2) (200 mM) were considered according with Thullner et al. [18]. The wt.% of magnetite (M) is indicated in brackets. [a] Yield = mol of biomass produced / mol of substrate consumed. [b] In anoxic conditions, the Monod term Fe^{3+} / (K_{Fe3+} + Fe^{3+}) in eq. (2.1) was assumed ≈ 1 given the relatively high amount of Fe^{3+} in most of the samples. [c] In C4 sample, hematite (≈ 40 wt.%) was also present. [d] In H sample a small amount of MnO_2 (≈ 0.1 wt.%) was determined (see section 9).

Table A1. 5. Results obtained by model simulations with PHREEQC

	Initial (0 days)		Final (113 days)							
Sample	Fe^{3+} solid	Magnetite Stoichiometry	$Fe(II)_{aq}$	Secondary magnetite	Siderite	Total Fe(II) from solid Fe^{3+}	Fe^{3+} reduction	Total lactate consume	SI siderite[a]	Comments
Magnetite-bearing	mM	Fe^{2+}/Fe^{3+}	mM	mM	mM	mM	%	%		
M (Syn)	88.4	0.35	0.07	1.06	---	3.3	3.7	13.3	0.29	
C5-T (M~90)	80.5	0.33	0.02	0.46	---	1.4	1.7	9.8	0.41	
C1 (M~89)	79.6	0.33	0.02	0.33	---	1.0	1.3	8.2	-0.09	
S2 (M~79)	69.9	0.35	0.03	0.39	---	1.2	1.7	8.5	0.21	
S1 (M~35)	31.8	0.30	0.04	0.31	---	1.0	3.0	8.1	0.35	
C3 (M~08)	7.7	0.20	0.03	0.11	2.2	2.6	33.2	12.2	0.00	
C2 (M < 5)	2.9	0.20	0.04	0.06	0.9	1.1	38.5	8.6	0.35	
CT (M < 5)	1.9	0.20	0.01	0.006	1.7	1.7	90.1	9.9	-0.42	
Iron (hydr)oxides										
G (Syn)	106.6	---	0.04	1.1	---	1.1	1.1	7.8	-0.83	
F (Syn)	89.2	---	1.2	28.4	1.9	31.6	35.4	100	1.85	
Mixed oxides										
C4 (H~40 / M~19)[b]	47.4	---	0.04	0.33	---	1.0	1.5	8.3	0.36	*Hematite*
	18.3	0.2								*Magnetite*
H~99.9 / MnO_2~0.1 (Syn)[c]	118.5	---	0.2	1.5	---	1.7	1.4	11.5	1.22	*(0.1 mM Mn^{4+})*

Initial contents of Fe^{3+} in the solid samples were calculated considering nonstoichiometric (or partially oxidized) magnetite. The wt.% of magnetite (M) is indicated in brackets. [a] SI, Saturation Index. [b] In C4 sample, hematite (≈ 40 wt.%) was also present. For C4 sample, the % of Fe^{3+} reduction was indicated relative to the content of ferric iron in both hematite and magnetite. [c] In H sample a small amount of MnO_2 (≈ 0.1 wt.%) was determined (see Section 9).

8. Fe(II) uptake on magnetite

Previous studies showed that the uptake of dissolved Fe(II) by magnetite depends on its initial stoichiometry ($X = Fe^{2+}/Fe^{3+}$) [19, 20]. In this study, the uptake of dissolved Fe(II) was simulated using the Langmuir isotherm equation (EA1.5):

$$C_{ad} = \frac{\alpha \cdot C_L \cdot C_{aq}}{1 + \alpha \cdot C_{aq}} \qquad \text{(EA1.5)}$$

where C_{ad} (mmol g^{-1}) is the concentration of Fe(II) adsorbed, C_{aq} (mM) is the aqueous Fe(II) concentration, C_L is the limiting sorbate concentration and a is the equilibrium constant related with energy of sorption. C_L and a are empirical fitting constants. As observed in Figure A1.4A, the equation EA1.5 describes well the results obtained by Gorski and Scherer [19]. These authors also reported the maximum uptake of Fe(II) from solution for different initial Fe^{2+}/Fe^{3+} ratios of magnetite. This information (Fig. A1.4B) was used to determine the values of C_L and a in eq. EA1.5 for the different Fe^{2+}/Fe^{3+} ratios considered for the magnetite-bearing samples (from 0.20 to 0.35, Table A1.5). These ratios are similar to the range available in the literature (e.g., $0.23 < Fe^{2+}/Fe^{3+} < 0.34$ for natural magnetite samples [19] and $Fe^{2+}/Fe^{3+} = 0.24$ after exposing stoichiometric synthetic magnetite to ambient air for 24 h [21]).

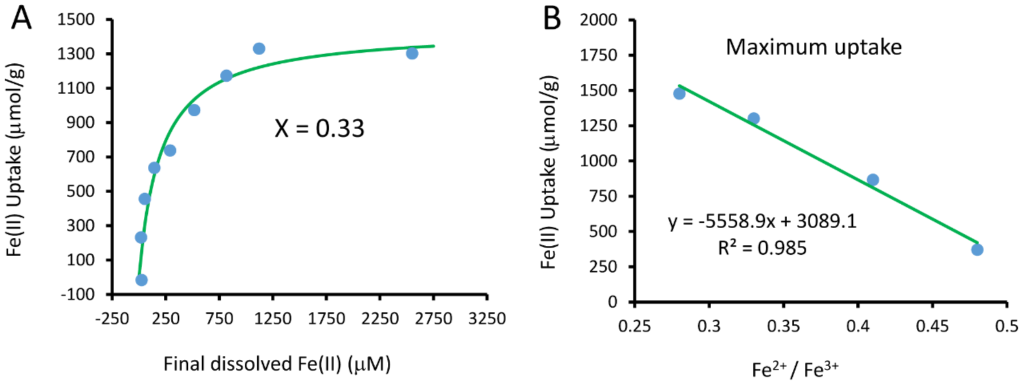

Figure A1. 4. (A) Uptake of Fe(II) from solution in an experiment with nonstoichiometric magnetite ($Fe^{2+}/Fe^{3+} = 0.33$) [20] .The solid green line shows the data fit according with eq. (EA1.5). (B) Effect of initial magnetite stoichiometry on the maximum Fe(II) uptake. The solid green line represents the linear correlation. Data points in (A) and (B) were obtained from Gorski and Sherer [19].

9. Magnetite (bio)reduction experiments

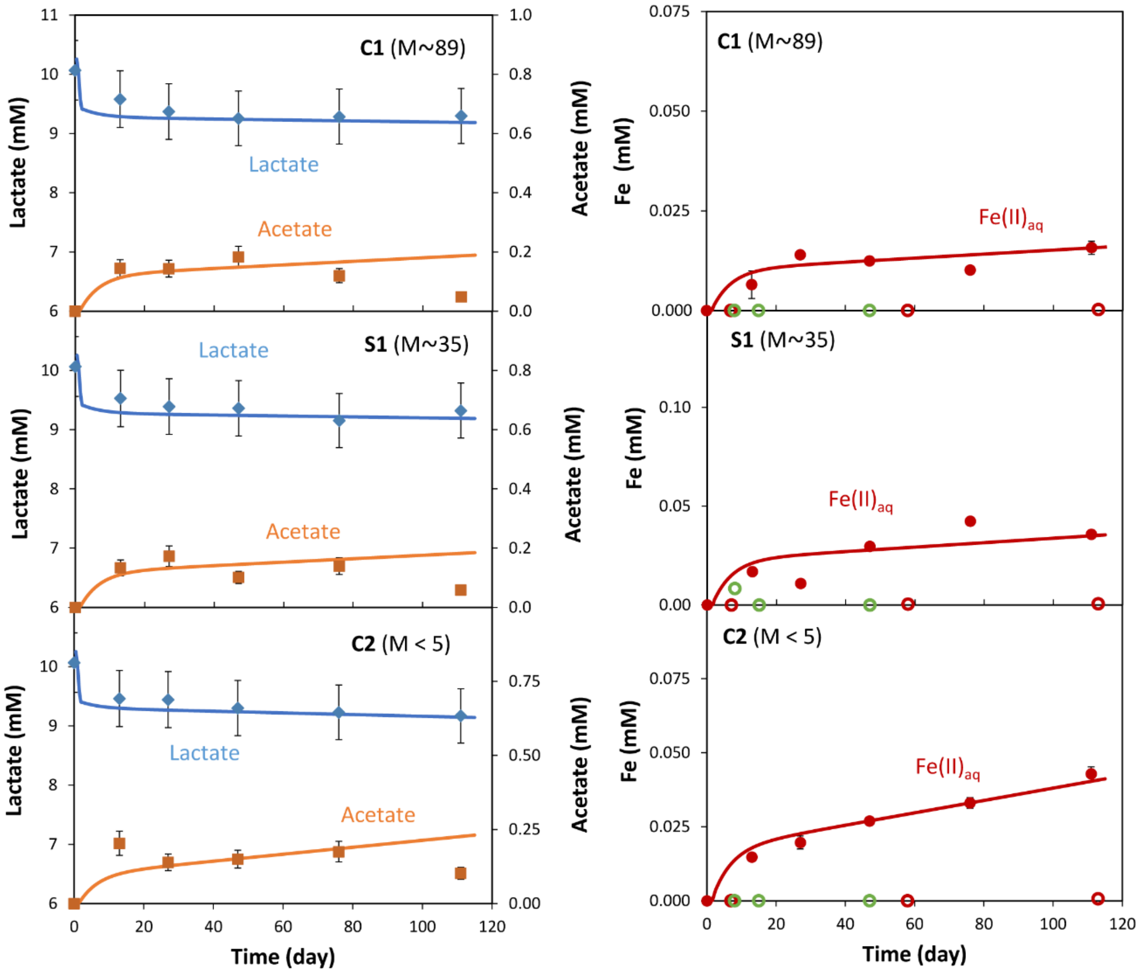

Figure A1. 5. Evolution of lactate, acetate and dissolved Fe(II) during the experiments. Solid lines show the trends obtained by model simulations. Empty circles in the right panels show the $Fe(II)_{aq}$ concentrations from abiotic controls (red) and from the anoxic abiotic controls prepared using O_2-free ASW (violet) or Milli-Q water (green). Weight % of magnetite (M) is indicated in brackets.

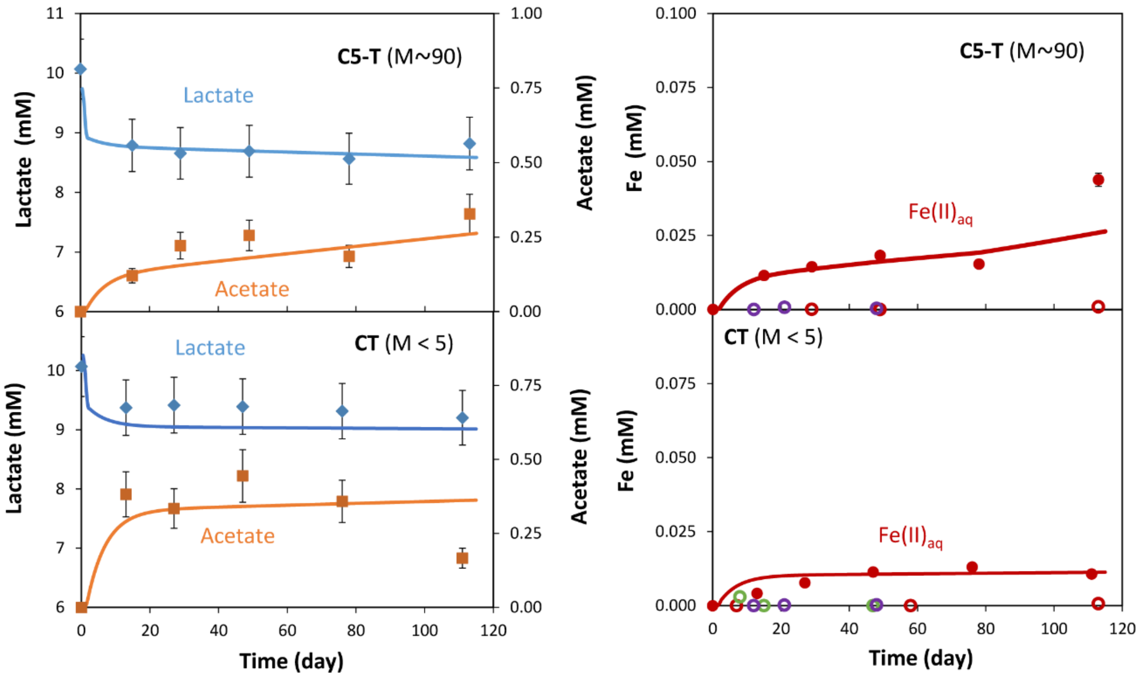

Figure A1.5. (Continuation).

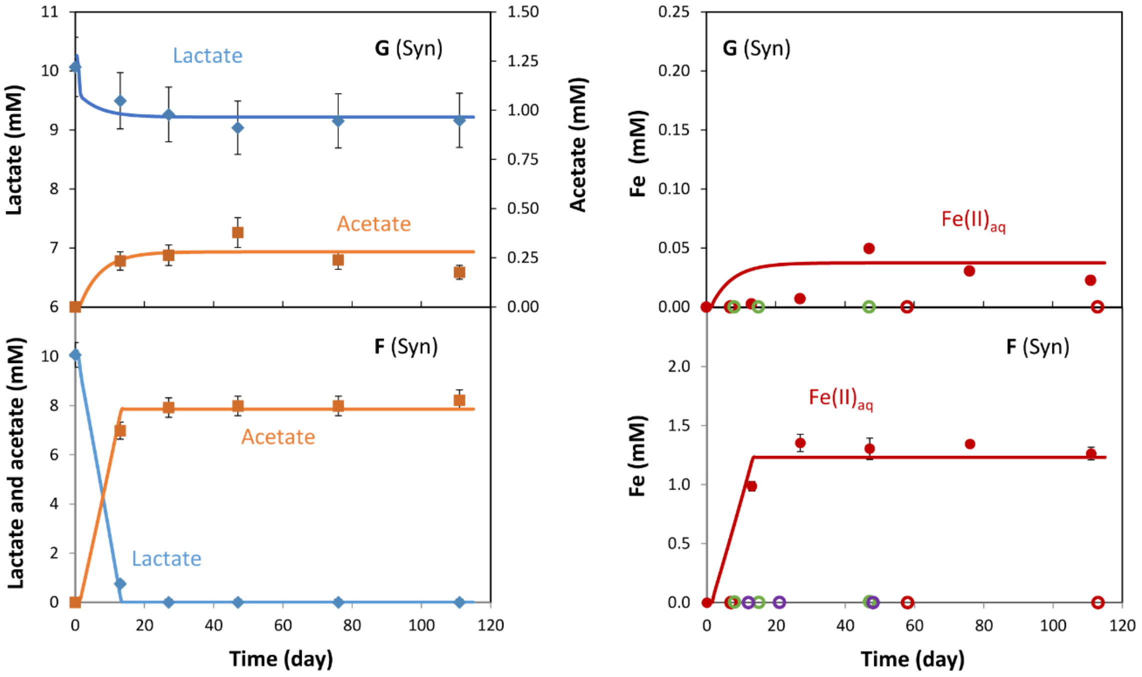

Figure A1.5. (Continuation).

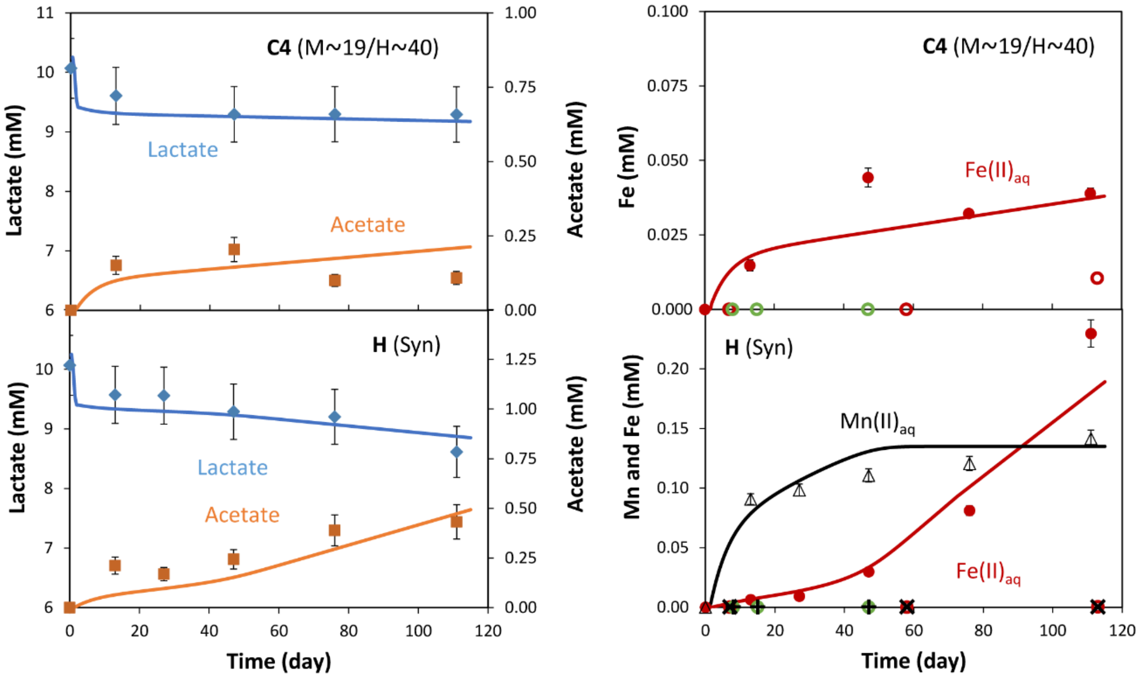

Figure A1.5. (Continuation). For the experiment with H sample, concentrations of dissolved Mn(II) in the microcosms (empty triangles), abiotic controls (x) and anoxic abiotic controls prepared with O_2-free Milli-Q water (+) are shown in the right panel.

In the experiment performed with synthetic hematite (H sample), high amounts of dissolved Mn(II) were observed, from 5.0 to 7.8 mg/L, suggesting the presence of Mn^{4+}-oxide in the solid and its bioreduction. Thus, MnO_2 was included in the geochemical model and a small amount of ≈ 0.1 wt.% of MnO_2 was estimated, which might be explained as a sample impurity. The geochemical model showed that reduction of Mn^{4+} inhibited Fe^{3+} bioreduction at the beginning of the experiment, which explains the different trend observed for the dissolved Fe(II) concentration in the experiment with H sample.

10. Mineralogical analysis by FE-SEM and ATR-FTIR of the solid samples collected at the end of the experiments.

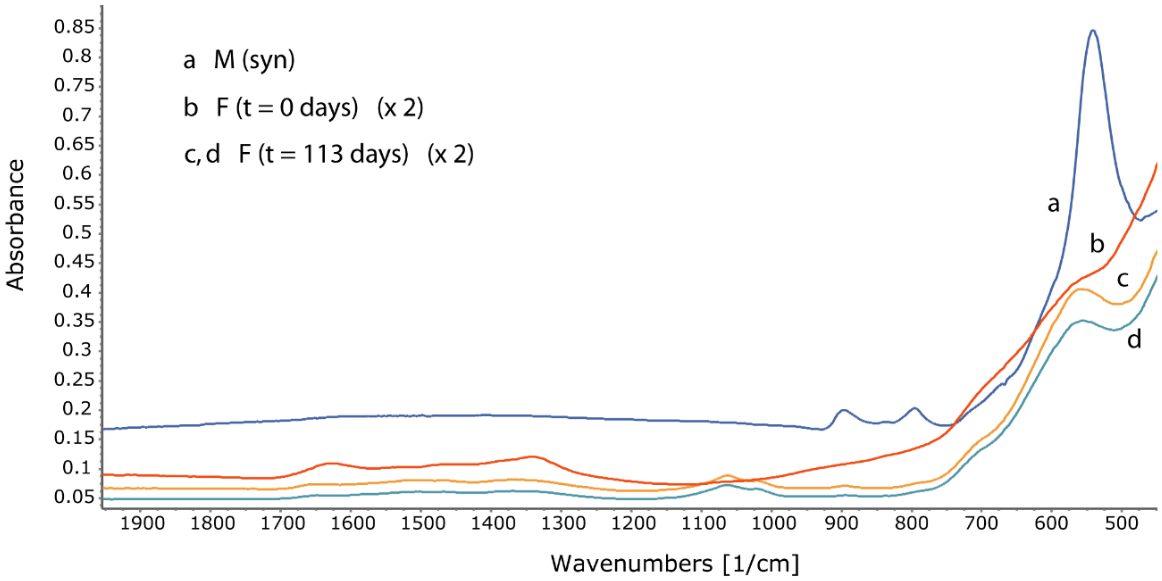

Figure A1. 6. ATR-FTIR spectra of: (a) synthetic magnetite, (b) ferrihydrite used in the experiments and (c, d) solid sample retrieved at the end of the experiments with ferrihydrite.

Formation of secondary magnetite in the experiments with ferrihydrite was detected by ATR-FTIR (Fig. A1.6). A characteristic absorbance peak of magnetite at around 545 cm^{-1}, observed for the synthetic magnetite sample (Fig. A1.6 a), was also observed for the samples retrieved at the end of the experiment with ferrihydrite (Fig. A1.6c, d). However, in the ferrihydrite this absorbance peak shifted to a slightly higher wavenumber (560 cm^{-1}) compared to that of synthetic magnetite. This shift was also observed in a previous study and the authors suggested that it may be due to an alteration of the crystal structure associated with the incorporation of substantial amounts of intra-crystalline organic matter during biogenic magnetite formation [22] .

The potential precipitation of siderite was also investigated in the samples C3, C2 and CT (Table A1.5) by ATR-FTIR (Fig. A1.7b-e). The most prominent adsorption features within carbonate spectra (at 1400 and 875 cm^{-1}) arise from the CO_3^{2-} ion [23] . The characteristic peaks of the siderite (Fig. A1.7a) were not observed in any of the samples, which is consistent with the small amounts of siderite (< 2.5 wt.%) estimated from the geochemical model (Table A1.5)

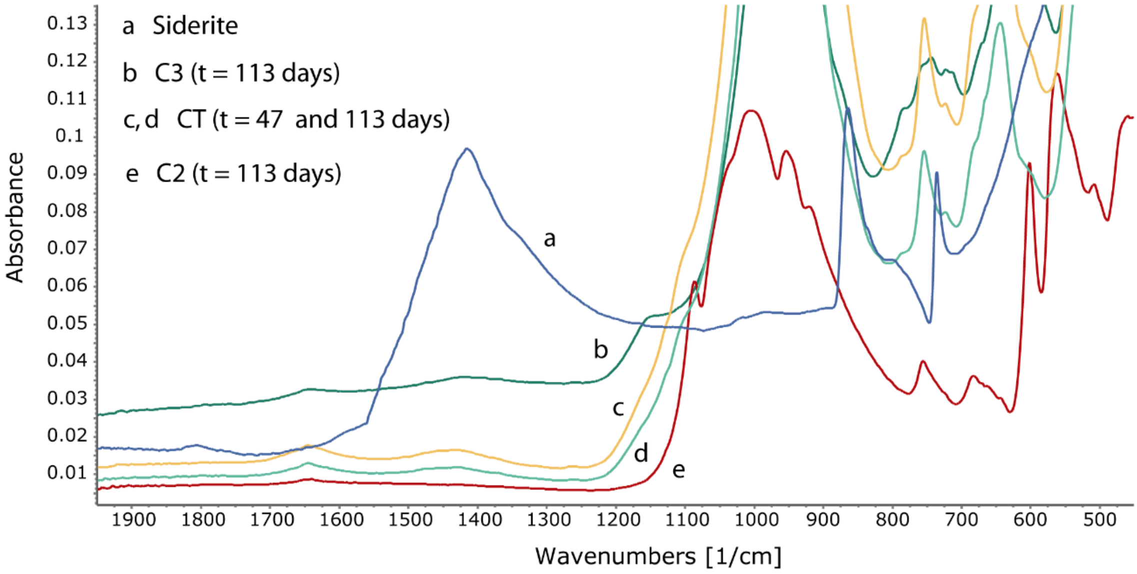

Figure A1. 7. ATR-FTIR spectra of: (a) natural siderite (86.6 wt.% $FeCO_3$), (b) C3, (c, d) CT and (e) C2.

11. Cell viable counts in the microcosm experiments

For some samples, cell counts showed an increase of cell number at the beginning of the experiment (Fig. A1.8), which was mainly associated with microbial growth in aerobic conditions. This observation is in agreement with the results obtained from the geochemical model. For the experiments with ferrihydrite, initial lactate concentration (10 mM) was totally consumed after 20 days, which may explain the very low cell numbers measured after 40 days. However, data from Fig. A1.8 must be used with caution since cell counts were performed in aqueous samples and, therefore, cells adsorbed on the solid phase were not taken into account.

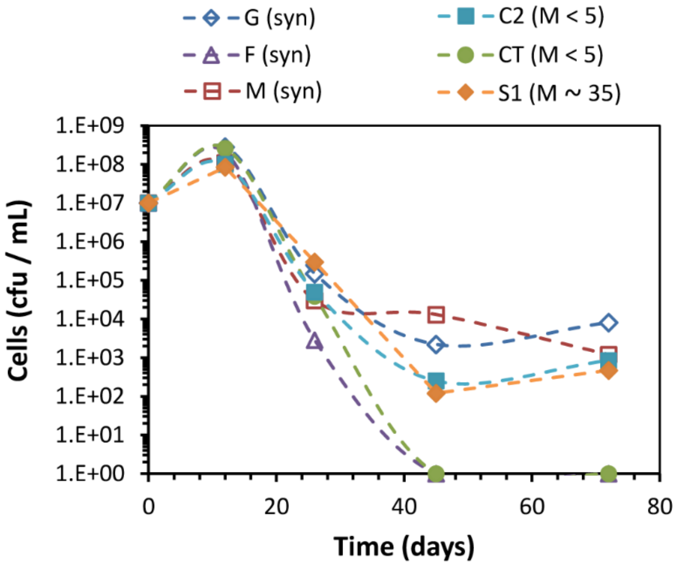

Figure A1. 8. Cell viable counts (*aqueous phase*)

12. Trace elements release in the microcosm experiments

Co and Ni

As indicated in the main text, despite Co and Ni concentrations were relatively high in the magnetite ore samples used in the experiments, they were never detected in solution or only in few samples, respectively. Zachara et al., [24] investigated the solubilization of coprecipitated Co(III) and Ni(II) from synthetic goethite during Fe(III) bioreduction at circumneutral pH, and indicated that both Co(II) and Ni(II) were released from goethite structure at a concentration and rate, relative to Fe(II), proportional to their mole fraction. However, these authors stated that a combination of geochemical reactions, including coprecipitation within biogenic Fe(II) secondary minerals, controlled whether the released metals were solubilized into the aqueous phase or remained associated with the solid fraction. In this study, [24] biogenic siderite appeared to structurally incorporate Co(II). Coker et al., [25] reported the incorporation of Co and Ni into the structure of biogenic magnetite, obtained through Fe(III) bioreduction of synthetic oxyhydroxides containing the appropriate substitution cations, and determined their site occupancies. A recent study [26] exploring the stabilization of different cations during ferrihydrite transformation induced by Fe(II) at pH 6.5, indicated that the transformations involving cations with high binding abilities (i.e., Ni(II), Co(II) and Zn(II)), resulted in larger amounts of stabilized metals in the secondary minerals (goethite and magnetite). These studies may thus help to explain the low solubilization of Co and Ni observed in the present study.

Stoichiometric coefficients of Mn, V, As, Ga and Cu estimated by model calibration

For Mn (samples C5-T and CT, Fig. 2.4) and Ga (CT), estimated stoichiometric coefficients by model calibration were consistent with the range of concentrations determined for these elements by LA-ICP-MS and EMPA in the respective magnetite samples. However, the estimated stoichiometric coefficients for As and specially V in the experiments with C5-T and CT samples (Fig. 2.4) were lower than those calculated according to their content in the respective magnetite samples (see discussion in the main text). For Cu (C1 sample, Fig. 2.4) a higher stoichiometric coefficient was estimated in comparison to that calculated from Cu concentration in the magnetite. The highest uncertainty of the concentration analyses of TEs in solution was observed for Cu (see above), which might explain in part this result.

REFERENCES

1. Knipping, J.L., et al., *Trace elements in magnetite from massive iron oxide-apatite deposits indicate a combined formation by igneous and magmatic-hydrothermal processes.* Geochimica et Cosmochimica Acta, 2015. **171**: p. 15-38.

2. Bish, D.L. and S. Howard, *Quantitative phase analysis using the Rietveld method.* Journal of Applied Crystallography, 1988. **21**(2): p. 86-91.

3. Young, R., *The Rietveld method Oxford Univ*. 1995, Press.

4. Brunauer, S., P.H. Emmett, and E. Teller, *Adsorption of gases in multimolecular layers.* Journal of the American chemical society, 1938. **60**(2): p. 309-319.

5. Jochum, K.P., et al., *Determination of reference values for NIST SRM 610–617 glasses following ISO guidelines.* Geostandards and Geoanalytical Research, 2011. **35**(4): p. 397-429.

6. Paton, C., et al., *Iolite: Freeware for the visualisation and processing of mass spectrometric data.* Journal of Analytical Atomic Spectrometry, 2011. **26**(12): p. 2508-2518.

7. Paul, B., et al., *CellSpace: a module for creating spatially registered laser ablation images within the Iolite freeware environment.* Journal of Analytical Atomic Spectrometry, 2012. **27**(4): p. 700-706.

8. Torres, E. and M. Auleda, *A sequential extraction procedure for sediments affected by acid mine drainage.* Journal of Geochemical Exploration, 2013. **128**: p. 35-41.

9. Stucki, J., *The Quantitative Assay of Minerals for Fe2+ and Fe3+ Using 1, 10-Phenanthroline: II. A Photochemical Method.* Soil Science Society of America Journal, 1981. **45**(3): p. 638-641.

10. Nystroem, J.O. and F. Henriquez, *Magmatic features of iron ores of the Kiruna type in Chile and Sweden; ore textures and magnetite geochemistry.* Economic geology, 1994. **89**(4): p. 820-839.

11. Dare, S.A., S.-J. Barnes, and G. Beaudoin, *Did the massive magnetite "lava flows" of El Laco (Chile) form by magmatic or hydrothermal processes? New constraints from magnetite composition by LA-ICP-MS.* Mineralium Deposita, 2015. **50**(5): p. 607-617.

12. Müller, B., M.D. Axelsson, and B. Öhlander, *Trace elements in magnetite from Kiruna, northern Sweden, as determined by LA-ICP-MS.* Gff, 2003. **125**(1): p. 1-5.

13. Kim, K.J., et al., *Magnetic and electronic properties of vanadium-substituted magnetite VxFe3− xO4 thin films.* Journal of Magnetism and Magnetic Materials, 2007. **310**(2): p. e876-e877.

14. Yeary, L.W., et al., *Magnetic properties of bio-synthesized zinc ferrite nanoparticles.* Journal of magnetism and magnetic materials, 2011. **323**(23): p. 3043-3048.

15. Roden, E.E. and Q. Jin, *Thermodynamics of microbial growth coupled to metabolism of glucose, ethanol, short-chain organic acids, and hydrogen.* Applied and environmental microbiology, 2011. **77**(5): p. 1907-1909.

16. Gao, H., et al., *Shewanella loihica sp. nov., isolated from iron-rich microbial mats in the Pacific Ocean.* International Journal of Systematic and Evolutionary Microbiology, 2006. **56**(8): p. 1911-1916.

17. Lee, S. and J.A. Fuhrman, *Relationships between biovolume and biomass of naturally derived marine bacterioplankton.* Applied and environmental microbiology, 1987. **53**(6): p. 1298-1303.

18. Thullner, M., P. Van Cappellen, and P. Regnier, *Modeling the impact of microbial activity on redox dynamics in porous media.* Geochimica et Cosmochimica Acta, 2005. **69**(21): p. 5005-5019.

19. Gorski, C.A. and M.M. Scherer, *Fe2+ sorption at the Fe oxide-water interface: A revised conceptual framework*, in *Aquatic Redox Chemistry*. 2011, ACS Publications. p. 315-343.

20. Gorski, C.A. and M.M. Scherer, *Influence of magnetite stoichiometry on FeII uptake and nitrobenzene reduction.* Environmental science & technology, 2009. **43**(10): p. 3675-3680.

21. Cheng, W., R. Marsac, and K. Hanna, *Influence of magnetite stoichiometry on the binding of emerging organic contaminants.* Environmental science & technology, 2018. **52**(2): p. 467-473.

22. Perez-Gonzalez, T., et al., *Magnetite biomineralization induced by Shewanella oneidensis.* Geochimica et Cosmochimica Acta, 2010. **74**(3): p. 967-979.

23. Müller, C.M., et al., *Infrared attenuated total reflectance spectroscopy: an innovative strategy for analyzing mineral components in energy relevant systems.* Scientific reports, 2014. **4**: p. 6764.

24. Zachara, J.M., et al., *Solubilization of Fe (III) oxide-bound trace metals by a dissimilatory Fe (III) reducing bacterium.* Geochimica et Cosmochimica Acta, 2001. **65**(1): p. 75-93.

25. Coker, V.S., et al., *Probing the site occupancies of Co-, Ni-, and Mn-substituted biogenic magnetite using XAS and XMCD.* American Mineralogist, 2008. **93**(7): p. 1119-1132.

26. Liu, C., et al., *Fe (II)-induced phase transformation of ferrihydrite: The inhibition effects and stabilization of divalent metal cations.* Chemical Geology, 2016. **444**: p. 110-119.

APPENDIX 2

1. Ferrihydrite (Fh) synthesis

For preparation of approximately 10 g of 2L-ferrihydrite, a modified procedure based on Schwertmann and Cornell [1] was followed. Forty g of $Fe(NO_3)\cdot 9H_2O$ were dissolved in MilliQ water. 1 M KOH solution was used to bring pH of the previous solution to 7.5. The solution was then centrifuged at 4500 rpm for 10 min. After removing the supernatant clean water, dialysis cellulose tubular membranes were filled with the denser fraction, hermetically closed and submerged in 5 liters of Milli-Q. Electric conductivity was periodically checked, and water was renewed every 12 h approximately until conductivity reached the value of ~ 5µS cm^{-1}. The iron oxide slurry in the tubular membrane was then introduced into *falcon* vials and centrifuged at 4500 rpm for 10 min to eliminate excessive water. Finally, the solid was quickly frozen with liquid nitrogen and immediately freeze-dried for 48 h. The solid was retrieved and grinded in a mortar obtaining a final fraction size < 5µm in diameter.

2. Adsorption experiments

Non-stirred adsorption experiments were carried out with synthetic Fe(II), anoxic SSW, acetate and TRIS-buffer to quantify the amount of Fe(II) adsorbed during reductive dissolution of synthetized ferrihydrite. Figure A2.1 shows a rapid adsorption of injected Fe(II) on the ferrihydrite surface, where aqueous Fe(II) decreased to very low concentrations (0.09 mM) after 100 min.

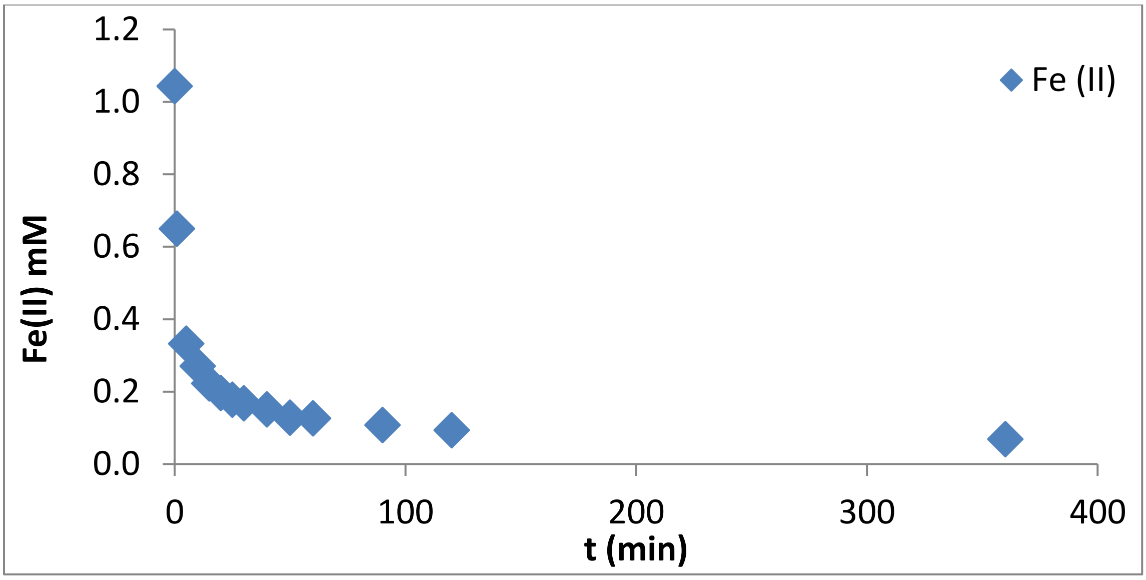

Figure A2. 1. Fe(II) adsorption onto ferrihydrite (experiment A2). The initial concentrations were: Fe(II) = 1.26 mM; acetate = 10 mM; Tris-HCl = 10 mM and pH = 8.2. Volume of synthetic seawater (SSW) = 250 mL and initial mass of ferrihydrite = 2.5 g. 90-95% of the initial Fe(II) concentration was adsorbed in approximately 2 h.

3. Fe(II) adsorption isotherm

A Fe(II) adsorption isotherm was carried out by means of stirred batch experiments with anoxic SSW, acetate, buffer and ferrihydrite as adsorbent and aqueous Fe(II) as adsorbate. The concentration of the latter was increased from 0.4 to 40 mM (maximum Fe(II) concentration expected (Eq. (4.1)). Fe(II) was measured under equilibrium conditions, which were reached within 4 h. The difference between the initial and equilibrium Fe(II) concentrations corresponded to adsorbed Fe(II) (Fig. 1.5 Chapter 1).

Given the theoretical average number of available sorption sites for ferrihydrite (i.e., 2.2-2.5 sites nm^{-2}) [2, 3], the measured specific surface area (160 m^2 g^{-1}), and the amount of ferrihydrite used in the experiments (2.5 g), the calculated concentration of sorption sites was 5.8×10^{-3} mmol sites g^{-1}. The typical shape of a site-limited adsorption isotherm in which Fe(II) adsorption rapidly occurs before reaching the maximum adsorption capacity was not observed. The concentration of adsorbed Fe(II) did not level off (Fig. 1.5 Chapter 1), resulting in an increase in adsorbed Fe(II). This behavior indicated that Fe(II) uptake by ferrihydrite was not only due to Fe(II) adsorption, but to an additional process such as the formation of a secondary Fe(II)-bearing phase (e.g. magnetite).

4. Heterotrophic nitrite reduction

A set of batch experiments was performed to estimate the nitrite reduction rate in the absence of Fe(II) and ferrihydrite and to evaluate a potential interference during abiotic nitrite reduction and oxidation of bio-produced Fe(II) caused by heterotrophic reduction of nitrite by *S. loihica*. Batch experiments were filled with anoxic SSW, TRIS-HCl buffer, *S.loihca* and lactate or acetate (Fig. A2.2). When organic matter was lactate (Fig. A2.2a), denitrification took place for approximately 10 h after an activation time of about 20 h. When organic matter was acetate (Fig. A2.2b), both the activation time and denitrification lasted much longer (one week and two months, respectively). These results allowed us to discard an interference of heterotrophic nitrite reduction in the abiotic experiments with bio-produced Fe(II) (see text).

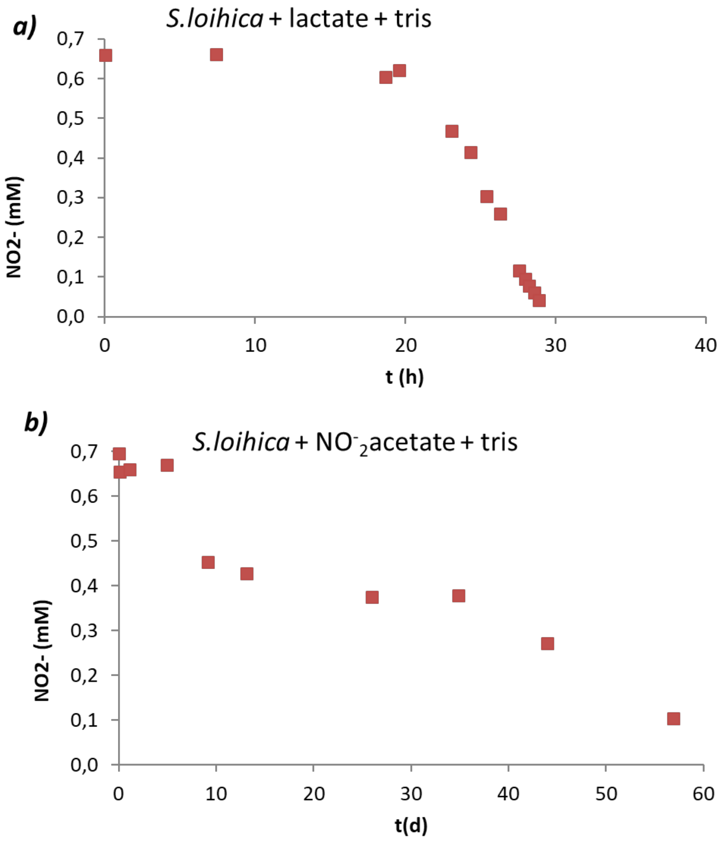

Figure A2. 2. Heterotrophic nitrite reduction mediated by *S.loihica* in the absence of Fe(II) and ferrihydrite. Organic matter is lactate (a) and acetate (b).

5. Control experiments

Control experiments were performed to test possible interferences of SSW, acetate, lactate, ferrihydrite on Fe(II) and/or nitrite (Table A1.1). Nitrite was analyzed in the presence of both ferrihydrite and acetate (C1), only with acetate (C2) and only with SSW (C3). Synthetic Fe(II) was analyzed only with acetate (C4) and only with SSW (C5). Nitrite and Fe(II) concentrations were periodically measured for a month and no significant change in their initial concentrations was observed. Aqueous Fe(II) in the presence of ferrihydrite and acetate in SSW was rapidly and fully adsorbed onto ferrihydrite (Fig. A2.1).

Table A2. 1. Control experiments filled with SSW and Tris-HCl buffer solution.

	sample	ferrihydrite (g)	volume (mL)	aqueous bio-Fe(II) (mM)	synthetic Fe(II) (mM)	NO^-_2 (mM)	acetate (mM)	lactate (mM)	*S.loihica*	antibiotics
CONTROL EXPERIMENTS	C1	2.5	250	-	-	0.65	10	-	-	-
	C2	-	250	-	-	0.65	10	-	-	-
	C3	-	250	-	-	0.65		-	-	-
	C4	-	250		0.75	-	10	-	-	-
	C5	-	250		1.00	-	-	-	-	-
	C6	-	50	1.2	-	-	10	-	-	chloramphenicol
	C7	-	50	1.2	-	-	10	-	-	riphampicine
	C8	-	50	1.2	-	-	10	-	-	spectynomicine

In addition, a potential interference of different antibiotics effective with *Shewanella s.p*. (chloramphenicol, rifampin and streptomycin [4]) on Fe(II) and/or NO_2^- concentration was investigated in experiments C6, C7 and C8. The results showed that these antibiotics oxidized about 30% of the initial Fe(II), probably because of the nitrogen content in their molecules. The use of antibiotics was therefore discarded to kill bacteria after ferrihydrite reduction.

In two experiments, after Fe(II) bio-production (stage 1 in experiment Ferr; Section 2.4), bacteria were killed by autoclaving. However, the initial Fe(II) concentration abruptly dropped (loss of about 60%) because of (a) O_2 penetration while autoclaving and subsequent Fe(II) oxidation and/or (b) an increase in temperature accelerated Fe(II) incorporation on ferrihydrite during transformation to magnetite [5]. Moreover, a bottle exploded while autoclaving. Hence, autoclaving was discarded to kill bacteria after Fe(II) bioproduction.

6. Nitrite reduction calculations

Rates of nitrite reduction were obtained using a second-order rate expression:

$$\frac{d[NO_2^-]}{dt} = -k_{obs}\,[Fe(II)]\,[NO_2^-] \qquad \text{(EA2.1)}$$

where k_{obs} is the nitrite reduction rate constant. The values for k_{obs} were determined for each experiment using the integrated form:

$$\frac{1}{[Fe(II)]_0-\alpha[NO_2^-]_0} \cdot ln\frac{[NO_2^-]_0([Fe(II)]_0-\alpha X)}{[Fe(II)]_0([NO_2^-]_0-X)} = k_{obs} \cdot t \qquad \text{(EA2.2)}$$

where $[NO_2^-]_0$ and $[Fe(II)]_0$ are the initial concentrations of nitrite and total ferrous iron concentration, respectively, X denotes the disappearance of nitrite and -α corresponds to the Fe(II) mols reacted per mol of nitrite reduced (see below). For each experiment, the rate constant (k_{obs}) was derived from the slope on the right-hand side of Eq. (EA2.2) versus time (t) (Fig. A2.3). The values used in Eq. (EA2.2) and the results obtained are shown in Table A2.2.

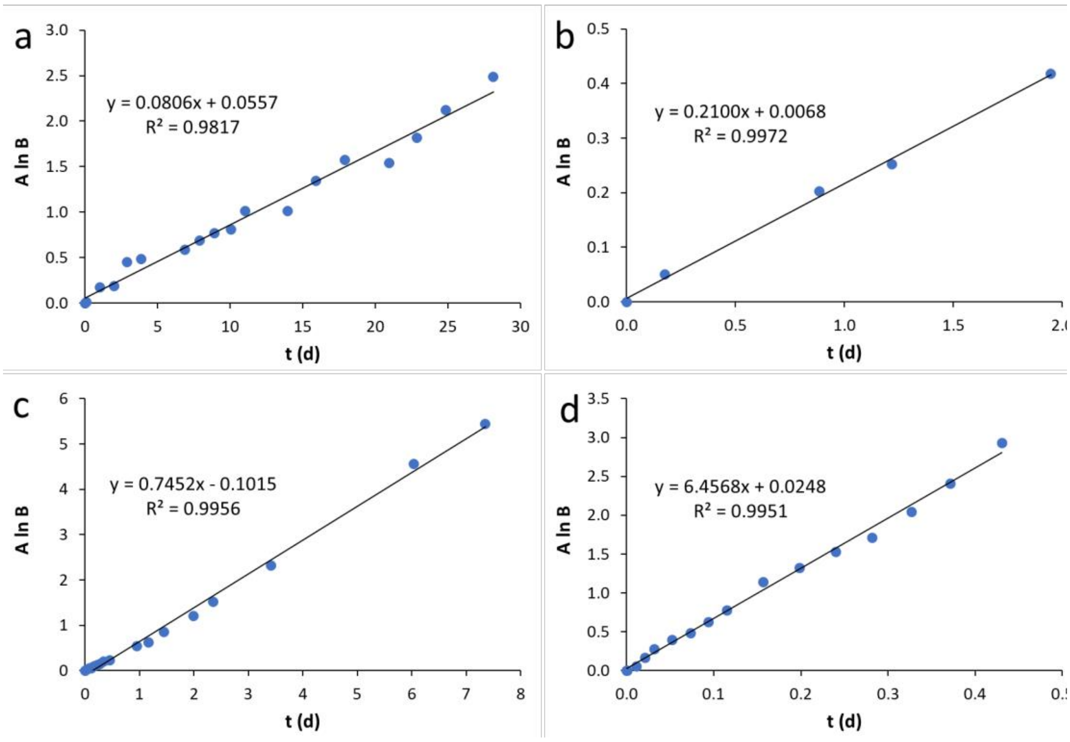

Figure A2. 3. Linear regressions based on Eq. (EA2.2): $A = 1/[Fe(II)]_0 - \alpha[NO_2^-]_0$ and $B = [NO_2^-]_0([Fe(II)]_0 - \alpha X)/[Fe(II)]_0([NO_2^-]_0 - X)$. The results for the exeriments shown in Fig. 4.3 are illustrated: (a) A1-1, (b) A2-1, (c) A3-1 and (d) NFerr-1.

Table A2. 2. Parameters used in Eq. (EA2.2) and calculated half-life values of NO_2^-. α was a fitting parameter. Concentrations of initial NO_2^-, dissolved Fe(II) and total Fe(II) are also indicated.

Experiment	α	Initial NO_2^- (mM)	Initial dissolved Fe(II) (mM)	Initial total Fe(II) (mM)	k_{obs} (mM^{-1} d^{-1})	R^2	Half-life NO_2^- (d)
A1-1	2.7	0.65	1.25	1.25	0.081	0.982	12.7
A1-2	2.7	0.65	1.25	1.25	0.047	0.882	21.9
A1-3	2.7	0.65	1.25	1.25	0.048	0.863	21.6
A2-1	2.7	0.76	< d.l.[i]	1.26	0.21	0.997	-[ii]
A2-2	2.7	0.76	< d.l.[i]	1.26	0.25	0.943	-[ii]
A2-3	2.7	0.76	< d.l.[i]	1.26	0.25	0.966	-[ii]
A3-1	2.7	0.74	1.15	2.60	0.75	0.996	0.47
A3-2	2.7	0.75	1.19	2.60	0.74	0.995	0.47
A3-3	2.7	0.73	1.16	2.60	0.74	0.992	0.47
NFerr-1	2.7	0.77	1.18	2.10[iii]	6.47	0.995	0.07
NFerr-2	2.7	0.22	0.36	2.10[iii]	0.45	0.987	0.79

i = d.l.: detection limit; ii = nitrite reduction extent for the simulated period was <50%; iii =value obtained by data fitting.

7. Isotopic data

A

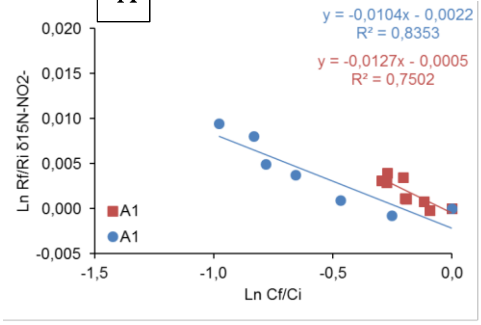

B

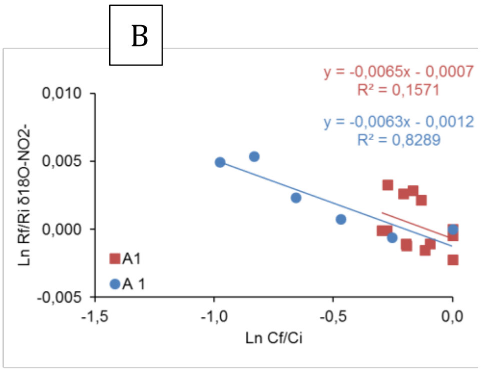

C

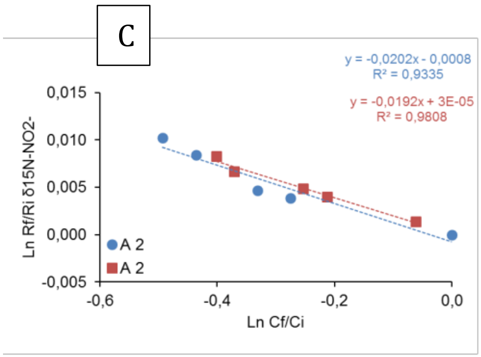

D

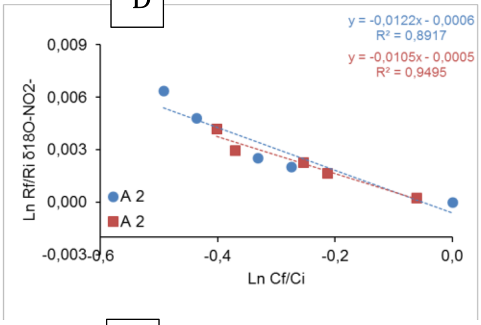

E

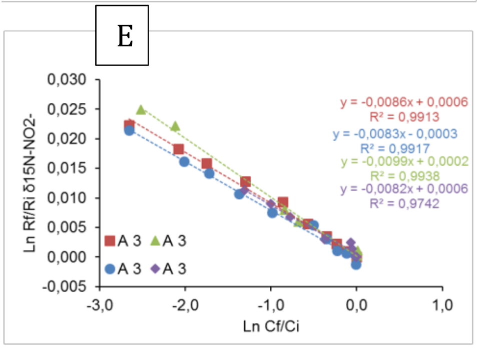

F

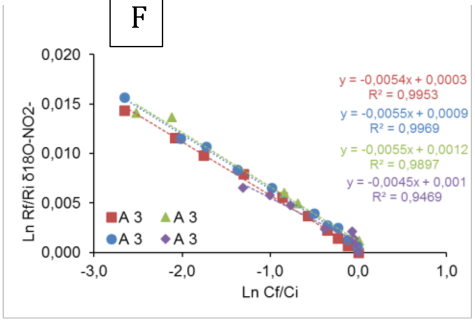

G

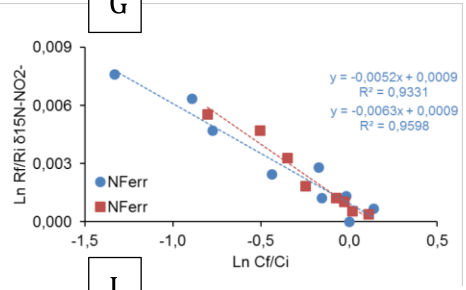

H

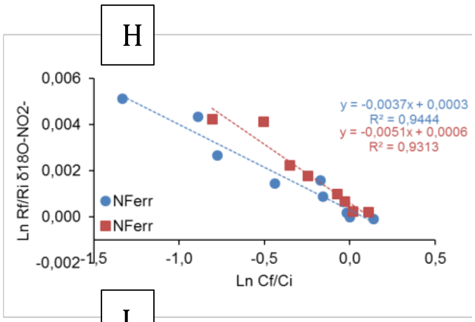

I

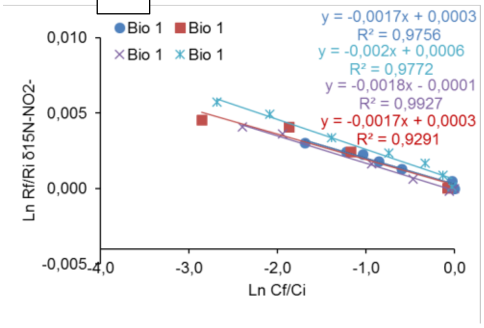

J

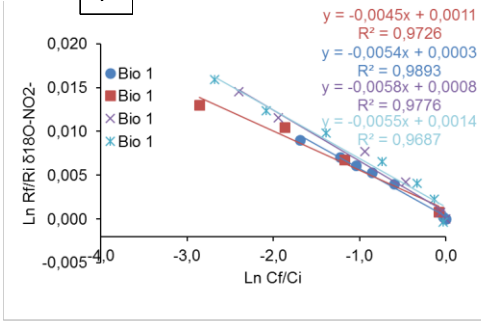

Figure A2. 4. Linear correlation between the natural logarithm of the substrate remaining fraction and the determined isotope ratios. The ε^{15}N-NO_2^- (A, C, E, G, I) and ε^{18}O-NO_2^- (B, D, F, H, J) are calculated by means of a Rayleigh distillation equation (Eq. (4.3) in text) for all replicates of each tested condition (A and B = A1, C and D = A2, E and F = A3, G and H = NFerr and I and J =Bio1).

REFERENCES

1. Schwertmann, U. and R.M. Cornell, *Iron oxides in the laboratory: preparation and characterization*. 2008: John Wiley & Sons.

2. Dzombak, D.A. and F.M. Morel, *Surface complexation modeling: hydrous ferric oxide*. 1990: John Wiley & Sons.

3. Hiemstra, T. and W.H. Van Riemsdijk, *A surface structural model for ferrihydrite I: Sites related to primary charge, molar mass, and mass density.* Geochimica et Cosmochimica Acta, 2009. **73**(15): p. 4423-4436.

4. Brink, A., A. Van Straten, and A. Van Rensburg, *Shewanella (Pseudomonas) putrefaciens bacteremia.* Clinical infectious diseases, 1995. **20**(5): p. 1327-1332.

5. Das, S., M.J. Hendry, and J. Essilfie-Dughan, *Transformation of two-line ferrihydrite to goethite and hematite as a function of pH and temperature.* Environmental science & technology, 2011. **45**(1): p. 268-275.

APPENDIX 3

Marine Environmental Research 151 (2019) 104782

Contents lists available at ScienceDirect

Marine Environmental Research

journal homepage: www.elsevier.com/locate/marenvrev

Dissimilatory bioreduction of iron(III) oxides by *Shewanella loihica* under marine sediment conditions

Robert Benaiges-Fernandez[a,b,*], Jordi Palau[b,c], Francesco G. Offeddu[b], Jordi Cama[b], Jordi Urmeneta[a,d], Josep M. Soler[b], Bernhard Dold[e,f]

[a] *Department of Genetics, Microbiology and Statistics, Universitat de Barcelona, Barcelona, Catalonia, Spain*
[b] *Institute of Environmental Assessment and Water Research (IDAEA, CSIC), Barcelona, Catalonia, Spain*
[c] *Department of Mineralogy, Petrology and Applied Geology, Universitat de Barcelona, Barcelona, Catalonia, Spain*
[d] *Biodiversity Research Institute (IRBio), Universitat de Barcelona, Barcelona, Catalonia, Spain*
[e] *Department of Civil, Environmental and Natural Resources Engineering, Luleå University of Technology, Luleå, Sweden*
[f] *Sustainable Mining Research & Consultancy EIRL, San Pedro de La Paz, Chile*

ARTICLE INFO

Keywords:
Iron bioreduction
Marine sediment
Iron oxide
Dissolution
Shewanella loihica

ABSTRACT

Shewanella is a genus of marine bacteria capable of dissimilatory iron reduction (DIR). In the context of deep-sea mining activities or submarine mine tailings disposal, dissimilatory iron reducing bacteria may play an important role in biogeochemical reactions concerning iron oxides placed on the sea bed. In this study, batch experiments were performed to evaluate the capacity of *Shewanella loihica* PV-4 to bioreduce different iron oxides (ferrihydrite, magnetite, goethite and hematite) under conditions similar to those in anaerobic sea sediments. Results showed that bioreduction of structural Fe(III) via oxidation of labile organic matter occurred in all these iron oxides. Based on the aqueous Fe (II) released, derived Fe(II)/acetate ratios and bioreduction coefficients seem to be only up to about 4% of the theoretical ones, considering the ideal stoichiometry of the reaction. A loss of aqueous Fe (II) was caused by adsorption and mineral transformation processes. Scanning electron microscope images showed that *Shewanella lohica* was attached to the Fe(III)-oxide surfaces during bioreduction. Our findings suggest that DIR of Fe(III) oxides from mine waste placed in marine environments could result in adverse ecological impacts such as liberation of trace metals in the environment.

1. Introduction

Iron is one of the most important elements on Earth due to its involvement in key biological processes, such as photosynthesis. However, the low solubility of Fe makes it not much bioavailable in most environments (Raiswell and Canfield, 2012). Iron is one of the controlling elements in many ecosystems, especially in marine environments (Field et al., 1998; Morel and Price, 2003). Some studies have shown that iron stimulates the growth of phytoplankton in high-nitrate, low-chlorophyll waters, which account for 25% of the ocean (De Baar et al., 2005). Furthermore, iron participates in important biological processes such as atmospheric carbon dioxide consumption, dimethyl sulfide (DMS) production and organic matter (OM) degradation in sediments (Boyd and Ellwood, 2010). Bioavailability of iron in the sea also played a crucial role in the modulation of carbon dioxide concentration in the atmosphere in the geological past (Martin et al., 1990).

A marine sediment is an aphotic nutrient-rich and low-production zone where most microorganisms are heterotrophic (Fenchel, 1969). In anoxic reduced zones of the sediment, there are OM-degrading anaerobic microorganisms that use inorganic compounds other than oxygen as terminal electron acceptors (TEAs) for the electron transport respiratory chain (Lovley, 1991). Dissimilatory iron reduction mediated by microorganisms uses Fe(III) as TEA to produce Fe(II) species. This process is coupled to the degradation of simple OM and is carried out by different genera of bacteria, like *Geobacter* or *Shewanella* (Lovley and Phillips, 1986). In marine sediments, metabolic products of degradation serve as electron donors for the terminal oxidizing bacteria, which use inorganic TEAs for a complete oxidation of organic matter. Moreover, iron reduction besides sulfate reductors are the most important terminal oxidation processes in the upper anoxic zone (Thamdrup, 2000). For instance, in artic marine sediments lactate (among acetate, propionate and isobutyrate) is degraded in the marine sediment by iron and sulfate reducers (Finke et al., 2007).

---

[*] Corresponding author. Department of Genetics, Microbiology and Statistics, Universitat de Barcelona, Barcelona, Catalonia, Spain.
E-mail address: robert.benaiges@idaea.csic.es (R. Benaiges-Fernandez).

https://doi.org/10.1016/j.marenvres.2019.104782
Received 10 May 2019; Received in revised form 30 August 2019; Accepted 2 September 2019
Available online 05 September 2019
0141-1136/ © 2019 Elsevier Ltd. All rights reserved.

Table 1
Surface area and mineralogical composition (wt. %) of the studied samples.

Sample	Hematite	Goethite	Magnetite	Ferrihydrite	V1	M1	TB
hydroxylapatite ($Ca_5(PO_4)_3(OH)$)						16%	11%
magnetite ($Fe^{2+}Fe^{3+}_2O_4$)			100%		19%	79%	89%
horblende ($Ca_2(Mg, Fe, Al)_5$ $(Al, Si)_8O_{22}(OH)_2$)					41%		
hematite (Fe_2O_3, α-Fe_2O_3)	100%				40%		
ferro-actinolite ($Ca_2(Mg_{2.5\text{-}0.0}Fe^{2+}_{2.5\text{-}5.0})Si_8O_{22}(OH)_2$)						5%	
goethite (α-$FeO(OH)$)		100%					
ferrihydrite ($(Fe^{3+})_2O_3{\cdot}0.5H_2O$)				100%			

The *Shewanella* genus is well known for its presence in marine sediments and for its metabolic capacity (Hau and Gralnick, 2007). *Shewanella* can use oxygen, nitrate and heavy metals as TEAs. Some strains may even degrade recalcitrant organic compounds, such as chlorinated solvents, providing the genus with the potential to be applied in bioremediation studies (Roh et al., 2006). *Shewanella loihica* is a species from the genus *Shewanella* isolated from a submarine volcano in Loihi, Hawaii (Gao et al., 2006). The metabolic versatility and ubiquitous presence in the marine environment make *Shewanella loihica* a suitable candidate for bioreduction studies. Earlier studies on the capacity and mechanisms of *Shewanella* to bioreduce ferric iron in fresh water have shown that (i) it is able to reduce not only soluble Fe (III) compounds but also (Fe) (III)-bearing minerals such as magnetite (Fe_3O_4) through polysaccharide attachment (Dong et al., 2000) and that (ii) biotic iron reduction coupled to OM degradation requires a direct contact between the microorganisms and the poorly soluble mineral surface (Tugel et al., 1986). However, bioreduction of magnetite and other iron oxides and hydroxides (ferrihydrite, goethite and hematite) under marine conditions has not yet been studied.

The fate of iron oxides in seafloor sediments has a major interest for potential sea water contamination caused by deep-sea mining activities or marine disposal of mine tailings, which were practices widely spread worldwide (Ellis and Ellis, 1994) although currently banned in most of the countries (Dold, 2014). For instance, marine contamination associated with continuous tailings disposal has been reported in. Chañaral Bay in northern coast of Chile (Dold, 2006; Medina et al., 2005) and Portman Bay in the south-east coast of Spain (Manteca et al., 2014). In mine tailings originated from sulfide-rich ores the contained Fe(III)-oxides incorporate Mn, Al, Cr, Co, Ni, Zn, V, Pb and As (Knipping et al., 2015; Nadoll et al., 2014). Valence II and III metal cations can be absorbed on the iron oxides or isomorphously substitute iron in the crystalline oxide structure (Cornell and Schwertmann, 1996). Offshore disposal of these mine tailings may result in adverse ecological impacts as bioreductive dissolution of Fe(III) oxides releases aqueous Fe(II) together with trace metals and metalloids co-precipitated or structurally incorporated in Fe (III) oxides (Zachara et al., 2001). Thus, an undesired bioaccumulation of metals and metalloids in sea sediments, in secondary plumes and in the water column and an increase in trophic transfer of metals could occur (Morello et al., 2016; Ramirez-Llodra et al., 2015). A better understanding of the interaction between Fe(III) oxides and microorganisms capable to bioreduce Fe(III) sheds new light on the bioavailability of iron in the ocean and on potential environmental consequences of sea mining activities and marine disposal of mine tailings.

To this end, Fe(III) oxides (synthetic ferrihydrite, commercial goethite, magnetite and hematite and field specimens with different contents of iron oxides and other minerals) were reacted in the laboratory in the presence of *Shewanella loihica* strain PV-4, whose ecophysiology makes it optimal for Fe(III)-bioreduction under marine sediment conditions. Two different experiments were performed to elucidate the kinetics of Fe(III) bioreduction and to examine the bacteria-mineral surface interaction.

2. Materials and methods

2.1. Sample characterization

The iron oxide samples used in this study have three different sources: three samples were commercial powders of magnetite, hematite and goethite purchased from Sigma Aldrich; one sample of 2L ferrihydrite was synthesized in the laboratory following the procedure described by Cornel and Shwertmann (1991); and three samples were field specimens with different contents of magnetite (V1 from Distrito Algarrobo, Chile, TB from Lago Sur, Chile, and M1 from Malmberget, Sweden). Sample V1 also contained hematite. Powder X-ray diffraction (XRD) analysis and Rietveld refinement (Young, 1995), using a Bruker D8 A25 Advance X-ray diffractometer θ- θ with CuKα1 radiation, showed that the commercial and synthesized samples were composed of the respective iron oxides and no accessory minerals were identified. Rietveld analysis confirmed that no impurities were present in the samples. As for the field samples, magnetite was present in all of them (ranging from 19 to 89 wt % for V1 and M1, respectively), hematite was only present in V1 (40 wt %) and goethite was not detected (Table 1). Other minerals identified were silicates (hornblende, and Fe-actinolite) and phosphates (hydroxyapatite) (Table 1).

The size fraction of the commercial powders was about 5 μm. Synthesized 2L ferrihydrite was ground using an agate mortar and pestle and sieved to a size fraction of 5–60 μm. Fragments of field samples were similarly ground and sieved to a size fraction of 60–100 μm. These powdered samples were used in batch experiments to study the Fe(III) bioreduction reaction. The specific surface area of all these samples was determined by the Brunauer-Emmett-Teller (BET) method (Brunauer et al., 1938) using a Gemini 2370 surface area analyzer and 5-point N_2 adsorption isotherms. Sample degassing with nitrogen lasted for 2 h at 137 °C. Data uncertainty was around 10%. Synthesized ferrihydrite showed the largest value ($181\ m^2\ g^{-1}$) and M1 and TB the lowest ones (0.6 and $0.2\ m^2\ g^{-1}$, respectively; Table 2).

2.2. Bacterial culture

Shewanella loihica strain PV-4 was obtained from the German Collection of Microorganisms and Cell Cultures (DSMZ 17748). To obtain a bacterial suspension for the starting inoculum, cells were cultivated in M1 medium (Gao et al., 2006) supplemented with 10 mM of sodium lactate as electron donor and carbon source and 10 mM of Fe (III) citrate as electron acceptor. Cultures were incubated anaerobically for 24 h at 30 °C and then harvested by centrifugation (5000 rpm for 10 min). The pellet was re-suspended in synthetic seawater prepared previously following the standard protocol D1141-98 (ATSM International). Centrifugation and pellet resuspension were repeated three times as a washing step.

A medium simulating seawater (hereafter referred to as marine medium) was developed for the experiments. A basal medium of synthetic seawater (ASTM D1141-98) was amended with sodium lactate (10 mM) as an electron donor and carbon source, ammonium chloride (1.87 mM) as a source of nitrogen, and TRIS-HCl (10 mM) as a pH-buffer. The pH of the medium was adjusted to 8.2 with 0.1 N NaOH

Table 2
Microbial bioreduction activity coefficients calculated from measured acetate and ferrous iron concentrations.

sample	Specific (BET) surface area (m^2 g^{-1})	$k_{biored\text{-}Fe}$ (μmol $g_{oxide}{}^{-1}$ d^{-1})	$k_{biored\text{-}Ac}$ (μmol $g_{oxide}{}^{-1}$ d^{-1})	$k_{biored\text{-}Fe}$ (μmol m^{-2} d^{-1})	$k_{biored\text{-}Ac}$ (μmol m^{-2} d^{-1})	$Fe(II)_{aq}$/acetate (k-Fe/k-Ac)[a]
Hematite	5.4	0.033	0.61	0.006	0.114	0.0530
Goethite	12.3	0.026	0.95	0.002	0.077	0.0276
Magnetite	6.9	0.232	1.72	0.034	0.249	0.1349
Ferrihydrite	181	5.490	32.03	0.030	0.177	0.1714
V1	1.8	0.316	13.06	0.297	0.59	0.5073
TB	0.6	0.057	0.57	0.080	0.80	0.0995
M1	0.2	0.073	1.26	0.309	5.31	0.0583

[a] Bio-reduction stoichiometry is given by the Fe (II)aqueous/acetate ratio (theoretical value = 4).

solution. The final medium was sterilized by autoclave (121 °C for 20 min).

2.3. Batch experiments with powdered samples

In all batch experiments, 0.25 ± 0.01 g of powdered sample were placed in 25 mL glass vials capped with Teflon plugs and then sterilized by autoclave (121 °C for 20 min). Previous studies (Das et al., 2010; Mazzetti and Thistlethwaite, 2002) showed a thermal transformation of ferrihydrite to hematite could occur. A test performed with ferrihydrite showed that XRD analyses after the sterilization revealed no mineral changes in this stage.

The vials were filled with 25 mL of marine medium, keeping a 1% solid/liquid ratio (g/mL), and inoculated with *Shewanella loihica* to an approximate final number of $1{\cdot}10^7$ colony-forming units (cfu) mL^{-1}, measured by agar culture (LB). The vials were sealed with screw caps, leaving a minimal head space (small air bubble) to prevent overpressure, and statically immersed in a thermostatic water bath at 10 ± 1 °C in the dark. These conditions with the use of the marine medium mimicked the suboxic zone in marine sediments (Jørgensen and Kasten, 2006; Rosselló-Mora et al., 1999). Abiotic controls without inoculum of *Shewanella loihica* were also prepared under the same conditions as biotic experiments.

For each solid sample, a single-point batch experiment was carried out. Five vials were prepared as replicates, and each one was sacrificed at different time spans (13, 27, 47, 70 and 111 days). Sampling was performed in a glove box with N_2 atmosphere to maintain the anoxic conditions. The vials were shaken just before sampling and then the medium from the vial was totally recovered, sampled and filtered using a sterile syringe and syringe filters (0.22 μm pore size). Sample aliquots were used for pH/Eh measurements and for chemical analyses of cations and anions. To evaluate the carbon and energy source consumption, lactate and acetate, being the latter the oxidation end product under anaerobic conditions, were measured. For ion analysis a volume of 10 mL was preserved at pH < 2 by adding 100 μL of 60% (v/v) HNO_3 solution. For Fe(II)/Fe(III) measurements by Phenanthroline colorimetry (Stucki, 1981), an additional volume of 10 mL was preserved with the addition of 100 μL of 6 M HCl solution. Thereafter, all samples were stored at 4 °C in the dark until analysis.

2.3.1. Chemical analyses

Measurements of pH (± 0.02 pH units) and Eh (± 10 mV) were performed in the glove box using pH and Eh electrodes (Crison and SenTix ORP, Ag/AgCl, WTW, respectively). Oxidation-reduction potential readings were converted to standard Eh values by correcting for the electrode potential of the reference hydrogen electrode. Total iron was analyzed by Inductively Coupled Plasma Mass Spectrometry (ICP-MS, Perkin- Elmer 3000). Owing to the high dissolved iron concentrations in the experiments with ferrihydrite, iron measurements were performed using ICP–Optical Emission Spectroscopy (ICP-OES). The uncertainty of the ICP-MS (and ICP-OES) measurements was better than ± 5%. Total iron measured was checked to be Fe (II) with a modified protocol of the Phenanthroline method. Lactate and acetate concentrations were determined by high performance liquid chromatography (HPLC). The equipment used consisted of a Waters 600 HPLC pump controller equipped with an Aminex HPX-87H column (300 × 7.8 mm), BioRad, and a Waters 717 plus autoinjector. Triplicates were performed for iron, lactate and acetate measurements.

2.4. Fe (II)-ferrihydrite adsorption experiments

Fe(II) adsorption on powdered ferrihydrite in marine medium (0.5 g of ferrihydrite and 50 mL of solution, 1% w/v) was determined in gently mixed batch experiments at room temperature (23 ± 2 °C). Different amounts of $FeCl_2$ were added to distinct vials, from 0.4 to 40 mM, in order to get a wide range of initial Fe(II) aqueous concentration in the experiment. Samples were collected after reaching equilibrium at 24 h (Dzombak and Morel, 1990) to measure total and ferrous iron by the phenanthroline method. At the end of the experiments the solid fractions were retrieved, freeze dried and preserved under nitrogen atmosphere until analysis. Subsequently, XRD-Rietveld analyses and measurement of BET specific surface areas were performed. The concentration of adsorbed Fe(II) was determined by subtracting the aqueous ferrous iron concentration after equilibration from the initial concentration according to (1):

$$C_{Fe-ads} = (C_{Fe-i} - C_{Fe-eq})\cdot\frac{V}{M} \tag{1}$$

where $C_{Fe\text{-}ads}$ is the amount of adsorbed iron per gram of ferrihydrite, $C_{Fe\text{-}i}$ and $C_{Fe\text{-}eq}$ are the initial and equilibrium aqueous concentrations of Fe(II), respectively, V is the volume of solution and M is the mass of ferrihydrite.

2.5. Experiments with microbial cells and field samples

Surface mineral-bacteria interaction was investigated by scanning electron microscope (SEM). Fragments of field samples (M1 and TB) were cut down to small rectangular pieces (surface of ≈10 mm^2 and ≈3 mm thick) in order to fit into sample holders used for the critical point drying technique. These pieces were used to study the interaction between *Shewanella* and the surface of the iron oxides. Top surfaces were polished by conventional metallographic polishing to improve the observation of the surface mineral-bacteria interaction by SEM. The M1 and TB pieces were placed in 200 mL bottles filled with marine medium (synthetic sea water) without head space and incubated with $1{\cdot}10^7$ cfu mL^{-1} of *Shewanella loihica*. Experiments were conducted in the N_2-atmosphere glove box in the dark for 115 days at 25 °C.

At the end of the experiments, the pieces incubated with *Shewanella* were retrieved and treated for 2 h with a glutaraldehyde 2.5% w/v in 0.1 M phosphate buffered saline (PBS) cell-fixation solution. Several washes with PBS (10 min each) were done, and post-fixation of the mineral pieces was carried out using 1% osmium tetraoxide and 0.8% potassium ferricyanide in 0.1 M PBS for up to 2 h in darkness. To evaluate potential effects of the dehydration process on the bacteria

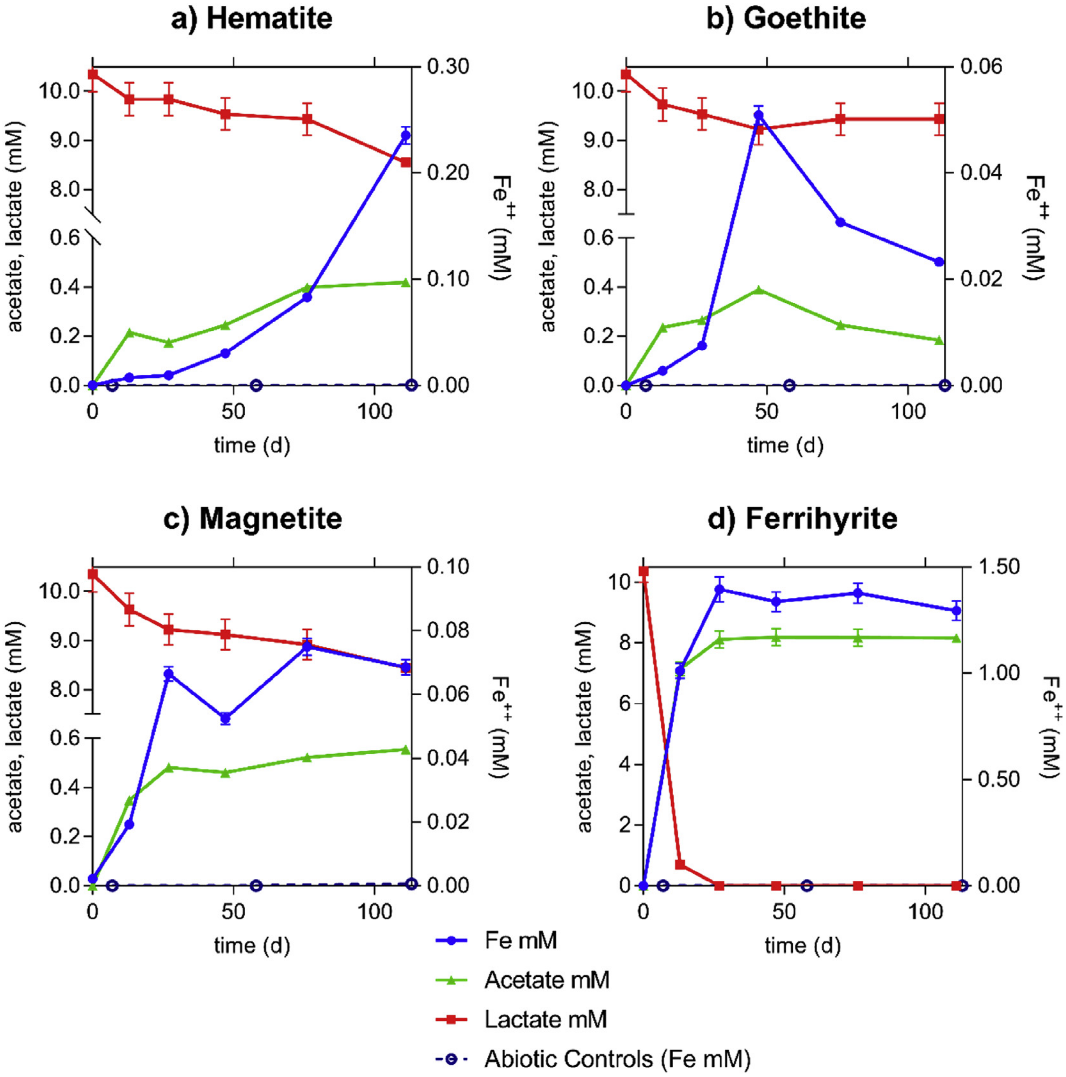

Fig. 1. Variation in concentration of lactate, acetate and total aqueous Fe over time in the bioreductive dissolution experiments with synthetic and commercial iron oxide samples: a. Hematite, b. Goethite, c. Magnetite, d. Ferryhydrite. Key: (☐) Lactate; (▲) Acetate; (●) Total dissolved iron and (o) Abiotic controls. Error bars correspond to the analytical uncertainty (SD).

structure, two different dehydration methods were carried out. In one dehydration method the critical point drying technique was performed by replacing water in the samples with increasing concentrations of ethanol (50–100%) (Anderson, 1951). In the other method sample dehydration was performed using a hexamethyldisilazane (HMDS) solution (Nation, 1983). Thereafter, all samples were coated with carbon before SEM observation (Hitachi H-4100FE instrument under a 15–20 kV potential in a high vacuum) using the backscattered electron detector (BSD) in Field Emission (FE) and an energy-dispersive spectrometer (EDS).

3. Results

3.1. Bioreductive dissolution of Fe-oxides

Dissolution of the iron oxide minerals and production of aqueous Fe (II) did not take place in the abiotic control experiments. In contrast, bioreductive dissolution occurred in all experiments inoculated by *Shewanella loihica*. Fig. 1 shows the variation of total aqueous iron concentration over time for the experiments with synthetic and commercial samples. Measured total aqueous iron in all the experiments was confirmed to be Fe (II) by the phenanthroline method. Aqueous iron concentration increased over time in the experiment with hematite (Fig. 1a), initially increased and then decreased in the case of goethite (Fig. 1b) and increased and levelled off in the experiments with magnetite and ferrihydrite (Fig. 1c and d). The highest Fe(II) concentration (1.3 mM) was reached in the ferrihydrite experiment. In all experiments, the change in aqueous ferrous iron concentration was accompanied by consumption of lactate and production of acetate. Only in the case of ferrihydrite experiment lactate was totally consumed. For the experiments prepared with field samples, reductive dissolution of the iron oxides showed similar trends (Fig. 2), in which iron increased in different steps (Fig. 2a,c) or gradually (Fig. 2b). The concentrations of released iron were lower than those of the synthetic and commercial samples (< 0.03 mM). As observed for the experiments with synthetic and commercial samples, consumption of lactate and production of acetate accompanied the ferrous iron release.

The measured ferrous iron and acetate concentrations throughout the experiments were used to estimate initial bioreduction coefficients based on the initial release of iron and acetate associated with the microbial activity. These coefficients were calculated by linear regression of the first two sampling points for ferrihydrite and the first three ones for the other oxide experiments using the following expressions (2,3):

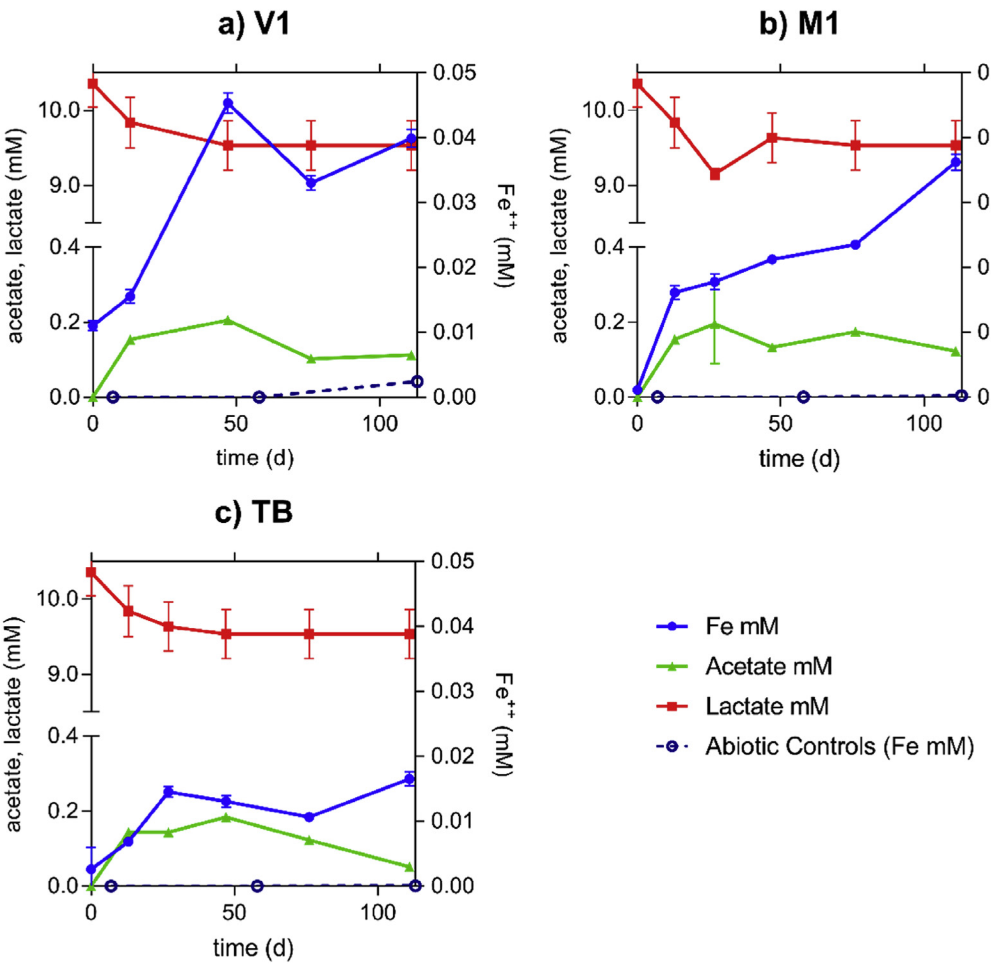

Fig. 2. Variation in concentration of lactate, acetate and total aqueous Fe over time in the bioreductive dissolution experiments with field powdered samples. a. Sample V1 (Distrito Algarrobo, Chile); b. Sample M1 (Malmberget, Sweden); c. Sample TB (Lago Sur, Chile). Key: (□) Lactate; (▲) Acetate; (●) Total dissolved iron and (o) Abiotic controls. Error bars correspond to the analytical uncertainty (SD).

$$k_{biored-Fe} = \frac{C_{Fe(II)} \cdot V}{\Delta t \cdot M} \tag{2}$$

$$k_{biored-Ac} = \frac{C_{acetate} \cdot V}{\Delta t \cdot M} \tag{3}$$

where $C_{Fe(II)}$ and $C_{acetate}$ are the measured iron and acetate concentrations (μM), V is the solution volume (L), M is the Fe(III)-oxide mass (g) and t is time (d). Linear regressions showed R^2 values between 0.8 and 0.99. The values of the iron and acetate bioreduction coefficients are listed in Table 2. Fig. 3a shows that the bioreduction coefficient (μmol g_{oxide}^{-1} d^{-1}) for the ferrihydrite experiment is much larger than those of the other samples. However, when the coefficients are normalized with the specific BET surface area (μmol m^{-2} d^{-1}) the coefficients of magnetite are higher (Fig. 3b).

In all experiments, pH slightly decreased from 8.2 to an average pH of 7.8 (Fig. S1) whereas Eh significantly decreased from 300 mV to an average value of 18.5 mV (Fig. S1).

3.2. Fe(II)-ferrihydrite adsorption

Due to the high specific surface area of ferrihydrite (181 m^2 g^{-1}) compared to the other iron oxides investigated (Table 1), this phase was used to evaluate Fe(II) adsorption on Fe(III)-oxides in the marine medium. Fig. 4 shows the measured adsorption of Fe(II) on powdered ferrihydrite. The amount of adsorbed Fe (II) increased with Fe (II) aqueous concentration, exceeding the theoretical adsorption capacity of ferryhydrite (0.6 mmol g^{-1}) (Hiemstra, 2013). The XRD patterns and Rietveld semi-quantitave analysis of the retrieved ferrihydrite allowed us to elucidate the mineralogical change at the end of the experiment and showed the presence of both ferrihydrite (≈10 wt%) and magnetite (≈90 wt%) (Fig. 5).

3.3. Bacteria and Fe-oxide surfaces

Independently of the dehydration technique used to preserve the bacteria structure, SEM images of the reacted field samples showed the presence of bacteria (*S. loihica*) attached on the iron-oxide surfaces (Fig. 6). Bacteria cells colonized the iron-oxide surfaces, either as individual cells or forming clusters. Most of the cells were attached preferably on the iron-oxide surfaces rather than on the surfaces of the other minerals present in the field samples (Fig. 6a). Extracellular structures by *S. loihica* have been observed suggesting that bacteria connect with the mineral surface and with other cells (Fig. 6b and c).

4. Discussion

4.1. Aqueous chemistry

The capacity of *Shewanella* to reduce soluble (e.g. iron citrate) or structural (e.g. biogenic magnetite) ferric iron has been studied (Kostka and Nealson, 1995), but its capacity to reduce magnetite and other iron-oxide minerals under marine conditions remained unknown. Our study demonstrates that *S. loihica* was able to bioreduce not only magnetite, but also hematite, goethite and ferrihydrite in conditions similar to

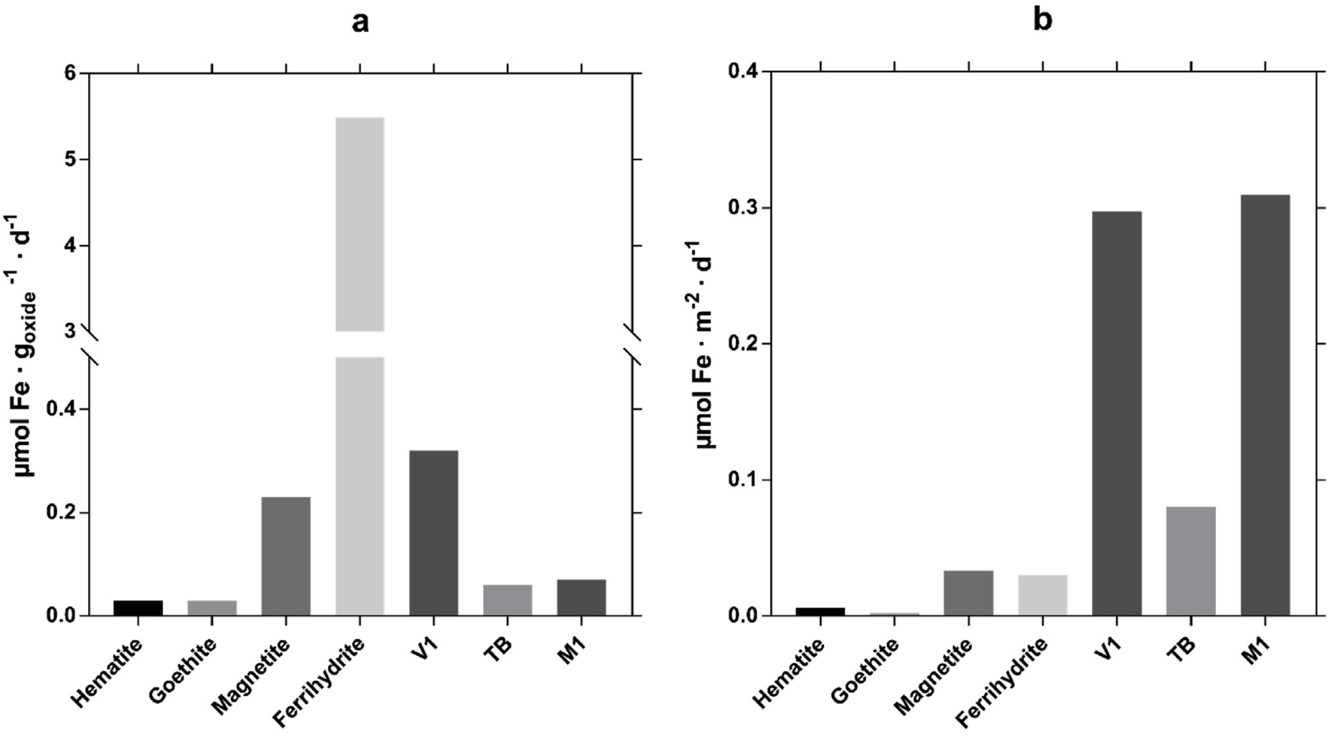

Fig. 3. Iron bioreduction coefficients of the iron oxides mediated by *S. loihica*: a) values normalized to mass and b) normalized to surface area.

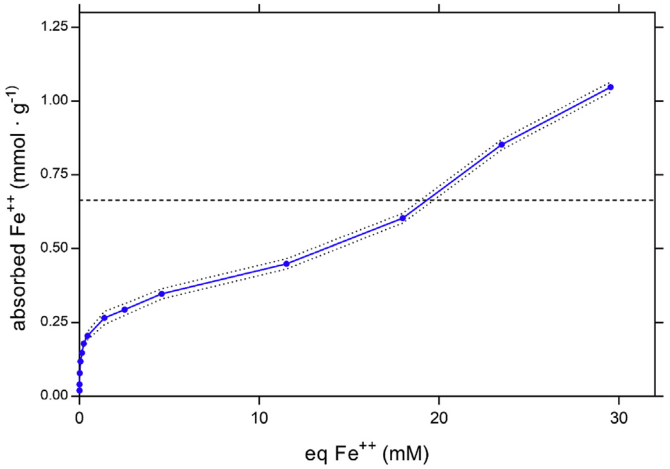

Fig. 4. Ferrous iron adsorption isotherm onto ferrihydrite in the marine medium. Dashed line indicates the saturation point based on the calculated number of sorption sites for ferrihydrite. Dotted lines indicate the SD of the experiment.

those found in anoxic marine environments, such as in seafloor sediments and in offshore mine-tailings disposal sites (Ramirez-Llodra et al., 2015). It appeared that *S. loihica* used the structural ferric iron of the iron oxides as an electron acceptor in the respiratory chain (Tugel et al., 1986). In the experiments, a simultaneous consumption of light organic matter (lactate) to produce acetate was observed along with an increase in aqueous Fe(II). Production of acetate was attributed to the anaerobic metabolism of the bacteria during ferric iron reduction. This finding is in agreement with previous studies showing that the metabolism of *S. loihica* was sustained by the production of acetate from lactate, which acts as electron donor (Scott and Nealson, 1994; Tang et al., 2007).

Bioreduction may be expressed in a simple form as (Lovley, 1991) (4):

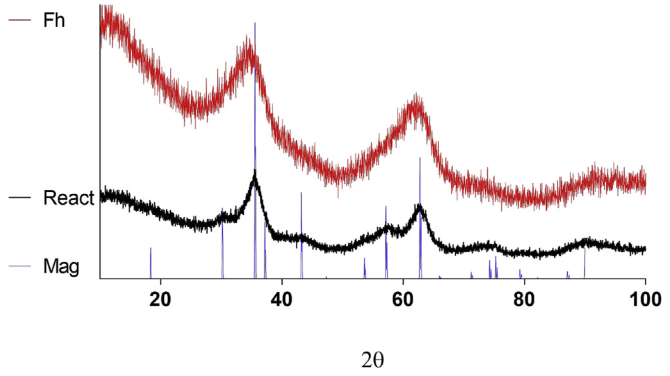

Fig. 5. XRD patterns of non-reacted pure ferrihydrite (red) and reacted ferrihydrite after absorption experiments (black). Blue lines indicate the position of the main XRD peaks of pure crystalline magnetite (blue) obtained from Ruff database. Most of the reacted ferrihydrite transformed to magnetite after surface adsorption of iron (II). Rietveld analysis of the reacted sample indicates that 10% of the sample is ferrihydrite and 90% is magnetite with nanocrystalline morphology. (For interpretation of the references to color in this figure legend, the reader is referred to the Web version of this article.)

$$\text{Lactate}^- + 4\text{Fe}^{3+} + 2\text{H}_2\text{O} \rightarrow \text{acetate}^- + \text{HCO}_3{}^- + 4\text{Fe}^{2+} + 5\text{H}^+ \tag{4}$$

Where one and 4 mol of acetate and ferrous iron are respectively produced (i.e., Fe(II)/acetate ratio = 4). Experiments with high lactate consumption and acetate formation correlated well with those having high aqueous ferrous iron concentration. In the ferrihydrite experiment, however, bioreduction was halted by total exhaustion of lactate (Fig. 1d). Mass balance between lactate consumption and acetate production showed carbon deficit in all experiments (lactate consumed > acetate produced). In a first stage (≈ < 12 h) of bioreduction experiments, *Shewanella loihica* consumed all the remaining oxygen in solution in the full oxidation of lactate to CO_2 via the aerobic metabolic pathway. The observed carbon mismatch (reaching up to ≈20%) was attributed to both carbon assimilation in biomass formation during

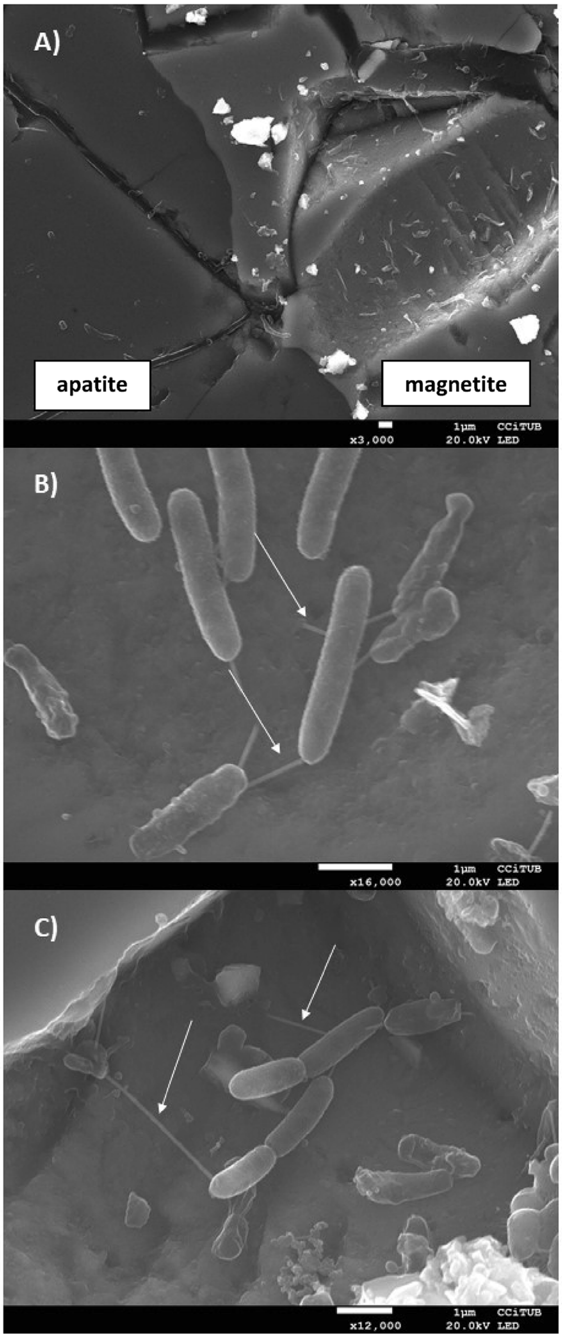

Fig. 6. SEM images of *S. loihica* cells colonizing an iron-oxide surface: a) Bacteria growing preferably on the oxide surfaces (magnetite); b,c) Bacteria growing on the surface of magnetite (M1) with developed extracellular structures (see arrows) interconnecting cells and/or connecting cells with the mineral surface.

microbial growth and the use of the aerobic metabolic pathway in oxygen consumption by *Shewanella loihica*.

According to the bioreduction reaction (Eq. (4)), a significant deficit of ferrous iron, based on measured aqueous Fe(II) relative to acetate, was found in all experiments. The Fe(II)/acetate ratios range between 0.03 and 0.17, which is between 0.7% and 4.3% of the stoichiometric ratio (Table 2). Several previous studies (Benner et al., 2002; Bonneville et al., 2004; Roden et al., 2000) reported a similar Fe(II) deficit, suggesting that (1) the apparent extent of bioreduction based on measured aqueous Fe(II) reached only about 3% solubilization of initial Fe(III) and (2) Fe(III) reduction could then be largely underestimated due to adsorption of Fe(II) on the dissolving iron oxides and/or formation of secondary mineral phases containing structural Fe(II).

In the current study, the measurement of adsorption of Fe(II) on powdered ferryhidrite in marine medium (Fig. 4) indicated a probable adsorption of solubilized ferrous iron, as it has also been found for other Fe(III)-oxides in previous studies using aqueous solutions with a composition different than in our study (Larese-Casanova and Scherer, 2007; Rajput et al., 2016). Considering the adsorption capacity of ferryhidrite ($0.6\ \text{mmol g}^{-1}$) and the released acetate in the ferrihydrite bioreduction experiment (Fig. 1d), a Fe(II)/acetate ratio of 3.25 would be obtained if only adsorption of ferrous iron had occurred. Therefore, the marked Fe deficit observed (Fe(II)/acetate = 0.17; Table 2) cannot be explained by adsorption of ferrous iron alone. Moreover, the Fe(II)-ferrihydrite adsorption experiments showed that the adsorbed Fe(II) exceeded the maximum capacity ($0.6\ \text{mmol g}^{-1}$; Fig. 4). This indicated that an additional process, such as ferrihydrite transformation to magnetite, could be responsible for the extra Fe(II) uptake. A comparison between the XRD patterns of non-reacted and reacted ferrihydrite samples showed the presence of magnetite, a more crystalline phase (Fig. 5), confirming the occurrence of magnetite formation. Previous studies suggested that the Fe(III)-oxide-magnetite transformation is driven by an electron transfer between the absorbed Fe(II) and Fe(III) in iron oxides, resulting in the formation of nano-crystalline, stoichiometric magnetite (Byrne et al., 2011; Williams and Scherer, 2004). This mineralogical transformation may be expressed as (5):

$$2Fe(OH)_3 + Fe^{2+} \leftrightarrow Fe_3O_4 + 2H_2O + 2H^+ \tag{5}$$

It is suggested that in alkaline environments magnetite is the most stable iron oxide phase (Tronc et al., 1992), in contrast to lepidocrocite and goethite in neutral environments (Boland et al., 2014). Simultaneous Fe(II) adsorption and mineral transformation could therefore explain the systematically high deficit of aqueous ferrous iron. These two processes, which act as a sink for dissolved biogenic ferrous iron, were also observed in *Geobacter* mediated ferrihydrite bioreduction (Chen et al., 2018).

The estimated initial bioreduction coefficients differed between the different oxides studied (Table 2). Bioreduction kinetics is dependent on the reactive surface area of the iron oxides, which plays a key role in the process (Burdige et al., 1992). Ferrihydrite has the largest surface area (Table 1), up to three orders of magnitude higher than that of the other minerals. As a result, the bioreduction coefficient of ferrihydrite shows the highest value ($5.49\ \mu\text{mol of Fe(II)}\ g_{\text{oxide}}^{-1}\ d^{-1}$;Fig. 3a). In contrast, the lowest bioreduction coefficient corresponds to goethite (Table 2), commercial powder ($0.026\ \mu\text{mol of Fe(II)}\ g_{\text{oxide}}^{-1}\ d^{-1}$; Fig. 3a). Nevertheless, when microbial bioreduction coefficients were normalized with the specific surface area of the oxides, magnetite, either synthetic or natural (Magnetite and M1) shows the highest bioreduction coefficient ($0.034\ \mu\text{mol Fe(II)}\ m^{-2}\ d^{-1}$ for Magnetite and $0.309\ \mu\text{mol Fe(II)}\ m^{-2}\ d^{-1}$ for M1; Fig. 3b). According to the normalized acetate coefficients, both commercial and field magnetite samples showed the highest acetate production compared to other commercial and synthetic samples ($0.249\ \mu\text{mol acetate}\ m^{-2}\ d^{-1}$ and $5.31\ \mu\text{mol acetate}\ m^{-2}\ d^{-1}$, respectively). These phases therefore show high preference for *Shewanella*'s bioreduction. Yet, the high values of the magnetite bioreduction coefficient could be also associated with an extra release of ferrous iron from the lattice of the magnetite (Kostka and Nealson, 1995). Furthermore, if Fe(III) of the magnetite lattice is reduced to Fe(II), an increase in crystal radius (with IV coordination) from 63 to 77 p.m. might destabilize magnetite structure, yielding high coefficient values (Shannon, 1976). The variability in the bioreduction coefficients of the studied iron oxides could be attributed to the differences in the intrinsic mineral properties, such as the degree of crystallinity, grain size and impurity content (Li et al., 2012; O'Loughlin et al., 2010).

4.2. *Shewanella loihica* and Fe-oxide surfaces

Bacteria use several strategies to perform bioreduction process. A well-known strategy is the contact of bacteria with mineral surfaces, allowing the electron transport (Burdige et al., 1992). SEM images showed *Shewanella loihica* cells colonizing the iron-oxide surfaces (Fig. 6a), either as individual cells or forming clusters. In addition, the SEM images revealed the presence of extracellular structures apparently connecting single cells with the mineral surface and/or with other cells (Fig. 6b and c). In fact, previous studies have shown that the genera *Shewanella* is able to develop extracellular structures to perform the electron exchange in the bioreduction process (i.e. nanowires) (Gorby et al., 2006; Pirbadian et al., 2014; Shi et al., 2016). A similar morphology between the extracellular structures in our study and those reported in previous studies exist. Nevertheless, to fully prove the electron-exchange capacity of the extracellular structures observed in this work, further studies are necessary.

5. Conclusions

Shewanella loihica is able to dissolve Fe (III) oxides via dissimilatory iron reduction under conditions of anoxic marine sediments. The deficit of aqueous ferrous iron relative to acetate produced during bioreduction was explained by adsorption of Fe(II) on the dissolving iron oxides and transformation of the iron oxides into stoichiometric magnetite. Hence, calculated bioreduction coefficients based on measured aqueous Fe(II) account for only up to about 4% of the actual reaction, considering the theoretical release of Fe (II) and acetate productions. During bioreduction, *Shewanella loihica* colonizes the surface of the iron oxides.

Results indicate a potential unfavorable role of iron-oxide bioreduction in deep-sea mining activities or coastal mine-tailings disposal, where release of trace and toxic metals represents an environmental threat. Furthermore, the iron released from metal mine tailings disposed offshore could affect primary production, jeopardizing the resilience of offshore ecosystems. However, a positive implication of iron-oxide bioreduction is found for biotechnology as iron-oxide bioleaching could potentially be used for recovery of iron and trace elements in metallurgical treatments.

Acknowledgements

Thanks are due to Javier García-Veigas, Eva Prats and Maite Romero (Scientific and Technical Services of the University of Barcelona) for technical assistance in the SEM-EDX and ICP-AES analyses, and to Jordi Bellés (IDAEA-CSIC) for technical assistance in the laboratory. We are indebted to Natàlia Moreno (IDAEA-CSIC) for her assistance in the XRD analyses. This study was funded by the Chilean Government through the Research Fund for Fishery and Aquaculture (Fondo de Investigación Pesquera y de Acuicultura; FIPA) of SUBPESCA, Project No. FIP 2015-11 and the Catalan Government through project 2017SGR 1733.

Appendix A. Supplementary data

Supplementary data to this article can be found online at https://doi.org/10.1016/j.marenvres.2019.104782.

References

Anderson, T.F., 1951. Techniques for the PRESERVATION OF three-dimensional structure IN preparing specimens for the electron microscope. Trans. N. Y. Acad. Sci. 13, 130–134.

Benner, S.G., Hansel, C.M., Wielinga, B.W., Barber, T.M., Fendorf, S., 2002. Reductive dissolution and biomineralization of iron hydroxide under dynamic flow conditions. Environ. Sci. Technol. 36, 1705–1711.

Boland, D.D., Collins, R.N., Miller, C.J., Glover, C.J., Waite, T.D., 2014. Effect of solution and solid-phase conditions on the Fe (II)-accelerated transformation of ferrihydrite to lepidocrocite and goethite. Environ. Sci. Technol. 48, 5477–5485.

Bonneville, S., Van Cappellen, P., Behrends, T., 2004. Microbial reduction of iron (III) oxyhydroxides: effects of mineral solubility and availability. Chem. Geol. 212, 255–268.

Boyd, P., Ellwood, M., 2010. The biogeochemical cycle of iron in the ocean. Nat. Geosci. 3, 675.

Brunauer, S., Emmett, P.H., Teller, E., 1938. Adsorption of gases in multimolecular layers. J. Am. Chem. Soc. 60, 309–319.

Burdige, D.J., Dhakar, S.P., Nealson, K.H., 1992. Effects of manganese oxide mineralogy on microbial and chemical manganese reduction. Geomicrobiol. J. 10, 27–48.

Byrne, J., Telling, N., Coker, V., Pattrick, R., Van Der Laan, G., Arenholz, E., Tuna, F., Lloyd, J., 2011. Control of nanoparticle size, reactivity and magnetic properties during the bioproduction of magnetite by Geobacter sulfurreducens. Nanotechnology 22, 455709.

Chen, Z., Zhang, Y., Luo, Q., Wang, L., Liu, S., Peng, Y., Wang, H., Shen, L., Li, Q., Wang, Y., 2018. Maghemite (γ-Fe2O3) nanoparticles enhance dissimilatory ferrihydrite reduction by Geobacter sulfurreducens: impacts on iron mineralogical change and bacterial interactions. J. Environ. Sci. 78, 193–203.

Cornel, R., Shwertmann, U., 1991. Iron Oxides in the Laboratory. Preparation and Characterization. VCH Editions, Weinhein, Germany.

Cornell, R., Schwertmann, U., 1996. The Iron Oxides: Structures, Properties, Reactions, Occurrences and Uses. VCH Verlagsgesellshaft GMBH, Weinheim, Germany, pp. 533–559.

Das, S., Hendry, M.J., Essilfie-Dughan, J., 2010. Transformation of two-line ferrihydrite to goethite and hematite as a function of pH and temperature. Environ. Sci. Technol. 45, 268–275.

De Baar, H.J., Boyd, P.W., Coale, K.H., Landry, M.R., Tsuda, A., Assmy, P., Bakker, D.C., Bozec, Y., Barber, R.T., Brzezinski, M.A., 2005. Synthesis of iron fertilization experiments: from the iron age in the age of enlightenment. J. Geophys. Res.: Oceans 110.

Dold, B., 2006. Element flows associated with marine shore mine tailings deposits. Environ. Sci. Technol. 40, 752–758.

Dold, B., 2014. Submarine tailings disposal (STD)—a review. Minerals 4, 642–666.

Dong, H., Fredrickson, J.K., Kennedy, D.W., Zachara, J.M., Kukkadapu, R.K., Onstott, T.C., 2000. Mineral transformations associated with the microbial reduction of magnetite. Chem. Geol. 169, 299–318.

Dzombak, D.A., Morel, F., 1990. Surface Complexation Modeling: Hydrous Ferric Oxide. John Wiley & Sons.

Ellis, D., Ellis, K., 1994. Very deep STD. Mar. Pollut. Bull. 28, 472–476.

Fenchel, T., 1969. The ecology of marine microbenthos IV. Structure and function of the benthic ecosystem, its chemical and physical factors and the microfauna communities with special reference to the ciliated protozoa. Ophelia 6 1-182.

Field, C.B., Behrenfeld, M.J., Randerson, J.T., Falkowski, P., 1998. Primary production of the biosphere: integrating terrestrial and oceanic components. Science 281, 237–240.

Finke, N., Vandieken, V., Jørgensen, B.B., 2007. Acetate, lactate, propionate, and isobutyrate as electron donors for iron and sulfate reduction in Arctic marine sediments, Svalbard. FEMS (Fed. Eur. Microbiol. Soc.) Microbiol. Ecol. 59, 10–22.

Gao, H., Obraztova, A., Stewart, N., Popa, R., Fredrickson, J.K., Tiedje, J.M., Nealson, K.H., Zhou, J., 2006. Shewanella loihica sp. nov., isolated from iron-rich microbial mats in the Pacific Ocean. Int. J. Syst. Evol. Microbiol. 56, 1911–1916.

Gorby, Y.A., Yanina, S., McLean, J.S., Rosso, K.M., Moyles, D., Dohnalkova, A., Beveridge, T.J., Chang, I.S., Kim, B.H., Kim, K.S., 2006. Electrically conductive bacterial nanowires produced by Shewanella oneidensis strain MR-1 and other microorganisms. Proc. Natl. Acad. Sci. 103, 11358–11363.

Hau, H.H., Gralnick, J.A., 2007. Ecology and biotechnology of the genus Shewanella. Annu. Rev. Microbiol. 61, 237–258.

Hiemstra, T., 2013. Surface and mineral structure of ferrihydrite. Geochem. Cosmochim. Acta 105, 316–325.

Jørgensen, B., Kasten, S., 2006. Marine Geochemistry. Bacteria and.

Knipping, J.L., Bilenker, L.D., Simon, A.C., Reich, M., Barra, F., Deditius, A.P., Wälle, M., Heinrich, C.A., Holtz, F., Munizaga, R., 2015. Trace elements in magnetite from massive iron oxide-apatite deposits indicate a combined formation by igneous and magmatic-hydrothermal processes. Geochem. Cosmochim. Acta 171, 15–38.

Kostka, J.E., Nealson, K.H., 1995. Dissolution and reduction of magnetite by bacteria. Environ. Sci. Technol. 29, 2535–2540.

Larese-Casanova, P., Scherer, M.M., 2007. Fe (II) sorption on hematite: new insights based on spectroscopic measurements. Environ. Sci. Technol. 41, 471–477.

Li, X., Liu, T., Li, F., Zhang, W., Zhou, S., Li, Y., 2012. Reduction of structural Fe (III) in oxyhydroxides by Shewanella decolorationis S12 and characterization of the surface properties of iron minerals. J. Soils Sediments 12, 217–227.

Lovley, D.R., 1991. Dissimilatory Fe (III) and Mn (IV) reduction. Microbiol. Rev. 55, 259–287.

Lovley, D.R., Phillips, E.J., 1986. Organic matter mineralization with reduction of ferric iron in anaerobic sediments. Appl. Environ. Microbiol. 51, 683–689.

Manteca, J.I., García, J.Á.L., Oyarzun, R., Carmona, C., 2014. The beach placer iron deposit of Portman Bay, Murcia, SE Spain: the result of 33 years of tailings disposal (1957–1990) to the Mediterranean seaside. Miner. Depos. 49, 777–783.

Martin, J.H., Fitzwater, S.E., Gordon, R.M., 1990. Iron deficiency limits phytoplankton growth in Antarctic waters. Glob. Biogeochem. Cycles 4, 5–12.

Mazzetti, L., Thistlethwaite, P., 2002. Raman spectra and thermal transformations of ferrihydrite and schwertmannite. J. Raman Spectrosc. 33, 104–111.

Medina, M., Andrade, S., Faugeron, S., Lagos, N., Mella, D., Correa, J., 2005. Biodiversity of rocky intertidal benthic communities associated with copper mine tailing discharges in northern Chile. Mar. Pollut. Bull. 50, 396–409.

Morel, F., Price, N., 2003. The biogeochemical cycles of trace metals in the oceans.

Science 300, 944–947.

Morello, E.B., Haywood, M.D., Brewer, D.T., Apte, S.C., Asmund, G., Kwong, Y.J., Dennis, D., 2016. The Ecological Impacts of Submarine Tailings Placement, Oceanography and Marine Biology. CRC Press, pp. 323–374.

Nadoll, P., Angerer, T., Mauk, J.L., French, D., Walshe, J., 2014. The chemistry of hydrothermal magnetite: a review. Ore Geol. Rev. 61, 1–32.

Nation, J.L., 1983. A new method using hexamethyldisilazane for preparation of soft insect tissues for scanning electron microscopy. Stain Technol. 58, 347–351.

O'Loughlin, E.J., Gorski, C.A., Scherer, M.M., Boyanov, M.I., Kemner, K.M., 2010. Effects of oxyanions, natural organic matter, and bacterial cell numbers on the bioreduction of lepidocrocite (γ-FeOOH) and the formation of secondary mineralization products. Environ. Sci. Technol. 44, 4570–4576.

Pirbadian, S., Barchinger, S.E., Leung, K.M., Byun, H.S., Jangir, Y., Bouhenni, R.A., Reed, S.B., Romine, M.F., Saffarini, D.A., Shi, L., 2014. Shewanella oneidensis MR-1 nanowires are outer membrane and periplasmic extensions of the extracellular electron transport components. Proc. Natl. Acad. Sci. 111, 12883–12888.

Raiswell, R., Canfield, D.E., 2012. The iron biogeochemical cycle past and present. Geochem. Perspect. 1, 1–2.

Rajput, S., Pittman Jr., C.U., Mohan, D., 2016. Magnetic magnetite (Fe3O4) nanoparticle synthesis and applications for lead (Pb2+) and chromium (Cr6+) removal from water. J. Colloid Interface Sci. 468, 334–346.

Ramirez-Llodra, E., Trannum, H.C., Evenset, A., Levin, L.A., Andersson, M., Finne, T.E., Hilario, A., Flem, B., Christensen, G., Schaanning, M., 2015. Submarine and deep-sea mine tailing placements: a review of current practices, environmental issues, natural analogs and knowledge gaps in Norway and internationally. Mar. Pollut. Bull. 97, 13–35.

Roden, E.E., Urrutia, M.M., Mann, C.J., 2000. Bacterial reductive dissolution of crystalline Fe (III) oxide in continuous-flow column reactors. Appl. Environ. Microbiol. 66, 1062–1065.

Roh, Y., Gao, H., Vali, H., Kennedy, D.W., Yang, Z.K., Gao, W., Dohnalkova, A.C., Stapleton, R.D., Moon, J.-W., Phelps, T.J., 2006. Metal reduction and iron biomineralization by a psychrotolerant Fe (III)-reducing bacterium, Shewanella sp. strain PV-4. Appl. Environ. Microbiol. 72, 3236–3244.

Rosselló-Mora, R., Thamdrup, B., Schäfer, H., Weller, R., Amann, R., 1999. The response of the microbial community of marine sediments to organic carbon input under anaerobic conditions. Syst. Appl. Microbiol. 22, 237–248.

Scott, J.H., Nealson, K.H., 1994. A biochemical study of the intermediary carbon metabolism of Shewanella putrefaciens. J. Bacteriol. 176, 3408–3411.

Shannon, R.D., 1976. Revised effective ionic radii and systematic studies of interatomic distances in halides and chalcogenides. Acta Crystallogr. - Sect. A Cryst. Phys. Diffr. Theor. Gen. Crystallogr. 32, 751–767.

Shi, L., Dong, H., Reguera, G., Beyenal, H., Lu, A., Liu, J., Yu, H.-Q., Fredrickson, J.K., 2016. Extracellular electron transfer mechanisms between microorganisms and minerals. Nat. Rev. Microbiol. 14, 651.

Stucki, J., 1981. The quantitative assay of minerals for Fe2+ and Fe3+ using 1, 10-phenanthroline: II. A photochemical method 1. Soil Sci. Soc. Am. J. 45, 638–641.

Tang, Y.J., Meadows, A.L., Kirby, J., Keasling, J.D., 2007. Anaerobic central metabolic pathways in Shewanella oneidensis MR-1 reinterpreted in the light of isotopic metabolite labeling. J. Bacteriol. 189, 894–901.

Thamdrup, B., 2000. Bacterial Manganese and Iron Reduction in Aquatic Sediments, Advances in Microbial Ecology. Springer, pp. 41–84.

Tronc, E., Belleville, P., Jolivet, J.P., Livage, J., 1992. Transformation of ferric hydroxide into spinel by iron (II) adsorption. Langmuir 8, 313–319.

Tugel, J.B., Hines, M.E., Jones, G.E., 1986. Microbial iron reduction by enrichment cultures isolated from estuarine sediments. Appl. Environ. Microbiol. 52, 1167–1172.

Williams, A.G., Scherer, M.M., 2004. Spectroscopic evidence for Fe (II)− Fe (III) electron transfer at the iron oxide− water interface. Environ. Sci. Technol. 38, 4782–4790.

Young, R., 1995. The Rietveld Method. International Union of Crystallography Monographs on Crystal and Oxford Science Publications, Oxford, UK.

Zachara, J.M., Fredrickson, J.K., Smith, S.C., Gassman, P.L., 2001. Solubilization of Fe (III) oxide-bound trace metals by a dissimilatory Fe (III) reducing bacterium. Geochem. Cosmochim. Acta 65, 75–93.

Chemosphere 260 (2020) 127554

Contents lists available at ScienceDirect

Chemosphere

journal homepage: www.elsevier.com/locate/chemosphere

Geochemical and isotopic study of abiotic nitrite reduction coupled to biologically produced Fe(II) oxidation in marine environments

R. Benaiges-Fernandez [a, b, 1, *], F.G. Offeddu [a, 1], R. Margalef-Marti [c, d], J. Palau [a, c, d], J. Urmeneta [b, e], R. Carrey [c, d], N. Otero [c, d, f], J. Cama [a]

[a] *Institute of Environmental Assessment and Water Research (IDAEA, CSIC), 08034, Barcelona, Catalonia, Spain*
[b] *Departament de Genètica, Microbiologia I Estadística, Universitat de Barcelona, 08028, Barcelona, Catalonia, Spain*
[c] *Grup MAiMA, SGR Mineralogia Aplicada, Geoquímica I Geomicrobiologia, Departament de Mineralogia, Petrologia I Geologia Aplicada, Facultat de Ciències de La Terra, Universitat de Barcelona (UB), 08028, Barcelona, Catalonia, Spain*
[d] *Institut de Recerca de L'Aigua (IdRA), Universitat de Barcelona (UB), 08001, Barcelona, Catalonia, Spain*
[e] *Institut de Recerca de La Biodiversitat (IRBio), Universitat de Barcelona, 08028, Barcelona, Catalonia, Spain*
[f] *Serra Húnter Fellowship. Generalitat de Catalunya, Catalonia, Spain*

HIGHLIGHTS

- Anoxic marine experiments to study nitrite reduction coupled with Fe oxidation.
- Bio-produced Fe (II) by *Shewanella loihica* promotes abiotic nitrite reduction.
- Abiotic and biotic reduction of nitrite is distinguished using isotopic analysis.
- Fe(II) presence in aqueous and solid-bound forms leads to faster denitrification.

ARTICLE INFO

Article history:
Received 23 March 2020
Received in revised form
25 June 2020
Accepted 27 June 2020
Available online 10 July 2020

Handling Editor: Hyunook Kim

Keywords:
Iron reducing bacteria
Chemodenitrification
Nitrite reduction
Fe(II) oxidation
Nitrite isotope

ABSTRACT

Estuarine sediments are often characterized by abundant iron oxides, organic matter, and anthropogenic nitrogen compounds (e.g., nitrate and nitrite). Anoxic dissimilatory iron reducing bacteria (e.g., *Shewanella loihica*) are ubiquitous in these environments where they can catalyze the reduction of Fe(III) (oxyhydr)oxides, thereby releasing aqueous Fe(II). The biologically produced Fe(II) can later reduce nitrite to form nitrous oxide. The effect on nitrite reduction by both biologically produced and artificially amended Fe(II) was examined experimentally. Ferrihydrite was reduced by *Shewanella loihica* in a batch reaction with an anoxic synthetic sea water medium. Some of the Fe(II) released by S. loihica adsorbed onto ferrihydrite, which was involved in the transformation of ferrihydrite to magnetite. In a second set of experiments with identical medium, no microorganism was present, instead, Fe(II) was amended. The amount of solid-bound Fe(II) in the experiments with bioproduced Fe(II) increased the rate of abiotic NO_2^- reduction with respect to that with synthetic Fe(II), yielding half-lives of 0.07 and 0.47 d, respectively. The $\delta^{18}O$ and $\delta^{15}N$ of NO_2^- was measured through time for both the abiotic and innoculated experiments. The ratio of $\varepsilon^{18}O/\varepsilon^{15}N$ was 0.6 for the abiotic experiments and 3.1 when NO_2^- was reduced by *S. loihica*, thus indicating two different mechanisms for the NO_2^- reduction. Notably, there is a wide range of the $\varepsilon^{18}O/\varepsilon^{15}N$ values in the literature for abiotic and biotic NO_2^- reduction, as such, the use of this ratio to distinguish between reduction mechanisms in natural systems should be taken with caution. Therefore, we suggest an additional constraint to identify the mechanisms (i.e. abiotic/biotic) controlling NO_2^- reduction in natural settings through the correlation of $\delta^{15}N$-NO_2^- and the aqueous Fe(II) concentration.

© 2020 Elsevier Ltd. All rights reserved.

1. Introduction

Sediments in estuarine and coastal areas often contain terrigenous organic matter and other constituents such as iron and

---

* Corresponding author. Institute of Environmental Assessment and Water Research (IDAEA, CSIC), 08034, Barcelona, Catalonia, Spain.
E-mail address: robert.benaiges@idaea.csic.es (R. Benaiges-Fernandez).
[1] They both contributed equally in the study.

https://doi.org/10.1016/j.chemosphere.2020.127554
0045-6535/© 2020 Elsevier Ltd. All rights reserved.

nitrogen compounds (e.g., NO_x), which arrive via rivers and submarine groundwater inputs (Jani and Toor, 2018). Currently, the intensive use of nitrogen-based fertilizers and the systematic release of domestic and industrial waste account for the majority of nitrogen input to these systems (Guerbois et al., 2014). When oxygen is limited in these environments, dissimilatory iron reducing bacteria (e.g., *Shewanella loihica*) are able to reduce Fe(III) (oxyhydr) oxides minerals (Melton et al., 2014) producing Fe(II) (Eq. (1)) (Lovley, 1991). Further, the biologically produced Fe(II) can reduce available nitrite (NO_2^-) to form nitrous oxide (N_2O) (Eq. (2)) (Tai and Dempsey, 2009).

$$CH_3CHOHCOO^- + 4Fe(OH)_3 + 7H^+ \rightarrow CH_3COO^- + HCO_3^- + 4Fe^{2+} + 10H_2O \quad (1)$$

$$4Fe^{2+} + 2NO_2^- + 5H_2O \rightarrow 4FeOOH + N_2O + 6H^+ \quad (2)$$

Nitrous oxide is a potent greenhouse gas and the single greatest ozone-depleting substance (Ravishankara et al., 2009). In recent years, nitrite reduction by Fe(II) oxidation (i.e. chemodenitrification) has been the subject of much research given its environmental relevance (Tai and Dempsey, 2009; Grabb et al., 2017; Lu et al., 2017; Buchwald et al., 2016; Carlson et al., 2013).

Both iron and nitrogen cycles are related in anaerobic environments where bioreduction of hydrous ferric oxides (HFO), such as ferrihydrite, leads to nitrite reduction coupled with Fe(II) oxidation (Melton et al., 2014; Kampschreur et al., 2011; Bryce et al., 2018). Since nitrite reduction occurs in the presence of aqueous Fe(II) and in the absence of HFO (Robertson et al., 2016; Devol, 2015), higher abiotic NO_2^- reduction rates have been observed in the presence of solid iron phases (Tai and Dempsey, 2009; Wu et al., 2015; Dhakal et al., 2013). Tai and Dempsey (2009) observed higher NO_2^- reduction rates when the initial aqueous Fe(II)/HFO ratio was 0.3. They demonstrated that ratio values higher than 0.3 indicate a halt of the reduction even in the presence of mineral-associated Fe(II). Furthermore, they showed that the abiotic NO_2^- reduction was negligible in the absence of HFO. In experiments with aqueous Fe(II) and nitrite, precipitation of HFO or mixed valence (Fe(II), Fe(III)) iron minerals, such as green rust (Pantke et al., 2012), will probably occur due to the oxidation of aqueous Fe(II) (Lu et al., 2017; Chen et al., 2018).

Solid Fe(II) (also referred to as structural or solid-bound Fe(II)) may be involved in nitrite reduction (Rakshit et al., 2008) together with the dissolved Fe(II). Dhakal et al. (Dhakal et al., 2013) studied the ability of magnetite to reduce nitrite and showed that abiotic NO_2^- reduction by magnetite had a greater impact on nitrite removal than microbially mediated denitrification. However, Lu et al. (Lu et al., 2017) showed that magnetite was not able to reduce nitrite in a wide NO_2^- concentration range (30–280 mg L^{-1}) in the absence of solid-bound Fe(II). Few studies on abiotic nitrite reduction in experiments with fresh biogenic magnetite in marine conditions are available to date (Otte et al., 2019).

Currently, the evaluation of abiotic nitrogen reduction coupled with oxidation of Fe(II) in heterogenous systems at laboratory scales has been performed by the addition of synthetic Fe(II) (e.g., $FeCl_2$) to aqueous solutions with different iron minerals (Lu et al., 2017; Robertson et al., 2016; Robertson and Thamdrup, 2017). However, in natural settings Fe(II) can derive from microbial reduction of Fe(III)-minerals. Dissimilatory Fe(III) reduction could alter the properties of the iron mineral surface or result in the formation of secondary iron mineral phases such as magnetite or siderite (Roh et al., 2006). The evaluation of abiotic nitrite reduction therefore requires that experiments be carried out under conditions more comparable to natural settings (e.g., marine environment).

In this study, ferrihydrite was the Fe(III) mineral used in biotic and abiotic nitrite reduction experiments with synthetic seawater at pH 8.2 because it is abundant in marine sediments (Canfield, 1989) and therefore comparable to natural systems. Fe(II) was either added as $FeSO_4$ or biologically produced by *Shewanella loihica* (strain PV-4) at similar Fe(II) aqueous concentrations. This strain of *S. loihica* is known to reduce Fe(III) (oxyhydr)oxides in seawater under anoxic conditions (Benaiges-Fernandez et al., 2019). Given its thermodynamic instability and large surface area, ferrihydrite has a high reactivity in the presence of aqueous Fe(II), which may lead to a mineral transformation made up of more crystalline phases containing Fe(II) such as magnetite (Tomaszewski et al., 2016; Boland et al., 2014; Yang et al., 2010; Yee et al., 2006; Hansel et al., 2003; Piepenbrock et al., 2011).

Isotopic analysis is a useful tool for tracing NOx transformation processes. The enzymatic NO_3^- reduction provokes an enrichment in the heavy isotopes of the unreacted substrate (Böttcher et al., 1990; Fukada et al., 2003; Mariotti et al., 1981; Aravena and Robertson, 1998) unlike processes such as dilution that lead to a decrease in concentration without influencing the isotopic ratios. The same pattern is expected for the biotic reduction of all N intermediate products (e.g., NO_2^- or N_2O), which will be initially depleted in ^{15}N and ^{18}O with respect to the substrate. However, data on the dual N-O isotope systematics during the biotic reduction of intermediate compounds such as NO_2^- remain scarce (Bryan et al., 1983; Martin and Casciotti, 2016). Moreover, two recent isotopic studies on the abiotic NO_2^- reduction by Fe(II) found results similar to what is expected from the biotic reaction (Grabb et al., 2017; Buchwald et al., 2016). Essentially, it is unclear to what degree the isotopic characterization might help in distinguishing biotic and abiotic NO_2^- reduction. Further studies on the application of isotopic data to elucidate the process controlling the fate of nitrite in natural systems are therefore warranted.

In the present study, biotic and abiotic NO_2^- reduction experiments using synthetic and biologically produced Fe(II) were performed with anoxic synthetic sweater to (1) shed light on the kinetics of NO_2^- reduction in marine environments and (2) evaluate the possible use of isotopic analysis to distinguish between abiotic and biotic (heterotrophic) NO_2^- reduction. In addition, the reductive dissolution of ferrihydrite by *Shweanella loihica* and the fate of bioproduced Fe(II) was investigated.

2. Materials and methods

2.1. Solutions

Synthetic sea water (SSW) was prepared to simulate marine sediment conditions following the standard protocol D1141-98 (ATSM International). In addition to this basal medium, 10.0 mM of sodium lactate as both a carbon source and electron donor, and 10.0 mM of TRIS-HCl (Tris) as a buffer (pH ≈ 8.2) were added. Hereafter, this medium will be referred to as M-SSW.

Stock solutions of Fe(II) at pH 1 (HCl) and NO_2^- (230.0 mM 60.0 mM, respectively) were prepared in an anoxic glove box dissolving suitable amounts of $FeSO_4$ and KNO_2 into nitrogen degassed ultrapure (18.1 MΩ) Milli-Q water. Both solutions were subsequently filtered with a 0.22 μm membrane and stored in sterile bottles.

All solutions used in this study were sterilized by autoclave (121 °C, 20 min) unless stated otherwise. Dissolved oxygen concentrations were measured by luminescent dissolved oxygen (LDO) probe (detection limit 0.01 mg L^{-1}).

2.2. Bacterial culture

Shewanella loihica strain PV-4 was purchased from the German Collection of Microorganisms and Cell Cultures (DSMZ 17748). Bacteria were recovered and cultivated in M1 medium (Gao et al., 2006) with 10.0 mM of lactate as the electron donor and carbon source and 10.0 mM of Fe(III) citrate as the electron acceptor. To obtain bacterial suspensions, cells were cultivated for 24 h and then harvested by centrifugation (5000 rpm for 10 min). The pellet was then re-suspended in SSW. This step was repeated three times as a washing protocol. *S. loihica* was inoculated with a concentration of $1\cdot10^7$ colony-forming units (cfu) mL^{-1}.

2.3. Ferrihydrite: synthesis and characterization

2L-ferrihydrite was synthesized according to a modified protocol of Schwertmann and Cornell (Schwertmann and Cornell, 2008) (see supporting information (SI) for more details). The specific surface area was measured by the Brunauer-Emmett-Teller (BET) method (Brunauer et al., 1938) with a Gemini 2370 surface area analyzer using 5-point N_2 adsorption isotherms. Sample degassing with nitrogen lasted for 2 h at 137 °C. The BET specific surface area measured for unreacted samples varied between 140 and 180 m^2g^{-1}, and for the bioreacted samples it was between 144 and 152 $m^2\ g^{-1}$.

The reacted and unreacted samples were examined by three techniques: (1) scanning electron microscopy (SEM) using a Hitachi H-4100FE instrument under a 15–20 kV potential in a high vacuum and utilizing the backscattered electron detector (BSD) in field emission (FE) and coating the samples with carbon, (2) X-ray diffraction (XRD) using a *PANalytical X'Pert PRO MPD θ/θ* Bragg-Brentano powder diffractometer of 240 mm in radius and Cu Kα radiation ($\lambda = 1.5418$ Å) together with Rietveld analysis to quantify the amount of phases, and (3) Fourier transform infrared spectrometry (FTIR) utilizing a PerkinElmer frontier/ATR diamond/detector DTGS, accumulation at 16 scans, spectral resolution 4 cm^{-1}, spectral range 4000–225 cm^{-1}.

2.4. Experimental setup and sampling procedure

Table 1 lists the initial experimental conditions. Most of the batch experiments were run in the dark (bottles wrapped with aluminum foil) and in triplicate at 22 ± 2 °C. Bottles (reactors) were placed in an anoxic glove box purged with N_2 and equipped with UV germicidal light for periodic sterilization. Glassware, septa, caps, tips, and media solutions were sterilized by autoclave at 121 °C for 20 min before the experiments.

2.4.1. Abiotic nitrite reduction experiments with biologically produced Fe(II)

Batch experiments consisted of two stages. In the first stage, no nitrate was amended while Fe(II) was produced biologically (experiment Ferr; Table 1). The anaerobic reductive dissolution of ferrihydrite mediated by *S. loihica* was performed in cultures prepared with the M-SSW medium described above. Bottles of 500 mL were sealed with a screw cap, silicone O-ring and blue butyl rubber stopper before being wrapped in aluminum foil to avoid exposure to light. Autoclaved ferrihydrite powder was put into the bottles (1:100 w/v ratio). Each reactor consisted of a multi-point batch experiment in which the butyl rubber stopper allowed for multiple collection of samples with a syringe over time. Before sampling, the reactors were thoroughly shaken for liquid-solid homogenization. Aliquots of 5 mL were extracted about every 48 h, filtered through a 0.22 μm membrane, and acidified with 200 μL of 6 M HCl solution. 1 mL was used for immediate Fe(II) analysis, and the remaining 4 mL were stored in the dark at 4 °C for further lactate/acetate measurements.

In the second stage, nitrite was amended to the reactors and reduced by the biologically produced Fe(II) (NFerr experiment in Table 1). In other words, the initial conditions of stage two correspond to the final conditions of stage one, in which lactate was consumed and ferrihydrite bioreduction ended. The concentrations of bioproduced Fe(II) and acetate were 1.15 and 8.1 mM, respectively, for at least 10 days. On the tenth day, 4.81 mL of a 60.0 mM NO_2^- stock solution were injected into the reactors under anoxic conditions, resulting in a NO_2^- concentration of 0.76 mM. NFerr experiment was performed in duplicate to ensure reproducibility.

Three sample aliquots were extracted at each sampling interval: a 5 mL aliquot for aqueous Fe(II) and Fe(III) concentration measurements, another 5 mL aliquot to measure the nitrite isotopic composition ($\delta^{15}N$-NO_2^- and $\delta^{18}O$-NO_2^-), and a 1 mL aliquot to measure the NO_2^- concentration. Concentrations of dissolved iron and nitrite were analyzed immediately to prevent measurement error due to subsequent iron oxidation/nitrite reduction. The aliquots taken for isotope analysis were immediately frozen and later defrosted before measurement preparation (Section 2.6).

2.4.2. Abiotic nitrite reduction experiments with synthetic Fe(II)

To investigate the role of solid and aqueous Fe(II) in nitrite reduction, three abiotic experiments were performed with synthetic Fe(II) in the presence and the absence of ferrihydrite. The $\delta^{15}N$ and $\delta^{18}O$ of nitrite were monitored through time. In the experiments containing ferrihydrite, the liquid/solid ratio was the same as in the NFerr experiment. Three distinct experimental conditions were employed: (1) dissolved Fe(II) + NO_2^- without ferrihydrite, (2) ferrihydrite + synthetic Fe(II) (totally solid-bound on by ferrihydrite) + NO_2^- in the absence of aqueous Fe(II) and (3) ferrihydrite + both solid-bound and dissolved Fe(II) + NO_2^-, which

Table 1

Initial conditions for the different experiments. *Ferr*: Fe(II) bio-production; *NFerr*: nitrite addition after completion of Fe(II) bio-production in experiment *Ferr* (same bottle); *A1*: abiotic nitrite reduction in the absence of ferrihydrite; *A2*: abiotic nitrite reduction in the presence of ferrihydrite and solid-bound Fe(II); *A3*: abiotic nitrite reduction in the presence of ferrihydrite, solid-bound Fe(II) and aqueous Fe(II); *Bio1* and *Bio2*: biotic nitrite reduction in the absence of ferrihydrite with either lactate or acetate as carbon source, respectively. n.d. Below detection limit.

	Experiment	Ferrihydrite (g)	Volume (mL)	Aqueous bio-Fe(II) (mM)	Synthetic Fe(II) (mM) Added/ Aqueous	NO_2^- (mM)	Acetate (mM)	Lactate (mM)	*S.loihica*
Fe(II) bio-production	Ferr	5.0	500	–	–	–	–	10.8	yes
Abiotic $NO_{2\ red}^-$/ $Fe(II)_{ox}$	NFerr	3.8	380	1.15	–	0.76	8.1	–	–
	A1	–	250	–	1.20/1.20	0.65	10.0	–	–
	A2	2.5	250	–	1.20/n.d.	0.76	10.0	–	–
	A3	2.5	250	–	2.60/1.20	0.76	10.0	–	–
Biotic NO_2^- reduction	Bio1	–	250	–	–	0.65	–	10.0	yes
	Bio2	–	250	–	–	0.65	10.0	–	yes

are labeled A1, A2, and A3, respectively (Table 1). Three replicates were performed for these experiments. All experiments consisted of a basal medium of SSW supplemented with 10.0 mM acetate and 10.0 mM Tris-HCl buffer. Acetate was added to match the initial conditions in the NFerr experiment (8.1 mM of acetate final concentration; Table 1). Control experiments with autoclaved culture of *Shewanella loihica* were carried out to examine an effect of dead cells on the overall process, and no residual nitrite reduction was observed.

In experiment A1, the abiotic reduction of NO_2^- (0.65 mM concentration) by aqueous Fe(II) (1.20 mM concentration) took place in batch reactors with 250 mL of SSW basal solution. The decrease in aqueous Fe(II) and NO_2^- was monitored to evaluate the nitrite reduction rate by implementing a multi-point approach. In multi-point batch experiment A2, reactors contained 2.5 g of ferrihydrite and 250 mL of SSW basal solution amended with Fe (II) (1.20 mM concentration). The aqueous Fe(II) was consumed in 400 min due to its uptake on ferrihydrite (see SI and Fig. S1). Once aqueous Fe(II) was depleted, 3.16 mL of 60.0 mM nitrite (0.76 mM concentration) were added to the reactor to promote nitrite reduction by solid-bound Fe(II).

The multi-point batch experiment A3 contained 2.5 g of ferrihydrite and significantly more synthetic Fe(II) (2.60 mM final concentration; Table 1) than A2 experiments. Similar to experiment A2, a fast uptake of approximately 1.40 mM Fe(II) occurred, yielding a fairly constant aqueous Fe(II) concentration of approximately 1.20 mM for 8 days. Subsequently, 3.16 mL of 60.0 mM of nitrite (0.76 mM final concentration) were injected into the reactor to promote nitrite reduction by oxidation of both solid bound and aqueous Fe(II). Note that the aqueous Fe(II) concentration in the experiments A1, A2, A3 and in the NFerr experiment, previous to the addition of nitrite, were approximately the same (i.e., 1.20 mM). The identical sample collection and preservation method used for NFerr was also implemented in experiments A1, A2 and A3 (Section 2.4.1).

2.4.3. Biotic nitrite reduction experiments with S. loihica

Bio1 and Bio2 experiments were performed to investigate the heterotrophic nitrite reduction mediated by *S.loihica* in the absence of ferrihydrite and aqueous Fe(II) (Table 1). Each reactor was amended with SSW and adjusted to 10.0 mM of either lactate or acetate as electron donor and carbon source, 10.0 mM of Tris-HCl buffer, and 0.65 nM of nitrite. This enabled the comparison of the biological and abiotic denitrification rates to further characterize of the isotopic signature for each mechanism. Moreover, these experiments allowed an evaluation of the potential contribution of the heterotrophic nitrite reduction in the abiotic experiments with biologically produced Fe(II).

2.4.4. Control and adsorption experiments

Control reactors with SSW were performed to examine any potential interference between acetate and Fe(II), nitrite and acetate or buffer, acetate and Fe(II) and only nitrite or Fe(II) in SSW (details in SI). Adsorption experiments were carried out to quantify the amount of Fe(II) adsorbed during reductive dissolution of synthetized ferrihydrite (see SI). An Fe(II) adsorption isotherm was performed with increasing concentrations of aqueous Fe(II) in anoxic SSW, acetate and TRIS pH buffer to investigate the mechanisms responsible for the Fe(II) uptake on ferrihydrite (Fig. S2 in SI).

2.5. Chemical analyses

Concentrations of dissolved iron and nitrite were both measured by spectrophotometry (SP-830 PLUS, Metertech Inc.) at wavelengths of 510 nm and 540 nm, respectively. Fe(II) and total iron concentrations were measured immediately after sampling by the phenanthroline method (Stucki, 1981). Nitrite concentration was measured following the method defined by Garcia-Robledo et al. (2004) (García-Robledo et al., 2014). The total iron dissolved was also measured using a PerkinElmer 3000 inductively coupled plasma optical emission spectrometer (ICP-OES). Differences in Fe concentrations measured by the phenanthroline method and ICP-OES were smaller than 5%. Concentrations of lactate and acetate were measured by high performance liquid chromatography (Waters 600 HPLC pump controller equipped with an Aminex HPX-87H column (300 × 7.8 mm), BioRad column, and a Waters 717plus autoinjector). The associated uncertainty was less than 3%. The pH of the initial medium was measured in a glove box using a Thermo Orion pH electrode (±0.02 pH units) and periodically calibrated with standard solutions of pH 2, 4 and 7.

2.6. Isotopic analyses

δ^{15}N-NO_2^- and δ^{18}O-NO_2^- were determined following the azide reduction method (McIlvin and Altabet, 2005; Ryabenko et al., 2009). N_2O was analyzed using a Pre-Con (Thermo Scientific) coupled with a Finnigan MAT 253 Isotope Ratio Mass Spectrometer (IRMS, Thermo Scientific). Notation is expressed in terms of delta per mil (δ ‰) (i.e., $\delta = (R_{sample}\text{-}R_{standard})/R_{standard}$, where R is the ratio between the heavy (^{15}N, ^{18}O) and the light (^{14}N, ^{16}O)isotopes) (Coplen, 2011). The δ^{15}N and δ^{18}S values are reported against international atmospheric N_2 (AIR) and Vienna Standard Mean Oceanic Water (V-SMOW). According to Coplen (Coplen, 2011), several international and laboratory (in-house) standards were interspersed among samples for normalization of analyses. Two international standards (USGS 34 and 35) and two internal laboratory standards (UB-$NaNO_3$ ($\delta^{15}N = +16.9$‰ and $\delta^{18}O = +28.5$‰) and UB-KNO_2 ($\delta^{15}N = -28.5$‰)) were employed to calibrate the δ^{15}N-NO_2^- and δ^{18}O-NO_2^- raw values to the international scales. The reproducibility (1σ) of the samples, calculated from the standards systematically interspersed in the analytical batches, was ±1.0‰ for δ^{15}N-NO_2^- and ±1.5‰ for δ^{18}O-NO_2.

Under closed system conditions, the isotopic fractionation values ($\varepsilon^{15}N_{NO2}$ and $\varepsilon^{18}O_{NO2}$) are calculated according to the Rayleigh distillation equation (Eq. (3)):

$$\ln\left(\frac{R_{residual}}{R_{initial}}\right) = \varepsilon \times \ln\left(\frac{C_{residual}}{C_{initial}}\right) \tag{3}$$

where ε is the slope of the linear regression between the natural logarithms of the substrate remaining fraction ($\ln(C_{residual}/C_{initial})$, where C refers to the analyte concentration, and the determined isotope ratios ($\ln(R_{residual}/R_{initial})$, where $R = \delta+1$.

Given that the use of NO_3^- (and NO_2^-) standards to correct δ^{18}O-NO_2^- may cause a bias on their values for the loss of one O atom during NO_3^- to NO_2^- reduction, the results were interpreted according to the changes in the NO_2^- isotopic composition with respect to the initial one.

3. Results and discussion

3.1. Bioreduction of ferrihydrite

Fig. 1 shows the three distinct stages of the bioreduction experiment. In the first stage (approximately 10 days), a significant drop in the initial concentration of lactate (from 10.8 to 3.9 mM) was accompanied by a sharp increase in acetate concentration (up to 3.8 mM). However, aqueous iron was not detected during this interval. In the second stage (from 10 to 30 days), a gradual decrease in lactate and a progressive increase in acetate were

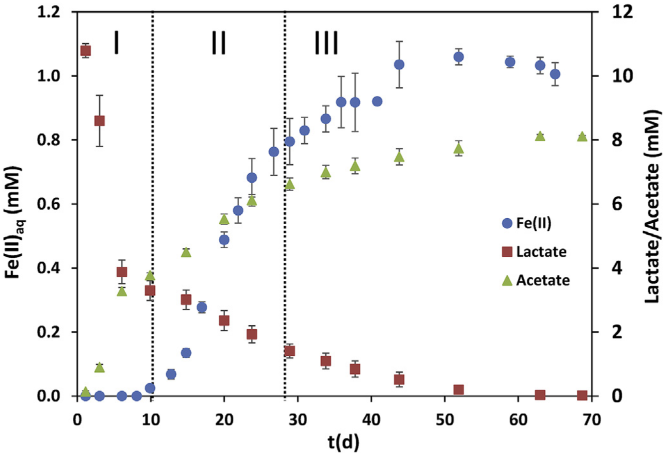

Fig. 1. Fe(II) bio-production experiment describing microbial reductive dissolution of ferrihydrite. The vertical error bars show the uncertainty calculated from three replicates (see text). Lactate consumption correspond to acetate and Fe(II) production. Three stages were differentiated throughout the experiment: (I) biomass production, (II) maximum release of Fe (II) and (III) halt of microbial metabolism.

observed together with a significant increase in dissolved iron. In the third stage, lactate was totally depleted after about 60 days, and acetate and Fe(II) concentrations stabilized at 8.1 and 1.15 mM, respectively. The total consumption of lactate (i.e. the electron donor) effectively halted Fe(III)-bioreduction and, therefore, the acetate and aqueous Fe(II) concentrations remained constant.

Referring to the bioreduction reaction (Eq. (1)), the molar ratio of [acetate]/[lactate] is 1. Nevertheless, based on the measured lactate consumption, a 20% deficit of acetate was observed throughout the experiments (Fig. 1). This non-stoichiometric behavior was mainly attributed to the use of lactate as a carbon source for biomass formation during microbial growth (Lanthier et al., 2008). Further, since the stoichiometric [Fe(II)]/[acetate] ratio is 4 (Eq. (1)) and the highest measured concentrations of aqueous Fe(II) and acetate were 1.15 and 8.1 mM, respectively, only a minor fraction of Fe(II) produced (i.e.≈ 3.5%) was found in solution. This Fe(II) deficit could be explained by a large Fe(II) adsorption on ferrihydrite. For instance, Dzomback and Morel (Dzombak and Morel, 1990) demonstrated that at relatively high pH (e.g. pH ≈ 8.2), ferrihydrite that has a large surface area combined with a poor crystalline organization can cause an exceptionally large sorption capacity of cations. In order to evaluate the Fe(II) adsorption process under the investigated conditions, several Fe(II)-adsorption assays were performed to obtain a Fe(II) adsorption isotherm (Figs. S1 and S2 in SI). The results confirmed a maximum uptake of Fe(II) on ferrihydrite of ≈ 1.20 mM (Fig. S1 in SI) and revealed that, in addition to adsorption, an additional process (ferrihydrite transformation) was responsible for the Fe(II) uptake on ferrihydrite (Fig. S2 in SI).

Earlier studies indicated that re-adsorption of Fe(II) on ferrihydrite can result in ferrihydrite transformation to goethite, magnetite or lepidocrocite (Yang et al., 2010; Hansel et al., 2003; Piepenbrock et al., 2011; Xiao et al., 2017, 2018; Dippon et al., 2015). In addition, the thermodynamic properties of the minerals involved, the aqueous Fe(II) concentration, the biological and physical settings, the presence of humic substances or the design of the experimental setup can play a role in ferrihydrite transformation (Dippon et al., 2015; Amstaetter et al., 2012). SEM images (Fig. 2a) show that the surface of the reacted ferrihydrite grains is rougher than that of the unreacted ones. XRD and FTIR analyses of the solid samples before and after the Fe(III) bioreduction process show that ferrihydrite indeed transformed into magnetite ($Fe^{2+}Fe^{3+}{}_2O_4$) (Fig. 2b and c). Yang et al. (Yang et al., 2010) pointed out that this transformation is caused by the inclusion of the biologically produced Fe(II) into the mineral lattice. Fig. 2b compares two XRD patterns after performing high statistic wide range scans of pristine and bioreduced samples. In addition to initial ferrihydrite, two new phases (nanocrystalline magnetite and microcrystalline hematite) were determined to be present in the reacted sample (NFerr experiment) with estimated amounts of 96 wt% (magnetite) and 4 wt% (hematite). The much smaller content of the latter was formed during the ferrihydrite autoclave process (Das et al., 2011).

3.2. NO_2^- reduction coupled with Fe(II) oxidation

Fig. 3 shows the evolution through time of the concentrations of nitrite and Fe(II) during abiotic (Fig. 3a-c) and biotic (Fig. 3d) nitrite reduction. Fig. 3a shows the variation in Fe(II) and NO_2^- in a representative A1 experiment with an initial aqueous Fe(II) concentration of ≈ 1.0 mM in the absence of ferrihydrite. After a week, Fe(II) depletion was approximately 50% of the initial concentration and 35% of nitrite was reduced. After a month, the Fe(II) depletion was 70% of the initial concentration and nitrite concentration fell to 65% of the initial concentration. The average nitrite reduction rate constant (k_{obs}) was estimated to be 0.059 mM^{-1} d^{-1} with a half-life value ($t_{1/2}$) of 18.7 d (second-order rate equation (Eq. (S1)) and parameters in Table S2 in SI).

Fig. 3b depicts the variation in Fe(II) and nitrite concentration in a representative A2 experiment in the presence of solid-bound Fe(II) with (i) product magnetite and (ii) Fe(II) adsorbed on the remaining ferrihydrite. About 27% of the initial NO_2^- was reduced within 2 days, indicating that in the absence of aqueous Fe(II), Fe(II) in the solid phase was able to reduce some NO_2^-. After 2 days, the reaction stopped, and nitrite concentration remained constant. An average nitrite reduction rate of 0.22 mM^{-1} d^{-1} was calculated for all replicates (Eq. (S1)) and Table S2 in SI). Fig. 3c shows the variation in Fe(II) and nitrite concentration in a representative A3 experiment in the presence of both aqueous Fe(II) and solid bound Fe(II). NO_2^- and aqueous Fe(II) concentrations dropped 13% and 62% from the initial value, respectively, within about 2 d, yielding an average nitrite reduction rate of 0.74 mM^{-1} d^{-1} ($t_{1/2}$ = 0.47 d) (Fig. S4 Table S2 in SI).

Fig. 3d shows the evolution of bioproduced Fe(II) after the cessation of the Fe(III) reduction in the Ferr experiment (Fig. 1), along with the nitrite concentration added in a representative NFerr experiment. To ensure comparability of the results, the experiment NFerr (Fig. 3d) was selected for its high initial concentration of aqueous bioproduced Fe(II), which was similar to those of the experiments with synthetic Fe(II). Considering the reductive dissolution reaction (Eq. (1)) and acetate production, the total concentration of bioproduced Fe(II) was estimated to be 32.0 mM. Nevertheless, the initial concentration of aqueous Fe(II) in the NFerr experiment was 1.20 mM because most of the bioproduced Fe(II) was adsorbed on ferrihydrite and incorporated in to form magnetite (see section 3.1). During the first 2 h, both nitrite and aqueous Fe(II) fell to about 50% and 30% of their initial concentrations, respectively. After 10 h, 87% of the initial nitrite and 38% of the initial aqueous Fe(II) were removed. The nitrite calculated reduction rate was 6.47 mM^{-1} d^{-1} ($t_{1/2}$ = 0.07 d) (Fig. S4 in SI). In the NFerr experiment with lower concentrations of Fe(II) and nitrite, the rate calculated are within the same range of that from A3 experiment (Table S2 in SI).

S. loihica used for the bioproduction of Fe(II) in the Ferr experiment (prior to nitrite addition in the NFerr experiment) could not be eliminated because both autoclave and antibiotics interfered

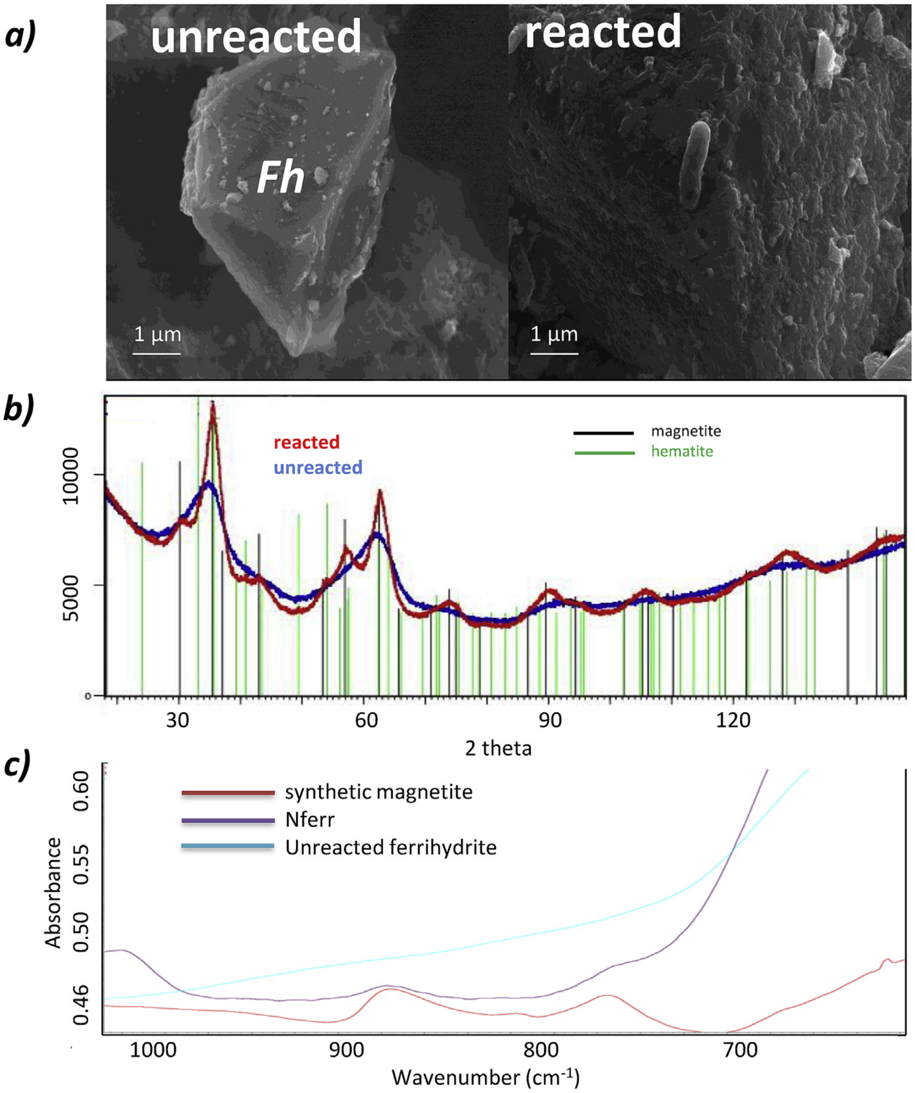

Fig. 2. Characterization of the solid sample: a) SEM images show an unreacted particle and a close-up surface of a reacted ferrihydrite particle with attached cell of *S. loihica*); b) X-ray powder diffraction patterns of the unreacted (blue line) and reacted (red line) ferrihydrite samples; black and green vertical lines show the 2θ positions of peaks of magnetite and hematite, respectively; c) FTIR spectra of unreacted ferrihydrite (blue line), reacted ferrihydrite (purple line) and pure magnetite (red line); magnetite peaks are visible in the reacted ferrihydrite sample. (For interpretation of the references to colour in this figure legend, the reader is referred to the Web version of this article.)

with dissolved Fe(II) (Table S2 in SI). However, as explained in Sections 3.3 and 3.4, the evidence resulting from (i) the isotopic data from the NFerr experiment (Fig. S5 in SI) and (ii) the observed biotic nitrite reduction by *S. loihica* in the Bio1 and Bio2 experiments ruled out any microbial reduction of nitrite.

The fastest abiotic nitrite reduction rate was observed in the NFerr experiment where bioproduced Fe(II) was the electron donor. In experiments with synthetic Fe(II), the rate was slower, despite both experiments having similar aqueous Fe(II) concentrations. In experiments with synthetic Fe(II), the nitrite reduction rate was highest in the presence of both aqueous and solid Fe(II) (e.g. A3 experiment), slower in the presence only of solid-bound Fe(II) (e.g. A2 experiment), and slowest in the experiment with only aqueous Fe(II) (e.g. A1 experiment). The highest nitrite reduction rate in the NFerr experiments compared to A3 experiment, both with aqueous and solid-bound Fe(II), suggests that the larger amount of solid-bound Fe(II) obtained in the NFerr experiments could play a crucial role on the nitrite reduction rate. Previous studies suggested that solid-bound Fe(II) is able to reduce nitrite (Tai and Dempsey, 2009; Rakshit et al., 2008; Byrne et al., 2011), and that an enhanced Fe(II)-rich surface (e.g. magnetite) of bioreduced Fe(III) (oxyhydr)oxides is able to consume electron acceptors (e.g., toxic hexavalent chromium).

The highest nitrite reduction rates were observed in the presence of both aqueous and solid-bound Fe(II). This is in accordance with Gorski and Scherer (Gorski and Scherer, 2011) who showed that aqueous Fe(II) removal by iron oxide could affect the reduction potential of the oxide, as a decrease in its oxidation grade leads to an increase in the reducing capacity of the oxide. The difference between the reduction rates calculated in experiments with only solid-phase Fe(II) and experiments containing both solid-phase Fe(II) and dissolved Fe(II) is similar to that calculated in reductive dechlorination by Fe(II)-associated with goethite (Elsner et al., 2004).

3.3. Biotic (heterotrophic) NO_2^- reduction by *S. loihica*

Biotic experiments showed a lag in microbial activity before

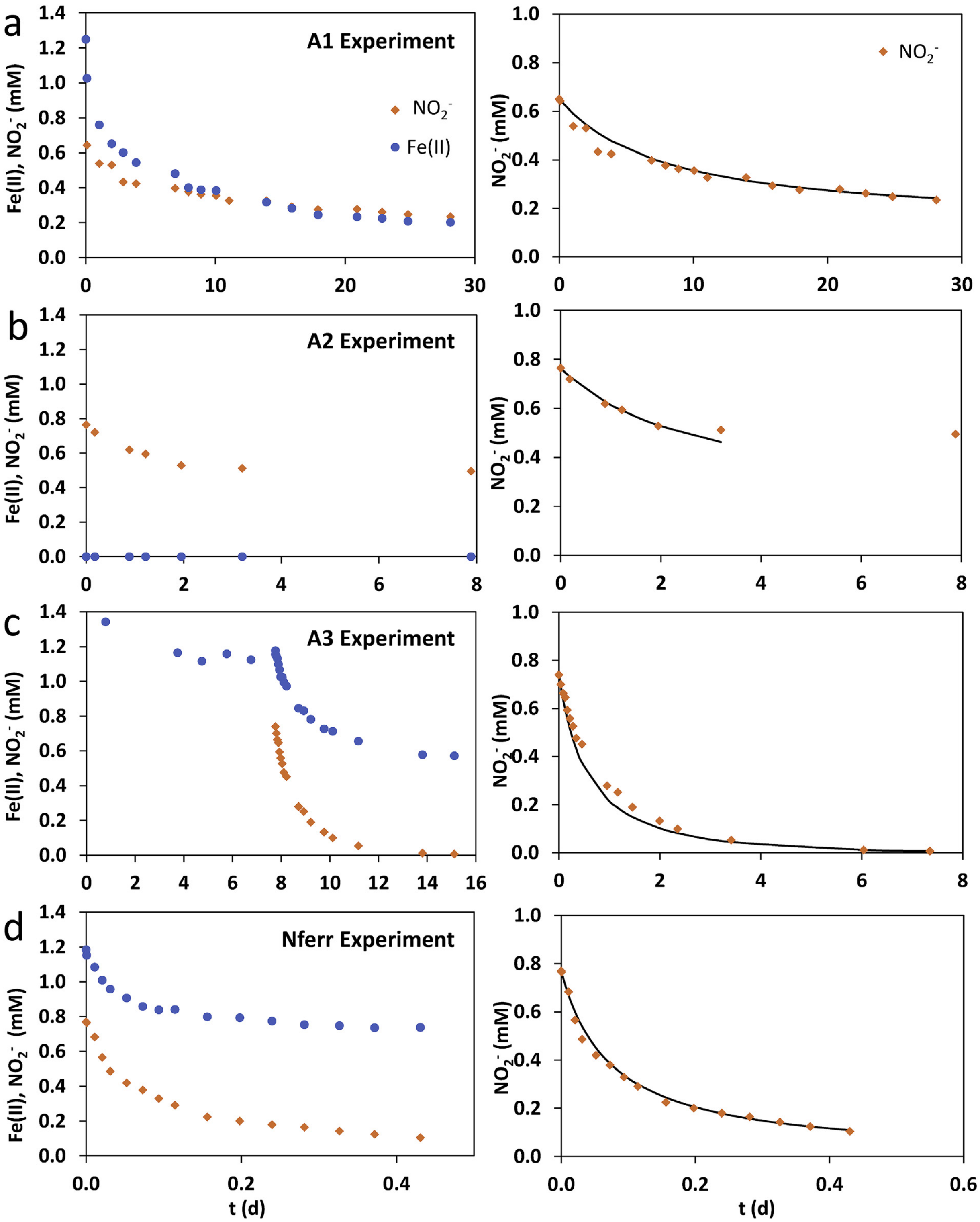

Fig. 3. Variation in concentrations of Fe(II) and NO_2^- throughout the experiments (left panels) and nitrite second-order decay fits using Eqs. (S1 and S2 in SI) (solid line in right panels): a) initial 0.65 mM nitrite and 1 mM of aqueous Fe(II) (A1 experiment); b) initial 0.76 mM nitrite and 1.2 mM of solid-bound Fe(II) with ferrihydrite (A2 experiment); c) Initial 2.6 mM Fe(II), after 8d adsorption of 1.39 mM Fe(II) in ferrihydrite forming solid-bound Fe(II). After that addition of 0.76 mM nitrite. (A3 experiment); d) initial 0.76 mM nitrite with ferrihydrite and 1.2 mM of bio-produced Fe(II) (Nferr experiment).

nitrite reduction commenced. In the reactors amended with lactate, nitrate reduction began after a 1-day lag period. For reactors amended with acetate, nitrite reduction began after a 10-day lag period (Fig. S3 in SI). Yoon et al. (Yoon et al., 2013) reported a similar behavior for *Shewanella* spp. In contrast, abiotic experiments with bioproduced Fe(II) and acetate, nitrite was consumed in only 10 h (Fig. 3d). These results suggest an absence of microbial nitrite reduction in the abiotic experiments with bioproduced Fe(II). As explained further in Sections 3.4 and 3.5, the isotopic data confirmed that the microbial nitrite reduction can be ruled out in the abiotic nitrite reduction experiments (NFerr experiment).

3.4. Isotopic fractionation during abiotic NO_2^- reduction owing to dissolved or solid-bound Fe(II)

As is commonly observed for denitrification (sources), the unreacted NO_2^- became enriched in the heavy isotopes of N and O (^{15}N and ^{18}O) during abiotic nitrate reduction. Table 2 lists the values determined for $\varepsilon^{15}N_{NO2}$, $\varepsilon^{18}O_{NO2}$ and $\varepsilon^{18}O/\varepsilon^{15}N$ (calculations shown in Fig. S5 in SI). These values are within the range reported in the literature for both the biotic (heterotrophic) and abiotic NO_2^- reductions (Table 3).

In the experiments to test the abiotic NO_2^- reduction, differences in NO_2^- isotopic fractionation were not observed (i) when using Fe(II) from biotic or synthetic sources (NFerr and A3 experiments, respectively) nor (ii) when using both aqueous and solid-bound Fe(II) or only aqueous Fe(II) (A1 and A3 experiments, respectively; Table 2). By contrast, in the experiments with solid-bound Fe(II) in the absence of aqueous Fe(II) (A2 experiment), the $\varepsilon^{15}N_{NO2}$ and $\varepsilon^{18}O_{NO2}$ determined were higher (Table 2).

In these abiotic NO_2^- reduction experiments, the observed variability of $\varepsilon^{15}N_{NO2}$ and $\varepsilon^{18}O_{NO2}$ could be caused by the different NO_2^- reduction rates or by a different reaction mechanism during oxidation of dissolved or solid-bound Fe(II). In earlier studies, lower ε values have been associated with higher NO_2^- reduction rates (Buchwald et al., 2016; Bryan et al., 1983). Buchwald et al. (Buchwald et al., 2016) observed differences in ε and NO_2^- removal rates using aqueous Fe(II) as electron donor or Fe(II) associated with the oxide surface. However, our results do not show a correlation between the NO_2^- reduction rates and the isotopic fractionation values (Table 2). For instance, $\varepsilon^{15}N_{NO2}$ and $\varepsilon^{18}O_{NO2}$ were similar in the A3 and NFerr experiments with highly dissimilar NO_2^- reduction rates (0.74 and 6.47 mM^{-1} d^{-1}, respectively).

The kinetics of the abiotic NO_2^- reduction could be affected by the initial concentration and proportion of the reactants (NO_2^- and Fe(II)), solution pH, and the presence of minerals that were added externally or those precipitated during the reaction (Grabb et al., 2017; Buchwald et al., 2016). In the latter case, the amount, composition (including the Fe oxidation state) and the mineral specific surface area could have influenced the reaction. In the present study, the formation of secondary magnetite during the Fe(II) oxidation in the Ferr experiment complicates a comparison between the effect of the conditions investigated in this study and earlier studies.

Therefore, it is difficult to determine whether the ε variability observed is only due to differences in the reduction rates or to the differences in mechanisms (oxidation of aqueous or solid-bound Fe(II) coupled with NO_2^- reduction).

A dual element isotope approach was used to further investigate the differences in the ε values in the different experiments (Fig. 4). The different slopes (i.e., $\Delta\delta^{18}O/\Delta\delta^{15}N \approx \varepsilon^{18}O/\varepsilon^{15}N$) suggest the occurrence of different nitrite reduction mechanisms. The higher ε values determined in the experiment A2 (solid-bound Fe(II)) compared with the similar values in the NFerr and A3 experiments (aqueous and solid-bound Fe (II)) and the A1 experiment (aqueous Fe (II)) suggest that nitrite reduction is controlled by a different mechanism in the presence of only solid-bound Fe(II). Nevertheless, the similar slopes in the dual N-O plot for A1, A2, A3 and NFerr ($\Delta\delta^{18}O/\Delta\delta^{15}N = 0.60 \pm 0.02$) indicates a common nitrite reduction mechanism in the abiotic experiments. Further research is needed to elucidate the process controlling the magnitude of ε values during nitrite reduction by solid-bound Fe(II).

Another consideration in the abiotic NO_2^- reduction experiments is the possible effect of $\delta^{18}O$-NO_2^- equilibration with $\delta^{18}O$-H_2O on the $\varepsilon^{18}O/\varepsilon^{15}N$ ratio. The magnitude of this effect depends on solution salinity, temperature and/or pH (Buchwald and Casciotti, 2013). Buchwald et al. (Buchwald et al., 2016) demonstrated that NO accumulated in a reversible reaction could re-oxidize to NO_2^- by incorporating an O atom from water, which could also influence the $\varepsilon^{18}O/\varepsilon^{15}N$ ratio. Nevertheless, Martin and Casciotti (Martin and Casciotti, 2016) have shown a negligible effect (0.0035‰) due to equilibrium isotopic exchange at room temperature and pH 7.6 over 2 h between sampling and the azide reaction. Given that our nitrite samples in synthetic seawater were retrieved at pH between 7.8 and 8.2, an oxygen equilibration effect was ruled out. The slopes obtained in the abiotic NO_2^- reduction experiments for relatively short (NFerr experiment) and long (A3 experiment) incubation periods (Table 2 and Fig. 4) reinforce the lack of $\delta^{18}O$-NO_2^- equilibration with $\delta^{18}O$-H_2O.

3.5. Use of isotopic tools to distinguish between abiotic and biotic NO_2^- reduction in the field

As in the abiotic reduction, a decrease in concentration resulted in an enrichment in the heavy isotopes (^{15}N and ^{18}O) of the unreacted substrate during biotic NO_2^- reduction. The isotopic fractionation results are listed in Table 2 (see calculations in Fig. S5 in SI). NO_2^- reduction by *S. loihica* using lactate as electron donor yielded $\varepsilon^{15}N_{NO2} = -1.6‰$, $\varepsilon^{18}O_{NO2} = -5.3‰$ and $\varepsilon^{18}O/\varepsilon^{15}N = 3.1$. The $\varepsilon^{15}N_{NO2}$ and $\varepsilon^{18}O_{NO2}$ obtained are within the range of the values reported in the literature for both the biotic (heterotrophic) and abiotic NO_2^- reduction (Table 3). Nevertheless, under the conditions of these experiments, the value of the isotopic fractionation of nitrogen ($\varepsilon^{15}N_{NO2}$) was smaller than those from our abiotic experiments. As a consequence, the value of the $\varepsilon^{18}O/\varepsilon^{15}N$ ratio obtained differs from those calculated for the abiotic experiments (Fig. 4 and Table 2) and becomes higher than prior values reported (Table 3).

In the biotic NO_2^- reduction, the magnitude of the $\varepsilon^{15}N_{NO2}$ and $\varepsilon^{18}O_{NO2}$ values could depend on the enzymes involved, on the NO_2^- transport across the cell and on the NO_2^- reduction rate. However, it is unknown whether the effect of pH or salinity could be negligible on the biotic nitrite reduction as it occurs in the biotic nitrate reduction (Granger et al., 2008; Wunderlich et al., 2012; Chen et al., 2002). Bacterial NO_2^- reduction can be catalyzed by two enzymes

Table 2
Average nitrite reduction rates (mM^{-1} d^{-1}), $\varepsilon^{15}N_{NO2}$, $\varepsilon^{18}O_{NO2}$ and $\varepsilon^{18}O/\varepsilon^{15}N$ ratio in the experiments. In NFerr experiment, nitrite reduction rate is calculated from a representative experiment. Fig. S6 (Supporting Information) shows the linear correlation between the natural logarithms of the substrate remaining fraction and the isotope ratios obtained. Values for $\varepsilon^{18}O/\varepsilon^{15}N$ are calculated from data indicated in Fig. S6.

	Experiment	Electron donor	electron donor distribution	Reduction rate (NO_2^-)	$\varepsilon^{15}N_{NO2}$‰	$\varepsilon^{18}O_{NO2}$‰	$\varepsilon^{18}O/\varepsilon^{15}N$
Abiotic	A1	Synthetic Fe(II)	Aqueous Fe(II)	0.059	−8.6	−6.3	0.7
	A2	Synthetic Fe(II)	Solid-bound Fe(II)	0.22	−19.7	−11.4	0.6
	A3	Synthetic Fe(II)	Aqueous & solid Fe(II)	0.74	−8.7	−5.2	0.6
	NFerr	Bio-produced Fe(II)	Aqueous & solid Fe(II)	6.47	−8.1	−4.6	0.6
Biotic	Bio1	Lactate			−1.6	−5.3	3.1

Table 3
$\varepsilon^{15}N$, $\varepsilon^{18}O$ (in ‰) and $\varepsilon^{18}O/\varepsilon^{15}N$ reported in the literature for the NO_2^- reduction. For NO_2^- biotic reduction, ε is calculated for conversion to N_2, whereas for NO_2^- abiotic reduction, the final product is assumed to be N_2O. n.a. = non analyzed.

Reaction type	Bacteria	e⁻ donor	e⁻ acceptor	$\varepsilon^{15}N$	$\varepsilon^{18}O$	$\varepsilon^{18}O/\varepsilon^{15}N$	reference
Biotic (heterotrophic)	*Pseudomonas aeruginosa* (Fe-NIR)	C_{org} (medium)	NO_2^-	−9.5	−4.2	0.4	(1) *
	Pseudomonas chlororaphis (Fe-NIR)	C_{org} (medium)	NO_2^-	−8.25	−9.75	1.2	(1) *
	Pseudomonas stutzeri (Fe-NIR)	C_{org} (medium)	NO_2^-	−7.0	−5.0	0.7	(1) *
	Pseudomonas aureofaciens (Cu-NIR)	C_{org} (medium)	NO_2^-	−20.5	−3.5	0.2	(1) *
	Achromobacter xylosoxidans (Cu-NIR)	C_{org} (medium)	NO_2^-	−21.0	−1.0	0.05	(1) *
	Ochrobactrum sp. (Cu-NIR)	C_{org} (medium)	NO_2^-	−23.5	−2.5	0.1	(1) *
	Pseudomonas stutzeri (Fe-NIR)	C_{org} (medium)	NO_2^-	−1.0	n.a.	n.a.	(2) *
	Kuenenia stuttgartiensis (Fe-NIR)	C_{org} (medium)	NO_2^-	−16.0	n.a.	n.a.	(3) *
Biotic	Environmental community	–	NO_2^-	−10	n.a.	n.a.	(4) *
Abiotic (heterogeneous)	–	Nontronite	NO_2^-	−11.1	−10.4	0.9	(5) *
	–	Nontronite + Fe(II) synth	NO_2^-	−2.3	−4.5	2.0	(5) *
	–	Green rust	NO_2^-	−4.2 to −9.4	−4.1 to −9.4	0.9 to 1.3	(5) *
	–	Fe(II) synth	NO_2^-	−6.1 to −33.9	−5.7 to −24.8	0.6 to 1.3	(6) *
	–	Goethite + Fe(II) synth	NO_2^-	−5.9 to 44.8	−5.2 to 33.0	0.7 to 1.0	(6) *

(1) Martin and Casciotti (2016) (average values of the data reported in Table 1).
(2) Bryan et al. (1983)
(3) Brunner et al. (2013).
(4) Jacob et al. (2016).
(5) Grabb et al. (2017)
(6) Buchwald et al. (2016)

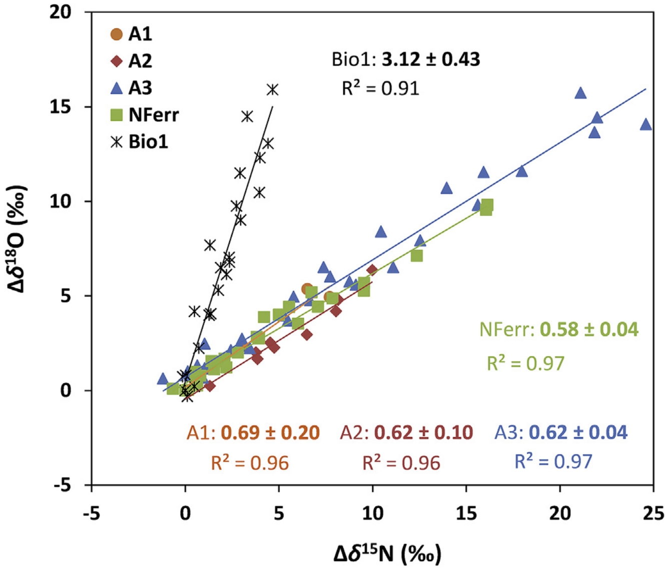

Fig. 4. Dual N-O isotope plot for the abiotic and biotic nitrite reduction experiments. Isotopic fractionation values respect to its initial isotopic composition for all carried out experiments are shown. Linear regression is represented by solid lines and formula. SD for all points is ±1.0‰ for $\delta^{15}N$-NO_2^- and ±1.5‰ for $\delta^{18}O$-NO_2.

located in the periplasm (Cu containing NO_2^- reductase encoded as *nirK* (Cu-NIR) and Fe-containing NO_2^- reductase encoded as *nirS* (Fe-NIR) ((Kuypers et al., 2018) and references therein). The $\varepsilon^{18}O/\varepsilon^{15}N$ ratio of 3.1 obtained for the biotic NO_2^- reduction by *S. loihica* bears no resemblance to those reported in a study on NO_2^- reduction with different bacterial species. Martin and Casciotti (Martin and Casciotti, 2016) attributed the variations in the $\varepsilon^{18}O/\varepsilon^{15}N$ ratio to the use of different enzymes since the species with Fe-NIR yielded higher $\varepsilon^{18}O/\varepsilon^{15}N$ ratios (from 0.4 to 1.2) than the species containing Cu-NIR (from 0.05 to 0.2). These authors suggested that Fe-NIR could produce a higher NO_2^--O isotopic fractionation because it allows cleavage of both N-O bonds since the Fe-NIR catalytic site might bind NO_2^--N (Fülöp et al., 1995; Maia and Moura, 2014). By contrast, the Cu-NIR catalytic site might bind both the NO_2^--O atoms and the N-O bond closest to the Asp98 residue, which is cleaved (Li et al., 2015; Murphy et al., 1997), independently of the isotopic composition. The NO_2 reductase associated with *S. loihica* is Cu-NIR (Simpson et al., 2010). However, our results are not indicative of this hypothesis. Our study showed an $\varepsilon^{18}O_{NO2}$ higher than $\varepsilon^{15}N_{NO2}$ in contrast to a lower $\varepsilon^{18}O_{NO2}$ associated with microorganisms containing Cu-NIR (Martin and Casciotti, 2016).

The $\varepsilon^{18}O/\varepsilon^{15}N$ of 3.1 ratio determined for the NO_2^- reduction by *S. loihica* differs from the range obtained for the abiotic experiments (0.6–0.7; Fig. 4). Thus, given that *S. loihica* is the only NO_2^- reducing microorganism in our experiments, the $\varepsilon^{18}O/\varepsilon^{15}N$ values calculated in the present study could allow us to distinguish the contribution of the biotic (heterotrophic) and abiotic NO_2^- reductions at the laboratory. However, considering the large variability of the $\varepsilon^{18}O/\varepsilon^{15}N$ ratio (from 0.05 to 3.1) in this study and in the literature for the biotic NO_2^- reduction (Tables 2 and 3), it would be difficult to distinguish between biotic and abiotic reactions in natural marine environments using this technique. One reason for this is the existence of complex bacterial communities with various NO_2^- reducing enzymes. Another reason is the overlap of biotic $\varepsilon^{18}O/\varepsilon^{15}N$ values with the ones attributed to the abiotic reduction (0.6–2.0; Tables 2 and 3).

Alternatively, the correlation between changes in nitrite isotopic composition ($\Delta\delta^{15}N_{NO2}$ or $\Delta\delta^{18}O_{NO2}$) and dissolved Fe(II) iron concentration (ln[Fe(II)]) during the abiotic nitrite reduction, could be useful to investigate the process controlling NO_2^- reduction under field conditions. A good correlation between $\delta(^{15}N$ or $^{18}O)$-NO_2^- and ln[Fe(II)] in field samples suggests NO_2^- reduction by Fe(II) oxidation, either abiotically or biotically (chemolithotrophically). By contrast, no correlation is expected for heterotrophic NO_2^- reduction. A decrease in Fe(II) concentration coupled with an increase in $\delta^{15}N_{NO2}$ and $\delta^{18}O_{NO2}$ was observed (Fig. 5). In the A1 experiment, the slopes for $\delta^{15}N_{NO2}$ and $\delta^{18}O_{NO2}$ (−5.4 and −3.8, respectively) were lower than those in the A3 (−32.2 and −20.3, respectively) and NFerr experiments (−32.6 and −18.9, respectively). This was due to the higher decrease in aqueous Fe(II) concentrations during the A1 experiment. In contrast to A3 and NFerr, which also contained solid-bound Fe(II) and the total amount of Fe(II) was thus higher than in A1, in the A1 experiment only aqueous Fe(II) was available for nitrite reduction (Table 1).

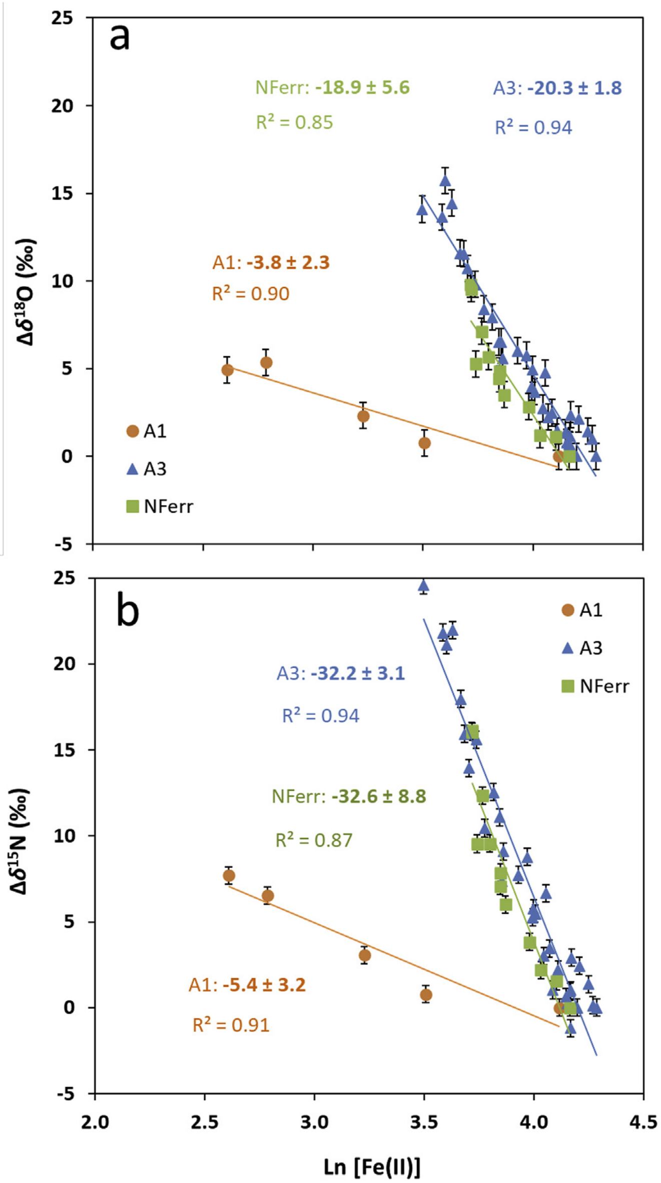

Fig. 5. Correlation between the NO_2^- isotopic composition and the Ln Fe(II) concentration. a) Isotopic $\delta^{18}O$-NO_2^- fractionation values respect to initial isotopic composition. b) Isotopic $\delta^{15}N$-NO_2^- fractionation values respect to initial isotopic composition. In the abiotic experiments containing dissolved Fe(II) (A1, A3 and NFerr), the linear regression of $\delta^{15}N$-NO_2^- and $\delta^{18}O$-NO_2^- is shown versus the Fe(II) concentration decrease.

Given that the equilibration between $\delta^{18}O_{NO2}$ and $\delta^{18}O_{H2O}$ could affect $\delta^{18}O_{NO2}$ under natural conditions, only the variation of $\delta^{15}N_{NO2}$ versus Fe(II) concentration could provide reliability of the NO_2^- fate in the environment. However, a possible effect of other N cycling processes (e.g. NO_2^- oxidation to NO_3^-, NO_2^- reduction to NH_4^+ or NH_4^+ oxidation to NO_2^-) on $\delta^{15}N_{NO2}$ should also be considered.

4. Conclusions

Experiments simulating an anoxic marine medium were carried out to study nitrite reduction coupled with (bioproduced and synthetic) Fe(II) oxidation. Fe(II) bioproduction was driven by ferrihydrite reduction mediated by *S. loihica*. Fe(II) released was partially re-incorporated into ferrihydrite, which transformed to nanocrystalline magnetite, producing solid Fe(II). Both the bioproduced aqueous Fe(II) and solid Fe(II) played a role in nitrite reduction.

Experiments with bioproduced or synthetic Fe(II) (aqueous and solid-bound Fe(II)) revealed that abiotic NO_2^- reduction is faster in a system with bioproduced Fe(II). The newly formed nano-crystalline magnetite with a high content of solid Fe(II) showed a significant reactivity in the presence of nitrite. Results obtained from the laboratory nitrite reduction experiments using synthetic Fe(II) suggest that with similar concentrations of aqueous Fe(II), nitrite reduction in natural systems could be stronger given the higher amounts of solid-bound Fe(II) obtained in the experiments with bioproduced Fe(II).

Experiments with only synthetic Fe(II) (aqueous, solid-bound Fe(II) or both) revealed that in the presence of Fe(II) in both aqueous and solid-bound forms, abiotic NO_2- reduction is faster and more effective in terms of nitrite removal than in the ones with only aqueous Fe(II) or only solid-bound Fe(II).

No differences in the $\varepsilon^{15}N_{NO2}$ and $\varepsilon^{18}O_{NO2}$ were found for the abiotic NO_2^- reduction regardless of wether the source of Fe(II) was biotic or synthetic. Differences in $\varepsilon^{15}N_{NO2}$ and $\varepsilon^{18}O_{NO2}$ were neither found for the abiotic NO_2^- reduction by (i) aqueous Fe(II) or (ii) aqueous and solid-bound Fe(II). By contrast, the isotopic fractionation was higher in the experiments with only solid-bound Fe(II). The similar slopes derived in the dual N-O isotope plot ($\varepsilon^{18}O/\varepsilon^{15}N = 0.6$) suggest a sole mechanism controlling the NO_2^- reduction in the abiotic experiments. The higher slope related to the biotic (heterotrophic) experiment ($\varepsilon^{18}O/\varepsilon^{15}N = 3.1$) contrasts with those of the abiotic experiments, becoming one of the highest values reported in the literature.

Hence, in laboratory microcosms, which mimic marine environments with *S. loihica* as the only existing NO_2^--reducing microorganism, the value of the $\varepsilon^{18}O/\varepsilon^{15}N$ ratio allows us to distinguish between the biotic and abiotic NO_2^- reduction. Given the wide range of $\varepsilon^{18}O/\varepsilon^{15}N$ values reported in the literature for the biotic and abiotic NO_2^- reduction by other heterotrophic bacteria, the use of the $\varepsilon^{18}O/\varepsilon^{15}N$ ratio to distinguish different NO_2^- reduction processes in field-scale studies should be discretionally applied.

Moreover, the correlation between $\delta^{15}N_{NO2}$ and the natural logarithm of the Fe(II) concentration observed could be used as an additional line of evidence to distinguish between NO_2^- reduction by Fe(II) oxidation, either abiotically or biotically (chemolithotrophically), and heterotrophic bacteria. This observation can improve the prospect of using isotopic data to investigate nitrite reduction processes in the field.

Sample CRediT author statement

Robert Benaiges-Fernandez: Conceptualization, Methodology, Investigation, Writing – Original Draft, Writing - Review & Editing; **Francesco G. Offeddu:** Conceptualization, Methodology, Investigation, Writing - Original Draft, Writing - Review & Editing; **Rosanna Margalef-Marti:** Methodology, Investigation, Writing - Review & Editing; **Jordi Palau:** Conceptualization, Investigation, Writing - Review & Editing; **Raul Carrey:** Methodology, Investigation; **Neus Otero:** Conceptualization, Validation, Writing - Review & Editing, Supervision; **Jordi Urmeneta:** Conceptualization, Supervision; **Jordi Cama:** Conceptualization, Validation, Writing - Review & Editing, Supervision, Project administration, Funding acquisition.

Declaration of competing interest

The authors declare that they have no known competing financial interests or personal relationships that could have appeared to influence the work reported in this paper.

5 Acknowledgements

This study was supported by projects CGL2017-87216-C4-1-R, CGL2017-82331-R and CEX2018-000794-S funded by the Spanish Ministry of Science and Innovation and AEI/FEDER funded by the European Union, and by MAG (2017 SGR 1733) financed by the Catalan Government. R. Margalef-Marti wishes to thank the Spanish Government for the Ph.D. grant BES-2015-072882. The authors are indebted to Jordi Bellés (IDAEA-CSIC), Natàlia Moreno (IDAEA-CSIC) and Xavier Alcové (SCTT-Barcelona University) for laboratory assistance and XRD analyses, respectively. The isotopic analyses were prepared at the MAiMA-UB research group laboratory and analyzed at the scientific and technical services of Barcelona University (CCiT-UB). We acknowledge Max Giannetta for his scientific discussions during the manuscript elaboration. We also wish to thank the Editor and three anonymous reviewers for their constructive comments that have improved the quality of the paper.

Appendix A. Supplementary data

Supplementary data to this article can be found online at https://doi.org/10.1016/j.chemosphere.2020.127554.

References

Amstaetter, K., Borch, T., Kappler, A., 2012. Influence of humic acid imposed changes of ferrihydrite aggregation on microbial Fe (III) reduction. Geochem. Cosmochim. Acta 85, 326–341.

Aravena, R., Robertson, W.D., 1998. Use of multiple isotope tracers to evaluate denitrification in ground water: study of nitrate from a large-flux septic system plume. Groundwater 36 (6), 975–982.

Benaiges-Fernandez, R., et al., 2019. Dissimilatory bioreduction of iron (III) oxides by Shewanella loihica under marine sediment conditions. Mar. Environ. Res. 151, 104782.

Boland, D.D., et al., 2014. Effect of solution and solid-phase conditions on the Fe (II)-accelerated transformation of ferrihydrite to lepidocrocite and goethite. Environ. Sci. Technol. 48 (10), 5477–5485.

Böttcher, J., et al., 1990. Using isotope fractionation of nitrate-nitrogen and nitrate-oxygen for evaluation of microbial denitrification in a sandy aquifer. J. Hydrol. 114 (3–4), 413–424.

Brunauer, S., Emmett, P.H., Teller, E., 1938. Adsorption of gases in multimolecular layers. J. Am. Chem. Soc. 60 (2), 309–319.

Bryan, B.A., et al., 1983. Variable expression of the nitrogen isotope effect associated with denitrification of nitrite. J. Biol. Chem. 258 (14), 8613–8617.

Bryce, C., et al., 2018. Microbial anaerobic Fe (II) oxidation–Ecology, mechanisms and environmental implications, 20 (10), 3462–3483.

Buchwald, C., Casciotti, K.L., 2013. Isotopic ratios of nitrite as tracers of the sources and age of oceanic nitrite. Nat. Geosci. 6 (4), 308–313.

Buchwald, C., et al., 2016. Constraining the role of iron in environmental nitrogen transformations: dual stable isotope systematics of abiotic NO2– reduction by Fe (II) and its production of N2O. Geochem. Cosmochim. Acta 186, 1–12.

Byrne, J., et al., 2011. Control of nanoparticle size, reactivity and magnetic properties during the bioproduction of magnetite by Geobacter sulfurreducens. Nanotechnology 22 (45), 455709.

Canfield, D.E., 1989. Reactive iron in marine sediments. Geochem. Cosmochim. Acta 53 (3), 619–632.

Carlson, H.K., et al., 2013. Fe (II) oxidation is an innate capability of nitrate-reducing bacteria that involves abiotic and biotic reactions, 195 (14), 3260–3268.

Chen, G., et al., 2002. Dual nitrogen-oxygen isotopic analysis and kinetic model for enzymatic nitrate reduction coupled with Fe (II) oxidation by Pseudogulbenkiania sp. Strain 534, 119456, 2020.

Chen, D., et al., 2018. Biological and chemical processes of microbially mediated nitrate-reducing Fe (II) oxidation by Pseudogulbenkiania sp. strain 2002. Chem. Geol. 476, 59–69.

Coplen, T.B., 2011. Guidelines and recommended terms for expression of stable-isotope-ratio and gas-ratio measurement results. Rapid Commun. Mass Spectrom. 25 (17), 2538–2560.

Das, S., Hendry, M.J., Essilfie-Dughan, J., 2011. Transformation of two-line ferrihydrite to goethite and hematite as a function of pH and temperature. Environ. Sci. Technol. 45 (1), 268–275.

Devol, A.H., 2015. Denitrification, anammox, and N2 production in marine sediments. Annual review of marine science 7, 403–423.

Dhakal, P., et al., 2013. Nitrite reactivity with magnetite. Environ. Sci. Technol. 47 (12), 6206–6213.

Dippon, U., et al., 2015. Secondary mineral formation during ferrihydrite reduction by Shewanella oneidensis MR-1 depends on incubation vessel orientation and resulting gradients of cells, Fe2+ and Fe minerals. Geomicrobiol. J. 32 (10), 878–889.

Dzombak, D.A., Morel, F.M., 1990. Surface Complexation Modeling: Hydrous Ferric Oxide. John Wiley & Sons.

Elsner, M., et al., 2004. Reactivity of Fe (II)-bearing minerals toward reductive transformation of organic contaminants, 38 (3), 799–807.

Fukada, T., et al., 2003. A dual isotope approach to identify denitrification in groundwater at a river-bank infiltration site. Water Res. 37 (13), 3070–3078.

Fülöp, V., et al., 1995. The anatomy of a bifunctional enzyme: structural basis for reduction of oxygen to water and synthesis of nitric oxide by cytochrome cd1. Cell 81 (3), 369–377.

Gao, H., et al., 2006. Shewanella loihica sp. nov., isolated from iron-rich microbial mats in the Pacific Ocean. Int. J. Syst. Evol. Microbiol. 56 (8), 1911–1916.

García-Robledo, E., Corzo, A., Papaspyrou, S., 2014. A fast and direct spectrophotometric method for the sequential determination of nitrate and nitrite at low concentrations in small volumes. Mar. Chem. 162, 30–36.

Gorski, C.A., Scherer, M.M., 2011. Fe2+ sorption at the Fe oxide-water interface: a revised conceptual framework. In: Aquatic Redox Chemistry. ACS Publications, pp. 315–343.

Grabb, K.C., et al., 2017. A dual nitrite isotopic investigation of chemodenitrification by mineral-associated Fe (II) and its production of nitrous oxide. Geochem. Cosmochim. Acta 196, 388–402.

Granger, J., et al., 2008. Nitrogen and oxygen isotope fractionation during dissimilatory nitrate reduction by denitrifying bacteria. Limnol. Oceanogr. 53 (6), 2533–2545.

Guerbois, D., et al., 2014. Nitrite reduction by biogenic hydroxycarbonate green rusts: evidence for hydroxy-nitrite green rust formation as an intermediate reaction product. Environ. Sci. Technol. 48 (8), 4505–4514.

Hansel, C.M., et al., 2003. Secondary mineralization pathways induced by dissimilatory iron reduction of ferrihydrite under advective flow. Geochem. Cosmochim. Acta 67 (16), 2977–2992.

Jani, J., Toor, G.S., 2018. Composition, sources, and bioavailability of nitrogen in a longitudinal gradient from freshwater to estuarine waters. Water Res. 137, 344–354.

Kampschreur, M.J., et al., 2011. Reduced iron induced nitric oxide and nitrous oxide emission. Water Res. 45 (18), 5945–5952.

Kuypers, M.M., Marchant, H.K., Kartal, B., 2018. The microbial nitrogen-cycling network. Nat. Rev. Microbiol. 16 (5), 263.

Lanthier, M., Gregory, K.B., Lovley, D.R., 2008. Growth with high planktonic biomass in Shewanella oneidensis fuel cells. FEMS Microbiol. Lett. 278 (1), 29–35.

Li, Y., Hodak, M., Bernholc, J., 2015. Enzymatic mechanism of copper-containing nitrite reductase. Biochemistry 54 (5), 1233–1242.

Lovley, D.R., 1991. Dissimilatory Fe (III) and Mn (IV) reduction. Microbiol. Mol. Biol. Rev. 55 (2), 259–287.

Lu, Y., et al., 2017. Microbial mediated iron redox cycling in Fe (hydr) oxides for nitrite removal. Bioresour. Technol. 224, 34–40.

Maia, L.B., Moura, J.J., 2014. How biology handles nitrite. Chem. Rev. 114 (10), 97.

Mariotti, A., et al., 1981. Experimental determination of nitrogen kinetic isotope fractionation: some principles; illustration for the denitrification and nitrification processes. Plant Soil 62 (3), 413–430.

Martin, T.S., Casciotti, K.L., 2016. Nitrogen and oxygen isotopic fractionation during microbial nitrite reduction. Limnol. Oceanogr. 61 (3), 1134–1143.

McIlvin, M.R., Altabet, M.A., 2005. Chemical conversion of nitrate and nitrite to nitrous oxide for nitrogen and oxygen isotopic analysis in freshwater and seawater. Anal. Chem. 77 (17), 5589–5595.

Melton, E.D., et al., 2014. The interplay of microbially mediated and abiotic reactions in the biogeochemical Fe cycle. Nat. Rev. Microbiol. 12 (12), 797–808.

Murphy, M.E., Turley, S., Adman, E.T., 1997. Structure of nitrite bound to copper-containing nitrite reductase from Alcaligenes faecalis mechanistic implications. J. Biol. Chem. 272 (45), 28455–28460.

Otte, J.M., et al., 2019. N 2 O formation by nitrite-induced (chemo) denitrification in coastal marine sediment, 9 (1), 1–12.

Pantke, C., et al., 2012. Green rust formation during Fe (II) oxidation by the nitrate-reducing Acidovorax sp. strain BoFeN1, vol. 46, pp. 1439–1446, 3.

Piepenbrock, A., et al., 2011. Dependence of microbial magnetite formation on humic substance and ferrihydrite concentrations. Geochem. Cosmochim. Acta 75 (22), 6844–6858.

Rakshit, S., Matocha, C.J., Coyne, M.S., 2008. Nitrite reduction by siderite. Soil Sci. Soc. Am. J. 72 (4), 1070–1077.

Ravishankara, A., Daniel, J.S., Portmann, R.W., 2009. Nitrous oxide (N2O): the dominant ozone-depleting substance emitted in the 21st century. Science 326 (5949), 123–125.

Robertson, E.K., Thamdrup, B., 2017. The fate of nitrogen is linked to iron (II) availability in a freshwater lake sediment. Geochem. Cosmochim. Acta 205, 84–99.

Robertson, E.K., et al., 2016. Dissimilatory nitrate reduction to ammonium coupled to Fe (II) oxidation in sediments of a periodically hypoxic estuary. Limnol. Oceanogr. 61 (1), 365–381.

Roh, Y., et al., 2006. Metal reduction and iron biomineralization by a psychrotolerant Fe (III)-reducing bacterium, Shewanella sp. strain PV-4. Appl. Environ. Microbiol. 72 (5), 3236–3244.

Ryabenko, E., Altabet, M.A., Wallace, D.W., 2009. Effect of chloride on the chemical conversion of nitrate to nitrous oxide for δ15N analysis. Limnol Oceanogr. Methods 7 (7), 545–552.

Schwertmann, U., Cornell, R.M., 2008. Iron Oxides in the Laboratory: Preparation and Characterization. John Wiley & Sons.

Simpson, P.J., Richardson, D.J., Codd, R., 2010. The periplasmic nitrate reductase in Shewanella: the resolution, distribution and functional implications of two NAP isoforms, NapEDABC and NapDAGHB. Microbiology 156 (2), 302–312.

Stucki, J., 1981. The quantitative assay of minerals for Fe2+ and Fe3+ using 1, 10-phenanthroline: II. A photochemical method. Soil Sci. Soc. Am. J. 45 (3), 638–641.

Tai, Y.-L., Dempsey, B.A., 2009. Nitrite reduction with hydrous ferric oxide and Fe (II): stoichiometry, rate, and mechanism. Water Res. 43 (2), 546–552.

Tomaszewski, E.J., et al., 2016. The role of dissolved Fe (II) concentration in the mineralogical evolution of Fe (hydr) oxides during redox cycling. Chem. Geol. 438, 163–170.

Wu, D., et al., 2015. Denitrification of nitrite by ferrous hydroxy complex: effects on nitrous oxide and ammonium formation. Chem. Eng. J. 279, 149–155.

Wunderlich, A., Meckenstock, R., Einsiedl, F., 2012. Effect of different carbon substrates on nitrate stable isotope fractionation during microbial denitrification. Environ. Sci. Technol. 46 (9), 4861–4868.

Xiao, W., et al., 2017. Use of fourier transform infrared spectroscopy to examine the Fe (II)-Catalyzed transformation of ferrihydrite. Talanta 175, 30–37.

Xiao, W., et al., 2018. Effect of Shewanella oneidensis on the kinetics of Fe (II)-catalyzed transformation of ferrihydrite to crystalline iron oxides. Environ. Sci. Technol. 52 (1), 114–123.

Yang, L., et al., 2010. Kinetics of Fe (II)-catalyzed transformation of 6-line ferrihydrite under anaerobic flow conditions. Environ. Sci. Technol. 44 (14), 5469–5475.

Yee, N., et al., 2006. The rate of ferrihydrite transformation to goethite via the Fe (II) pathway. Am. Mineral. 91 (1), 92–96.

Yoon, S., Sanford, R.A., Löffler, F.E., 2013. Shewanella spp. use acetate as an electron donor for denitrification but not ferric iron or fumarate reduction. Appl. Environ. Microbiol. 79 (8), 2818–2822.